



# *Environmentally friendly phosphorus flame retardant systems for acrylonitrilebutadiene-styrene (ABS): strategies to enhance mechanical properties and development of novel phosphorus/cork powder hybrid solutions*

**Farnaz Ghonjizadehsamani**

**ADVERTIMENT** La consulta d'aquesta tesi queda condicionada a l'acceptació de les següents condicions d'ús: La difusió d'aquesta tesi per mitjà del repositori institucional UPCommons (<http://upcommons.upc.edu/tesis>) i el repositori cooperatiu TDX (<http://www.tdx.cat/>) ha estat autoritzada pels titulars dels drets de propietat intel·lectual **únicament per a usos privats** emmarcats en activitats d'investigació i docència. No s'autoritza la seva reproducció amb finalitats de lucre ni la seva difusió i posada a disposició des d'un lloc aliè al servei UPCommons o TDX. No s'autoritza la presentació del seu contingut en una finestra o marc aliè a UPCommons (*framing*). Aquesta reserva de drets afecta tant al resum de presentació de la tesi com als seus continguts. En la utilització o cita de parts de la tesi és obligat indicar el nom de la persona autora.

**ADVERTENCIA** La consulta de esta tesis queda condicionada a la aceptación de las siguientes condiciones de uso: La difusión de esta tesis por medio del repositorio institucional UPCommons (<http://upcommons.upc.edu/tesis>) y el repositorio cooperativo TDR (<http://www.tdx.cat/?locale-attribute=es>) ha sido autorizada por los titulares de los derechos de propiedad intelectual **únicamente para usos privados enmarcados** en actividades de investigación y docencia. No se autoriza su reproducción con finalidades de lucro ni su difusión y puesta a disposición desde un sitio ajeno al servicio UPCommons No se autoriza la presentación de su contenido en una ventana o marco ajeno a UPCommons (*framing*). Esta reserva de derechos afecta tanto al resumen de presentación de la tesis como a sus contenidos. En la utilización o cita de partes de la tesis es obligado indicar el nombre de la persona autora.

**WARNING** On having consulted this thesis you're accepting the following use conditions: Spreading this thesis by the institutional repository UPCommons (<http://upcommons.upc.edu/tesis>) and the cooperative repository TDX (<http://www.tdx.cat/?locale-attribute=en>) has been authorized by the titular of the intellectual property rights **only for private uses** placed in investigation and teaching activities. Reproduction with lucrative aims is not authorized neither its spreading nor availability from a site foreign to the UPCommons service. Introducing its content in a window or frame foreign to the UPCommons service is not authorized (*framing*). These rights affect to the presentation summary of the thesis as well as to its contents. In the using or citation of parts of the thesis it's obliged to indicate the name of the author.





UNIVERSITAT POLITÈCNICA  
DE CATALUNYA  
BARCELONATECH

*Environmentally friendly phosphorus  
flame retardant systems for acrylonitrile-  
butadiene-styrene (ABS): strategies to  
enhance mechanical properties and  
development of novel phosphorus/cork  
powder hybrid solutions*

by

**Farnaz Ghonjizadehsamani**



DOCTORATS  
INDUSTRIALS



# Environmentally friendly phosphorus flame retardant systems for acrylonitrile-butadiene-styrene (ABS): strategies to enhance mechanical properties and development of novel phosphorus/cork powder hybrid solutions

By:

**Farnaz Ghonjizadehsamani**

In partial fulfillment of the requirements for the degree of Doctor of Philosophy  
in  
**Materials Science and Engineering**

Director:

**Dr. Vera Cristina de Redondo Realinho**

Co-directors:

**Dr. Laia Haurie Ibarra**

**Dr. Ramón Malet Murillo**

2024, Barcelona



UNIVERSITAT POLITÈCNICA DE CATALUNYA  
BARCELONATECH

Departament de Ciència i Enginyeria  
de Materials





## Acknowledgments

First of all, I would like to express my gratitude to my thesis supervisors, Dr. Vera Cristina Realinho, Dr. Laia Haurie and Dr. Ramón Malet for all their continuous encouragement, lead, advice and helpful evaluations in my studies to carry out this thesis. I would like to thank Elix Polymers and the Industrial Doctorate program of the Generalitat de Catalunya for their financial support on this project. I am greatly thankful to all my colleagues at Elix Polymers, especially to Pedro, Marc, Anna and also all professors and employees in Materials Science and Engineering department of ESEIAAT (CEM-UPC), Poly2 research group, Prof. José Ignacio Velasco, Dr. David Arencón, Dr. Marcelo Antunes, Dr. Farayde Matta and all people at Centre Català del Plàstic (CCP), for their kind supports. I would like to thank those who helped me during the experimental procedures Fran and Josep in the Materials Science and Engineering department of ESEIAAT (CEM-UPC), and Dr. Antonia Navarro in the Material laboratory of EPSEB-UPC. I would also like to thank Prof. Tarik Eren and his research group for their kind hospitality and help during my stay at Yildiz Technical University. Finally, special appreciation to my family and friends who helped me with their support, comprehension and love during my PhD time.







## Table of contents

Acknowledgments.....	I
Confidential.....	
Confidential.....	
Confidential.....	
Table of contents.....	XII
Abbreviations.....	XVI
List of figures.....	XXI
List of tables.....	XXV
Chapter I: Introduction.....	3
<i>I.1 Objectives</i> .....	8
<i>I.2 Outline of thesis</i> .....	10
Chapter II: State of the art.....	15
<i>II.1 Strategies to improve polymers' flame retardancy</i> .....	17
<i>II.2 Bio-flame retardants</i> .....	23
<i>II.3 Modification of bio-based materials</i> .....	26
<i>II.4 Flame retardant acrylonitrile-butadiene-styrene composites</i> .....	33
<i>II.5 Effect of flame retardants on the ABS or ABS blends' mechanical properties</i> .....	36
Chapter III: Materials and methods .....	45
<i>III.1 Materials</i> .....	45
<i>III.1.1 ABS</i> .....	45
<i>III.1.2 Impact modifiers</i> .....	46
<i>III.1.3 Phosphorus flame retardants</i> .....	46
<i>III.1.4 Cork powder</i> .....	47
<i>III.1.5 Components for cork's phosphorylation</i> .....	49
<i>III.2 Chemical extraction of cork powder's components</i> .....	50
<i>III.3 Phosphorylation of cork powder</i> .....	51
<i>III.4 Melt-compounding and specimens' preparation</i> .....	55
<i>III.5 Morphological and physical characterization</i> .....	58
<i>III.5.1 Scanning electron microscopy</i> .....	58
<i>III.5.2 Cork particle size and density</i> .....	58
<i>III.6 Thermal analysis</i> .....	59
<i>III.6.1 Thermogravimetric analysis</i> .....	59

<i>III.7 Dynamic mechanical thermal analysis</i> .....	59
<i>III.8 Mechanical characterization</i> .....	61
<i>III.8.1 Three-point bending test</i> .....	61
<i>III.8.2 Charpy impact test</i> .....	62
<i>III.9 Chemical characterization</i> .....	62
<i>III.9.1 Attenuated total reflectance and Fourier transform infrared spectroscopy</i> .....	62
<i>III.9.2 TGA-FTIR</i> .....	63
<i>III.9.3 Thin layer chromatography</i> .....	64
<i>III.9.4 Gas chromatography–mass spectrometry</i> .....	65
<i>III.9.5 X-ray photoelectron spectroscopy</i> .....	65
<i>III.10 Fire performance analysis</i> .....	66
<i>III.10.1 Limiting oxygen index</i> .....	66
<i>III.10.2 UL-94 flammability test</i> .....	66
<i>III.10.3 Micro-scale combustion calorimetry</i> .....	68
<i>III.10.4 Cone calorimetry</i> .....	68
Chapter IV: Confidential .....	
Chapter V: The components' roles in thermal stability and flammability of cork powder .....	101
<i>V.1 Introduction</i> .....	101
<i>V.2 Results and Discussion</i> .....	103
<i>V.2.1 Particle size distribution, density and morphology of cork powder</i> .....	103
<i>V.2.2 Chemical composition and analysis of cork components</i> .....	104
<i>V.2.3 Thermal stability of cork powder and its main components</i> .....	108
<i>V.2.4 Potential flammability of cork powder and its main components</i> .....	113
<i>V.3 Conclusions</i> .....	119
Chapter VI: Cork powder as an adjuvant bio-flame retardant in ABS flame retardant formulations .....	123
<i>VI.1 Introduction</i> .....	123
<i>VI.2 Composition of ABS formulations</i> .....	126
<i>VI.3 Results and discussion</i> .....	126
<i>VI.3.1 Morphology of ABS composites</i> .....	126
<i>VI.3.2 Dynamic mechanical thermal analysis</i> .....	129
<i>VI.3.3 Pyrolysis: thermogravimetric analysis</i> .....	131
<i>VI.3.4 Evolved pyrolysis gasses: FTIR analysis</i> .....	139
<i>VI.3.5 Micro-scale combustion calorimetry</i> .....	144
<i>VI.3.6 Chemical analysis of MCC residue</i> .....	146
<i>VI.3.7 Fire behavior</i> .....	147

VI.3.8 Morphological and chemical analysis of CC residue .....	153
VI.4 Conclusions .....	157
Chapter VII: Effect of cork powder's phosphorylation on thermo-mechanical, thermal stability and fire behavior of ABS formulations .....	163
VII.1 Introduction .....	163
VII.2 Composition of ABS formulations.....	165
VII.3 Results and discussion .....	165
VII.3.1 Chemical analysis of phosphorylated cork powder .....	165
VII.3.2 Morphology of ABS composites .....	174
VII.3.3 Dynamic mechanical thermal analysis .....	176
VII.3.4 Thermal stability .....	178
VII.3.5 Fire behavior .....	182
VII.3.6 Morphological and chemical analysis of CC residue .....	186
VII.4 Conclusions.....	193
Chapter VIII: Confidential.....	
Chapter IX: Patents and scientific dissemination.....	207
IX.1 Patents.....	207
IX.1 Publications.....	207
IX. International conferences.....	208
References .....	209



## Abbreviations

ABS	Acrylonitrile-butadiene-styrene
ABS P	ABS with 20 wt.% of phosphorus-based flame retardant system
ABS-g-MA	ABS grafted maleic anhydride
ABS-R	Polybutadiene grafted SAN, containing a 70 wt.% of polybutadiene
AHP	Aluminum hypophosphite
AlPi	Aluminium diethyl phosphinate
APBu	Aluminum isobutylphosphinate
APP	Ammonium polyphosphate
APTES	3-aminopropyltriethoxysilane
ATR-FTIR	Attenuated total reflectance-Fourier transform infrared
BDEs	Brominated diphenyl ethers
BDP	Bisphenol A bis diphenyl phosphate
C	Cork powder
CA	Carbonization agent
CC	Cone calorimetry
C <sub>d</sub>	Cork powder modified with DTSP
C <sub>g</sub>	Cork powder modified with glyphosate
CNIS	Charpy notched impact strength
COP	Carbon monoxide production
CPCs	Cork polymer composites
CPD	Construction products directive
C <sub>t</sub>	Cork powder modified with TEP
DCM	Dichloromethane
DMTA	Dynamic mechanical thermal analysis
DOPO	9,10-dihydro-9-oxa-10-phosphaphenanthrene-10-oxide
DPER	Dipentaerythritol

DPP	Poly-4-nitrophenoxy-phosphazene
dTG	First derivative of TG curves
DTSP	Dimethyl-3-triethoxysilanepropylphosphoramidate
E'	Storage modulus
E''	Loss modulus
EDX	Energy-dispersive X-ray spectroscopy
EG	Expandable graphite
EHC	Effective heat of combustion
EMA	Ethylene methylacrylate
E24	EMA with 24 wt.% of MA
E29	EMA with 29 wt.% of MA
EMA-GMA	Ethylene-methyl acrylate-glycidyl methacrylate
EN	European standards
EnBACO-MAH	Ethylene-n butyl acrylate-carbon monoxide-maleic anhydride
EVA	Ethylene–vinyl acetate
EVA18	EVA with 18 wt.% VA
EVA40	EVA with 40 wt.% VA
FF	Flax fabric
FIGRA	Fire index growth rate
FM	Factory mutual
FR	Flame retardant
FRI	Fire retardancy index
FTIR	Fourier-transformed infrared
FTT	Fire Testing Technology
GC–MS	Gas chromatography–mass spectrometry
GF	Glass fiber
HBCD	Hexabromocyclododecane
HFFR	Halogen-free flame retardant

HNTTP	Hexakis 4-nitrophenoxy cyclotriphosphazene
HRR	Heat release rate
IFR	Intumescent flame retardant
INIS	Izod notched impact strength
IPA	Isopropyl alcohol
LBR	Linear burning rate
LDS	Laser diffraction particle size analyzer
LOI	Limiting oxygen index
MA	Methyl acrylate
MARHE	Maximum average rate of heat emission
Max tan $\delta$	Maximum of the tan $\delta$
MBS	Methacrylate–butadiene–styrene
MCC	Microscale combustion calorimeter
MFAHP	Microencapsulated aluminum hypophosphite
MH	Magnesium hydroxide
ML	Mass loss
MLR	Mass loss rate
MMT	Montmorillonite
MPP	Melamine polyphosphate
NC	Nanoclay
PA	Polyamide
PA6	Polyamide 6
PA6T	Poly(hexamethylene terephthalamide)
PAPP	Piperazine pyrophosphate
PB	Polybutadiene
PBDE	Polybromodiphenylether
PC	Polycarbonate
PCFC	Pyrolysis combustion flow calorimeter



PER	Pentaerythritol
PETA	Poly-N,N'-ethyleneterephthalamide
PFR	Phosphorus based flame retardant
pHRR	Peak heat release rate
P-LIG	Phosphorylated lignin
PP	Polypropylene
PPTA	Poly(p-propane terephthalamide)
PS	Polystyrene
RDP	Resorcinol bis (diphenyl phosphate)
RP	Red phosphorus
SAN	Styrene-acrylonitrile
SBI	Single burning item
SBS	Styrene-butadiene-styrene
SEBS-g-MA	Styrene-ethylene-butylene-styrene grafted maleic anhydride
SEM	Scanning electron microscope
Si-MAH	silicone/poly(n-butyl acrylate) with a SAN-maleic anhydride terpolymer
SPR	Smoke production rate
T <sub>5%</sub>	Temperature corresponding to 5% of mass loss
TBBPA	Tetrabromobisphenol A
TBPA	Tetrabromophthalic anhydride
TC	Technical Committees
t <sub>combustion</sub>	Time of the combustion
TD	Thermal decomposition
TEA	Trimethylamine
TEP	Triethyl phosphate
T <sub>g</sub>	Glass transition temperature
TG	Thermogravimetric
TGA	Thermogravimetric analysis

THE	Total heat emitted
THF	Tetrahydrofuran
THR	Total heat release
TLC	Thin layer chromatography
$T_{\text{peak}}$	Temperature at maximum mass loss rate
$T_{\text{pHRR}}$	Temperature of the pHRR
$t_{\text{pHRR}}$	Time to pHRR
TPP	Triaryl phosphates
TPP	Triphenyl phosphates
TSP	Total smoke production
TTI	Time to ignition
UHMW-SR	Ultrahigh molecular weight silicone rubber
UL	Underwriters Laboratories
VA	Vinyl acetate
VPA	Vinyl phosphonic acid
XPS	X-ray Photoelectron Spectroscopy
ZB	Zinc borate

## List of figures

<b>Figure II.1.</b> Fire tetrahedron. ....	16
<b>Figure II.2.</b> Schematic representation of a burning polymer. ....	17
<b>Figure II.3.</b> Potential char forming mechanism of APP/poly(1,3,5-triazin-2-aminoethanol diethylenetriamine) (CA). ....	23
<b>Figure II.4.</b> Phosphorylation of hydroxy functions with A) Esterification with $H_3PO_4$ , B) Phosphorylation with $P_4O_{10}$ and C) Reaction of Williamson reaction (R = aliphatic or aromatic groups and R' = chloro, alkyl, aryl or oxyalkyl groups). ....	27
<b>Figure II.5.</b> Pudovik reaction. ....	28
<b>Figure II.6.</b> Atherton and Todd's reaction. ....	28
<b>Figure II.7.</b> Phosphorylation of a triglyceride containing 2.4 $\alpha,\beta$ -unsaturated ketone derived from high oleic sunflower oil ....	30
<b>Figure II.8.</b> Phosphorylation of lignin by Pudovik reaction . ....	31
<b>Figure II.9.</b> Phosphorylation of sugarcane bagasse . ....	31
<b>Figure II.10.</b> Lignin phosphorylation with phosphorus pentoxide ( $P_2O_5$ ) . ....	32
<b>Figure II.11.</b> Izod notched and Charpy notched impact strength results of ABS and its composites, respectively . ....	37
<b>Figure II.12.</b> Charpy notched impact strength of flame retarded ABS composites . ....	38
<b>Figure III.1.</b> ABS chemical structure. ....	45
<b>Figure III.2.</b> EMA chemical structure . ....	46
<b>Figure III.3.</b> APP chemical structure. ....	47
<b>Figure III.4.</b> AlPi chemical structure. ....	47
<b>Figure III.5.</b> Suberin chemical structure . ....	48
<b>Figure III.6.</b> Lignin chemical structure. ....	48
<b>Figure III.7.</b> Polysaccharides chemical structure. ....	48
<b>Figure III.8.</b> Glyphosate chemical structure. ....	49
<b>Figure III.9.</b> Triethyl phosphate (TEP) chemical structure. ....	49
<b>Figure III.10.</b> Dimethyl-3-triethoxysilanepropylphosphoramidate (DTSP) chemical structure . ....	50
<b>Figure III.11.</b> Soxhlet extraction procedure of cork powder. ....	51
<b>Figure III.12.</b> Proposed reaction of cork powder and glyphosate. ....	52
<b>Figure III.13.</b> Digital photograph of reaction setup of cork/glyphosate in water at room temperature. ....	52
<b>Figure III.14.</b> Digital photograph of reaction setup of cork/glyphosate in water at 120 °C. ....	53
<b>Figure III.15.</b> Digital photograph of reaction setup of cork/glyphosate in toluene at 120 °C. ....	53
<b>Figure III.16.</b> Proposed reaction of cork powder and TEP. ....	54
<b>Figure III.17.</b> Proposed reaction of cork powder and DTSP. ....	54
<b>Figure III.18.</b> Digital photograph of Brabender mixing chamber. ....	55
<b>Figure III.19.</b> Digital photograph of the hot-plate press. ....	56
<b>Figure III.20.</b> Digital photograph of sputter coater and SEM. ....	58
<b>Figure III.21.</b> Digital photograph of LDS analyzer. ....	59
<b>Figure III.22.</b> Digital photograph of DMTA. ....	60
<b>Figure III.23.</b> Digital photograph of three-point bending testing machine. ....	61
<b>Figure III.24.</b> Digital photograph of Charpy impact strength testing machine. ....	62
<b>Figure III.26.</b> Digital photograph of ATR-FTIR and FTIR spectrometers. ....	63
<b>Figure III.25.</b> Digital photograph of TGA coupled FTIR analyzer. ....	63
<b>Figure III.27.</b> Scheme of TLC technique. ....	64
<b>Figure III.28.</b> Gas chromatography-mass spectrometry system. ....	65

<b>Figure III.29.</b> Scheme of LOI measurement setup. ....	66
<b>Figure III.30.</b> Scheme of horizontal UL-94 setup. ....	67
<b>Figure III.31.</b> Scheme of vertical UL-94 setup. ....	67
<b>Figure III.32.</b> Digital photograph of MCC. ....	68
<b>Figure III.33.</b> Digital photograph of cone calorimeter while burning a sample. ....	69
<b>Figure V.1.</b> Schematic of cork cells wall presenting the position of each main component. ....	102
<b>Figure V.2.</b> SEM micrographs of cork powder at 250×, 500× and 5000× with a scale bar of 100, 50 and 5 μm, respectively. ....	104
<b>Figure V.3.</b> ATR-FTIR spectra of cork powder, extractive-free cork, desuberized cork, suberin and lignin. ....	105
<b>Figure V.4.</b> ATR-FTIR spectra of DCM, ethanol and water extractives. ....	107
<b>Figure V.5.</b> TG and dTG curves of cork and extractive-free cork obtained at 10 °C/min under N <sub>2</sub> atmosphere. ....	109
<b>Figure V.6.</b> TG curves of cork extractives obtained at 10 °C/min under N <sub>2</sub> atmosphere. ....	110
<b>Figure V.7.</b> Experimental and calculated TG and dTG of curves of cork at 10 °C/min under N <sub>2</sub> atmosphere. ....	111
<b>Figure V.8. (a)</b> TG and <b>(b)</b> dTG curves of cork and extractive-free cork obtained at 10 °C/min under N <sub>2</sub> atmosphere. ....	112
<b>Figure V.9.</b> Heat release rate vs. temperature of cork and extractive-free cork. ....	115
<b>Figure V.10.</b> Heat release rate vs. temperature of cork extractives. ....	116
<b>Figure V.11.</b> Experimental and calculated heat release rate curves of cork. ....	117
<b>Figure V.12.</b> Heat release rate vs. temperature of cork powder and its components. ....	118
<b>Figure VI.1.</b> SEM micrographs of ABS, ABS/30APP and ABS/30C, at 250 × and 1500 ×, with a scale bar of 100 and 10 μm, respectively. ....	127
<b>Figure VI.2.</b> SEM micrographs of ABS/3C/27APP and ABS/20C/10APP, at 250 × and 1500 ×, with a scale bar of 100 and 10 μm, respectively. ....	128
<b>Figure VI.3.</b> Storage modulus (E') and tan δ of ABS and ABS formulations. ....	129
<b>Figure VI.4.</b> Storage modulus (E') of ABS / Storage modulus (E') of ABS formulations. ....	131
<b>Figure VI.5. (a)</b> Mass and <b>(b)</b> dTG curves of ABS, APP and cork powder obtained at 10 °C/min under N <sub>2</sub> atmosphere. ....	132
<b>Figure VI.6. (a)</b> Mass and <b>(b)</b> dTG of curves of ABS, ABS/30APP and ABS/30C obtained at 10 °C/min under N <sub>2</sub> atmosphere. ....	134
<b>Figure VI.7.</b> dTG curves of ABS formulations with <b>(a)</b> C/APP weight ratio <1 and <b>(b)</b> C/APP ≥ 1 cork obtained at 10 °C/min under N <sub>2</sub> atmosphere. ....	135
<b>Figure VI.8.</b> Experimental and calculated mass and dTG curves of <b>(a)</b> and <b>(b)</b> composite with individual components (APP and C) in ABS, and representative examples of thermal decomposition behavior of ABS composites with C/APP weight ratio <b>(c)</b> lower than 1 and <b>(d)</b> equal or higher than 1. ....	138
<b>Figure VI.9.</b> Experimental and calculated residue value at 800 °C of flame retarded ABS formulations. ....	139
<b>Figure VI.10.</b> FT-IR spectra of <b>(a)</b> ABS, <b>(b)</b> cork and <b>(c)</b> APP pyrolysis products between the beginning of decomposition (T <sub>5%</sub> ) and the maximum mass loss rate (T <sub>peak</sub> ). ....	140
<b>Figure VI.11.</b> FT-IR spectra of <b>(a)</b> ABS/30C, <b>(b)</b> ABS/30APP, <b>(c)</b> ABS/3C/27APP and <b>(d)</b> ABS/20C/10APP pyrolysis products between the beginning of decomposition (T <sub>5%</sub> ) and the maximum mass loss rate (T <sub>peak</sub> ). ....	142
<b>Figure VI.12.</b> Heat release rate of ABS and ABS formulations obtained by MCC. ....	144
<b>Figure VI.13.</b> FTIR spectra of the ABS/30APP, ABS/3C/27APP, ABS/20C/10APP and ABS/30C residue after MCC test. ....	147

<b>Figure VI.14.</b> Heat release rate vs. time curves of ABS, ABS/30APP and ABS/30C.....	148
<b>Figure VI.15.</b> Heat release rate vs. time curves of ABS formulations with (a) C/APP < 1 and ABS/30APP (b) C/APP ≥1 and ABS/30C.....	151
<b>Figure VI.16.</b> Total heat release rate of ABS and ABS formulations.....	152
<b>Figure VI.17.</b> Digital photographs of (a) ABS/30APP, (b) ABS/1C/29APP, (c) ABS/3C/27APP, (d) ABS/5C/25APP, (e) ABS/10C/20APP, (f) ABS/15C/15APP, (g) ABS/20C/10APP, and (h) ABS/25C/5APP residue after cone calorimetry. The approximate residue thickness is indicated on the scale (in centimeters). .....	154
<b>Figure VI.18.</b> SEM micrographs of the upper (left) and down surface (right) of the ABS formulations after the cone calorimeter tests (at 250 × with a scale bar of 100 μm). .....	155
<b>Figure VI.19.</b> FTIR spectra of the ABS/30APP, ABS/3C/27APP and ABS/20C/10APP residue after cone calorimeter test.....	156
<b>Figure VII.1.</b> ATR-FTIR spectra of cork powder, glyphosate and phosphorylated cork with glyphosate under condition 1. ....	166
<b>Figure VII.2.</b> ATR-FTIR spectra of phosphorylated cork with glyphosate under condition 2 and 3.....	166
<b>Figure VII.3.</b> ATR-FTIR spectra of TEP and phosphorylated cork with TEP under condition 1 and 2. ....	168
<b>Figure VII.4.</b> ATR-FTIR spectra of DTSP and phosphorylated cork with DTSP before and after washing. ....	169
<b>Figure VII.5.</b> Digital photographs of TLC plates for glyphosate and phosphorylated cork with glyphosate. ....	170
<b>Figure VII.6.</b> Digital photograph of TLC plates for TEP and phosphorylated cork with TEP.....	170
<b>Figure VII.7.</b> Digital photograph of TLC plates for DTSP and phosphorylated cork with DTSP, test was done with the ratio of 2:1 DCM: methanol as the solvent system. ....	171
<b>Figure VII.8.</b> GC-MS chromatogram of phosphorylated cork with (a) glyphosate, (b) TEP and (c) DTSP. ....	172
<b>Figure VII.9.</b> SEM micrographs of ABS with 30 wt.% of cork and phosphorylated cork, at 250 × and 1500 ×, with a scale bar of 100 and 10 μm, respectively.....	174
<b>Figure VII.10.</b> SEM micrographs of ABS with 20 wt.% of cork and phosphorylated cork, at 250 × and 1500 ×, with a scale bar of 100 and 10 μm, respectively.....	175
<b>Figure VII.11.</b> SEM micrographs of ABS with 3 wt.% of cork and phosphorylated cork, at 250 × and 1500 ×, with a scale bar of 100 and 10 μm, respectively.....	176
<b>Figure VII.12.</b> Storage modulus (E') and tan δ of ABS formulations, effect of phosphorylation.....	177
<b>Figure VII.13.</b> TG curves of cork and phosphorylated cork samples obtained at 10 °C/min under N <sub>2</sub> atmosphere. ....	179
<b>Figure VII.14.</b> TG curves of ABS composites containing 30 wt.% of cork or phosphorylated cork, obtained at 10 °C/min under N <sub>2</sub> atmosphere.....	180
<b>Figure VII.15.</b> TG curves of ABS composites containing 20 wt.% of cork or phosphorylated cork with 10 wt.% APP, obtained at 10 °C/min under N <sub>2</sub> atmosphere. ....	181
<b>Figure VII.16.</b> TG curves of ABS composites containing 3 wt.% of cork or phosphorylated cork with 27 wt.% APP, obtained at 10 °C/min under N <sub>2</sub> atmosphere. ....	181
<b>Figure VII.17.</b> Heat release rate vs. time curves of ABS formulations with 30 wt.% cork, the effect of phosphorylation.....	183
<b>Figure VII.18.</b> Heat release rate vs. time curves of ABS formulations with 20 wt.% cork and 10 wt.% APP, the effect of phosphorylation. ....	184
<b>Figure VII.19.</b> Heat release rate vs. time curves of ABS formulations with 3 wt.% cork and 27 wt.% APP, the effect of phosphorylation. ....	184

**Figure VII.20.** SEM micrographs of the upper (left) and down surface (right) of the ABS formulations with 30 wt.% of unmodified cork or phosphorylated cork after the cone calorimeter tests (at 250 × with a scale bar of 100 mm)..... 189

**Figure VII.21.** SEM micrographs of the upper (left) and down surface (right) of the ABS formulations with 20 wt.% of unmodified cork or phosphorylated cork after the cone calorimeter tests (at 250 × with a scale bar of 100 mm)..... 190

**Figure VII.22.** SEM micrographs of the upper (left) and down surface (right) of the ABS formulations with 3 wt.% of unmodified cork or phosphorylated cork after the cone calorimeter tests (at 250 × with a scale bar of 100 mm)..... 191

**Figure VII.23.** FTIR spectra of the ABS formulations with 30, 20 and 3 wt.% different phosphorylated cork residue after cone calorimeter test. .... 192

## List of tables

<b>Table II.1.</b> Different types of phosphorus flame retardants used for ABS in the literature. ....	35
<b>Table II.2.</b> Charpy notched impact strength of flame retarded ABS composites. ....	39
<b>Table III.1.</b> Samples identification and composition in weight %.....	57
<b>Table III.2.</b> Vertical UL-94 materials classifications. ....	67
<b>Table V.1.</b> Chemical composition of cork powder.....	104
<b>Table V.2.</b> TG and dTG data of thermal degradation and residue of cork and its main components. ....	108
<b>Table V.3.</b> Main results obtained from micro-scale combustion calorimetry. ....	114
<b>Table VI.1.</b> Materials identification and weight percentage (wt.%) of the components. ....	126
<b>Table VI.2.</b> Storage modulus ( $E'$ ), intensity of $\tan \delta$ and glass transition temperature ( $T_g$ ) of ABS and ABS formulations. ....	130
<b>Table VI.3.</b> Thermal decomposition data obtained from TGA (mass and dTG curves) of ABS, APP and cork (C). ....	133
<b>Table VI.4.</b> Mass and dTG data of ABS and ABS formulations. ....	136
<b>Table VI.5.</b> Summary of data obtained by MCC for ABS and ABS composites. ....	145
<b>Table VI.6.</b> Main results obtained from cone calorimeter tests. ....	149
<b>Table VI.7.</b> UL-94 horizontal results of ABS and ABS composites.....	153
<b>Table VII.1.</b> Materials identification and weight percentage (wt.%) of the components. ....	165
<b>Table VII.2.</b> Cork powder, and phosphorylated cork samples XPS component ratios of $C_{1s}$ , $O_{1s}$ , $N_{1s}$ , $Si_{2p}$ and $P_{2p}$ elements.....	173
<b>Table VII.3.</b> Storage modulus ( $E'$ ) and glass transition temperature ( $T_g$ ) of ABS formulations, effect of phosphorylation.....	178
<b>Table VII.4.</b> Mass and dTG data of cork and phosphorylated cork samples. ....	179
<b>Table VII.5.</b> Mass and dTG data of ABS formulations with cork and phosphorylated cork.....	182
<b>Table VII.6.</b> Main results obtained from cone calorimeter tests, the effect of cork phosphorylation. ....	185
<b>Table VII.7.</b> UL-94 horizontal results of ABS and ABS composites, the effect of cork phosphorylation. ....	186
<b>Table VII.8.</b> Digital photographs of ABS formulations residue after cone calorimetry, the effect of phosphorylation.....	187







Introduction

Chapter

I





## Chapter I: Introduction

The use of polymeric materials in our everyday life is increasing rapidly due to their remarkable combination of properties such as, high strength or modulus to weight ratios, toughness, resilience, resistance to corrosion, heat and electrical insulation, low cost, low weight and ease of processing [1]. In the early 1950s, a thermoplastic polymer referred as acrylonitrile-butadiene-styrene (ABS), consists of three monomers, acrylonitrile, butadiene and styrene, was commercialized and quickly gained popularity due to its excellent mechanical properties like high impact resistance, toughness, as well as chemical, heat resistance and processability. It has been used in a wide range of applications, including automotive parts, electronic housings, household appliances and toys [2]. However, ABS is inherently highly flammable and releases toxic gasses during the combustion that significantly limits its industrial applications; therefore, it has always been a challenge to tailor a suitable flame retardant (FR) system for ABS to control its fire hazard [3, 4].

By introducing brominated FRs to the market in the 1960s, most of the concerns regarding the flame retardancy of ABS were considered accomplished [5]. However, in the 1990s the use of these halogenated flame retardants was reported to endanger the environment and human health. In the past decades, the use of these additives, such as tetrabromobisphenol A (TBBPA) and brominated diphenyl ethers (BDEs), has been strictly limited [6-8]. Consequently, the halogen-free flame retardants (HFFRs) were developed and introduced to the industry as environmental friendly alternatives. The HFFRs, mainly based on phosphorus, are reported to be the most effective flame retardant systems to improve the fire behavior of polymeric matrices. The most widely used phosphorus based flame retardants (PFRs) in ABS or in its polymer blends are based on organic and inorganic phosphorus compounds such as: triphenyl phosphates (TPP) [9], bisphenol A bis (diphenyl phosphate) (BDP) [10], aluminum hypophosphite (AHP) [4], red phosphorus (RP) [11], piperazine pyrophosphate (PAPP) [12] and ammonium polyphosphate (APP) [13]. These phosphorus-based flame retardants have a prominent action in the condensed phase or gas phase, depending on their chemical composition [14]. Some of them, such as APP, PAPP and BDP during the thermal decomposition are converted to phosphoric acid leading to the formation of pyrophosphate and polyphosphate structures acting mainly in the condensed phase.

They catalyze the dehydration reaction of polymer end chains and induce char formation. On the other hand, TPP, AHP and RP have a major action in the gas phase during decomposition. They mainly volatilize to produce free radicals ( $\text{PO}_2\bullet$ ,  $\text{PO}\bullet$  and  $\text{HPO}\bullet$ ), which scavenge  $\text{H}\bullet$  and  $\text{OH}\bullet$  radicals, forming less reactive or even inert molecules in the flame, and suppressing the radical reactions of combustion in the gas phase [15-17].

APP, composed of inorganic salt of poly phosphoric acid and ammonia, has attracted the industry attention due to its low loadings, lower cost, processability and its function in intumescent flame retardant systems [18]. APP has been used to enhance the fire behavior of different polymers in intumescent flame retardant (IFR) systems, where it was used with other substances that act as charring agents such as pentaerythritol (PER) [19], dipentaerythritol (DPER) [20], poly-(4-nitrophenoxy)-phosphazene (DPP) [21] and poly-N,N'-ethyleneterephthalamide (PETA) [22]. These charring agents act by catalyzing the esterification reaction of APP, promoting the release of non-flammable gasses such as  $\text{H}_2\text{O}$ ,  $\text{CO}$ ,  $\text{CO}_2$  and  $\text{NH}_3$  in the gas phase and the formation of a cohesive and cross-linked char in the condensed phase. For example, the occurrence of synergistic interactions between APP and aluminium diethyl phosphinate (ALPi) revealed to enable the liberation of phosphorus radicals at a temperature range which acted like scavengers of those radicals yielded during ABS decomposition, as well as, to promote the formation of a more effective protective layer in the condensed phase [13].

On the other hand, in the present days, there is a remarkable surge of interest towards novel flame retardants derived from renewable sources. This attention is driven by the accessibility of these sustainable alternatives and growing awareness of environmental issues associated with the increased use of fossil resources. Moreover, the advancement of flame retardant systems sourced from renewable materials is well-suited to be a solution for the increasing use of polymers in many technical fields, by reducing their environmental footprint [23]. It has been reported that in some cases, bio-based materials act more efficiently in the condensed phase by producing a thermally stable char residue [24, 25]. For instance, the incorporation of a system consists of low-cost starch, flax fabric (FF) and APP was reported to exhibit an improvement in the flame retardancy of a biodegradable polymer by the formation of a compact cross-linked 3D network (P-O-P and P-O-C) as a protective char layer due to the presence of both APP and starch as a charring agent [26]. In another study the influence of lignin on the thermal and fire properties of ABS blends was

investigated and it was concluded that the presence of lignin could have a positive impact on the fire behavior by increasing the char formation [27].

Recently, the interest in valorization of industrial and forestry by-products and wastes is increasing rapidly in order to promote the circular economy. Portugal and Spain are considered the main manufacturers of cork products with the production rate of 46% and 33% of the world total production (200 thousand tons per year), respectively [28, 29]. However, an important waste of approximately 30% (of the total production), with no economic value, called cork powder, a term used to cover all cork wastes, is produced during this industrial cork processing [30, 31]. In order to valorize this forest waste, some studies have been carried out by employing cork powder in polyolefinic matrices, mainly focusing on the effect of cork powder composition in water absorbance, mechanical and insulation properties of cork polymer composites (CPCs) [32-34]. In addition, there are different strategies reported to be applied in order to improve the desired properties of CPCs such as, chemical modification of cork [35], the use of coupling agents [35, 36] to promote cork matrix bonding and the use of different natural or synthetic fibers to reinforce CPCs [37, 38]. Moreover, the charring ability of cork attributed to the presence of lignocellulosic components can help to slow down the combustion process by forming a protective barrier when exposed to heat.

Moreover, to enhance the flame retardant properties of cork through chemical modifications, some treatments such as phosphorylation can be proposed. By introducing phosphorus groups into the surface of cork particles, the material's flame retardancy can be significantly improved by not only enhancing the charring ability of cork but also provides probable additional fire protection benefits such as releasing phosphorus radicals. Overall, the combination of cork's inner flame retardant properties and its charring ability, along with advancements in chemical modification techniques, positions cork as a versatile and eco-friendly material for enhancing fire safety in diverse industries. Further research and development in this area hold great potential for unlocking new opportunities for using cork powder, a bio-waste, in flame retardant applications while promoting environmental sustainability.

Although there is no study regarding cork phosphorylation, there are some related to the phosphorylation of lignocellulosic materials. For instance, bisphosphonic acid and vinyl phosphonic acid (VPA) have been used to introduce phosphorus moieties into the lignin-rich miscanthus fibers and lignin-poor flax fibers [39]. By using hexane-1,6-diylbisphosphonic acid,

phosphorus content in miscanthus fibers reached 1.4 wt.% while a lower content of 0.3 wt.% for flax fibers was registered. Bisphosphonic acid was more efficiently grafted onto miscanthus fibers than flax fibers due to the presence of a higher lignin content. VPA grafting was less effective than bisphosphonic acids and phosphorus levels were lower than 0.3 wt.% for both flax and miscanthus fibers. However, microscale combustion calorimetry (MCC) and thermogravimetric analysis (TGA) results showed that VPA modified miscanthus fibers released less heat and promoted more char than those modified by bisphosphonic acids. It was observed that the higher thermal stability of bisphosphonic acid did not allow it to act as effectively as VPA at microscale. On the contrary, VPA decomposed simultaneously with miscanthus or flax fibers and promoted the charring of the fibers. Therefore, it was reported that the final thermal stability and fire performance not only depended on the phosphorus content but also on the thermal stability of the used phosphorus component. Furthermore, adding phosphorylated lignin (P-LIG) to ABS has also presented promising results by improving the thermal stability of the ABS composites and promoting a higher formation of the protective char [40]. It was observed when P-LIG with 4.1% of phosphorus content was synthesized and 30 wt.% of P-LIG was added to ABS composites, it promoted char formation by reacting with ABS during thermal decomposition leading to a significant reduction of the peak of heat release rate pHRR and THR of 58% and 20%, respectively. It was shown that P-LIG was acting mainly in the condensed phase by interacting with ABS during the decomposition of the composite. These interactions induced less release of combustibles to the flame while a charring protective barrier was formed on the composite surface. A slight inhibition effect in the flame was observed as well, probably caused by release of phosphorus species into the gas phase.

On the other hand, while flame retardants play an important role in improving the fire resistance of ABS, they can also adversely affect its mechanical properties. In general, addition of large amounts of flame retardants to polymers decreases their mechanical properties particularly, their toughness and flexibility. Therefore, some treatments, such as incorporation of compatibilizers and/or impact modifiers, have been suggested. For instance, the impact strength enhancement of an ABS with an IFR composed of APP, melamine and calcium 3-hydroxy-2,2-bis(hydroxymethyl) propyl phosphate at the ratio of 3:1:1 was reported [41]. A polybutadiene grafted SAN rubber, containing a 70 wt.% of polybutadiene (ABS-R) at different loadings of 4-26 wt% was incorporated into the mentioned IFR-ABS. The highest increase of impact strength



(115%) was achieved for the composite containing 15 wt.% of ABS-R and related to an improvement in the boundary adhesion between the IFR and ABS matrix. The effect of styrene-ethylene/butylene-styrene-maleic anhydride-graft (SEBS-g-MA) on a recycled polymeric blend of ABS/high impact polystyrene/polystyrene (9:21:70), containing 2-10 wt.% of TPP and sepiolite with a ratio of 1:1 was also reported [42]. The blends with 8 wt.% of FR exhibited a V-1 classification in UL-94 and a 29% limiting oxygen index (LOI) value. nevertheless, the incorporation of flame retardants led to a drastic reduction of impact strength from 66.12 J/M to 23.5 J/m, while adding 2, 5 and 10 wt.% SEBS-g-MA increased it up to 69.4 J/m, 74.5 J/m and 80.4 J/m, respectively, by increasing the elastomeric phase and subsequently resilience property of the blend. Although, 2 and 5 wt.% SEBS-g-MA addition increased the tensile strength from 21.6 MPa to 28.6 MPa and 27.4 MPa, respectively, when 10 wt.% of SEBS-g-MA was added, a lower tensile strength of 25.5 MPa was registered due to the presence of a higher rubbery content where the elastomeric phase started dominating the blend. Therefore, the blend with 5 wt.% of SEBS-g-MA was chosen as the optimized one. In general, compatibilizers and impact modifiers act by reducing the crack growth rate and increasing the energy absorbed in the plastic region, which is also called stress whitened zone [43].

The present work proposes different approaches to develop flame retarded ABS composites: (i) improving the mechanical properties of a self-extinguished phosphorus flame retardant system composed of APP and AlPi, (ii) developing novel FR-ABS formulations with enhanced environmental sustainability by combining APP with cork powder, a bio-waste of the cork industry and (iii) modification and phosphorylation of cork powder to improve its flame retardancy behavior as a promising adjuvant bio-flame retardant.

## *I.1 Objectives*

Two general objectives were defined in the present thesis. The first one was focused on the development of new strategies to reduce the adverse impact of a highly efficient phosphorus-based flame retardant system on ABS, previously developed in the Poly2 group. The main requirements of this objective were to accomplish a minimum notched Charpy impact strength of 6 kJ/m<sup>2</sup> and a V-0 classification in UL-94 burning test, that was needed for extending the application window of ABS. The second goal was aimed to develop ABS formulations with even lower environmental impact by combining APP with cork powder, a renewable material from natural resources and a bio-waste of the cork industry, elucidating the effect of this novel system on the thermal stability and flame retardancy of ABS.

According to the general objectives, the particular ones were established as followed:

- **Developing a fireproof ABS composite with enhanced mechanical properties:**
  - Preparing of ABS composites containing a global 20 wt.% of APP/AlPi with 2-5 wt%. of the selected compatibilizers/impact modifiers.
  - Characterizing the Charpy impact strength and vertical burning UL 94 ranking of flame retarded ABS composites.
  - Discussing the effect of compatibilizers/impact modifiers on the microstructure, viscoelastic and mechanical behavior, thermal stability and fire performance of phosphorus flame retardant ABS composite with the optimal balance of impact strength and flammability.
  
- **Investigating the effect of combining APP with cork powder on thermal stability and fire behavior of ABS:**
  - Ascertaining the chemical composition of natural cork powder and analyzing its effect on the cork powder's thermal stability and flammability.
  - Preparing ABS composites containing APP and cork powder with a global filler weight content of 30 wt.%

- Characterizing ABS/cork/APP composites' microstructural morphology, thermal stability, thermo-mechanical and fire properties.
- Studying the possible synergistic or antagonistic effect of combining a phosphorus-based flame retardant and cork powder at different ratios on the thermal stability and fire behavior of the ABS matrix
- Discussing the possible mechanisms and modes of action of APP and cork flame retardant system.
  
- **Investigating the effect of cork powder phosphorylation on thermal stability and fire behavior of ABS:**
  - Modifying of cork powder surface by using different phosphorus components under different reaction conditions.
  - Analyzing the effect of different phosphorylation agents and conditions on the phosphorus bands' presence, phosphorus content and final product successful phosphorylation.
  - Preparing ABS composites containing a phosphorus-based flame retardant and phosphorylated cork powder at a global loading of 30 wt.%
  - Characterizing the microstructural morphology, thermal stability, thermo-mechanical and fire properties of ABS composites containing phosphorylated cork with and without APP.
  - Investigating the effect of phosphorylation on the fire performance of flame retarded ABS composites containing cork and/or APP and discussing their mechanisms of action.

## *1.2 Outline of thesis*

The content of this thesis has been divided into six chapters as below:

Chapter I contains the introduction, the motivation and objective of this work, as well as its structure.

In Chapter II, a bibliographic review is carried out on the state of the art of flame retardancy and mechanical properties of ABS.

Chapter III describes the raw materials, the compounding, specimens' preparation, the general characterization techniques, and experimental methods used along the whole thesis to determine the properties of the composites.

Chapter IV shows the materials, the discussion of the results regarding the properties of a flame retarded ABS and the conclusions with the purpose of improving its mechanical properties. The results of this preliminary work have been published: Farnaz Ghonjizade-Samani, Laia Haurie, Ramón Malet, Mark Pérez and Vera Realinho, "Phosphorus based flame retardant ABS with enhanced mechanical properties by combining ultrahigh molecular weight silicone rubber and ethylene methyl acrylate copolymer", *Polymers*, Vol. 16, NO. 7, PP. 923 (1-21), IF: 5.0, 27 March 2024, DOI: 10.3390/polym16070923. And regarding this chapter, a European patent application with the number EP23383250 was filed on December 4th, 2023.

Chapter V exhibits the discussion of the results and the conclusions related to the thermal and flammability of cork, as a bio-waste source, and its components. The results of this preliminary work have been published: Farnaz Ghonjizade-Samani, Laia Haurie, Ramón Malet and Vera Realinho, "The Components' Roles in Thermal Stability and Flammability of Cork Powder", *Materials*, Vol. 16, NO. 10, PP. 3829 (1-17), IF: 3.4, 18 May 2023, DOI: 10.3390/ma16103829.

Chapter VI displays the materials and the obtained results of bio-FR ABS composites containing cork and APP, as well as, the conclusions. The results of this preliminary work have been submitted: Farnaz Ghonjizade-Samani, Laia Haurie, Ramón Malet and Vera Realinho, "Study of using cork powder as an adjuvant bio-flame retardant in acrylonitrile-butadiene-styrene flame retardant formulations", *Polymer degradation and stability*.

Chapter VII presents the study of surface modification and phosphorylation of cork bio-waste and investigates the effect of its phosphorylation on the mechanical properties, thermal

stability and fire behavior of FR-ABS composites. It also exhibits the discussion of the results and the conclusions.

Chapter VIII illustrates the general conclusions and the proposed future studies.

In Chapter IX, the publications and conferences participations, regarding this thesis, are listed.



State of the art

Chapter

II

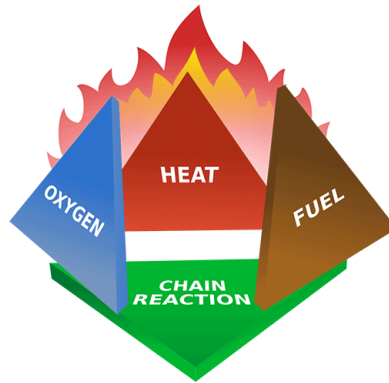




## Chapter II: State of the art

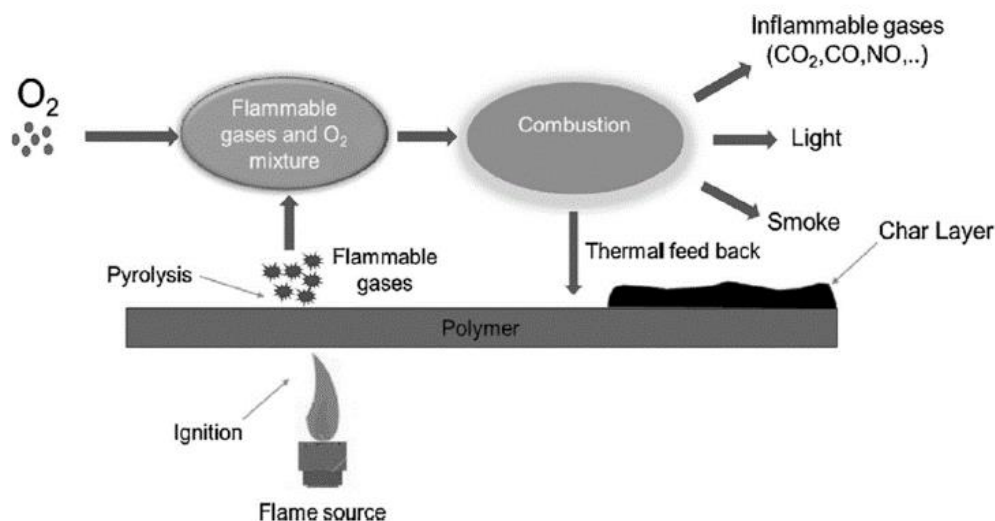
Polymers are considered a large and growing part of the fire load in homes, commercial environments, and transportation [44, 45]. Among them, the most widely used are the least expensive ones that tend to have the highest flammability. Flammability generally refers to the propensity of a substance to ignite easily and burn rapidly with a flame and is one of the most important indicators of fire hazard. Polymers due to their chemical structure, made up mainly of carbon and hydrogen, are highly combustible [46]. The combustion reaction involves two factors: one or more combustibles (reducing agents) and a combustive (oxidizing agent). In general, the combustive is the oxygen in the air. Polymer combustion can be simply summarized in four steps: (i) heating of the polymer; (ii) decomposition; (iii) ignition and (iv) combustion.

The whole process usually starts with an increase in the temperature of a polymeric material at the presence of a heat source, to such an extent that it induces the polymer bond scissions. Thermal decomposition of the solid material results in the formation of flammable volatiles mainly in the form of gaseous fuel further reacting with the oxidant in the air above the condensed phase, slowly at first, and when a critical concentration of free radicals is reached, ignition occurs leading to the flaming combustion above the solid material. The life span of the combustion cycle depends on the amount of heat released during the combustion of the fuel. When this amount reaches a certain level, new decomposition reactions are induced in the solid phase, and therefore more combustibles are produced [47, 48]. The combustion cycle is thus maintained and called a fire tetrahedron (Figure II.1).



**Figure II.1.** Fire tetrahedron [49].

On the other hand, flaming combustion also can be divided into physical and chemical processes which occur in three phases: gas, mesophase, and condensed (liquid/solid) phase [50, 51]. The mesophase is the interface between the gas and condensed phase during combustion. The physical processes include energy transport by radiation and convection between the gas phase and the mesophase and the energy loss from the mesophase by mass transfer, vaporization of the pyrolysis gasses and conduction into the solid. Fuel production is the rate-limiting step in polymer flaming combustion, and is controlled primarily by the rate at which heat and mass are transported to and from the polymer, respectively (Figure II.2) [52]. The important chemical processes are divided to the thermal degradation of the polymer in a thin surface layer (the mesophase) as a consequence of the physical processes (energy transport), mixing of the volatile pyrolysis products with air by diffusion, and combustion of the fuel-air mixture in a combustion zone. The combustion zone is bounded by a fuel-rich region on the inside and a fuel-lean region on the outside. Increasing the oxygen concentration in the environment increases the flame heat flux, either due to a higher flame temperature, resulting in an increase of the combustion zone volume or the luminosity of the flame [46].



**Figure II.2.** Schematic representation of a burning polymer [53].

### *II.1 Strategies to improve polymers' flame retardancy*

The need to protect materials against fire has been a scientific undertaking for centuries. The use of flame-retardant additives for polymeric materials was introduced as a solution in the early twentieth century. The first fire retardants for polymers were halogen-based such as halogenated hydrocarbons and waxes used in Army tents. New chemistries followed after that, in order to get a response to the need to improve fire resistance of materials. With the growing demand of synthetic polymers in daily use applications, fire safety engineers and insurance companies need to cover additional fire safety established by governmental regulations.

These fire safety regulations in force today began in the early twentieth century when insurance companies requested a greater employed fire safety for reducing the paying amount on losses due to the fire. Different fire safety standards in the United States were created by organizations like Underwriters Laboratories (UL) and Factory Mutual (FM) [50]. In Europe, European standards (EN) for reaction-to-fire are specified by the European Commission and Technical Committees (TC) (ISO/TC92 Fire Safety, TC 89 Fire Hazard Testing). The European reaction-to-fire classification system was introduced in support of the Construction Products Directive (CPD) with the aim of achieving harmonization and replacing the different national standards and tests [54]. Under the European classification system for reaction to fire as defined

in the standard EN13501 part 1, building products are tested for reaction to fire and divided into seven Euro-classes as A1, A2, B, C, D, E and F for materials for which performance has not yet been determined or failing Euro-class E criteria. Tests used to determine the Euro-class for all construction products except floor coverings and cables are: EN ISO 1182 (non-combustibility test), EN ISO 1716 (determination of the heat of combustion), EN ISO 13823 (single burning item (SBI)) and EN ISO 11925-2 (small flame ignitability test). For example, the first stage of testing is EN ISO 11925-2, that simulates a small flame ignition such as a cigarette lighter being applied for a short time (15 seconds) to the edge or surface of a product. This can result in an E or F classification, or it is a prerequisite for the SBI test (30 instead of 15 seconds exposure), when the aim is to achieve classes B, C or D. In the SBI test method according to EN ISO 13823, a specimen is exposed to a gas flame of 30 kW, simulating a single burning item in corner [54, 55].

There is no one universal fire standard worldwide, which is why fire risk scenarios set the fire test that a material must pass, and, why a particular flame-retardant system is designed to pass that test. It should be noted that no one system will pass all fire tests, and, in general, today a system is designed to meet a particular test, not to be flame retarded against all fire situations. Since the intensity of a flame will vary from a situation to another one, it is impossible to create a universal flame-retardant system. So, in industry, flame-retardant polymeric materials are designed to pass the test related to a specific fire risk scenario for example, fire in plastics used in cars (FMVSS 302 test) [56], polyurethane foam (Crib V test) [57], and polymers for electronics (UL-94 test) [58]. For instance, in the electronic fields if the plastic is UL-94 rated V-1 or better, nothing will happen, as the flame will go out; but if the plastic has a lower flame-retardant rating, the flame can spread rapidly, and in some cases can lead to a large fire.

To improve the reaction to fire different flame retardants have been used. They can be categorized in two groups, normal additives and reactive additives. The additives that do not chemically bond to the polymer and are mixed into the polymer during polymerization or melt compounding are called normal additives. Normal additives are part of polymer formulations and the most common type of FR. They are usually mineral fillers, hybrids or organic compounds, which can include macromolecules. Reactive additives are those which are added to the polymer during polymerization or a post processing. The modes of action of FRs can be classified in two different ways. One related to the mode of action by itself, which can be physical or chemical and

secondly regarding the location of the action, which can be in the condensed phase or the gas phase. The different modes of action of FRs are described in detail as below:

- **Physical modes of action:** The main physical mechanisms of a FR are via cooling and acting as a heat sink, dilution of the fuel and/or oxygen content, and protective layer formation. Some FRs like alumina trihydrate and magnesium hydroxide endothermically decompose resulting in decreasing the temperature of the reaction to a lower temperature than the combustion temperature and act through cooling or heat sink mechanisms. Other FRs like phosphorus based ones liberate nonflammable gasses during thermal decomposition, such as H<sub>2</sub>O, CO<sub>2</sub> or NH<sub>3</sub>. These gasses dilute the fuel and/or the oxygen supply, decreasing its concentration sufficiently to prevent ignition or sustained combustion. Some FRs, such as intumescent and nanocomposites, act by stopping fuel release through binding up fuel as carbon char and providing thermal insulation for polymeric matrix by the formation of protective char layers with acts as a thermal barrier that prevents or slows down the volatile fragments from escaping the material and the oxygen atoms from diffusing into it, thus inhibiting the exothermic reactions, and reduces the rate of heat transfer into the material, slowing down the pyrolysis of the polymer [47, 59].
- **Chemical modes of action:** FRs can also act via chemical mechanisms, such as radical scavenging led to flame inhibition, promotion of accelerated crosslinking and charring, and promotion of accelerated decomposition Radical scavenging or flame inhibition mechanism is initiated by the release of specific radicals, such as Br•, Cl• or PO• that are formed through decomposition of the halogen or phosphorus based FRs containing these elements. When the polymer decomposes into volatile radical fragments, the mentioned radicals capture these fuel fragments before they react with the oxygen atoms. Therefore, the exothermic processes are stopped or slowed down, and reduce the heat released by the combustion and interrupts the cycle. It is important to note that for an FR compound to be effective, its decomposition must occur before that of the polymeric matrix, so that the scavenger radicals are already present to capture the fuel fragments once these are released. The most favorable temperature is when the FR compound decomposes at

around 50 °C below the polymer. Furthermore, some FRs, such as phosphorus ones, can enhance the charring reaction, leading to a more intense formation of the protective layer. The accelerated crosslinking reaction also leads to reducing the release of volatile fragments, since the atoms are bound to the matrix by a larger number of bonds, therefore more energy is required in order to be released. Moreover, some FRs can catalyze the decomposition of the polymer and accelerate the thermal decomposition. This leads to a sudden reduction in the polymer melt viscosity, making it drip away from the location of the flame. As a result, the fuel is removed from the source of heat, leading to flame extinguishment due to the lack of fuel [59, 60].

- **Condensed phase and gas phase modes of action:** The mentioned physical or chemical mechanisms can also be categorized regarding the location where they act. Cooling through endothermic reactions, formation of a solid protective layer, accelerated crosslinking or charring, and accelerated polymer decomposition are the ones occurring in the condensed phase. Mechanisms that take place in the gas phase are dilution of the fuel or oxygen content, formation of a gaseous protective layer, and radical scavenging. Flame-retardant compounds can work in either or both of gas or condensed phase, and in one or a combination of the physical and chemical mechanisms.

Flame retardants can also be classified based on their chemical composition such as halogenated, mineral and phosphorus-based flame retardants. Halogenated flame retardants have been in use since the 1930s, and were considered a cost effective solution for flame retarding of polymeric materials. The most commonly used ones in polymers are TBBPA, Polybromodiphenylether (PBDE), Hexabromocyclododecane (HBCD) and Tetrabromophthalic anhydride (TBPA). However, there are some significant drawbacks which limit their use, such as an increase in smoke release during combustion and the release of corrosive gasses during burning. Therefore, in the 1990s, the use of these halogenated flame retardants was reported to endanger the environment and human health due to their high toxicity. As a result, the use of these additives, such as TBBPA and BDEs, has been highly limited [7, 8]. Consequently, HFFRs were developed and introduced to the industry as environmental friendly solutions.

On the other hand, the mineral FRs generally are reported to act by decomposing endothermically during the combustion, and reduce the temperature in the condensed phase, resulting in slowing down the thermal decomposition of the polymer. Then, the non-flammable residue which is left behind from thermal decomposition, usually a metal oxide, dilutes the total amount of polymer fuel and the liberation of non-flammable gasses from the mineral filler promoting the dilution of the available fuel in the gas phase. The most commonly used mineral FRs are metal hydroxides and metal carbonates. The chosen hydroxide or carbonate in the mineral FRs should be able to release the water or carbon dioxide at temperatures before the beginning of polymer matrix decomposition, such as aluminum, magnesium hydroxides, magnesium carbonate [61, 62].

Although mineral FRs are inexpensive and they produce a lower amount of smoke and toxic gasses, they have limited fire performance. When sufficient heat has consumed all the mineral filler and all the water/CO<sub>2</sub> has been released, the remaining metal oxide would not protect the polymer. So, the mineral filler can delay ignition and slow initial flame growth, but it cannot stop it completely while exposing to constant external heat. And another disadvantage of them is their high loading, which is necessary to make them effective, that reduces the mechanical properties of the composite. Therefore, mineral fillers have some practical limits of usefulness for a few polymeric materials, for instance polyolefin and rubbers [47, 60].

The most widely commercial non-halogenated FRs are based on phosphorus compounds. As the name describes, phosphorus-based FRs incorporate phosphorus into their structure, and the structure can vary greatly from inorganic to organic forms, and between different oxidation states (0, +3, +5) [63]. Phosphorus compounds can act both in gas phase and condensed phase, depending on their chemical structure and their interaction with the polymer [64-66]. This means that they can be useful even in low amounts when combined with polymers that inherently produce char. Further, phosphorus FRs tend to act well in high heat flux fire conditions, and through char formation, which can provide a significant fire protection in combination with other FRs [60].

This group of FRs includes as elemental red phosphorus, phosphines, phosphonium compounds, phosphonates, phosphites, phosphinates, and phosphates. These compounds act in the condensed phase by changing the pyrolysis process of the polymer and reducing the amount of gaseous combustibles. Their main modes of action are dehydration and char formation [67]. Then, they convert to phosphoric acid during thermal decomposition, which produces pyrophosphate and

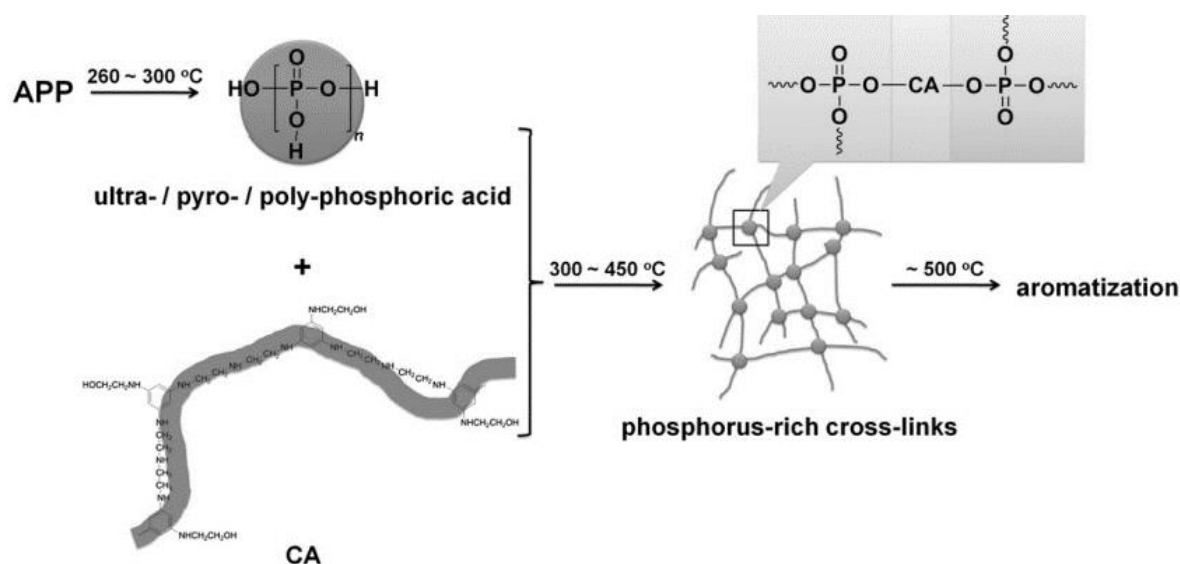
polyphosphate by elimination of water. They can cause the dehydration of polymer end chains and trigger char formation. The released water dilutes the oxidizing gas phase. In some cases, they volatilize into the gas phase to form  $\text{PO}_2^\bullet$ ,  $\text{PO}^\bullet$  and  $\text{HPO}^\bullet$  free radicals, and act as scavengers of  $\text{H}^\bullet$  and  $\text{OH}^\bullet$  radicals [59, 68].

Another common group of flame retardants are IFRs. They have been considered to be one of the most promising eco-friendly flame retardants because of their advantages of relatively high efficiency, low smoke, and low toxicity [69]. In these systems, materials swell when exposed to fire or heat to form a porous foamed mass, usually carbonaceous, that acts as a barrier to heat, oxygen and other pyrolysis products [70, 71]. Three agents are generally required in this approach: an acid, a carbonizing agent or a char forming agent, and a foaming agent. Initially, the released acid esterifies the carbon-rich source and later, the ester decomposes via dehydration yielding a carbonaceous residue. The released gasses from these reactions and decomposition products cause the carbonizing material to foam. It should be mentioned that the temperatures at which the acid has to be liberated should be below the decomposition temperature of the carbonizing agent and the decomposition temperature of the polymer should be around that of the dehydration reaction. One of the best known examples of this system is APP in combination with PER in polymers, such as polypropylene (PP) and polyamide (PA) [72, 73].

In these systems, synergists are also used to enhance the efficiency of intumescent FRs. For example, zeolite can effectively enhance the mechanical strength of the char layer and stabilize it by Si-O-P-C and Al-O-P-C bonds. Some recent investigations have noted the use of polymers like polyamide 6 (PA6) as char-forming agents instead of traditional organic compounds such as polyol to achieve improved mechanical properties and also to avoid problems of exudation and water solubility [59, 70]. An IFR system, composed of a carbonization agent (CA), poly(1,3,5-triazin-2-aminoethanol diethylenetriamine), and APP, was applied into polystyrene (PS) [74]. The results of LOI and UL-94 test demonstrated that when the content of APP and CA was 22.5 and 7.5 wt%, respectively, the LOI value of PS/IFR composite was 32.5%, and a V-0 classification was achieved. The cone calorimeter data showed that the heat release rate (HRR), the total heat release (THR) and the mass loss rate (MLR) were reduced largely with the addition of IFR. Some cone calorimeter data, such as smoke production rate (SPR), total smoke production (TSP) and carbon monoxide production (COP), revealed that the IFR could greatly suppress the generation of the smoke during the material flaming. The improvement in flame retardancy of this system



was reported to be due to the formed intumescent charred layer, which could act as isolating barriers to avoid heat transfer and flame propagation. The study on the flame-retardant mechanism of IFR indicated that a steady structure containing P-O-C was formed due to the reaction between APP and CA. A potential char-forming mechanism of this IFR is shown in Figure II.3.



**Figure II.3.** Potential char forming mechanism of APP/poly(1,3,5-triazin-2-aminoethanol diethylenetriamine) (CA) [74].

## II.2 Bio-flame retardants

The interest in biomaterials is rapidly growing due to the concerns about the environment and their unique characteristics. They are renewable, completely or partially recyclable, and biodegradable. Bio-based composites are those composites, in which at least one of the components is originating from biological products (biomass). This means that polymer composites, in which either the matrix or the reinforcement is bio-based, can be already considered as bio-based (partially bio-based or completely bio-based) [75, 76].

In order to understand how bio-based components can be used to develop flame retardants, their biochemical composition should be considered. Thus, four main families of compounds can be distinguished: proteins, lipids, phenolic and carbohydrates compounds [77].

i. Proteins and lipids:

Proteins are linear biological polymers found in living cells. They are made of sequences of amino acids bonded by peptidic linkage. The thermal stability and the pyrolysis products of proteins tightly depend on their amino-acid composition. There are some researches regarding their flame retardancy. A novel chicken-feather keratin-based flame retardant was synthesized to improve fire behavior of cotton. The agent showed high thermal stability and excellent char-forming ability, which produced much higher char yields at high temperature in nitrogen and obtained a higher LOI value in comparison with the untreated cotton [78].

Lipids are a group of naturally occurring molecules whose main biological functions are energy storing, signal transmission and structural material for cell walls [79]. Due to the presence of various functional groups (hydroxyls, carboxylic acids, double bonds) in their structure, a great variety of reactions are expected. Some lipid derivatives such as undecylenic acid or cardanol have been used to prepare phosphorus containing monomers that can act as reactive flame retardant. Also, phospholipids and sphingolipids are two categories of lipids containing phosphorus and nitrogen atoms in their backbone. Considering the influence of these atoms in the fire behavior of polymers, these lipids can be proposed as potential raw materials for new bio-based flame retardants.

ii. Phenolic and carbohydrates compounds:

Natural polyphenols are a class of organic molecules found in plants and characterized by the presence of phenolic units having one or several hydroxyl groups resulting in a high molecular weight complex structure. Lignin, from this group, is the second most abundant natural polymer after cellulose and the first aromatic polymer. Lignin is mainly found in higher plants and in some algae. In comparison with other components of biomass, lignin degrades over a broader range of temperature between 200 °C and 500 °C. The thermogravimetric curve generally shows a first weight loss between 100 °C and 180 °C that corresponds to the release of water physically bonded into the raw matter. In the first step of the decomposition (200-260 °C), low molecular weight products resulting from the propanoid side chain cleavage are released. Then, the main degradation step (275-450 °C) corresponds to the cleavage of the main chain either by C–C and  $\beta$ -scission or by aryl-ether cleavage. Above 500 °C, further rearrangements and condensation of the aromatic structure occur, leading to the formation of a significant char yield of 57% at 600 °C and the release of dihydrogen in the gas phase [80].

Carbohydrates, also known in biochemistry as saccharides, are biological molecules containing carbon, hydrogen and oxygen atoms. They include low molecular weight compounds such as glucose and lactose or more complex molecules such as oligo and polysaccharides. The compounds that attracted more attention for flame retardant development are polysaccharides, and more particularly starch and cellulose. Starch, a well-known biodegradable polymer, is widely utilized to develop bio-plastics for biodegradable films or biodegradable composites [81, 82]. Chemically, starch is a polysaccharide consisting of amylose and branched amylopectin ( $\alpha$ -D-glucose links with 1,4 and 1,6-branch) [26]. Starch is an ideal candidate to serve as a carbonization agent in an intumescent system. This charring ability of starch, if accompanied by an acidic source, can generate an effective IFR system [83]. Biodegradable flame-retardant composites using a compression technique on low-cost starch, FF and APP were developed [26]. The effect of APP on the flammability and thermal properties of the TPS with flax fabric composites was studied. LOI and horizontal-burning tests exhibited significant sustainability of the composites toward flame and direct flame self-extinguishment. The FR properties of the composites were speculated to be due to the protective compact cross-linked P-O-P and P-O-C network of the char. The reported effects of APP include improvement in mechanical and biodegradation properties.

Cellulose, another biomaterial from this family, is the most abundant one, having low density, high specific strength and modulus, low cost, low energy consumption non-toxic renewable biomass in the world. Its reactive OH groups makes it convenient for graft polymerization with synthetic polymers [84, 85]. A cellulose-g-poly (butyl acrylate) with and without nanoparticles of kaolin was used to prepare nanocomposites. The porous nature of the nanocomposites showed higher thermal behavior and enhanced mechanical properties. The LOI value and cone calorimetry test presented enhancement in fire retardancy of the nanocomposites. It was suggested that the nanocomposite may find use in the industries as fire-retardant materials and open the door of formulating self-extinguishing materials [86].

As it was previously discussed, fuel, heat and oxygen are the three important elements in a combustion process. Once the flame is ignited by stopping any of the mentioned three elements the propagation of flame can be terminated or reduced. In the case of lignocellulosic natural fibers, they start to decompose rapidly under heat sources while polymer matrices melt. The hemicellulose decomposition starts first in the beginning of combustion and with the increase in temperature lignin also gets decomposed. Mass is continuously lost during the decomposition

process because of the evaporating gasses. Different techniques has been used to study the flammability and thermal behavior of natural fiber reinforced polymer composites [87]. The most widely used natural fibers include flax, sisal [88], hemp [89], jute [90], and cotton [91] as well as wood [92]. In nature, some lignocellulosic plants have developed protective behaviors against fire growth. For example, the cork oak that is considered more fire-resistant than other trees owing to the slow combustion of cork, containing mainly suberin (33 wt.%–50 wt.%) (waxy substance composed of polyaliphatic and polyaromatic domains interlinked by glycerol) followed by lignin (20 wt.%–25 wt.%), polysaccharides (12 wt.%–20 wt.%) and extractives (14 wt.%–18 wt.%). In terms of structure, cork presents tiny hollow cells of hexagonal shape in a closed-cell foam [93-95].

These bio-based compounds can have advantages as flame retardant additives because of their molecular composition and structure providing them inherent ability to produce thermally stable charred residues when exposed to fire. This charring competency is particularly important for developing effective flame retardant systems. During the combustion, charring flame retardant systems act by creating an insulating layer at the surface of the burning material resulting in the improvement of its fire behavior by reducing both the thermal and oxygen diffusion, as well as the volatilization of combustible products [25].

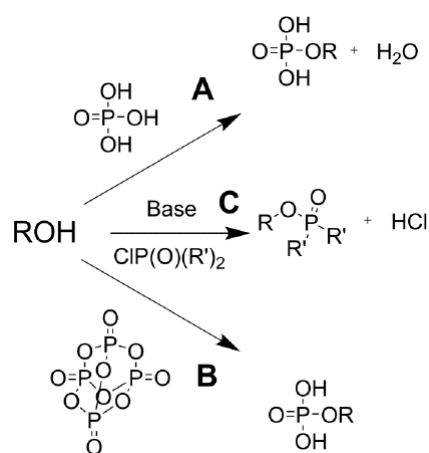
### *II.3 Modification of bio-based materials*

As it was previously discussed, the use of bio-based materials is getting a high attention in terms of the reduction of the environmental impact. In addition, the valorization of numerous by-products and wastes has become an interesting topic. Nevertheless, to achieve the optimized thermal stability and fire performance, chemical modifications for bio based materials can be proposed. For instance, the functionalization with phosphorus-containing-moieties modifies the fire retardancy performance of bio-based compounds. Numerous strategies have been developed to introduce phosphorus-containing moieties.

Materials from natural sources contain mainly hydroxy and phenolic hydroxy groups or unsaturated groups like amino groups in chitosan, carboxylic acid or aldehyde groups in lignin.

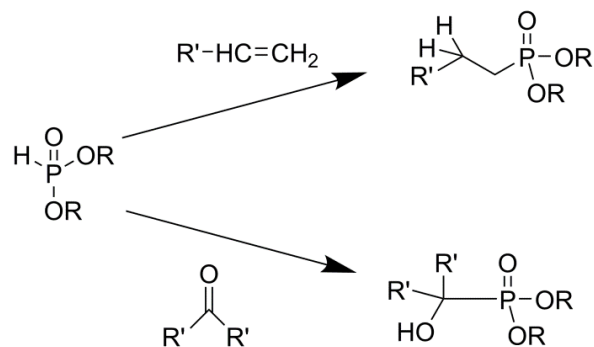
There are different methods to introduce the phosphorus compounds to organic bio-based backbones, such as R-OH, double bonds and amine functional groups phosphorylation.

There are two types of hydroxy groups available in bio based materials, the aliphatic OH such as in the cellulose and aromatic OH such as in the biophenols like lignin derivatives. To introduce phosphorus-containing functions to hydroxy groups, the esterification reactions with  $\text{H}_3\text{PO}_3$  or  $\text{H}_3\text{PO}_4$  has been used (Figure II.4). The phosphorus could be covalently attached to the renewable molecule chain via a reaction of hydroxy groups and produce phosphate groups, phosphite groups or phosphonic acid groups where these derivatives contain mobile hydrogen atoms directly attached to phosphor that lead to obtain phosphonated compounds [96].



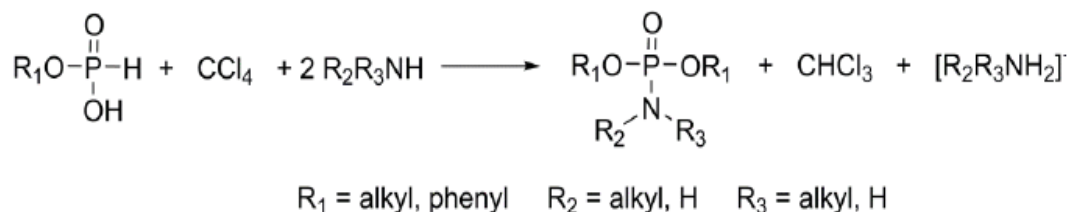
**Figure II.4.** Phosphorylation of hydroxy functions with A) Esterification with  $\text{H}_3\text{PO}_4$ , B) Phosphorylation with  $\text{P}_4\text{O}_{10}$  and C) Reaction of Williamson reaction (R = aliphatic or aromatic groups and R' = chloro, alkyl, aryl or oxyalkyl groups) [96].

The double bond phosphorylation can be done via the Pudovik reaction (Figure II.5) that is the addition of organophosphorus compounds containing P-H bonds. A reaction between Dialkyl phosphites and carbonyl compounds is reported to result in the production of chiral  $\alpha$ -hydroxy phosphonates and phosphonic acid [97].



**Figure II.5.** Pudovik reaction [96].

The Atherton–Todd reaction in Figure II.6 [98] is considered a typical reaction for amine functional groups phosphorylation. The reaction has been reported as an effective single-step route to yield phosphoramidates from diphenyl and dialkyl phosphonates. The reaction of carbon tetrachloride, an amine and an organophosphorus compound containing a P-H bond resulted in the formation of a P(O)Cl oxychloride species and the condensation of this intermediary with N-H containing substrates.



**Figure II.6.** Atherton and Todd's reaction [96].

As previously explained, cork consists of three main different components. Suberin is the main component of cork, that is a glyceridic polyester made of glycerol and long-chain fatty acids. The second major component of cork is lignin, a highly cross-linked aromatic phenolic polymer. Polysaccharides are also present in cork cellular structure as polysaccharide derivatives consisting of chains of mono-saccharides with intermediate linkages. Although, to the best of author knowledge, there is no study on cork or suberin phosphorylation, there are some published researches regarding the phosphorylation of bio components similar to the cork's. For instance,

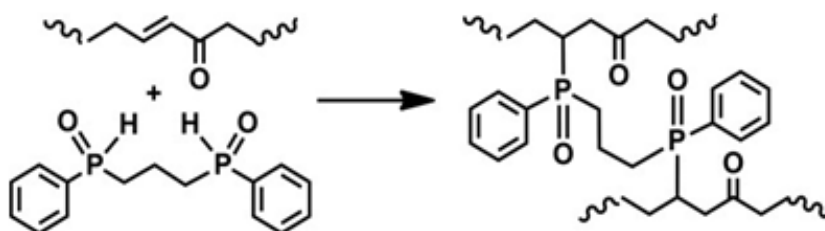
for phosphorylation of the triglyceride which is an ester derived from glycerol and three fatty acids found in plants and animals, some methods have been proposed.

There are different types of triglycerides depending on the oil source, highly unsaturated or less unsaturated. Vegetable oils are the most abundant, annually renewable natural resources available from various oilseeds with the carboxylic group and the unsaturated chains which can be functionalized. For triglycerides or fatty acids, the available functional groups are considered double bonds, hydroxy, carboxylic acids or epoxy. Acrylate and phosphine oxide-containing vegetable oils have been reported to be successfully synthesized in a one-pot two-step reaction. In presence of chlorodiphenylphosphine, allylic phosphinites were capable to undergo a 2,3-sigmatropic rearrangement leading to tertiary phosphine oxides directly linked to triglyceride. The obtained phosphorus-containing triglycerides with different hydroxyl content were activated to polymerization by acrylation and these acrylate triglycerides were radically cross-linked in presence of different amounts of pentaerythritol tetra-acrylate. The presence of overall 2.8 wt.% phosphorus content slightly increased the LOI values from 19.6% to 22.4%. Thermal degradation study under nitrogen and air, also showed that phosphorus-containing compounds were released upon heating acting through a gas phase mechanism. Moreover, the production of a char residue, observed by scanning electron microscope (SEM), that acts in the condensed-phase was reported [99].

Another method has been developed to introduce 9,10-dihydro-9-oxa-10-phosphaphenanthrene-10-oxide (DOPO) into the fatty acids structures [100]. DOPO reacted with p-benzoquinone to form a phosphonate diol and the hydroxy groups of DOPO derivatives were esterified with natural castor oil. With the double bond available from this derivative, acyclic diene metathesis polymerization of a phosphorus-containing  $\alpha,\omega$ -diene led to the formation of a series of phosphorus containing linear polyesters. The presence of a synthesized FR system in epoxy with overall 5.7 wt.% P content resulted in a LOI value as high as 32%. The SEM micrograph of the top surface view of the specimen after the LOI showed the appearance of a black charred material with small cavities. It was also reported that SEM energy-dispersive X-ray spectroscopy (EDX) demonstrated that the phosphorus density increased toward the top burned surface and a phosphorus-rich layer was formed. During combustion, phosphorus compounds can form glass-like polyphosphoric acid that protects the burning surface, or they can form phosphorus-carbon char by reacting with organic components. This protective layer protects the

underlying polymer from attack by oxygen and radiant heat as well as prevents the combustible gasses from transferring to the surface of the materials and feeding the flame, which resulted in improving the fire performance.

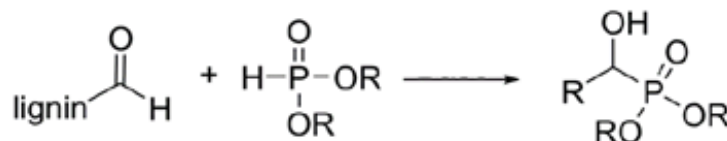
In general, the phosphorus function combined with aromatic groups allows balancing the aliphatic chains of triglycerides (Figure II.7). The use of these new structures have been reported to be capable of improving the flame retardancy of polymeric matrices both in gas and condensed phases. In a study, phosphorus-containing thermosetting resins derived from high oleic sunflower oil were prepared through phospho-Michael addition of a difunctional secondary phosphine oxide, the 1,3-bis (phenylphosphino) propane dioxide on the a triglyceride containing 2.4  $\alpha,\beta$ -unsaturated ketone groups per molecule derived from high oleic sunflower oil [101]. LOI value of 21.5% was reported for the phosphorus-free resin showing its high flammability. The presence of 1.6% of phosphorus resulted in a remarkable increase of the LOI value to 35.0%. This LOI value increased with the phosphorus content and a maximum value of 38.0% was obtained for the thermoset containing 4.7% of P. These results showed an important improvement on the flame retardant properties related to the presence of phosphorus.



**Figure II.7.** Phosphorylation of a triglyceride containing 2.4  $\alpha,\beta$ -unsaturated ketone derived from high oleic sunflower oil [101].

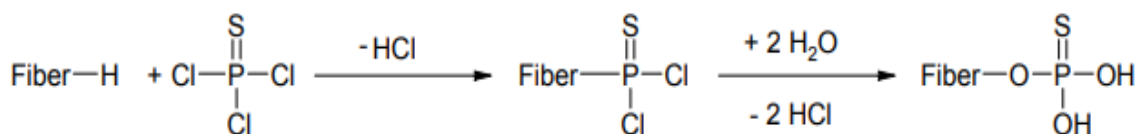
Furthermore, phosphorylation of biophenols and particularly lignin and lignocellulosic materials, due to their strong abundance as renewable resources, has gained a particular interest. The main application of phosphorylated lignin is as a flame retardant additive for polymers. The phosphorylated lignin is considered a high performance flame retardant since the aromatic structure of lignin combined with phosphorus groups can act as a very efficient char-forming additive (Figure II.8).





**Figure II.8.** Phosphorylation of lignin by Pudovik reaction [96].

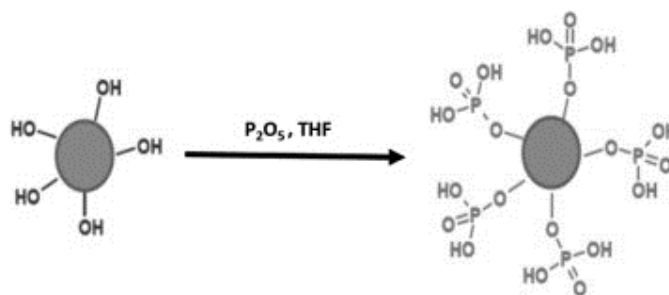
In addition, phosphorylation of a lignocellulosic compound, sugarcane bagasse, has been proposed via grafting of phosphorus groups by reacting thiophosphoryl chloride on hydroxy groups followed by hydrolyzation of the product [102]. A successful grafting with the presence of a phosphorus content of 4.08 wt.% was reported (Figure II.9).



**Figure II.9.** Phosphorylation of sugarcane bagasse [102].

The efficiency of lignin phosphorylation is difficult to evaluate since lignin is a natural macromolecule that its chemical structure depends on its resource. In general, the content of phosphorus presented in phosphorylated lignin depends on the type of phosphorylation and the phosphorus-containing precursor used. The phosphorus content of the modified lignin also depends on the hydroxy groups substitution degree. A phosphorylated lignin with 16.6 wt.% of phosphorus content was obtained by using phosphoric acid, while by using hypophosphorus acid and phosphoric anhydride, a 3.6 wt.% and 6-13 wt.% of phosphorus were registered, respectively [96]. An Enhancement of flame retardancy was reported for ABS composites containing 30 wt.% P-LIG with 4.1% of phosphorus content via the reaction presented in Figure II.10. The P-LIG thermal stability was significantly enhanced in comparison to that for lignin. Grafting phosphorus onto lignin increased the amount of residue at high temperature compared to ABS. It was shown that P-LIG promoted char formation by reacting with ABS during thermal decomposition leading to a significant reduction of the peak of heat release rate (pHRR) and THR of 58% and 20%, respectively. It was presented that P-LIG was acting mainly in the condensed phase by interacting with ABS during the decomposition of the composite. These interactions induced a lower release

of combustibles to the flaming zone while a charring protective barrier was formed on the composite surface. A slight inhibition effect in the flame was also observed probably due to the release of phosphorus species into the gas phase [40].



**Figure II.10.** Lignin phosphorylation with phosphorus pentoxide ( $P_2O_5$ ) [40].

Furthermore, for polysaccharides, the use of phosphorylating agents such as polyphosphorus and alkyl chlorophosphate have been introduced in order to prepare fireproof fabrics [103]. Phosphorylated polysaccharides are char-forming materials and they can prevent the combustion or delay the spread of the fire after ignition. During combustion, phosphorus generates a polymeric form of phosphoric acid that induces the formation of a char layer which can act as a protecting barrier for the material from oxygen. Chitosan derivatives, that are a polysaccharide, were phosphorylated with  $P_4O_{10}$  reaction with glycidyl methacrylate and then cross-linked under UV in order to prepare new flame retardant material for epoxy. MCC results showed that presence of phosphorylated chitosan significantly led to a 56% reduction of the peak heat release and 50% of total heat release of epoxy composites. Thermogravimetric analysis exhibited that the thermal stability of materials was improved at high temperature. Fourier transform infrared of evolved gasses and the residue revealed that phosphorylation promoted the formation of char and reduced the release of combustible gas [104].

A sodium alginate/carboxymethyl cellulose/chitosan polysaccharide-based composite aerogel was fabricated by freeze-drying [105]. It was reported that phosphorylation of polysaccharides-based composite with sodium hypophosphite resulted in a significant enhancement of flame retardancy. It was shown that peak heat release rate and total heat release of the composite decreased from 30 W/g to 20 W/g and 15 kJ/g to 10 kJ/g, respectively. Results

indicated that the ester cross-linking could improve the thermal stability of polysaccharide-based aerogels because of the phosphorylation of polysaccharide and easily form a thermostable carbonization layer. In addition, it was reported that the aerogel can serve as a thermal shielding layer and the second-degree burn time could reach up to 87.1 s under radiant heat exposures of 11.3 kW/m<sup>2</sup>. Therefore, the polysaccharide-based aerogels were proposed as an ideal material for thermal protective clothing application.

#### *II.4 Flame retardant acrylonitrile-butadiene-styrene composites*

ABS is an engineering thermoplastic polymer which consists of polybutadiene (PB) as a discrete phase and styrene-acrylonitrile (SAN) copolymer as a continuous phase. ABS, due to its good mechanical performance, chemical resistance and easy processing, is widely used in many applications especially in the electronics and automotive industries [106-109]. In different studies, fire behavior of ABS and its composites have been investigated. It was reported that ABS is not classified in the UL-94 test and its LOI value is 18-20% [110, 111]. This high flammability of ABS which is due to its chemical structure needs the incorporation of flame-retardant materials to achieve high flame retardancy and thermal stability.

The most widely used flame retardants in ABS are phosphorus-based ones. For instance, aluminum isobutylphosphinate (APBu) and its synergistic system with red phosphorus (APBu/RP) were reported to improve the fire behavior of ABS and it was observed that the addition of RP to ABS-APBu enhanced the flame retardation of APBu both in the gaseous phase and condensed phase, leading to a high synergistic effect [112]. Hexakis (4-nitrophenoxy) cyclotriphosphazene (HNTP) with APP were applied to ABS in order to improve the intumescent flammability and thermal properties of ABS. It was found that when the weight loading of FR was 30 wt.%, the ratio of HNTP and APP was 1:1, the ABS sample achieved V-0 classification and a higher LOI value. The cooperation of HNTP and APP could remarkably enhance the ability of charring with a high amount of residue of 8.11% at 800 °C under air [113].

Recently, it was also revealed that synergistic interactions between APP and AlPi promoted the liberation of phosphorus radicals at a temperature range which acted like scavengers of those radicals yielded during ABS decomposition, as well as, the formation of a more effective protective layer in the condensed phase resulted in a remarkable reduction of the peak heat release rate (74%) and of the maximum average rate of heat emission (65%), obtained by cone calorimetry

(CC). Analyzing the pyrolysis, flammability and fire behavior showed synergy in flammability by combining both flame retardants, a UL-94 V-0 classification and combined condensed (by APP) and gas phase-based (by AlPi) mode of action in the ABS matrix [13].

As previously discussed, lignocellulosic materials have shown potential in the field of flame retardant materials due to their excellent char forming ability. In a study, lignin was modified with aluminum phosphate and then coated with red phosphorus and used as a flame retardant in ABS. Addition of 25 wt.% of modified lignin was reported to result in a V-0 classification and the reduction of peak heat release rate, total heat release and total smoke release by 64.6%, 49.3%, and 30.1%, respectively. This significant reduction was due to the formation of  $\text{PO}\cdot$  and  $\text{HPO}\cdot$  free radicals via the decomposition of modified lignin that captured the  $\text{H}\cdot$  and  $\text{HO}\cdot$  free radicals produced during the combustion of ABS and inhibit the flame oxidation chain reaction; the decomposition of modified lignin absorbed heat, and its decomposition products were dehydrated and carbonized to form a protective char layer on the burning surface, that prevented the heat and oxygen transfer [114]. In another study, the alkali lignin was blended with ABS at different loading levels of 5, 10 and 20 wt.%, and the in situ reactive compatibilization was also employed to improve their interfacial compatibility. It was reported that lignin was uniformly dispersed in the ABS matrix. It was also observed that addition of lignin reduced the initial degradation temperature of ABS due to its lower thermal stability. However, lignin could enhance the high-temperature stability due to the char-formation of lignin at relatively lower temperature. The compatibilization only had a slight influence on the thermal stability and char formation of the composites. Adding 20 wt.% of lignin into ABS resulted in a 32% reduction in pHRR. THR and MLR also decrease with increasing lignin content. The in situ reactive compatibilization with SEBS-g-MA, can further reduce the flammability of ABS due to the improved char layer. As the amount of compatibilizer is 10 wt%, the pHRR reduction reaches 44% relative to pure ABS. The highly conjugated graphitic carbon layer is primarily responsible for the improved flame retardancy. Moreover, the free radical-trapping capacity of lignin also contributes to the reduced flammability of ABS [27].

In Table II.1, different types of phosphorus FR applied in ABS with the reported fire performance are presented.

**Table II.1.** Different types of phosphorus flame retardants used for ABS in the literature.

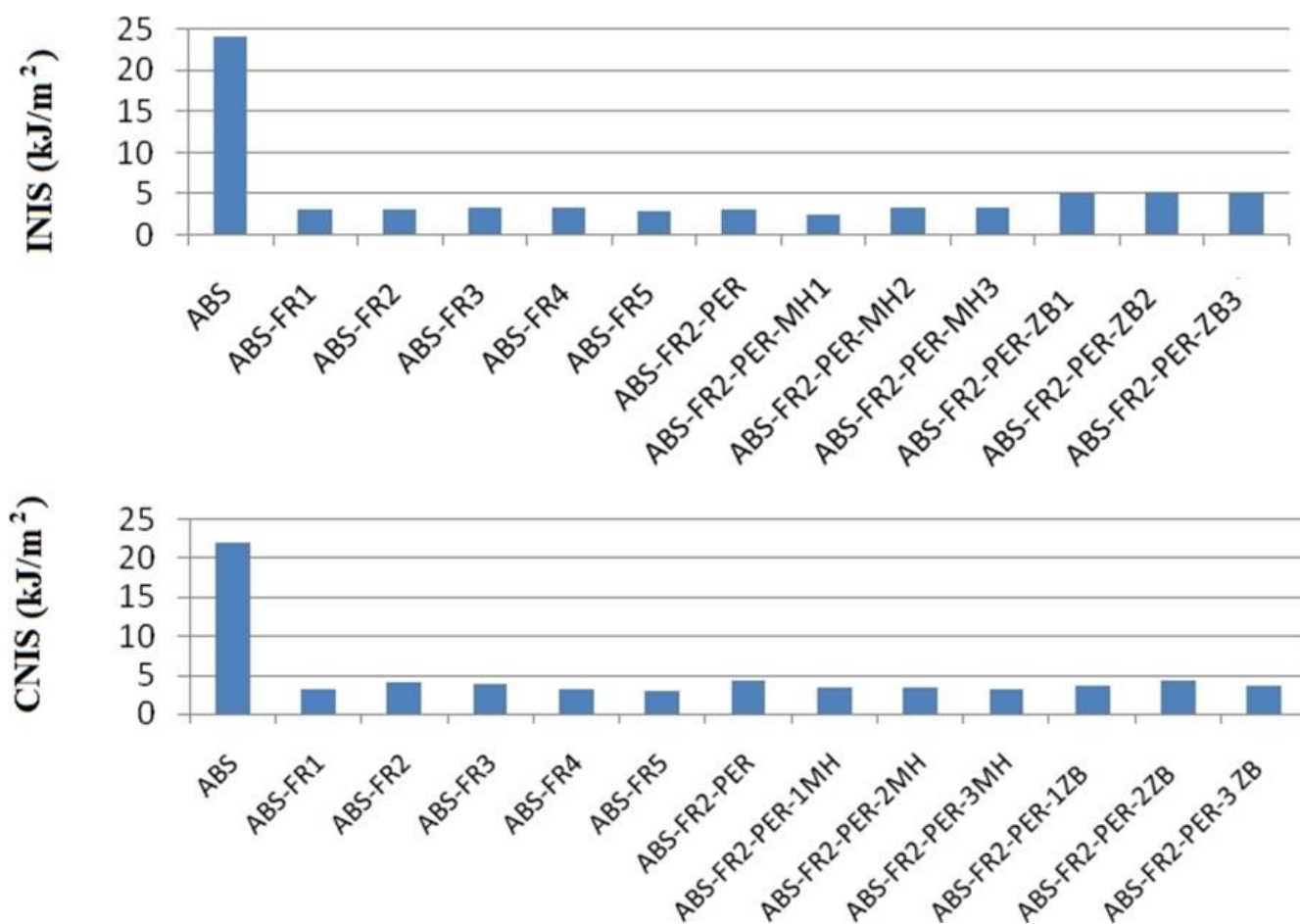
Flame retardant system	wt.%	UL-94	LOI (%)	pHRR reduction of CC (kW/m <sup>2</sup> )	References
APBu and RP	15:5	V-0	29.8	574 to 178	[112]
PAPP and AlPi	20:5	V-0	30.8	1059 to 260	[12]
AlPi, APP, PER and zinc borate (ZB)	12.5:12.5:5:3	V-0	28.1	712 to 354	[115]
AHP	25	V-0	25	1059 to 365	[4]
AHP	30	V-0	25.1	704 to 174	[116]
Poly(diethylenetriamine terephthalamide) and APP	7.5:22.5	V-0	31.5	649 to 556	[117]
APP:AlPi and organic montmorillonite	10:10:2	V-0	28.7	486 to 154	[118]
Microencapsulated aluminum hypophosphite with a shell of melamine formaldehyde resin	30	V-0	25.5	1059 to 242	[119]
Alkylphosphinate salt—aluminium β-( p-nitrobenzamide) ethyl methyl phosphinate	30	V-0	27.6	717 to 351	[120]
Hydroquinone bis(diphenyl phosphate) and novolac phenol	20:10	V-2	31	Reduced to 255	[121]
APP, AlPi and expandable graphite	7.5:7.5:5	V-0	-	Reduced to 306	[122]
APP, poly(hexamethylene terephthalamide) (PA6T) and Al(H <sub>2</sub> PO <sub>2</sub> ) <sub>3</sub>	23.3:4.7:2	V-0	28.5	-	[123]
APP and expandable graphite	3.75:11.25	V-0	31	-	[124]

Melamine phosphate microencapsulated with SiO <sub>2</sub> particles and dipentaerythritol	22.5:7.5	V-0	31.2	-	[125]
Tris(3-nitrophenyl) phosphine and triphenyl phosphate	14:21	V-1	25	-	[126]
Poly(p-propane terephthalamide) (PPTA) and APP	22.5:7.5	V-0	31.6	-	[127]
APP, pentaerythritol and organic montmorillonite	22.5:7.5:4	V-0	31.3	-	[128]
APP, poly-N,N'-ethyleneterephthalamide and AlPi	25:5:2	V-0	32	-	[22]
DOPO	27.5-30.0	V-0	-	-	[129]
APP and poly(diphenolic phenyl phosphate)(poly(DPA-PDCP)) derived from biomass	24:6	-	25.2	662 to 265	[130]
Phosphorylated lignin	30	-	-	602 to 411	[40]
Lignin-diethylenetriamine/red phosphorus nanoparticles	8	-	-	529 to 170	[131]
Modified lignin/aluminum phosphate coated red phosphorus	25	V-0	26.5	756 to 268	[114]

### *II.5 Effect of flame retardants on the ABS or ABS blends' mechanical properties*

In general, the addition of flame retardants decreases the mechanical properties of thermoplastics like ABS such as flexibility and impact strength that have an adverse effect on their processability limiting their industrial applications where both fire resistance and high mechanical performance

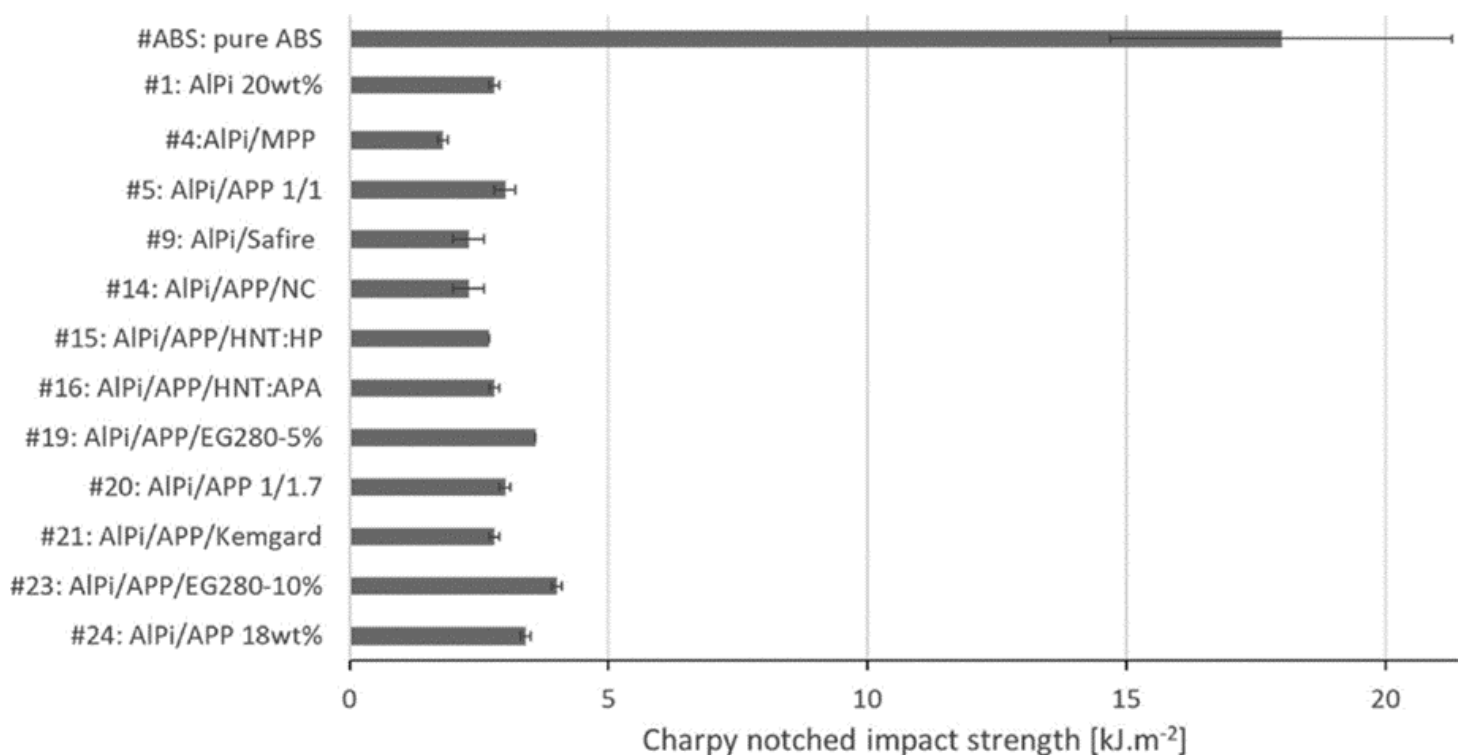
are essential, such as in automotive components, electronic devices, or structural elements. In Figure II.11, the effect of adding different flame retardant systems consist of 20-30 wt.% APP:AlPi (1:1) (FR) with 5 wt.% PER and 1-3 wt.% ZB or magnesium hydroxide (MH) is shown. Although all flame retardant systems showed an enhanced fire performance with V-0 classification, a drastic reduction in Izod and Charpy notched impact strength (INIS and CNIS) was observed [115].



**Figure II.11.** Izod notched and Charpy notched impact strength results of ABS and its composites, respectively [115].

In another study, effect of different FRs like APP, AlPi, brominated flame-retardant ether of 2,4,6-tribromophenol (FR245), melamine polyphosphate (MPP), nanocaly (NC), melamine poly(zinc phosphate) (safire), halloysite nanotubes-not modified (HNTs:HP), halloysite

nanotubes-modified with ammonium polyacrylate (HNTs:APA), expandable graphite and molybdate-coated magnesium silicate (kemgard) on Charpy impact strength was reported. As it can be seen, addition of these FRs also had an adverse effect on Charpy impact strength of flame retarded ABS composites (Figure II.12) [122].



**Figure II.12.** Charpy notched impact strength of flame retarded ABS composites [122].

It was revealed that the incorporation of 25 wt.% of microencapsulated aluminum hypophosphite (MFAHP) with a shell of melamine formaldehyde resin into ABS led to an enhancement of flame retardancy and a V-0 classification, while no remarkable change in flexural and tensile strength was observed [119]. However, the Izod notched impact decreased significantly from 17 kJ/m<sup>2</sup> to 2.6 kJ/m<sup>2</sup> due to the presence of the MFAHP flame retardant (Table II.2).



**Table II.2.** Charpy notched impact strength of flame retarded ABS composites [119].

Sample	Flexural strength (MPa)	Notched impact Strength (kJ/m <sup>2</sup> )
ABS	62.6 ± 0.5	17.0 ± 0.3
ABS/20% MFAHP	68.5 ± 0.3	2.6 ± 0.3
ABS/22% MFAHP	67.9 ± 0.3	2.5 ± 0.2
ABS/25% MFAHP	67.1 ± 0.2	2.6 ± 0.3

Therefore, some treatments, such as incorporation of compatibilizers and impact modifiers are required to improve the mechanical properties. Many studies have been carried out to investigate the effect of using various compatibilizers or impact modifiers such as ABS-g-(maleic anhydride) (ABS-g-MA), styrene-butadiene-styrene (SBS) block copolymer, ethylene-methyl acrylate-glycidyl methacrylate (EMA-GMA), methacrylate-butadiene-styrene (MBS) and ethylene-vinyl acetate (EVA) on mechanical properties of ABS blends, particularly in ABS/polycarbonate (PC) and ABS/ polyamide 6 (PA6). In a PC/ABS blend, adding ABS-g-MA compatibilizer resulted in an increase of impact strength compared to blends without compatibilizer. The maximum amount of increase was registered for the blends with an optimum content of 5 phr compatibilizer [132]. It was reported that the addition of SBS to the ABS/PC blend resulted in a decrease in the elasticity modulus, the tensile and yield strengths, while the percentage elongation and impact strength significantly increased [133]. In addition, it was shown that a small amount of ABS-g-MAH has a notable influence on the impact strength of the ABS/PC and the impact strength of the ABS/PC alloy increases with an increasing ABS-g-MAH content and it was confirmed by SEM that ABS-g-MAH could greatly enhance the compatibility of the ABS/PC blends [134]. EMA-GMA and ethylene-n butyl acrylate-carbon monoxide-maleic anhydride (EnBACO-MAH), were used at 0, 5, and 10% by weight to compatibilize the blend composed of ABS and polyamide 6 (PA6). It was shown by SEM that incorporation of compatibilizer resulted in a homogenous morphology with reduced dispersed particle diameter at the presence of 5 wt.% compatibilizer. Regarding the mechanical properties, different trends in yield strengths and strain at break values were observed depending on compatibilizer type, loading level, and blend composition. For the blend with 5 wt.% EnBACO-MAH, the highest toughness at room temperature was registered [135]. In another study,

the effect of different compatibilizers on mechanical properties of a flame retarded PC/ABS blend has been investigated. It was reported that the addition of MBS and EVA up to 3 phr increased the impact strength significantly for the PC/ABS containing a 10 and 15 phr flame retardant [136].

There are few studies regarding the improvement of ABS composites mechanical behavior that contain fillers. The impact strength enhancement of an ABS with an intumescent system composed of APP, melamine and calcium 3-hydroxy-2,2-bis(hydroxymethyl) propyl phosphate at the ratio of 3:1:1 was reported. For that, an ABS-R was added at different loadings of 4-26 wt% into the mentioned IFR-ABS. It was reported that the incorporation of ABS-R resulted in reduction of the storage modulus, damping behavior and glass transition temperature, obtained by dynamic mechanical thermal analysis (DMTA). By increasing the ABS-R loading, the tensile strength and the flexural strength gradually decreased; however, the notched impact strength increased. The highest increase of impact strength (115%) was reported for the composite containing 15 wt.% of ABS-R due to an improvement in the boundary adhesion between IFR and ABS matrix, confirmed by SEM [41]. In another work, the effect of SEBS-g-MA impact modifier on a recycled polymeric blend of ABS/high impact polystyrene/polystyrene (9:21:70), containing 2-10 wt.% of TPP and sepiolite with a ratio of 1:1, was investigated. The blends with 8 wt.% of FR showed a V-1 classification in UL-94 and a 29% LOI value. However, incorporation of FRs resulted in a drastic reduction of mechanical properties of the blends. Therefore, SEBS-g-MA impact modifier was added in order to improve the mechanical properties. The impact strength of the recycled blend without FR was 66.12 J/m, and after the addition of 8 wt.% FR, it was reduced to 23.5 J/m. However, the incorporation of 10 wt.% SEBS-g-MA resulted in a significant increase of impact strength to 80.4 J/m. It was also reported that the tensile strength was improved with the addition of an impact modifier, from 21 MPa to 27.4 MPa. It was shown that as wt.% of SEBS-g-MA increased, the tensile and flexural strength decreased due to the presence of a higher rubbery content where the elastomeric phase started dominating the blend. On the other hand, a higher wt.% of SEBS-g-MA resulted in an enhancement in the impact strength by increasing the elastomeric phase and subsequently resilience property of the blend [42].

In general, compatibilizers and impact modifiers act by reducing the crack growth rate and increasing the energy absorbed in the plastic region, which is also called stress whitened zone [43]. Ethylene methyl acrylate (EMA), and silicone/poly(n-butyl acrylate) with a styrene-acrylonitrile-maleic anhydride terpolymer (Si-MAH) were used as impact modifiers in a glass fiber (GF)-

reinforced PC composites. It was seen that by increasing EMA content, the tensile strength, the bending strength and modulus continuously decreased. The addition of 2 wt.% and 6 wt.% EMA reduced the tensile strength by 13.0% and 29.6% and the bending strength by 13.9% and 22.4%, respectively. Dispersed EMA elastomers in the GF-PC matrix acted as stress concentrators. A decrease in the modulus was also observed attributed to the enhanced mobility of the matrix molecules induced by the EMA elastomer. Addition of 2 wt.% of EMA resulted in an increase of impact strength by 39.7%, due to the high energy absorption capability of the flexible molecular chains in EMA. It was reported that further increasing the EMA content had no significant effect on the impact strength as a result of the balance between elastomer toughening and matrix continuity disruption caused by rubber coalescence. The same trend was also observed for incorporation of Si-MAH in GF-PC. By adding 2 wt.% of the Si-MAH, a significant enhancement of impact strength (152%) was registered. By further increase of Si-MAH, the impact strength increased; however, when the Si-MAH content increased to 4 and 6 wt.%, The impact strength remained almost constant. This improvement was the result of the high toughness of the silicone-poly(n-butyl acrylate) core and the good compatibility between the styrene acrylonitrile-maleic anhydride shell and PC. However, at a high Si-MAH content, large diameter rubber granules could appear and decrease the uniform contribution and energy absorbing capability of the additive. It was concluded that Si-MAH at 2 wt.% loading was the most efficient impact modifier for GF-reinforced PC composites. Then, the PC/GF/Si-MAH blend was chosen and its flame retardancy was enhanced by adding three different FRs: TPP, a TPP/RDP mixture and oligomeric siloxanecontaining potassium dodecyl diphenylsulfone sulfonate (SiKSS). For this formulation, a V-0 classification in UL-94 when 9 wt.% TPP, 6 wt.% TPP/RDP, or 0.2 wt.% SiKSS was reported [137].



Material and methods

Chapter

III



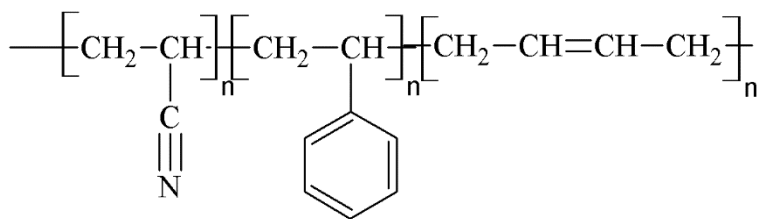
## Chapter III: Materials and methods

Prior to the presentation of experimental results, this chapter will provide the principal characteristics of materials used along the study, as well as the description of the preparation methodologies and testing procedures used for characterization of the prepared composites.

### *III.1 Materials*

#### *III.1.1 ABS*

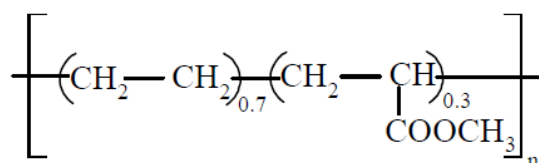
Two different grades of ABS were provided by Elix Polymers (Tarragona, Spain) and used as the polymeric matrix. According to the manufacturer, the first one, used in chapter IV, contains 37 wt.% ABS grafted with 13 wt.% SAN (total of 50 wt.% ABS) and 50 wt.% of ABS pellets and has an impact strength of 24 KJ/m<sup>2</sup> and a melt volume rate of 20 cm<sup>3</sup>/10 min, measured at 220 °C and 10 kg. Also, an ABS (used in chapter VI and VII), with the commercial name ELIX<sup>TM</sup> 128 IG, containing 26–28 wt.% of butadiene in a matrix of SAN and has a melt volume rate of 15 cm<sup>3</sup>/10 min, measured at 220 °C and 10 kg was used. The chemical structure of ABS is presented in Figure III.1.



**Figure III.1.** ABS chemical structure.

### III.1.2 Impact modifiers

Two different compatibilizers/impact modifiers, EVA and EMA, with different vinyl acetate (VA) content and different methyl acrylate (MA) content, respectively, have been used. Primeva<sup>®</sup> P1820C (EVA18) with average content of 18 wt.% VA and Primeva<sup>®</sup> P40055 (EVA40) with average content of 40 wt.% VA were provided by Repsol (Madrid, Spain) and used as compatibilizer and/or impact modifier. LOTRYL<sup>®</sup> 24MA07T (E24) with average content of 23-26 wt.% MA and LOTRYL<sup>®</sup> 29MA03T (E29) with average content of 27-31 wt.% MA were provided by Arkema (Colombes cedex, France) and used as compatibilizer and/or impact modifier. The chemical structure of EMA is presented in Figure III.2.



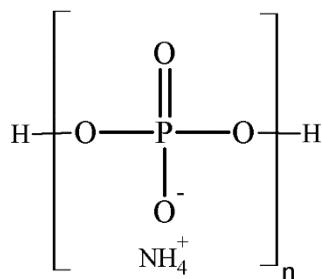
**Figure III.2.** EMA chemical structure [138].

Ultrahigh molecular weight silicone rubber (UHMW-SR), GENIOPLAST<sup>®</sup> PELLET S, a pelletized silicone gum formulation with a high loading of ultrahigh molecular weight siloxane polymer (70 wt.%) and 30 wt.% silica, was supplied by Wacker (Munich, Germany) and used as impact modifier.

### III.1.3 Phosphorus flame retardants

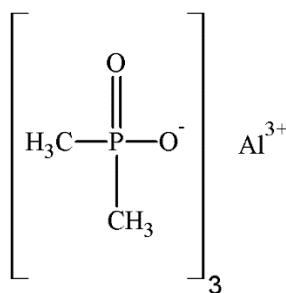
APP, Exolit<sup>®</sup> AP422, was supplied by Clariant Produkte (Sulzbach, Germany), and used as flame retardant. APP (see Figure III.3), with chemical formula  $(\text{NH}_4\text{PO}_3)_n$ , possesses a polymerization degree (n) higher than 1000 and a phosphorus and nitrogen content of 31–32 wt.% and 14–15 wt.% respectively, with average particle size of 17  $\mu$  and a density of 1.90 g/cm<sup>3</sup>.





**Figure III.3.** APP chemical structure.

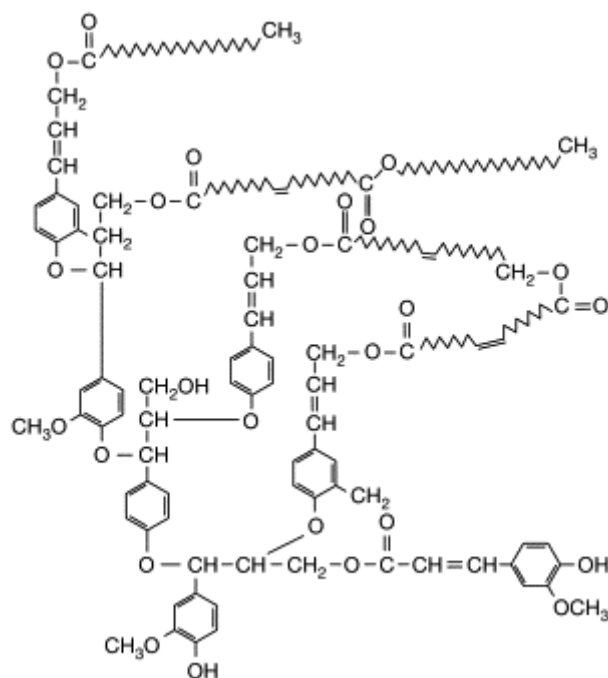
AlPi, OP1230, with chemical formula of  $((C_2H_5)_2PO_2)_3Al$ , was also supplied by Clariant Produkte and used as a flame retardant. A phosphorus content of 23.3-24 wt.%, a density of 1.35 g/cm<sup>3</sup> and an average particle size of 20-40 μ was reported by the manufacturer. The chemical structure of AlPi is shown in Figure III.4.



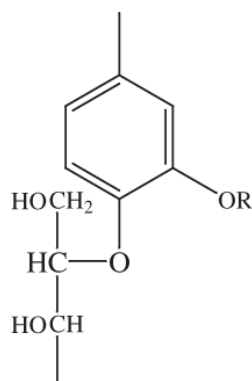
**Figure III.4.** AlPi chemical structure.

#### III.1.4 Cork powder

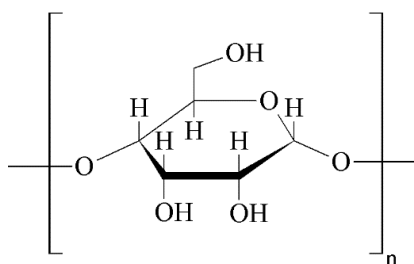
The cork powder was kindly provided by Corcho de Extremadura (Mérida, Spain); dichloromethane, ethanol, methanol, chloroform, sodium methoxide and sulfuric acid were purchased by LabKem (Barcelona, Spain). The components' composition of the employed cork powder as it was reported [95]: suberin (Figure III.5) is its main component with a 40 wt.% of the total weight, followed by 24 wt.% of lignin (Figure III.6), 19 wt.% of polysaccharides (Figure III.7) and 14 wt.% of extractives.



**Figure III.5.** Suberin chemical structure [139].



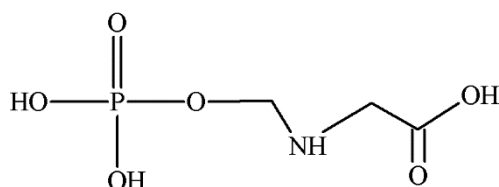
**Figure III.6.** Lignin chemical structure [140].



**Figure III.7.** Polysaccharides chemical structure.

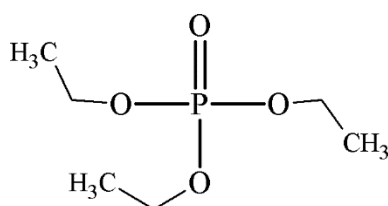
### III.1.5 Components for cork's phosphorylation

Three different phosphorus components were used as modifier agents for cork powder's phosphorylation. An analytical-grade of glyphosate 95% in powder form with a phosphorus content of 18 wt.%, a density of 1.7 g/cm<sup>3</sup> and solubility in water of 1.01g/100ml at 25°C was used as a phosphorus compound for cork phosphorylation. The chemical structure of glyphosate is shown in Figure III.8.



**Figure III.8.** Glyphosate chemical structure.

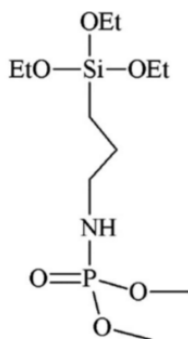
Triethyl phosphate (TEP), in liquid form, with a phosphorus content of 17 wt.% and molecular weight of 182.15 g/mol was supplied by Aldrich Chemical Co., Inc. with 98 % purity. The chemical structure of TEP is presented in Figure III.9.



**Figure III.9.** Triethyl phosphate (TEP) chemical structure.

Dimethyl-3-triethoxysilanepropylphosphoramidate (DTSP) was synthesized according to the Atherton and Todd reaction [141]. 0.2 mol of dimethyl phosphite and 0.2 mol of CCl<sub>4</sub> were dissolved in 200 mL tetrahydrofuran (THF) in a three-necked flask. The mixture was cooled down between 0 to 5 °C using an ice bath. Then a mixture of 0.2 mol of 3-aminopropyltriethoxysilane (APTES) and 0.2 mol of trimethylamine (TEA) dissolved in 50 mL THF was added dropwise into the above solution under an ice bath. After complete addition of APTES and TEA, the solution was allowed to warm up to room temperature and stirred for 12 h. The formed hydrochloride salt

of triethylamine was removed by filtration and yellow liquid was obtained by removal of the solvent. The chemical structure of the product, DTSP, is shown in Figure III.10. Analytical-grades of ammonia, isopropyl alcohol (IPA), dichloromethane (DCM) and toluene were used to wash the excessive remaining phosphorus on the surface of cork powder.

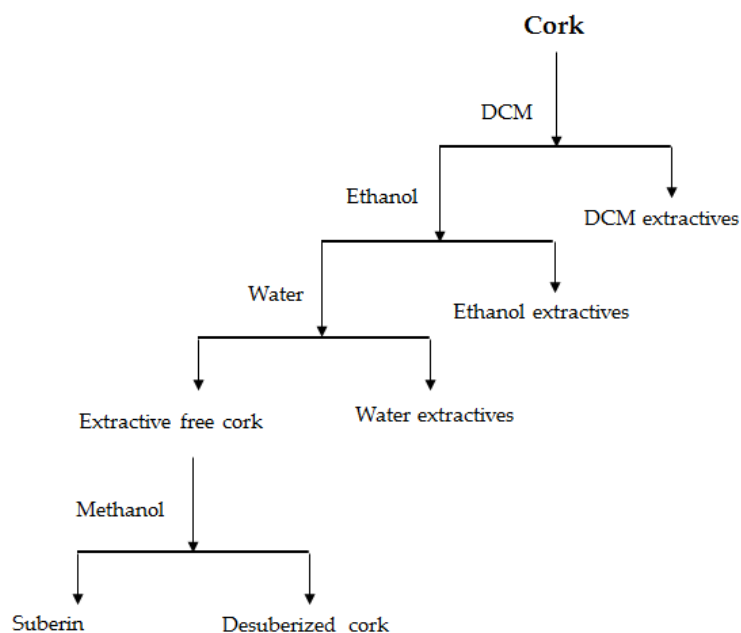


**Figure III.10.** Dimethyl-3-triethoxysilanepropylphosphoramidate (DTSP) chemical structure [141].

### *III.2 Chemical extraction of cork powder's components*

In order to determine cork composition, chemical analyses that included the determination of ash, extractives, suberin, lignin and cellulose were carried out. All experiments were performed in duplicate. The ash content was determined by incinerating 2 g of cork at 500 °C during 12 h, following TAPPI standard T 15 os-58. Successive Soxhlet extractions (Figure III.11) were performed using 3 g of samples to separate extractives with DCM for 6 h, ethanol for 8 h and water for 20 h, following TAPPI standards (T204 om-88 and T207 om-93) [142, 143]. After each extraction step, the solution was evaporated, and the solid residue weighed. The suberin content of the cork was determined using an extractive-free material by methanolysis for depolymerization [144]. A total of 1.5 g of extractive-free cork was refluxed with 250 mL of 3% NaOCH<sub>3</sub> in CH<sub>3</sub>OH over 3 h, filtered and then refluxed with CH<sub>3</sub>OH for 15 min. After filtration, the residue was acidified with 2 M H<sub>2</sub>SO<sub>4</sub> to pH 6 and evaporated in a rotating evaporator. The residue was suspended in 100 mL of water and extracted with 100 mL CHCl<sub>3</sub> three times; then the combined extracts were dried over Na<sub>2</sub>SO<sub>4</sub> salt, filtered, evaporated and weighted as suberin. Lignin was determined after acid hydrolysis with 72% H<sub>2</sub>SO<sub>4</sub> at 30 °C for 2 h and boiling for 4 h

after dilution with water to 4% H<sub>2</sub>SO<sub>4</sub>, following TAPPI T-222 standard. The residue was washed with hot water, dried and determined as lignin [145, 146].

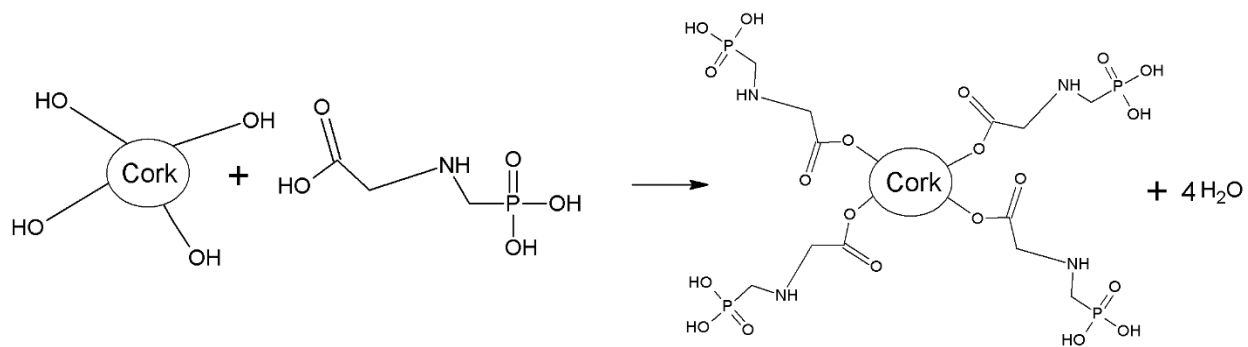


**Figure III.11.** Soxhlet extraction procedure of cork powder.

### *III.3 Phosphorylation of cork powder*

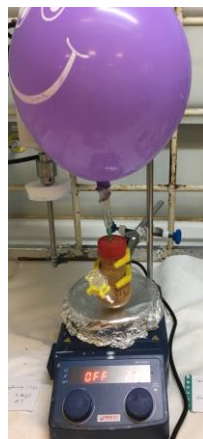
Glyphosate with a phosphorus content of 18 wt.%, TEPP with a phosphorus content of 17 wt.% and DTSP with a phosphorus content of 12 wt.% were used as phosphorus components and cork modifiers. The proposed reactions are as following:

1. Cork powder modified by glyphosate (C<sub>g</sub>) via proposed reaction presented in Figure III.12.



**Figure III.12.** Proposed reaction of cork powder and glyphosate.

- Condition 1 ( $C_g$ ): 1 gr of cork powder was mixed with 5 gr of glyphosate and 20 mL distilled water in a round bottom flask. The reaction was set at room temperature for 3 days under nitrogen atmosphere (Figure III.13).



**Figure III.13.** Digital photograph of reaction setup of cork/glyphosate in water at room temperature.

- Condition 2 ( $C_{g2}$ ): 1 gr of cork powder was mixed with 5 gr of glyphosate and 20 mL distilled water in a reaction set up shown in Figure III.14. The reaction was set at 120 °C for 12 hours.



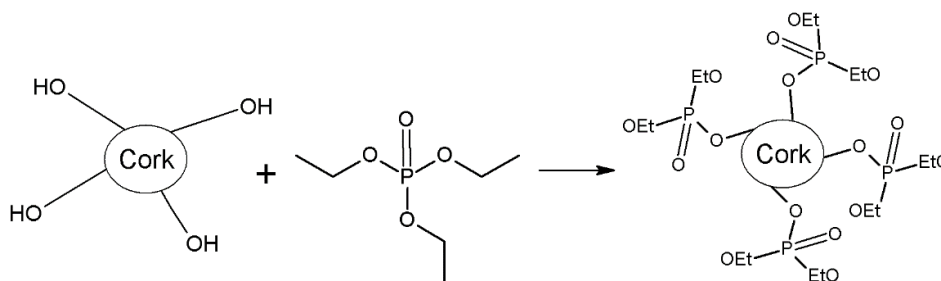
**Figure III.14.** Digital photograph of reaction setup of cork/glyphosate in water at 120 °C.

- Condition 3 ( $C_{g3}$ ): 1 gr of cork powder was mixed with 5 gr of glyphosate in 20 mL toluene under a reflux set up. The reaction was set at 120 °C for 12 hours under nitrogen atmosphere (Figure III.15).



**Figure III.15.** Digital photograph of reaction setup of cork/glyphosate in toluene at 120 °C.

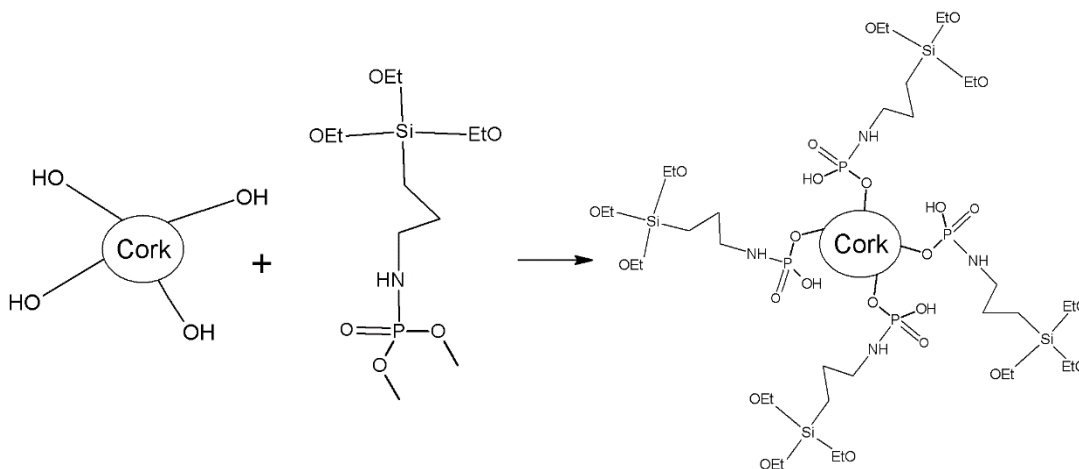
2. Cork powder modified by TEP (C<sub>t</sub>) through the proposed reaction shown in Figure III.16.



**Figure III.16.** Proposed reaction of cork powder and TEP.

- Condition 1 (C<sub>1</sub>): 1 gr of cork powder was mixed with 10 mL of TEP in a round bottom flask. The reaction was set at 120 °C for 12 hours under nitrogen atmosphere.
- Condition 2 (C<sub>2</sub>): 1 gr of cork powder was mixed with 10 mL of TEP in a PYREX set up. The reaction was set at room temperature for 3 days.

3. Cork powder modified by DTSP (C<sub>d</sub>) via the proposed reaction presented in Figure III.17.



**Figure III.17.** Proposed reaction of cork powder and DTSP.

- Condition 1: 1 gr of cork powder was mixed with 5 gr of DTSP in 20 mL toluene under a reflux set up. The reaction was set at 120 °C for 12 hours under nitrogen atmosphere.

Analytical grades of ammonia, IPA, DCM and toluene were used to wash the excessive remaining phosphorus on the surface of cork powder.



### *III.4 Melt-compounding and specimens' preparation*

The neat ABS and ABS composites were melt-compounded in a mixing chamber (Brabender, Duisburg, Germany) (Figure III.18) under fixed processing conditions including a blending time and temperature of 10 min and 160 °C respectively and a screws rotating rate of 60 rpm. Previous to melt compounding, ABS, APP, AlPi and cork were dried under vacuum in a convection oven in order to minimize the moisture and degradation during melt compounding. APP, AlPi and cork were dried overnight at 100 °C, ABS for 4 h at 80 °C.



**Figure III.18.** Digital photograph of Brabender mixing chamber.

Samples were prepared by using compression molding technique in a hot-plate press (IQAP-LAP PL-15) shown in Figure III.19. The materials after melt-compounding were directly placed into a square and circular molds with different dimensions. The circular mold with a diameter of 75 mm and thickness of 4 mm and the square mold with dimension of 120 mm and average of 3.2 mm thickness were used to prepare samples for different characterizations. A temperature of 170 °C was applied for 6 minutes and then 2 minutes under 80 bar of pressure. Subsequent cooling, under a constant pressure of 80 bar for 4 min, was applied at the end of the compression cycle. Then, specimens were cut for the characterizations following the standards.



**Figure III.19.** Digital photograph of the hot-plate press.

The composition of the melt-compounded materials studied in this thesis is listed in Table III.1.

**Table III.1.** Samples identification and composition in weight %.

<b>Materials</b>	<b>ABS</b>	<b>APP</b>	<b>AlPi</b>	<b>E24</b>	<b>E29</b>	<b>UHMW-SR</b>	<b>Cork</b>	<b>C<sub>g</sub></b>	<b>C<sub>d</sub></b>
ABS	100	-	-	-	-	-	-	-	-
ABS S	98	-	-	-	-	2	-	-	-
ABS E24	95	-	-	5	-	-	-	-	-
ABS E29	95	-	-	-	5	-	-	-	-
ABS E29 S	93	-	-	-	5	2	-	-	-
ABS P	80	10	10	-	-	-	-	-	-
ABS S P	78	10	10	-	-	2	-	-	-
ABS E24 P	75	10	10	5	-	-	-	-	-
ABS E29 P	75	10	10	-	5	-	-	-	-
ABS E24 S P	73	10	10	-	5	2	-	-	-
ABS E29 S P	73	10	10	-	5	2	-	-	-
ABS/30APP	70	30	-	-	-	-	-	-	-
ABS/1C/29APP	70	29	-	-	-	-	1	-	-
ABS/3C/27APP	70	27	-	-	-	-	3	-	-
ABS/5C/25APP	70	25	-	-	-	-	5	-	-
ABS/10C/20APP	70	20	-	-	-	-	10	-	-
ABS/15C/15APP	70	15	-	-	-	-	15	-	-
ABS/20C/10APP	70	10	-	-	-	-	20	-	-
ABS/25C/5APP	70	5	-	-	-	-	25	-	-
ABS/30C	70	-	-	-	-	-	30	-	-
ABS/30C <sub>g</sub>	70	-	-	-	-	-	-	30	-
ABS/30C <sub>d</sub>	70	-	-	-	-	-	-	-	30
ABS/20C <sub>g</sub> /10APP	70	10	-	-	-	-	-	20	-
ABS/20C <sub>d</sub> /10APP	70	10	-	-	-	-	-	-	20
ABS/3C <sub>g</sub> /27APP	70	27	-	-	-	-	-	3	-
ABS/3C <sub>d</sub> /27APP	70	27	-	-	-	-	-	-	3

### *III.5 Morphological and physical characterization*

#### *III.5.1 Scanning electron microscopy*

The morphology of fracture surface of the composites and the residue after cone calorimetry tests were analyzed using a JEOL JSM-5610 SEM. Samples were prepared by sputter depositing a thin layer of gold onto the fracture surface, the upper and inner surface of ashes in argon atmosphere using a BAL-TEC SCSD005 Sputter Coater (Figure III.20).



**Figure III.20.** Digital photograph of sputter coater and SEM.

#### *III.5.2 Cork particle size and density*

The particle size distribution of the cork powder, as received, was determined by a laser diffraction particle size analyzer (LDS), shown in Figure III.21, using LS 13 320 equipment (Beckman Coulter, Indiana, United States). LS 13 320 software (Beckman Coulter, Indiana, United States) was used to calculate the values such as  $D_{50}$ , which is the median diameter or the medium value of the particle size distribution and the value of the particle diameter at 50% in the cumulative distribution. The  $D_{90}$  was also calculated to describe the diameter where 90% of the distribution

has a smaller particle size and ten percent has a larger particle size. The mean value, a calculated value similar to the concept of average, was also obtained. An AccuPyc II 1340 helium pycnometer (Micrometritics, Georgia, United States) was used to determine the density of the cork powder.



**Figure III.21.** Digital photograph of LDS analyzer.

### *III.6 Thermal analysis*

#### *III.6.1 Thermogravimetric analysis*

Thermal stability under pyrolysis conditions was characterized by means of TGA under nitrogen atmosphere, using a Mettler Toledo STAR System model SMP/PF7548/MET/400W and a NETZSCH-Gerätebau GmbH equipment with a constant heating rate of 10 °C/min from 30 °C to 800 °C. For each experiment a mass of 5-10 mg and a gas flow rate of 250 mL/min were used.

#### *III.7 Dynamic mechanical thermal analysis*

DMTA was used to study the influence of the additives in thermo-mechanical behavior of ABS composites. A DMA Q800 model from TA instruments (Figure III.22) was used and calibrated in a single cantilever configuration. The experiments were performed from 30 °C to 150 °C at a

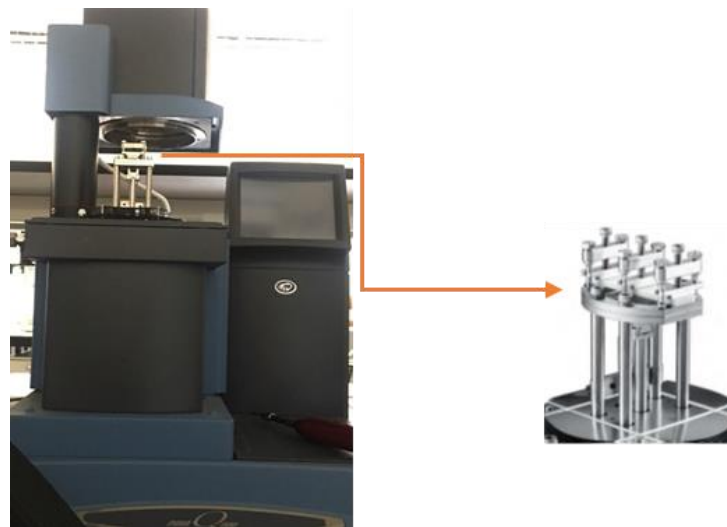
heating rate of 2 °C/min and frequency of 1 Hz applying a dynamic strain of 1%. Specimens were cut with an average length of  $35 \pm 0.1$  mm, width of  $12.75 \pm 0.1$  mm, and thickness of  $3 \pm 0.1$  mm. Dynamic mechanical properties of a material are described by the storage and loss modulus and tan delta through the following expressions:

$$E' = (\sigma/\varepsilon) \times \cos \delta \quad (1)$$

$$E'' = (\sigma/\varepsilon) \times \sin \delta \quad (2)$$

$$\tan \delta = E''/E' \quad (3)$$

Where  $E'$  is storage modulus,  $E''$  is loss modulus,  $\sigma$  is the stress,  $\varepsilon$  is the deformation and  $\delta$  is the phase difference between the applied strain and the tension produced. The peaks in loss modulus and tan delta curves present the window of the glass transition temperatures.

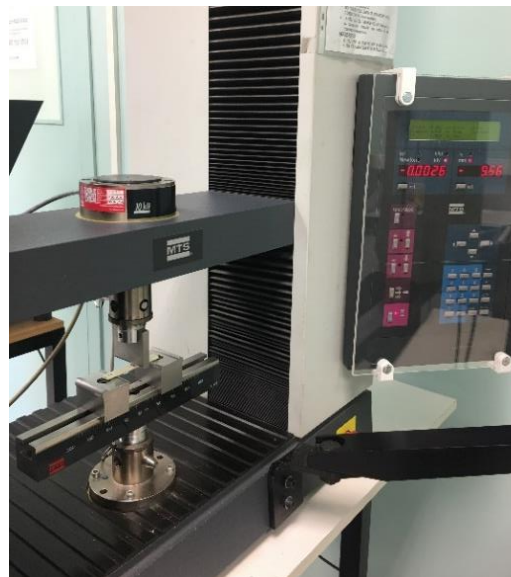


**Figure III.22.** Digital photograph of DMTA.

### III.8 Mechanical characterization

#### III.8.1 Three-point bending test

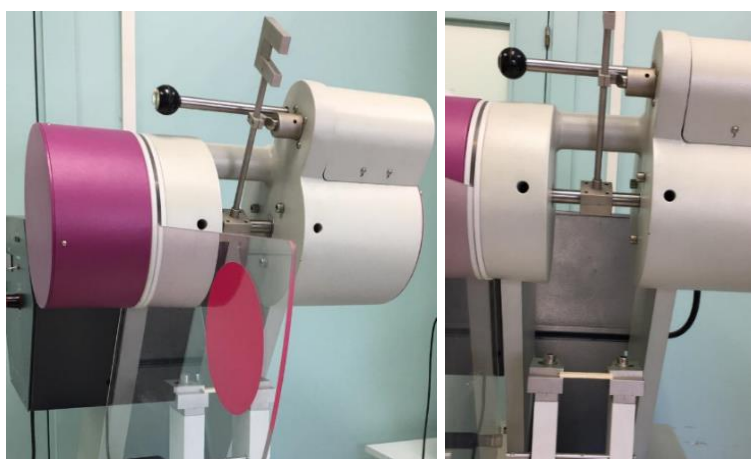
Flexural test was conducted according to ASTM D 790. Specimens of  $80 \times 10 \times 3.2 \text{ mm}^3$  were loaded in three point bending with a recommended span (L) to depth (d) ratio of 16:1 ( $L = 16d$ ). The test was conducted on the MTS 810 Material Test System (Figure III.23) using data acquisition software Test Works-II using a load cell of 10kN at 1 mm/min rate of loading. For each formulation, three to five specimens were tested and an average result was obtained. Flexural strength ( $\sigma_f$ ) was calculated according to maximum of  $\sigma_f = (3PL)/(2bd^2)$ , where  $\sigma_f$  (MPa) is the stress; P (N) is the load; L is the support span (mm); b is the width of beam tested (mm); and d is the depth of beam tested (mm). Flexural strain is given by  $\epsilon_f = (600sd)/(L^2)$ , where s is the deflection. The flexural modulus is calculated from the slope of the initial portion of the stress-strain curve.



**Figure III.23.** Digital photograph of three-point bending testing machine.

### *III.8.2 Charpy impact test*

Charpy notched impact strength was determined using a Zwick HIT 5.5P testing machine (Figure III.24). Specimens were tested according to ISO 179 standard. Specimens were  $70 \pm 0.5$  mm in length,  $10 \pm 0.1$  mm wide and  $4 \pm 0.1$  mm thick and a notch (type A) of 2 mm depth was done according to ISO 2818. All specimens were tested using a pendulum size of 1 J at room temperature.



**Figure III.24.** Digital photograph of Charpy impact strength testing machine.

## *III.9 Chemical characterization*

### *III.9.1 Attenuated total reflectance and Fourier transform infrared spectroscopy*

Attenuated total reflectance-Fourier transform infrared (ATR-FTIR) spectroscopy using a Nicolet™ 510 with ZnSe lenses and a single-reflection diamond ATR element, was employed to analyze the chemical nature of cork, its components and phosphorylated cork (Figure III.25). The measurements were obtained in the spectral range of  $4000\text{ cm}^{-1}$  to  $400\text{ cm}^{-1}$ . Also, the FTIR spectrometer, Nicolet™ 510, was used to analyze the chemical nature of ABS composites' residue after fire-reaction tests. The samples were prepared by mixing 1 mg of dried samples with 100 mg



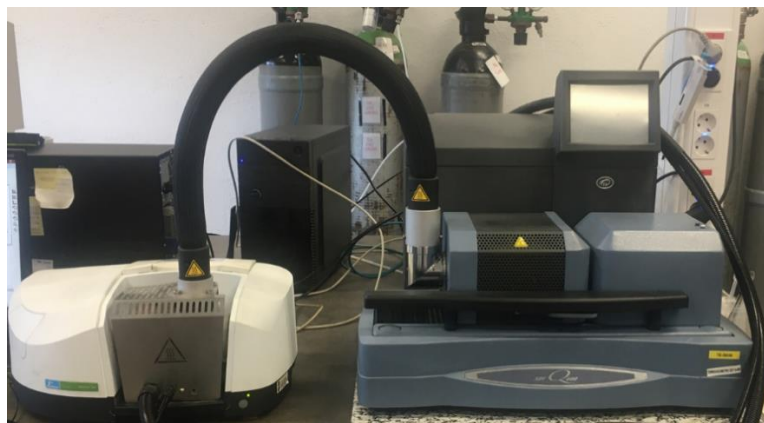
of pure KBr, pressed at a pressure of 10 Ton into pellets and analyzed using OMNIC™ software. Measurements were obtained in the spectral range of 4000 to 400  $\text{cm}^{-1}$ . Also,



**Figure III.25.** Digital photograph of ATR-FTIR and FTIR spectrometers.

### *III.9.2 TGA-FTIR*

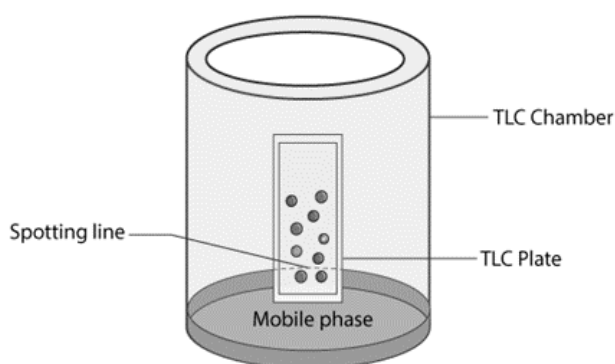
A TGA, using SDT Q600 equipment model (TA Instruments), coupled with a Fourier-transformed infrared spectrometer (FT-IR) presented in Figure III.26, was carried out in order to investigate the volatile emissions during the decomposition of the samples under study by means of a TG-IR-GCMS Interface TL8000 (Perkin Elmer, USA) and a IR Spectrum Two™ equipment (Perkin Elmer, USA). The interface device operated with a gas flow of 80 mL/min and a temperature of 250 °C.



**Figure III.26.** Digital photograph of TGA coupled FTIR analyzer.

### III.9.3 Thin layer chromatography

Thin layer chromatography (TLC), a chromatographic technique, was used to determine if a reaction is complete (Figure III.27). For the detection of phosphorus presence and confirming if the bonding was a chemical bonding or physical bonding to the surface of cork powder, pre-coated HPTLC plates (silica gel 60 F254, Merck Ltd., Darmstadt, Germany) were used. Different solvent systems for phosphorus residues for each reaction were prepared. Standard glyphosate, TEP, DTSP and modified cork were prepared in methanol and DCM (2 mg/mL) under 5 minutes of sonication. The samples were spotted on the HPTLC plates with fine capillary tubes along with pure phosphorus components as the control sample. The plates were dried, and the chromatogram was developed in a pre-saturated tank containing the solvent system. After developing the plates, the extra solvent was evaporated (dried) in a fume hood. The plates were then dipped in aqueous chromogenic reagent, potassium permanganate. After that, intense purple spots for the control samples were observed and if for the modified cork any spot showing presence of phosphorus residue was detected the samples were washed again to remove the phosphorus residue. The washing procedure continued until no spot appeared for the modified cork samples.



**Figure III.27.** Scheme of TLC technique.

### *III.9.4 Gas chromatography–mass spectrometry*

Gas chromatography–mass spectrometry (GC–MS) is an analytical method that combines the features of gas-chromatography and mass spectrometry to identify different substances within a test sample. The digital photograph of the GC-MS system is presented in Figure III.28. Analytical GC-MS was performed on a Carlo Erba Fractovap 2150 with a FID (DB5-column, 28 m; Carlo Erba, Thermo Finnigan, Hemel Hempstead, UK). Cork modified by different phosphorus compounds was sonicated in different solvents. C<sub>g</sub>, C<sub>t</sub> and C<sub>d</sub> samples as well as the reference samples of glyphosate, TEP and DTSP were prepared and sonicated for five minutes in DCM. The solvent was filtered and collected to perform GC-MS in order to detect the presence of the phosphorus components of glyphosate, TEP and DTSP.



**Figure III.28.** Gas chromatography-mass spectrometry system.

### *III.9.5 X-ray photoelectron spectroscopy*

X-ray Photoelectron Spectroscopy (XPS) is a technique which analyzes the elements constituting the sample surface, its composition, and chemical bonding state by irradiating x-rays on the sample surface, and measuring the kinetic energy of the photoelectrons emitted from the sample surface. XPS was carried out on a Thermo Scientific K-Alpha spectrometer using Al K<sub>α</sub> radiation to analyze the surface composition of phosphorylated cork powder.

### III.10 Fire performance analysis

#### III.10.1 Limiting oxygen index

LOI measurements was performed in an oxygen/nitrogen atmosphere (Figure III.29), in accordance with ISO 4589 standard, on  $80 \times 10 \times 4 \text{ mm}^3$  specimens.

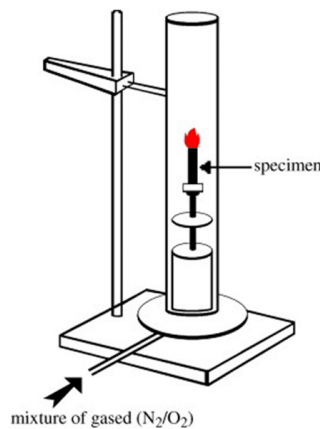
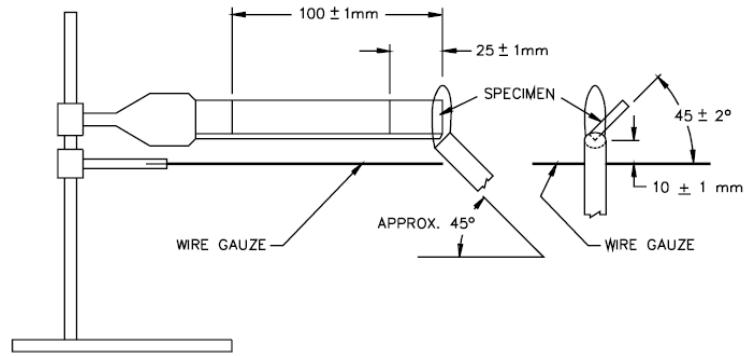


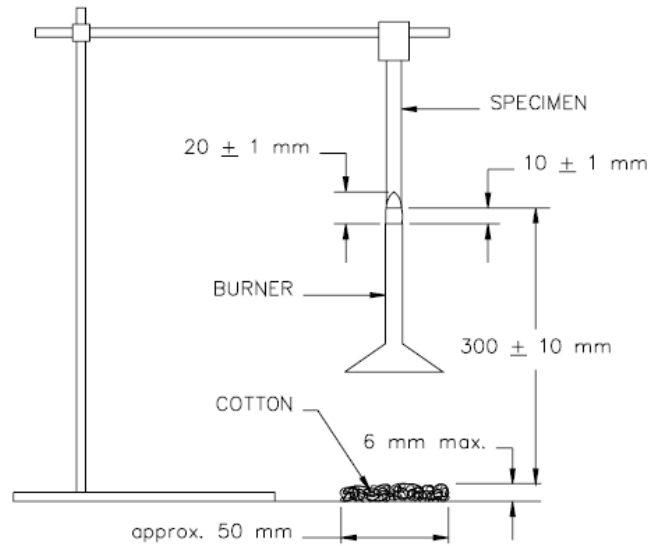
Figure III.29. Scheme of LOI measurement setup.

#### III.10.2 UL-94 flammability test

The flammability behavior was investigated by the UL-94 test on  $125 \times 12.5 \times 3.2 \text{ mm}^3$  specimens ignited from one side of specimens in the horizontal (Figure III.30) and the vertical (Figure III.31) configurations according to the standard of UL-94 (Underwriters Laboratories, USA). In vertical test, the samples were classified regarding Table III.2. Linear burning rate (LBR) was calculated in the horizontal configuration by standard through  $LBR = 60 L/t$  in mm/minute, where L is the damaged length in mm and t is time, in seconds (If the flame front passed the 100 mm mark of specimens,  $L = 75 \text{ mm}$ ).



**Figure III.30.** Scheme of horizontal UL-94 setup.



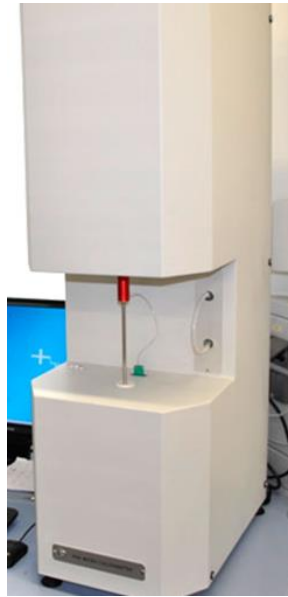
**Figure III.31.** Scheme of vertical UL-94 setup.

**Table III.2.** Vertical UL-94 materials classifications.

Criteria conditions	V-0	V-1	V-2
Afterflame time for each individual specimen $t_1$ or $t_2$	$\leq 10s$	$\leq 30s$	$\leq 30s$
Total afterflame time for any condition set ( $t_1$ plus $t_2$ for the 5 specimens)	$\leq 50s$	$\leq 250s$	$\leq 250s$
Afterflame plus afterglow time for each individual specimen after the second flame application ( $t_2+t_3$ )	$\leq 30s$	$\leq 60s$	$\leq 60s$
Afterflame or afterglow of any specimen up to the holding clamp	No	No	No
Cotton indicator ignited by flaming particles or drops	No	No	Yes

### III.10.3 Micro-scale combustion calorimetry

MCC, known as a pyrolysis combustion flow calorimeter (PCFC) from Fire Testing Technology (FTT) was used following ASTM D7309 standard (Figure III.32). A  $10 \pm 0.5$  mg of each sample was exposed to a heating rate of  $1 \text{ }^\circ\text{C/s}$  from  $150 \text{ }^\circ\text{C}$  to  $700 \text{ }^\circ\text{C}$  under  $\text{N}_2$ . The pyrolysis gasses were evacuated into an oven at  $900 \text{ }^\circ\text{C}$ , containing a gas flow of 80/20 of  $\text{N}_2/\text{O}_2$  mixture, where its total combustion took place and the oxygen consumption was determined. MCC is a useful instrument to evaluate the heat release rate and the fuel content of the decomposing volatile products. The curves of HRR versus temperature were plotted and the peak of heat release rate, the temperature of the pHRR ( $T_{\text{pHRR}}$ ), THR and residue were measured.



**Figure III.32.** Digital photograph of MCC.

### III.10.4 Cone calorimetry

Reaction-to-fire tests were carried out by means of a cone calorimeter (INELTEC, Barcelona, Spain) according to ISO 5660 standard procedure. Specimens of ABS and ABS composites with diameter of  $75 \pm 0.1$  mm and thickness of  $4 \pm 0.1$  mm were irradiated with a constant heat flux of  $35 \text{ kW/m}^2$  using a constant distance between the electrical resistance and the specimen of 25 mm. HRR vs. time curves were registered during the tests. Typical fire-reaction parameters such as time

to ignition (TTI), pHRR, the time to PHRR ( $t_{\text{PHRR}}$ ), time of combustion ( $t_{\text{combustion}}$ ), total heat emitted (THE), effective heat of combustion (EHC), maximum average rate of heat emission (MARHE) and residue were obtained from the cone calorimeter tests. Furthermore, a fire retardancy index (FRI) was also determined (Equation 1) to quantify the flame retardancy performance of ABS composites [147].

$$\text{FRI} = \frac{\left(\left(\frac{\text{pHRR}}{\text{TTI}}\right) \times \text{THR}\right)_{\text{neat polymer}}}{\left(\left(\frac{\text{pHRR}}{\text{TTI}}\right) \times \text{THR}\right)_{\text{composite}}} \quad (1)$$

The photograph of a burning sample under cone calorimeter is shown in Figure III.33.



**Figure III.33.** Digital photograph of cone calorimeter while burning a sample.





Confidential

Chapter

IV



The components' roles in thermal stability  
and flammability of cork powder

Chapter

V



## Chapter V: The components' roles in thermal stability and flammability of cork powder

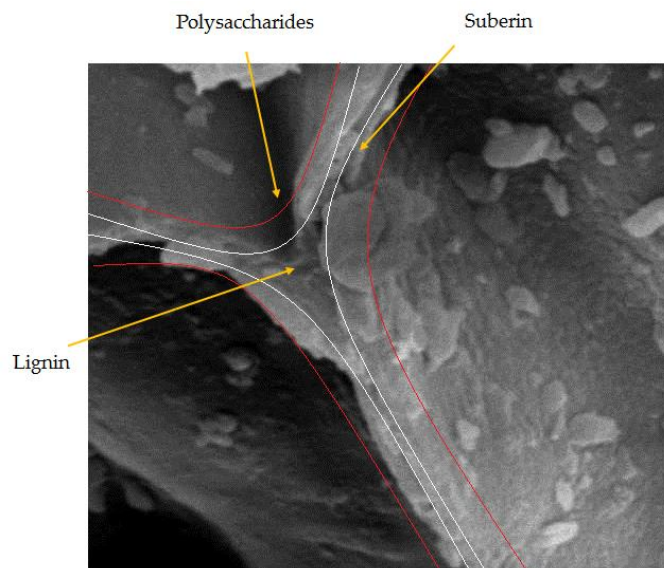
### *V.1 Introduction*

Interest in bio-materials is rapidly growing due to concerns about the environment and their unique characteristics: they are renewable, completely or partially recyclable and bio-degradable [23, 76, 169].

Cork is a biological tissue that is the outer bark of the oak tree *Quercus suber L.* that acts as a protective layer and is harvested each 9–12 years [32, 33, 35, 38, 170]. Due to cork's remarkable properties such as super compressibility without fracture, full recovery, impermeability and heat insulation, this lignocellulosic material has been widely used in various applications, for example, wine stoppers and construction materials for acoustic and thermal insulation [171-174].

The macroscopic cellular structure of cork presents an alveolar structure similar to a honeycomb with close cellular structure and thin-walled cells. The cells are rectangular prisms, packed base-to-base in columns parallel to the radial direction of the tree. The walls of cork cells are made of a thin, lignin-rich middle lamella (internal primary wall), a thick secondary wall of suberin and wax lamella and an outer tertiary wall of polysaccharides such as cellulose and hemicellulose (Figure V.1) [93, 94].

Suberin, the main component of cork, is a polyester consisting of natural aliphatic and aromatic macromolecules linked via ester bonds that provides cork with corrosion resistance and anti-aging characteristics [175]. The second major component of cork is lignin, a highly cross-linked aromatic phenolic polymer which causes durability of cork by increasing stress resistance, mechanical strength and hardness of cork cellular walls. Polysaccharides are also present in cork cellular structure as polysaccharide derivatives consisting of chains of mono-saccharides with intermediate linkages and contribute to the structural rigidity of the cork cells [172, 176, 177]. Finally, the last parts of cork chemical composition are extractives, which generally include phenolic compounds, terpenoids, fatty acids, resin acids and waxes [178].



**Figure V.1.** Schematic of cork cells wall presenting the position of each main component.

Different applications have been reported for components of cork; for example, suberin is used as a starting agent for production of polyurethane [179] and polyester polymers [180, 181] and a grafting agent for polymer composites [182], ink additives [183] and cosmetic and pharmaceuticals products [184, 185]. Lignin has applications within the sustainable construction industry such as lignin admixture and additives for concrete, lignin modified asphalts, lignin-based paints and coatings [186] or as reinforcing fillers in polymeric composites and an adhesive promoter in natural fiber composites [187, 188]. Polysaccharides are used in pharmaceutical [177], food and packaging applications [189, 190].

As a result of cork processing and manufacturing of different cork products, the cork industry generates substantial amounts of cork dust (the so-called “cork powder”), approximately 30% of the bulk material, which is usually considered a waste with low economic value and burned in boilers of industrial processes or disposed of in landfills [30, 36, 191]. Therefore, it is economically interesting to find a more valuable alternative application for this industrial waste bio-material. Recent studies were carried out in order to obtain “green materials” to improve polymers fire retardancy through the development of flame-retardant bio-composites [24]. Lignocellulosic-based materials are capable of producing charred residues, which can be particularly important for developing more sustainable intumescent flame retardants (IFR). Several studies reported that halogen-free flame retardants combined with bio-based materials

such as starch [26], lignin [192] and cellulose [193] resulted in an improvement in fire retardancy of thermoplastics by producing a foamed, thermally stable char and consequently protecting the underlying material against fire propagation.

In this sense, it is important to fully understand the chemical nature of cork powder to find a more valuable application for this bio-waste as, for instance, a potential synergistic in flame retardant systems. Although some studies are conducted to investigate the thermal stability of cork powder, to the best of authors' knowledge, there is a lack of studies regarding its flammability and the mechanisms of action of cork's main chemical components in its fire reaction.

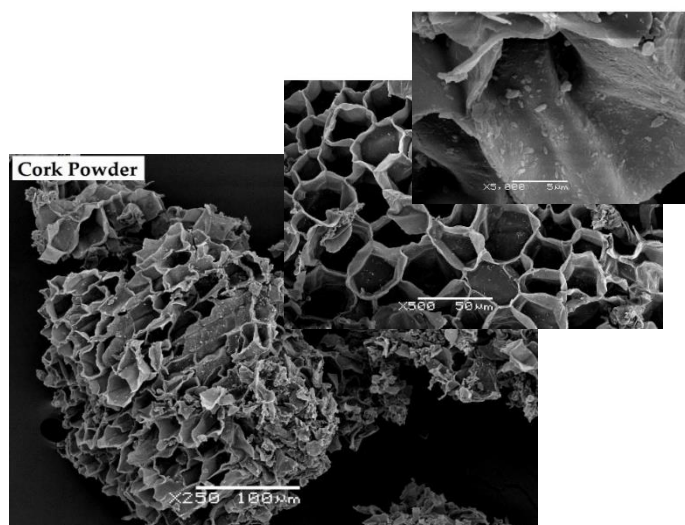
With all that in mind, in the present chapter, after the extraction of the main component of the cork, the chemical analysis, thermal stability and fire behavior of cork powder, its extractives, suberin and lignocellulosic components, are reported in detail.

## *V.2 Results and Discussion*

### *V.2.1 Particle size distribution, density and morphology of cork powder*

A density of 1.526 g/cm<sup>3</sup> was registered in accordance with the studies reported for the density of cork powder and cell walls [194, 195]. A symmetric distribution with a 218 μm average value of particle size, a D<sub>50</sub> of 147 μm and a D<sub>90</sub> of 500 μm for cork powder were obtained.

Cellular structure of cork powder was observed by SEM (Figure V.2). The cells are described as rectangular prisms in previous studies and are packed base-to-base in columns parallel to the radial direction of the tree [94]. The anisotropy of cork's cellular structure, which was observed in SEM, can result in its anisotropic properties [196]. In Figure 3, a representative particle with an average diameter size of 200–250 μm can be observed, in agreement with the obtained average dimensions. Likewise, it was observed that cutting or grinding cork during industrial processing results in the deformation or partial breakage of its cellular structure.



**Figure V.2.** SEM micrographs of cork powder at 250 $\times$ , 500 $\times$  and 5000 $\times$  with a scale bar of 100, 50 and 5  $\mu\text{m}$ , respectively.

### V.2.2 Chemical composition and analysis of cork components

The results obtained for the summative chemical composition of cork powder are summarized in Table V.1. The chemical composition of cork mainly depends on different factors such as geographic origin of cork, climate of the origin, soil, tree dimensions and growth conditions [94]. The results were in agreement with the range reported for cork components in the literature [175, 176].

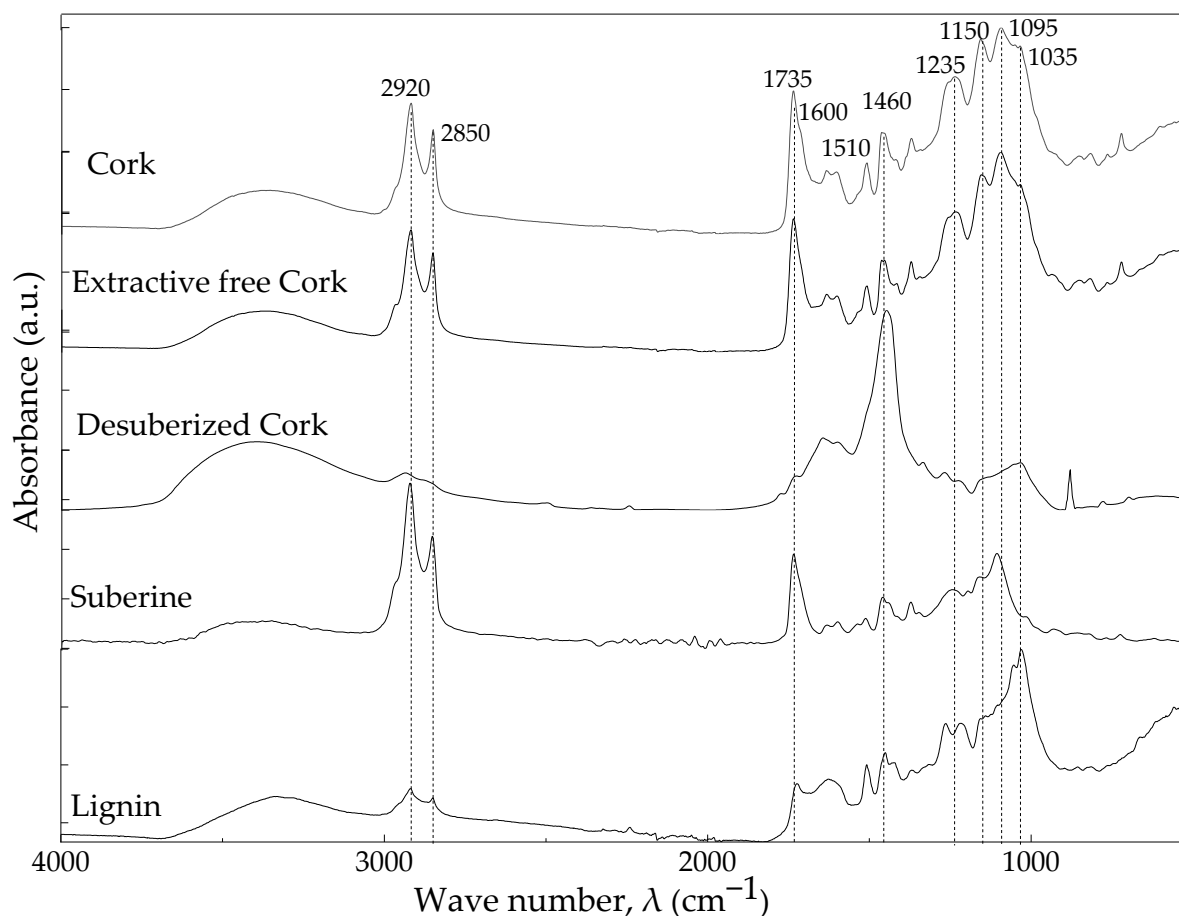
**Table V.1.** Chemical composition of cork powder.

Chemical Component	Wt.% *
Suberin	40
Lignin	24
Polysaccharides	19
Extractives	14
-DCM Extractives	7
-Ethanol Extractives	3
-Water Extractives	4
Ash	3
Total mass	100

\* Each value is the average of performed experiments with variation coefficients within 0.02–0.8.



The chemical nature of cork powder and its main components was characterized by means of ATR-FTIR spectrometry. Figure V.3 shows the normalized ATR-FTIR spectra of cork powder, extractive-free cork, desuberized cork, suberine and lignin.



**Figure V.3.** ATR-FTIR spectra of cork powder, extractive-free cork, desuberized cork, suberine and lignin.

All materials presented a broad absorbance band between  $3700\text{ cm}^{-1}$  and  $3000\text{ cm}^{-1}$ , characteristic of the hydroxyl groups stretching, presented in their chemical structure. Peaks at  $2920\text{ cm}^{-1}$  and  $2850\text{ cm}^{-1}$  were mainly attributed to the aliphatic chains of suberine, characteristics of asymmetric and symmetric C-H stretching vibrations, respectively [197-199]. The absorbance peaks at  $1735\text{ cm}^{-1}$ ,  $1235\text{ cm}^{-1}$  and  $1150\text{ cm}^{-1}$  were assigned to C=O, symmetric and asymmetric C-O stretching of the suberine ester group, respectively [197-203]. The peak registered at  $1460\text{ cm}^{-1}$  is also characteristics of C-H asymmetric deformation of suberine, as well as of lignin and

polysaccharides [198, 201]. Desuberized (lignin and polysaccharides) cork showed a disappearance of the main absorbance peaks of suberin at 2920, 2850, 1735, 1235 and 1150  $\text{cm}^{-1}$ . This fact indicates that suberin was successfully extracted from the cork powder. Furthermore, besides the mentioned characteristic peaks of suberin, peaks between 1600  $\text{cm}^{-1}$  and 1500  $\text{cm}^{-1}$  and at 1095  $\text{cm}^{-1}$  were registered in the Suberin spectra (see Figure V.3), which could be related to lignin and polysaccharide presence. Particularly, C=C stretching registered at 1600  $\text{cm}^{-1}$  and 1510  $\text{cm}^{-1}$  was assigned to the stretching of G-lignin aromatic ring vibrations [182]. The absorbance peaks at 1095  $\text{cm}^{-1}$  and 1035  $\text{cm}^{-1}$  are characteristic of C-O vibrations stretching the vibration of polysaccharides and lignin, respectively [198, 201, 203].

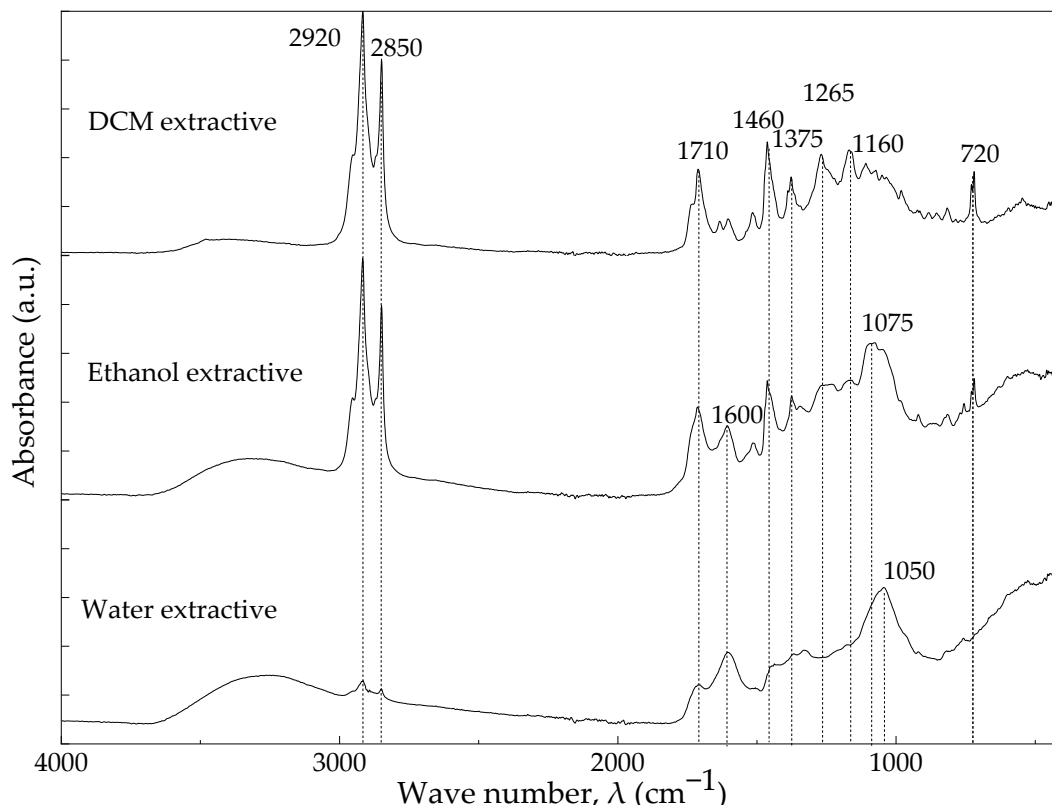
The spectrum of the extractive-free cork was identical to the one of the cork powder, which can be due to the relatively low amount of extractives in the cork (see Table 1).

Figure V.4 shows the ATR-FTIR spectra of cork extractives. In fact, extractives are not chemically bonded to the cork structure and can be extracted by polar and non-polar solvents [94]. Non-polar extractives were extracted by DCM, and polar extractives were extracted by ethanol and water. Non-polar extractives reportedly consist of waxes with aliphatic and aromatic compounds such as glycerol, fatty acids, triterpenes, while the main parts of polar extractives are phenolic compounds such as phenolic acids and tannins [94, 204].

Spectrum of DCM showed a broad absorbance band with low intensity between 3700  $\text{cm}^{-1}$  and 3000  $\text{cm}^{-1}$ , which is characteristic of hydroxyl groups. This band has a significantly lower intensity than that of polar extractives. The strong peaks at 2920  $\text{cm}^{-1}$  and 2850  $\text{cm}^{-1}$  are characteristic of symmetric and asymmetric C-H vibrations present in the aliphatic structure of terpenes of the waxy material. At 1710  $\text{cm}^{-1}$ , characteristic peaks of carbonyl as carboxylic acid function group and at 1460  $\text{cm}^{-1}$  characteristic of aromatic C-C vibration were presented [205-207]. In addition, the peak at 720  $\text{cm}^{-1}$  was attributed to the C-H bond related to the vinyl group of terpenes [202].

The absorbance band between 3700  $\text{cm}^{-1}$  and 3000  $\text{cm}^{-1}$  was also observed for ethanol extractives with a higher intensity compared to the non-polar one, corresponding to OH groups of tannins and phenolic compounds. The vibrations at 2920  $\text{cm}^{-1}$  and 2850  $\text{cm}^{-1}$  are characteristic of C-H vibrations present in aliphatic parts of phenolic acids found in ethanol extractives such as, ferulic acid, vanillic acid and cinnamic acid [94]. The signs at 1710  $\text{cm}^{-1}$ , 1600  $\text{cm}^{-1}$ , 1460  $\text{cm}^{-1}$  and 1075  $\text{cm}^{-1}$ , respectively, correspond to C=O carboxylic stretching, aromatic C=C stretch,

aromatic C-C vibration, C-O asymmetrical stretching, which are typically observed in phenolic compounds [202, 207, 208].



**Figure V.4.** ATR-FTIR spectra of DCM, ethanol and water extractives.

ATR-FTIR spectra of water extractive of cork also presented the same broad band of OH groups at  $3700\text{--}3000\text{ cm}^{-1}$ . The intensity of the peaks at  $2920\text{ cm}^{-1}$  and  $2850\text{ cm}^{-1}$ , corresponding to C-H vibrations, which are characteristics of phenolic compounds or water-soluble polysaccharides, was much lower compared to the rest of extractives. The signals of C=O stretching at  $1710\text{ cm}^{-1}$ , aromatic C-C vibration at  $1600\text{ cm}^{-1}$  and C-O asymmetrical stretching at  $1050\text{ cm}^{-1}$  were also registered for water extractives due to the presence of phenolic compounds [208]. Furthermore, compared to the rest of the extractives, the water extractive showed a decrease of  $1710\text{ cm}^{-1}$  and  $1460\text{ cm}^{-1}$  peaks intensity and a shift in C-O asymmetrical stretching from  $1075\text{ cm}^{-1}$  to  $1050\text{ cm}^{-1}$ .

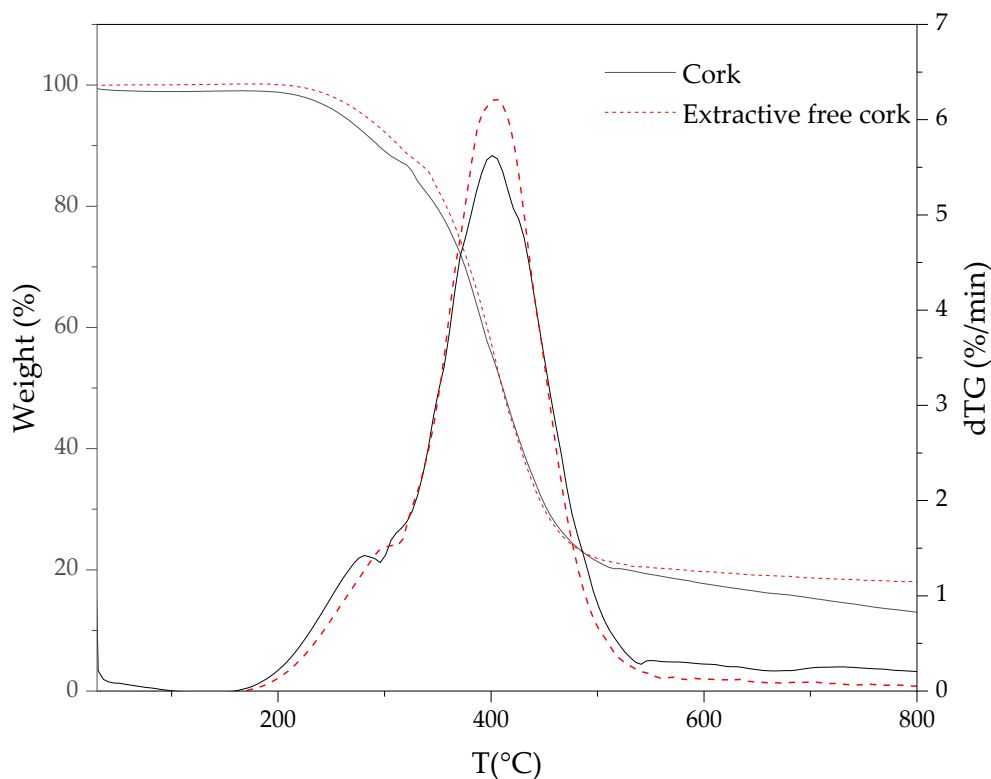
### V.2.3 Thermal stability of cork powder and its main components

Thermogravimetric analyses were carried out in order to characterize the role of each component in thermal stability of cork powder. Comparative thermogravimetric curves (TG) of pyrolysis and the first derivative of TG curves (dTG) obtained for cork and extractive-free cork are presented in Figure V.5. In addition, the temperature corresponding to  $T_{\text{peak}}$ , ML of each decomposition step and the amount of residue remained at 800 °C are shown in Table V.2.

**Table V.2.** TG and dTG data of thermal degradation and residue of cork and its main components.

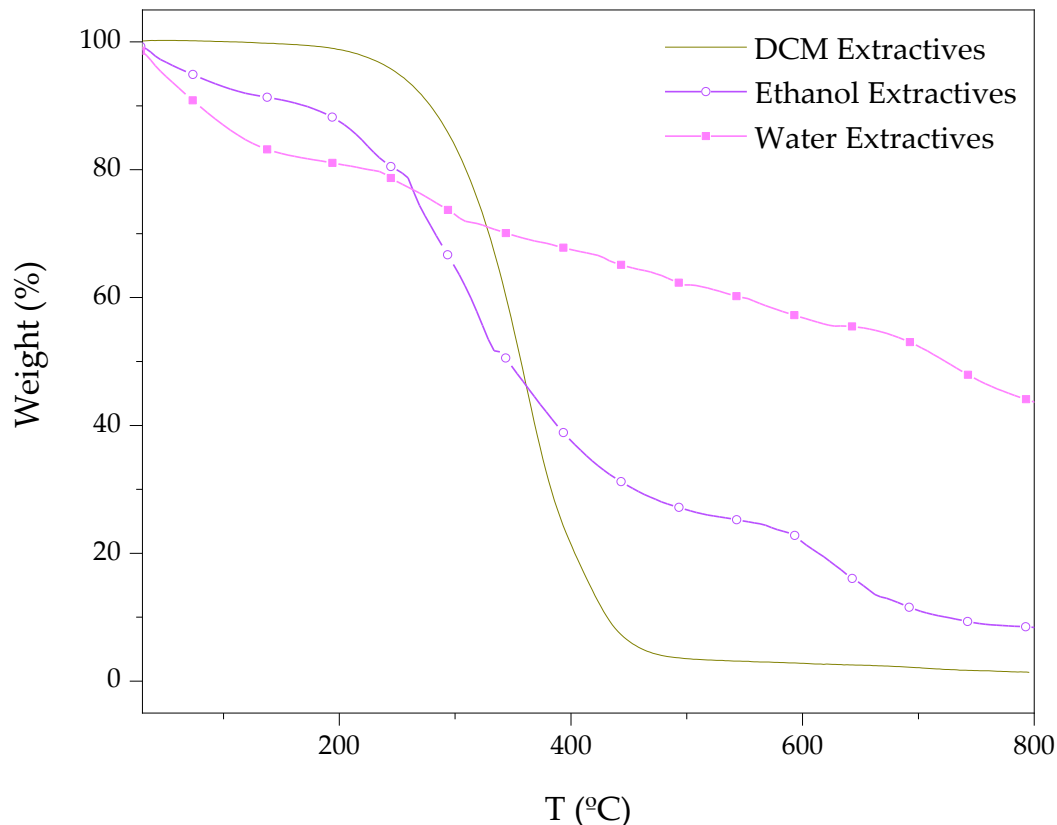
Materials	TD Step	T <sub>peak</sub> (°C)	ML (%)	R <sub>800 °C</sub> (%)
Cork	1	280	10.5	13.1
	2	400	70.1	
Extractive-free cork	1	300	8.7	17.1
	2	400	71.4	
Desuberized cork	1	65	5.1	32.6
	2	125	4.9	
	3	270	49.8	
Suberin	1	295	33.8	9.5
	2	420	52.1	
	3	740	1.5	
Lignin	1	60	6.7	29.4
	2	350	32.5	
DCM extractives	1	360	95.8	1.4
Ethanol extractives	1	310	66.1	16.7
	2	645	16.9	
Water extractives	1	280	16.3	60.1
	2	520	12.1	
	3	745	11.4	

Untreated cork started to decompose between 180 °C and 290 °C (see Figure V.5), followed by a higher mass loss of 70.1% between 290 °C and 600 °C.



**Figure V.5.** TG and dTG curves of cork and extractive-free cork obtained at 10 °C/min under N<sub>2</sub> atmosphere.

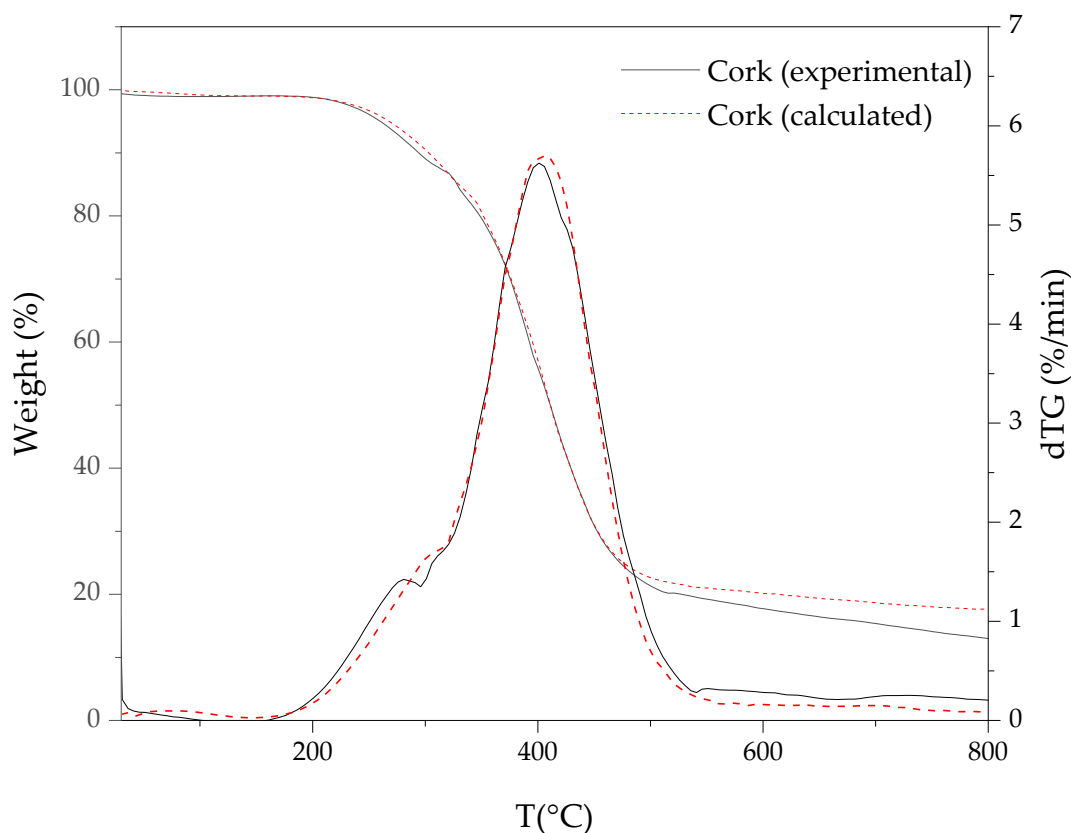
The removal of extractives from cork shifted the decomposition temperature, at a 5% of mass loss, from 260 °C to 280 °C and led to the formation of a more thermally stable residue between 500 °C and 800 °C. This fact implies that extractives can act as a catalyst by reducing the decomposition temperature of untreated cork and promoting the thermal decomposition of other components. Similar behavior was also observed for the contribution of extractives to the wood thermal degradation [209-211]. However, this effect contradicts the role of extractives in thermal stability improvement of cork in oxidative atmosphere [170]. An analysis of the different extractives' thermal stabilities was also conducted; the TG curves of the extractives are shown in Figure V.6.



**Figure V.6.** TG curves of cork extractives obtained at 10 °C/min under N<sub>2</sub> atmosphere.

As it is possible to see in Figure V.6, at 5% of mass loss, ethanol extractives showed a lower decomposition temperature compared to DCM and water extractives. Furthermore, above 350 °C, the polar extractives (ethanol and water extractives) showed a lower mass loss rate compared to the one observed for non-polar DCM extractives. In fact, the non-polar extractives only presented a 1.6% residue at 800 °C (see Table V.2). Meanwhile, the amount of residue at 800 °C for water and ethanol extractives was 60.1% and 16.7%, respectively.

In order to evaluate the possible catalytic effect of extractives on the cork thermal decomposition, the experimental and calculated TG and dTG curves of cork were compared (Figure V.7). The calculations were obtained from the TG/dTG contribution of the extractive-free cork and individual extractives; calculated cork = (86% × extractive-free cork + 7% × DCM extractives + 3% × ethanol extractives + 4% × water extractives).

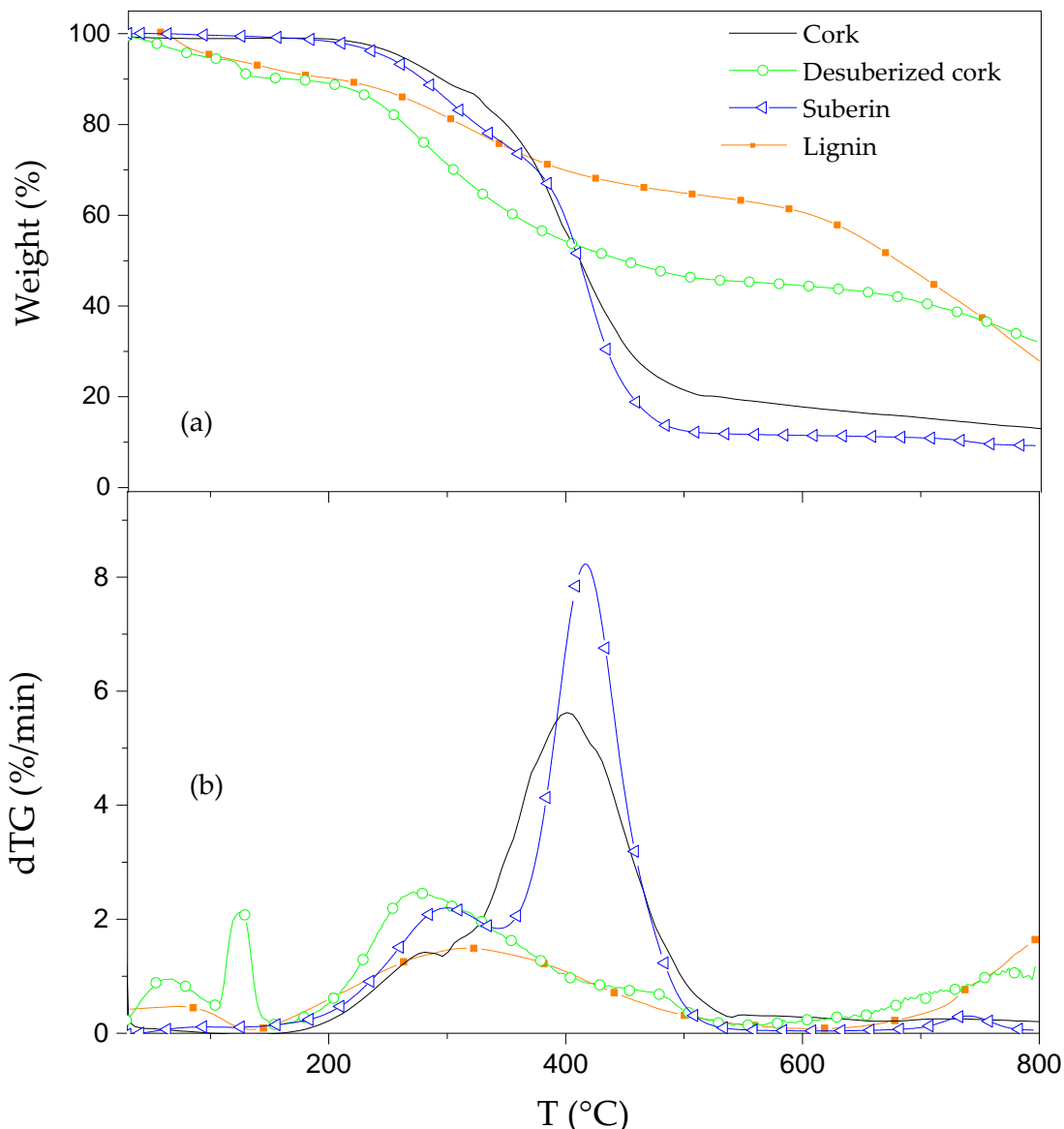


**Figure V.7.** Experimental and calculated TG and dTG of curves of cork at 10 °C/min under N<sub>2</sub> atmosphere.

The calculated curves show, between 200 °C and 300 °C, a slightly higher thermal stability than those registered in the experimental curves of cork. Thus, when extractives are inherently present in the cork composition, they promote a slightly higher thermal decomposition than expected in that range of temperature. Moreover, between 500 °C and 800 °C, the calculated curve shows a higher weight percentage than that of the experimental curve. These facts reinforce the catalytic effect of extractives on the beginning and end of cork thermal decomposition.

The comparative TG and dTG of cork, desuberized cork, suberin and lignin are shown in Figure V.8. Desuberized cork (or suberin free cork) showed a lower thermal stability than cork below 400 °C. This might be due to a higher loss of free and bounded water also observed in the case of polysaccharides from different bio-materials [212-214]. Its major mass loss occurred at 270 °C, 130 °C lower than that of cork, confirming the thermal stability effect of suberin on cork

thermal behavior. The higher residue observed in the desuberized cork samples could be due to the presence of sodium from the sodium methoxide, used for the extraction of suberin [170].



**Figure V.8.** (a) TG and (b) dTG curves of cork and extractive-free cork obtained at 10  $^{\circ}\text{C}/\text{min}$  under  $\text{N}_2$  atmosphere.

Suberin decomposes in two main steps, similar to cork. The first peak started slowly at 175  $^{\circ}\text{C}$  and continued to 390  $^{\circ}\text{C}$ , with a mass loss of 33.8%. It should be said that the mass loss of this step could be affected by the presence of residual lignin and polysaccharides detected in ATR-



FTIR curves. The second and major thermal decomposition step, between 390 °C and 500 °C, showed a 20 °C shift of  $T_{\text{peak}}$  to higher temperature compared to cork. This indicates that suberin contributes to increase the thermal stability of cork [202]. However, in both the mentioned thermal decomposition steps, the mass loss rate (%/min) was higher than that of cork.

Furthermore, it was reported that suberin is mainly composed of  $\omega$ -hydroxy acids and  $\alpha$ ,  $\omega$ -diacids [145]. The decomposition peaks of  $\omega$ -hydroxy acids and  $\alpha$ ,  $\omega$ -diacids, presented in suberin of different types of cork, were reported to be at 429 °C and 480 °C, respectively [145]. In this sense, it can be concluded that the present suberin is mainly composed of  $\omega$ -hydroxy acids. Lignin degraded in a broad step between 140 °C and 600 °C with a mass remaining of 59.4% at 600 °C. At lower temperatures, lignin decomposes due to the cleavage of alkyl-aryl ether linkages, while at higher temperatures the cleavage of aromatic rings and C-C bonds is the cause of thermal degradation [145, 170]. A small weight loss below 100 °C, due to free or bonded water, was also observed for lignin. By comparing lignin with desuberized cork (lignin and polysaccharides), it can be seen that lignin appears to be more thermally stable than polysaccharides at temperatures lower than 400 °C. Particularly, from the dTG desuberized and lignin curves, it is possible to observe that the mass loss rate of lignin was lower than that of desuberized sample. In addition, that  $T_{\text{peak}}$  of the major step decomposition, between 140 °C and 600 °C, was 75 °C higher in the case of lignin. This fact confirms that polysaccharides are the main responsible component for the first temperature peak in the thermal degradation of cork due to its lowest thermal stability among the other main components, and the same results were also observed for the cork components' contributions to the thermal behavior of cork in oxidative atmosphere [170].

#### *V.2.4 Potential flammability of cork powder and its main components*

In order to assess the flammability properties of cork and its components, MCC was used. In general, the fire behavior of materials is characterized by the amount of released heat when the material is exposed to a fire. MCC allows to obtain the HRR of materials using a low amount of the sample [215]. As it was described in Section 2, the MCC analysis consists of first heating the sample under pyrolysis conditions in a nitrogen atmosphere; then the degradation gasses are purged by an inert gas to the combustor, a chamber at 900 °C with a mixture of nitrogen (80%) and oxygen (20%), where these products are oxidized. The most representative flammability

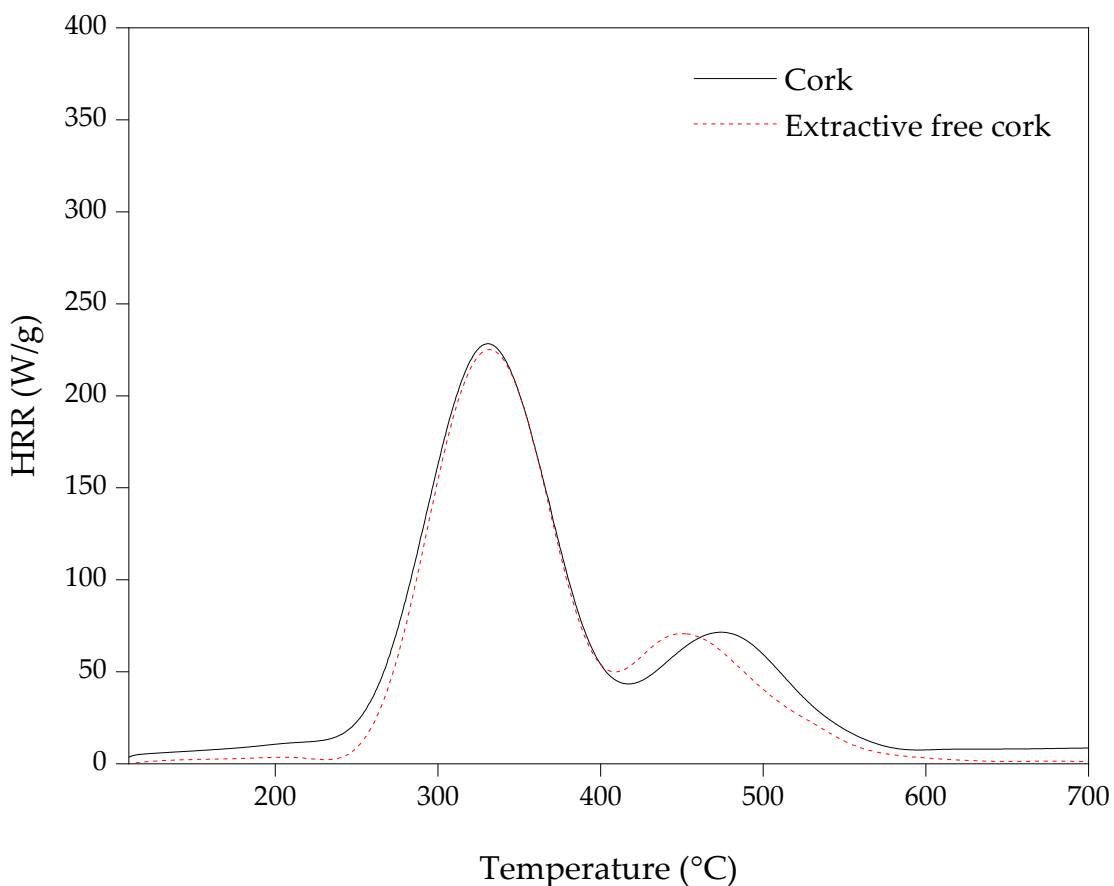
parameters, pHRR,  $T_{pHRR}$  and THR are summarized in Table V.3.  $T_{pHRR}$  represents the maximal heat flow temperature, and THR is obtained by integration of MCC curves.

**Table V.3.** Main results obtained from micro-scale combustion calorimetry.

Samples	pHRR (W/g)	THR (kJ/g)	Temperature to pHRR (°C)
Cork	230 ± 12	31.5 ± 0.3	330 ± 1
	70 ± 5		475 ± 1
Extractive-free cork	225 ± 12	27.7 ± 0.9	330 ± 2
	70 ± 5		455 ± 1
Desuberized cork	90 ± 2	24.1 ± 0.4	225 ± 1
	105 ± 8		365 ± 1
	80 ± 4		580 ± 0
Suberin	135 ± 17	27.2 ± 0.5	325 ± 1
	175 ± 11		390 ± 1
	80 ± 2		480 ± 0
Lignin	110 ± 12	26.8 ± 0.5	290 ± 1
	95 ± 12		490 ± 1
DCM extractive	365 ± 4	36.6 ± 0.7	410 ± 2
Ethanol extractive	220 ± 10	30.1 ± 0.9	385 ± 0
Water extractive	35 ± 0	4.1 ± 0.1	310 ± 2

Figure V.9 presents the heat release rate curves of cork powder and extractive-free cork. The cork started to degrade around 200 °C, and the heat release rate continued to increase by

increasing the temperature due to the release of combustible gasses during decomposition until it reached a maximum of 230 W/g at 330 °C.

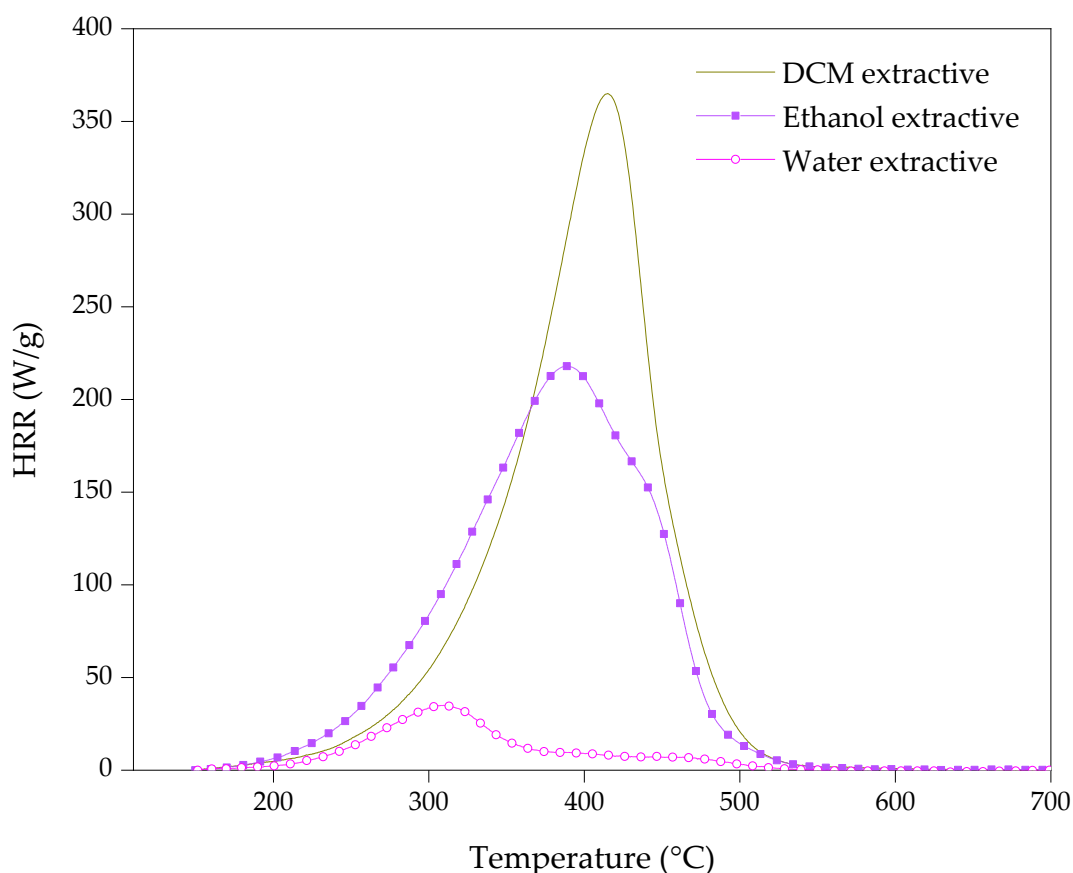


**Figure V.9.** Heat release rate vs. temperature of cork and extractive-free cork.

The removal of extractives from the cork shifted the starting temperature of degradation from 220 °C to 250 °C with a 12% lower THR, confirming that the extractives act as catalysts by reducing the decomposition temperature of cork and promoting the thermal decomposition of other components; a similar trend was also observed in TGA.

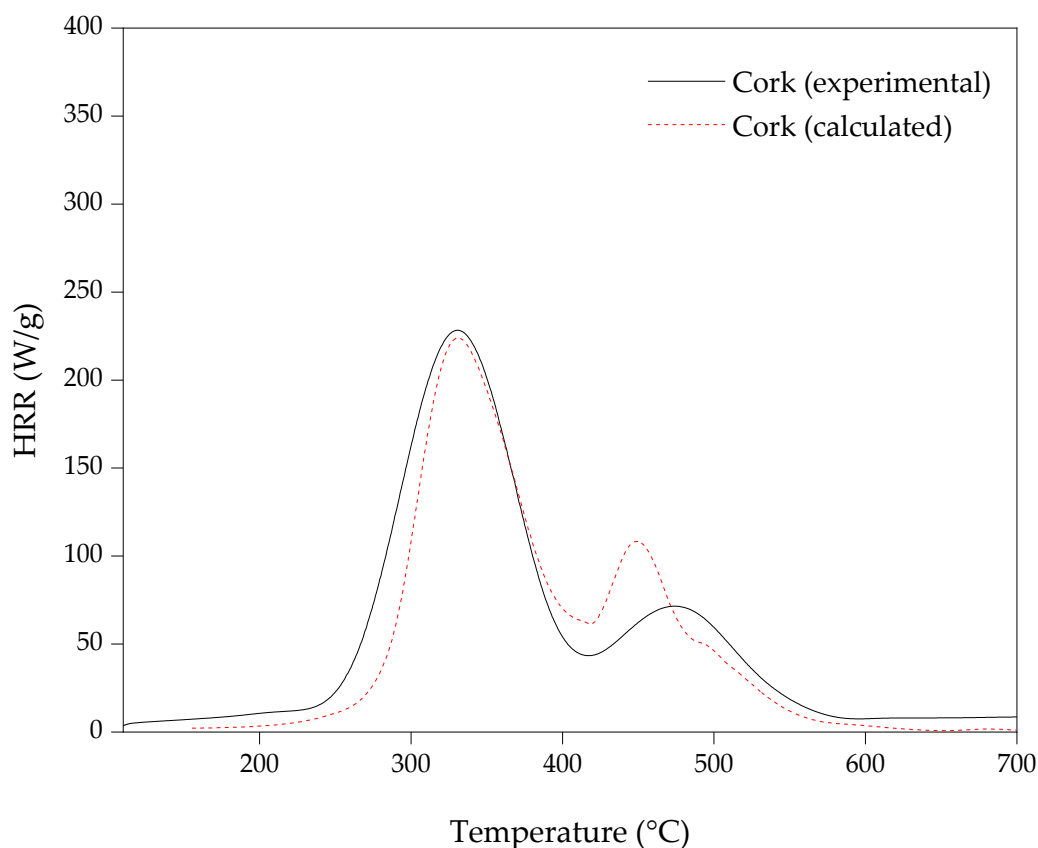
Heat release rate curves for cork extractives are presented in Figure V.10. The highest value of pHRR, 365 W/g at 410 °C, was registered for dichloromethane extractive. This non-polar extractive started to decompose at 190 °C in one step with almost no residue remaining, showing its high flammability. Ethanol extractive started at 180 °C with a pHRR of 220 W/g at 385 °C, and

then water extractive at about 200 °C with a pHRR of 35 W/g at 310 °C, which reached its pHRR at a lower temperature; however, its pHRR and THR were much lower compared to DCM and ethanol extractives. DCM extractives showed the highest  $T_{pHRR}$ , and together with ethanol extractive, they can be considered the main combustible parts of extractives with the highest pHRR and THR, which can be due to the presence of highly combustible compounds such as waxes, fatty acids and triterpene [204, 216].



**Figure V.10.** Heat release rate vs. temperature of cork extractives.

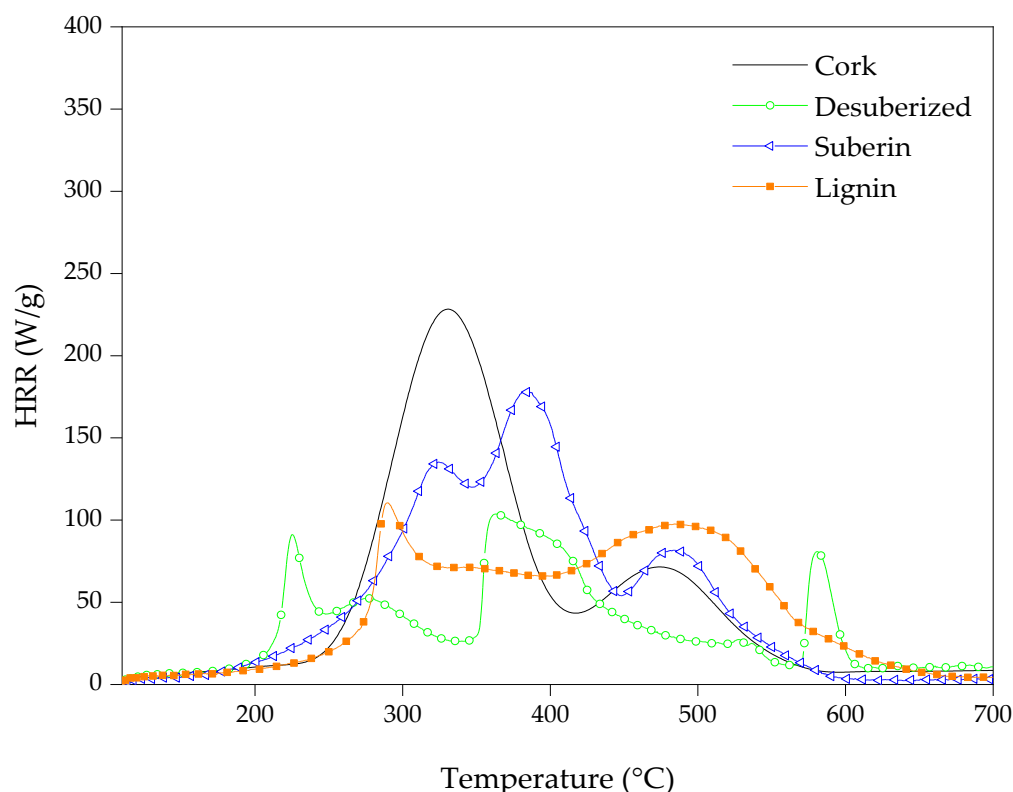
In Figure V.11, experimental and calculated HRR curves of cork are compared. The calculation was obtained from the HRR contribution of the extractive-free cork and individual extractives, calculated cork = (86% × extractive-free cork + 7% × DCM extractives + 3% × ethanol extractives + 4% × water extractives).



**Figure V.11.** Experimental and calculated heat release rate curves of cork.

The calculated curve exhibited higher onset decomposition than that obtained in the experimental curve of cork. This observation confirms the catalytic effect hypothesis of extractives, as it was also discussed previously in TGA analysis. Moreover, the second pHRR of cork powder compared to the calculated HRR vs. temperature curve of cork occurred at a higher temperature with a lowest HRR. This fact indicates that, as well as extractives catalyze the beginning of cork thermal decomposition, they also promote the formation of a more thermal-stable carbonaceous residue at higher temperatures (above 350 °C).

The comparative HRR curves of cork, desuberized cork, suberin and lignin are shown in Figure V.12.



**Figure V.12.** Heat release rate vs. temperature of cork powder and its components.

Following the same trend as it was observed in TGA, desuberized cork (or suberin free cork) decomposes at lower temperatures (150 °C) than cork (200 °C). The peaks observed between 200 °C and 320 °C of 90 W/g and 55 W/g, respectively, could be due to the release of polysaccharides of small-chain length [217]. The broad decomposition between 350 °C and 450 °C with a pHRR of 105 W/g could be attributed to the release of combustible volatile products from lignin [218]. The pHRR of 80 W/g at 580 °C is a result of the volatiles' released combustion when the charred layer formed during lignin pyrolysis was broken [219].

Lignin degraded in two broad steps with a lower  $T_{pHRR}$  (290 °C) compared to suberin and cork. By comparing lignin with desuberized cork (lignin and polysaccharides), it can be seen that lignin appears to be more stable than polysaccharides at lower temperatures as it started to decompose at 230 °C, about 50 °C higher than desuberized cork. As it was described by other authors [80, 218], the cleavage of the main chain of lignin involves the scission of several oxygen functional groups from its structure with different thermal stabilities. Therefore, a pHRR of 110 W/g at 290 °C that it is followed by a broad area of 70 W/g of HRR until approximately 425 °C

can be observed, when probably the char was broken and some flammable gasses were released, giving rise to a higher release of heat of 95 W/g at 490 °C.

The MCC curve of suberin shows three steps. The  $T_{pHRR}$  of the first peak is at 325 °C. This higher decomposition temperature in comparison with the other constituents of cork is in good agreement with the heat resistant characteristic reported in the literature [220]. The peaks at 390 °C and 480 °C with 175 W/g and 80 W/g of HRR are probably due to the decomposition of the different hydroxy and diacid chains of suberin [170].

### *V.3 Conclusions*

Chemical composition, thermal stability and fire behavior of cork and its main components were investigated in this work. The ATR-FTIR spectra of cork and the individual components showed that suberin was successfully extracted from cork powder; however, the presence of a small fraction of lignin and polysaccharides, in the spectrum of suberin, was detected. Thermal behavior of cork and extractive-free cork, in TGA analysis, revealed that polar and non-polar extractives had a catalytic effect on the thermal degradation of cork powder. It was also observed that by removing suberin from cork, the temperature of maximum mass loss rate shifted to lower temperatures, implying suberin plays an important role in enhancing the thermal stability of cork. Furthermore, MCC analysis was conducted to study the flammability of cork and its components. The removal of extractives from cork shifted the onset temperature of degradation from 220 °C to 250 °C and the temperature of the second pHRR from 475 °C to 450 °C, confirming that extractives act as catalysts at the beginning and end of cork combustion. Among extractives, non-polar extractives are the most combustible ones with the highest pHRR of 365 W/g. It was also concluded that, although suberin is the most heat-resistant component by delaying the thermal decomposition, it exhibits a high flammability as the temperature increases by releasing flammable gasses during the combustion without any significant charring effect. It was also noted that the lignocellulosic part of cork starts to degrade by the formation of a char barrier leading to the HRR reduction during the combustion; nevertheless, by increasing the temperature, the char layer was no longer effective and could not protect the underlying material. Further studies of cork powder or its main components as synergistic additives in flame retardant systems can be promising.





Cork powder as an adjuvant bio-flame

retardant in ABS flame retardant

formulations

Chapter

VI



## Chapter VI: Cork powder as an adjuvant bio-flame retardant in ABS flame retardant formulations

### *VI.1 Introduction*

ABS, an engineering thermoplastic polymer, consists of polybutadiene as a discrete phase and styrene-acrylonitrile copolymer as a continuous phase and, due to its toughness, impact resistance, chemical resistance and easy processing has been widely used in many applications such as in electrical and electronic industries, automotive and household appliances. [113, 148, 149, 221]. However, the high flammability of ABS combined with the smoke production could limit its applications. In order to improve its inherent high flammability and suppress the production of dark smoke, the use of different FRs in ABS has been reported. Most of the drawbacks related to flame retardancy of ABS were considered almost achieved with the development of brominated FRs [5]. However, in the 1990s it was revealed that some of these FRs release toxic gasses which adversely affect the environment and human health [7]. Therefore, more environmentally friendly FRs like mineral, carbon, nitrogen, silicon or phosphorus-based compounds were introduced as alternatives of brominated ones in ABS. A fire retardancy improvement for ABS with 60 wt.% of layered double hydroxides has been reported, by achieving a 28.3% LOI value and a 56% reduction of HRR compared to neat ABS [222]. ABS with 20 wt. % expandable graphite composites also showed a higher fire performance by increasing LOI value from 19.2% to 27.6% and a V-1 classification [223]. Nevertheless, to achieve a more efficient flame retardancy, many FRs systems are generally tailored based on the combination of the mentioned different families of flame retardants. For instance, combining SiO<sub>2</sub> particles microencapsulated with melamine phosphate and dipentaerythritol with the ratio of 3:1 at overall loading of 30 phr in ABS, has been reported to achieve a V-0 classification and a LOI value of 31.2% [125]. However, the most widely used multicomponent FR systems in ABS, or in its polymer blends, are based on organic and inorganic phosphorus compounds such as: TPP [9], BDP [10], AHP [4], RP [11], PAPP [12] and APP [13]. These have a prominent action in the condensed phase or gas phase, depending on their chemical composition [14]. Some of them, such as APP [19], PAPP [224] and BDP [9] during the thermal

decomposition are converted to phosphoric acid leading to the formation of pyrophosphate and polyphosphate structures acting mainly in the condensed phase. They catalyze the dehydration reaction of polymer end chains and induce char formation. Meanwhile, TPP [9], AHP [225] and RP [226] have a major action in the gas phase during decomposition. They mainly volatilize to produce free radicals ( $\text{PO}_2\bullet$ ,  $\text{PO}\bullet$  and  $\text{HPO}\bullet$ ), which scavenge  $\text{H}\bullet$  and  $\text{OH}\bullet$  radicals, forming less reactive or even inert molecules in the flame, and suppressing the radical reactions of combustion in the gas phase.

Within phosphorus flame retardants, APP has drawn industry attention due to its low loadings, lower cost and processability; however, APP by itself does not have an effective flame retardancy in ABS [18]. It is usually used as an acid source and foaming agent in bi-component IFRs [22]. In ABS, the use of APP with several charring agents such as PER [128], DPP [21] and PETA [22] have been reported. These charring agents act by catalyzing the esterification reaction of APP, promoting the liberation of non-flammable gasses such as  $\text{NH}_3$ ,  $\text{CO}$ ,  $\text{CO}_2$  and  $\text{H}_2\text{O}$  in the gas phase and a more cohesive and cross-linked char formation in the condensed phase. More recently, it was also revealed that synergistic interactions between APP and AlPi promoted the liberation of phosphorus radicals at a temperature range which acted like scavengers of those radicals yielded during ABS decomposition, as well as, the formation of a more effective protective layer in the condensed phase [13].

Furthermore, many studies have been carried out to obtain more environmentally friendly systems in the field of polymer science through the development of biocomposites [23]. Following the same trend, there is an increasing interest in fully or partially replacing synthetic flame retardants with bio-based ones. It has been reported that in some cases, bio-based materials act in the condensed phase by producing a more thermally stable char residue [24, 25]. For instance, the system containing low-cost starch, FF and APP showed an improvement in the flame retardancy of a biodegradable polymer due to the formation of a compact cross-linked 3D network (P-O-P and P-O-C) as a protective char layer due to the presence of both APP and starch as a charring agent [26]. A study about the influence of lignin on the thermal and fire properties of ABS blends concluded that the presence of lignin could have a positive impact on the fire behavior by increasing the char formation [27]. The strategy of adding P-LIG has also shown promising results by enhancing the thermal stability of the ABS composites and promoting the formation of a protective char [40].

The use of materials from renewable resources of forest-food-agricultural industrial wastes, as well as, replacing more traditional technologies by advanced green ones have been proposed, among other strategies, to come towards an ecological transition in multifunctional polymer composites development [227, 228]. In this context, in the past years, promoting circular economy by valorization of bio-wastes, like cork powder, has gained attention [229, 230]. Portugal and Spain are considered the main manufacturers of cork products and are responsible for 46% and 33% of the world total production (200 thousand tons per year), respectively [28, 29]. However, an important waste of approximately 30% (of total production), with no economic value, called cork powder, a term used to cover all cork wastes, is produced during industrial cork processing [30, 31]. Some few studies have been carried out by adding cork powder in polyolefinic matrices, focusing on the effect of cork powder composition in water absorbance, mechanical and insulation properties of cork-polymer composites [33, 34]. Nevertheless, there is yet a lack of knowledge regarding the effect of natural cork powder, mainly composed of suberin, lignin and polysaccharides, on the thermal stability and fire behavior of polymeric matrices, like ABS. Furthermore, analysis of cork powder ability as a potential charring agent in IFR systems has also not been reported.

Based on the previously exposed, the present chapter proposes to analyze the effect of cork powder (C) and APP on the thermo-mechanical behavior, thermal stability and fire performance of ABS composites. As well as, ascertain possible synergistic/antagonistic effects on the gas and/or condensed phase mechanism of action of such hybrid (natural-synthetic based additives) IFR in ABS.

## VI.2 Composition of ABS formulations

The composition of the melt-compounded materials studied in this chapter is listed in Table VI.1.

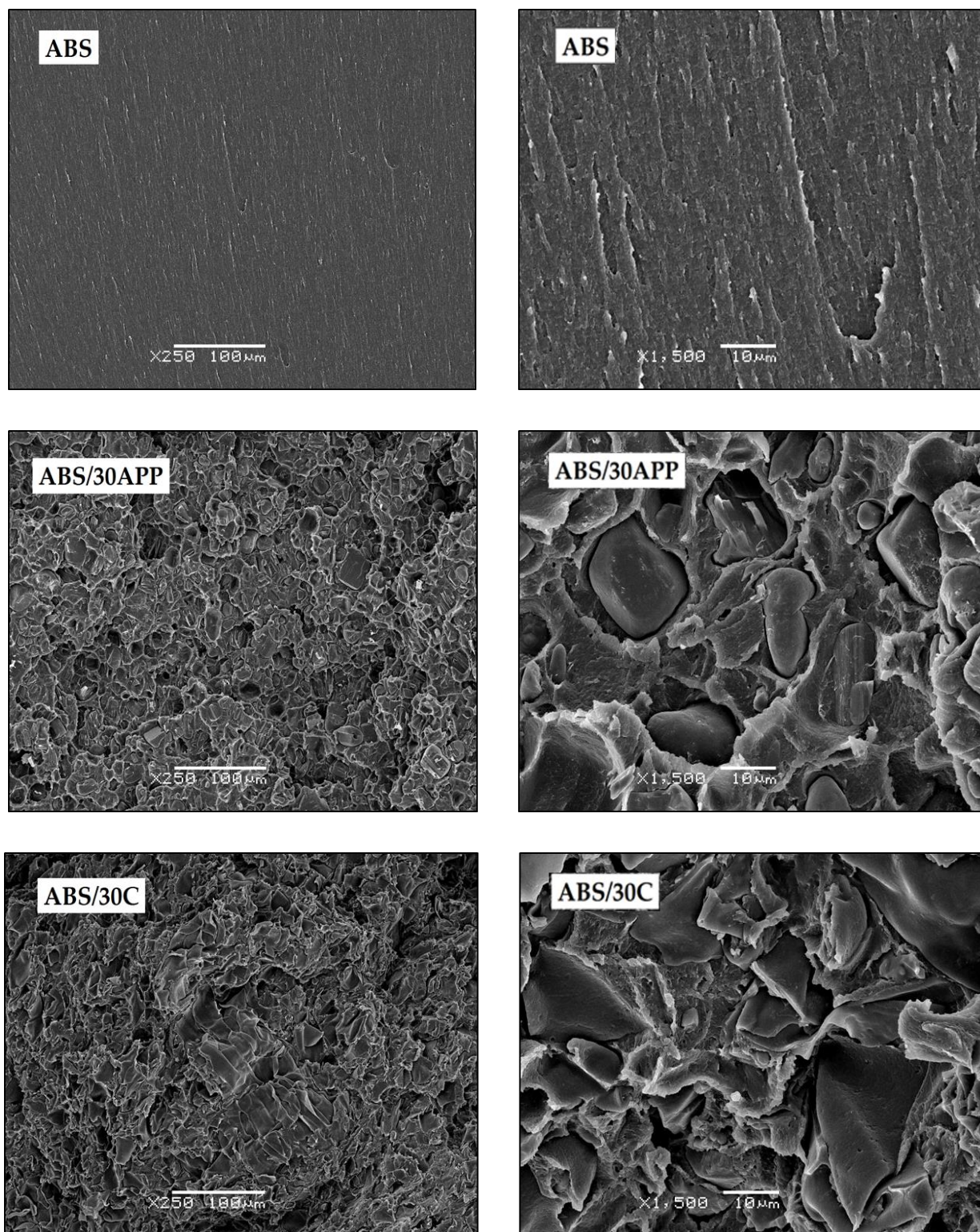
**Table VI.1.** Materials identification and weight percentage (wt.%) of the components.

<b>Materials</b>	<b>ABS (wt.%)</b>	<b>APP (wt.%)</b>	<b>Cork (wt.%)</b>
ABS	100	-	-
ABS/30APP	70	30	-
ABS/1C/29APP	70	29	1
ABS/3C/27APP	70	27	3
ABS/5C/25APP	70	25	5
ABS/10C/20APP	70	20	10
ABS/15C/15APP	70	15	15
ABS/20C/10APP	70	10	20
ABS/25C/5APP	70	5	25
ABS/30C	70	-	30

## VI.3 Results and discussion

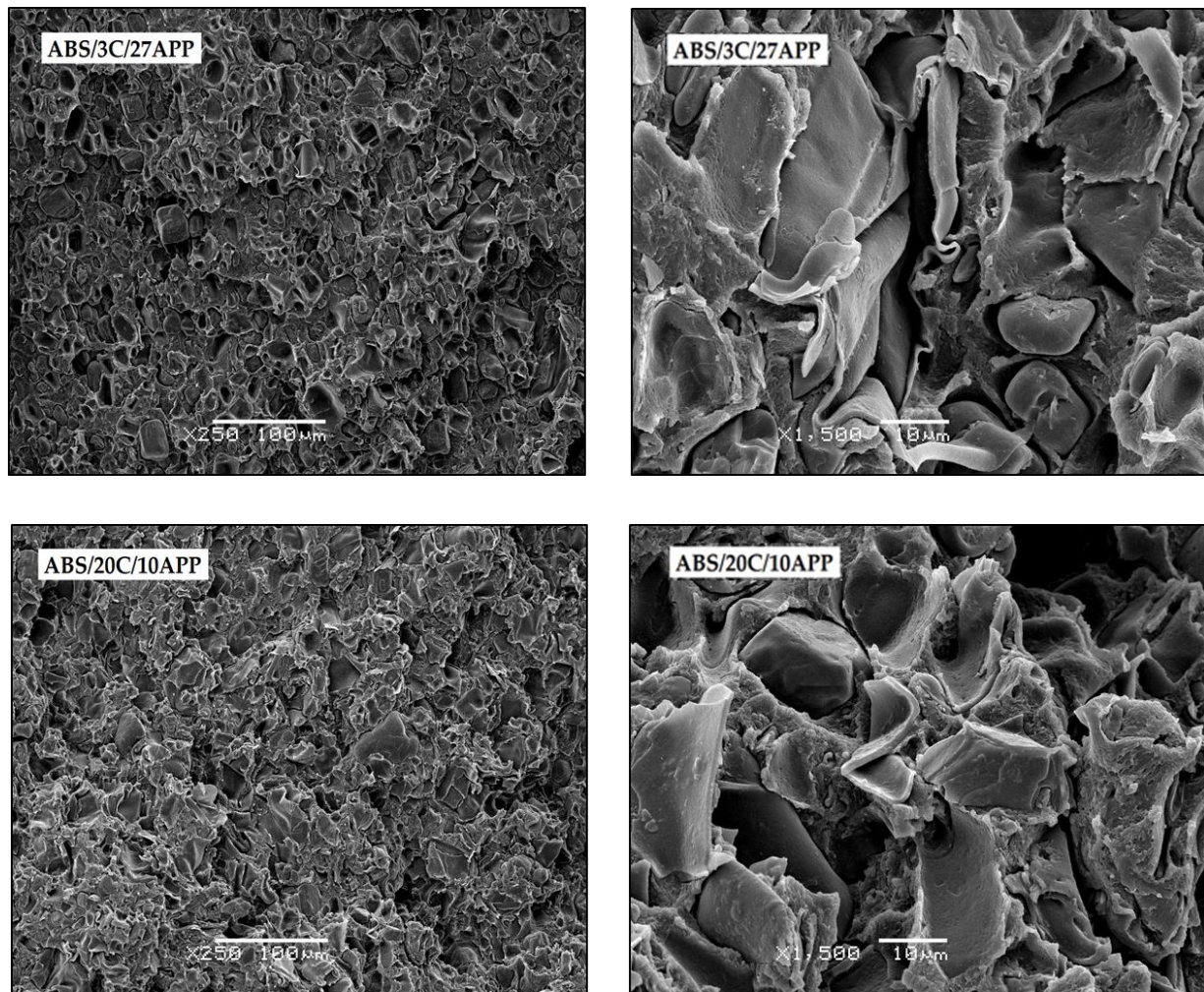
### VI.3.1 Morphology of ABS composites

Morphology of ABS, ABS/30APP and ABS/30C composites are shown in Figure VI.1. APP particles are well dispersed in the ABS matrix with the size of 3–20  $\mu\text{m}$  in accordance with what was reported by the supplier. For ABS/30C, it can be seen that the compression molding process of composite contains cork powder resulting in the deformation of cork cells.



**Figure VI.1.** SEM micrographs of ABS, ABS/30APP and ABS/30C, at 250 × and 1500 ×, with a scale bar of 100 and 10 μm, respectively.

In Figure VI.2, for ABS/3C/27APP and ABS/20C/10APP, cork cells were also observed compressed. Although ABS/C/APP composites exhibited a homogeneous microstructure with cork and APP particles well dispersed in the ABS matrix, there was evidence of poor interaction between cork or APP particles and the ABS matrix. It can be also seen that some of APP particles were removed during the fracture due to the weak particle-polymer interaction.



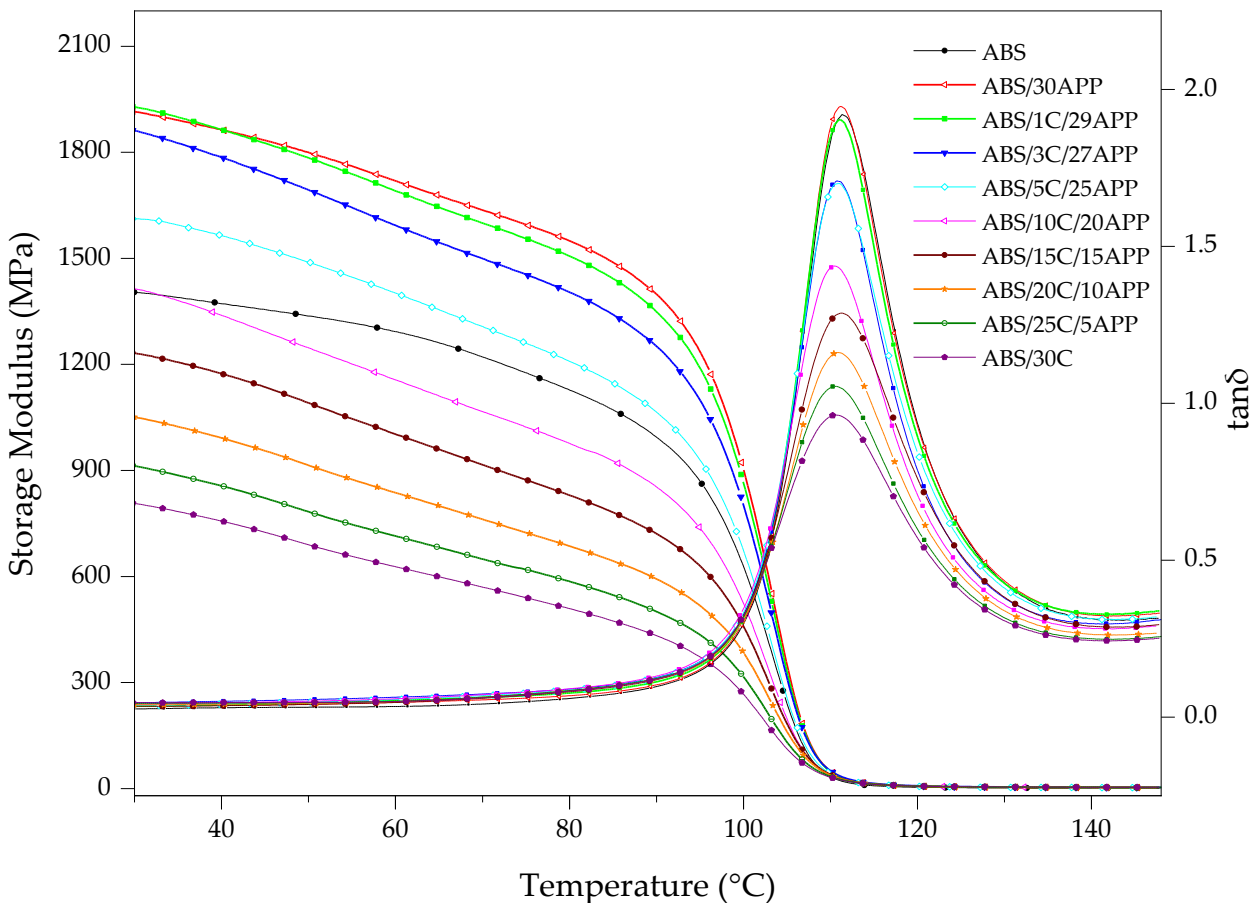
**Figure VI.2.** SEM micrographs of ABS/3C/27APP and ABS/20C/10APP, at 250 × and 1500 ×, with a scale bar of 100 and 10 μm, respectively.



### VI.3.2 Dynamic mechanical thermal analysis

The samples'  $T_g$  was obtained from the temperature corresponding to the maximum of the  $\tan \delta$  ( $\text{Max } \tan \delta$ ) curves. The  $E'$  was collected from the DMTA curves at 30 °C. There was a difference between the onset and the end of  $\tan \delta$  associated with the glass transition of SAN. The end of the transition was taken as reference to determine its intensity (peak of  $\tan \delta$  to the end of the curve).

Figure VI.3 shows the variation of the storage modulus and  $\tan \delta$  with temperature. As the temperature increased, the storage modulus decreased in the temperature region from 90-110 °C until reaching the energy of free movement of the SAN chain segments.



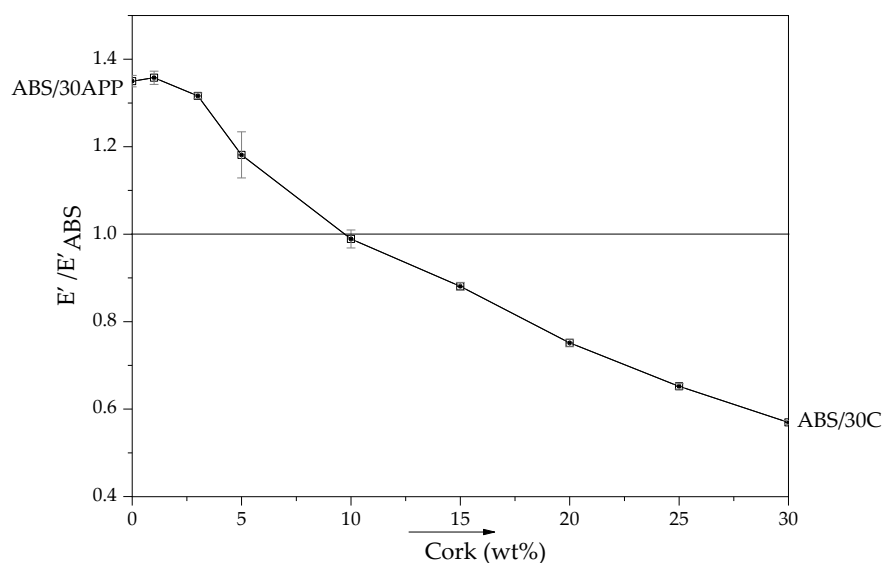
**Figure VI.3.** Storage modulus ( $E'$ ) and  $\tan \delta$  of ABS and ABS formulations.

The results of the DMTA of all samples are presented in Table VI.2. The glass transition temperature of the SAN phase of ABS, in general, was not significantly affected by the presence of APP or cork particles. Although adding both APP and cork to the polymer resulted in a clear decrease in the intensity of the  $\tan \delta$  and replacing cork by APP further decreased this intensity which implies a reduction of energy loss, structural relaxation and improvement in elasticity [231].

**Table VI.2.** Storage modulus ( $E'$ ), intensity of  $\tan \delta$  and glass transition temperature ( $T_g$ ) of ABS and ABS formulations.

Materials	$E'$ at 30 °C (MPa)	Intensity of $\tan \delta$	$T_g$ (°C)
			Max $\tan \delta$
ABS	1409 ± 8	1.64 ± 0.05	110 ± 0.4
ABS/30APP	1902 ± 18	1.62 ± 0.01	111 ± 0.2
ABS/1C/29APP	1913 ± 21	1.56 ± 0.01	111 ± 0.1
ABS/3C/27APP	1854 ± 10	1.38 ± 0.03	111 ± 0.1
ABS/5C/25APP	1664 ± 74	1.37 ± 0.01	111 ± 0.1
ABS/10C/20APP	1393 ± 29	1.14 ± 0.01	111 ± 0.1
ABS/15C/15APP	1241 ± 13	0.98 ± 0.02	111 ± 0.1
ABS/20C/10APP	1058 ± 12	0.89 ± 0.01	111 ± 0.7
ABS/25C/5APP	919 ± 9	0.89 ± 0.01	110 ± 0.4
ABS/30C	802 ± 6	0.72 ± 0.01	111 ± 0.1

In Figure VI.4, it is shown that with the 30 % addition of APP to ABS, the storage modulus increased in comparison with neat ABS. Then by substituting APP with C, the storage modulus decreased continuously. In addition, ABS/10C/20APP showed a similar behavior, in the elastic part, to neat ABS. It is clear with adding more than 10 wt.% of cork, the storage modulus decreased compared to the pure ABS which shows enhanced softening of the composites due to the low  $E'$  of cork (20-90 MPa) [232-234].



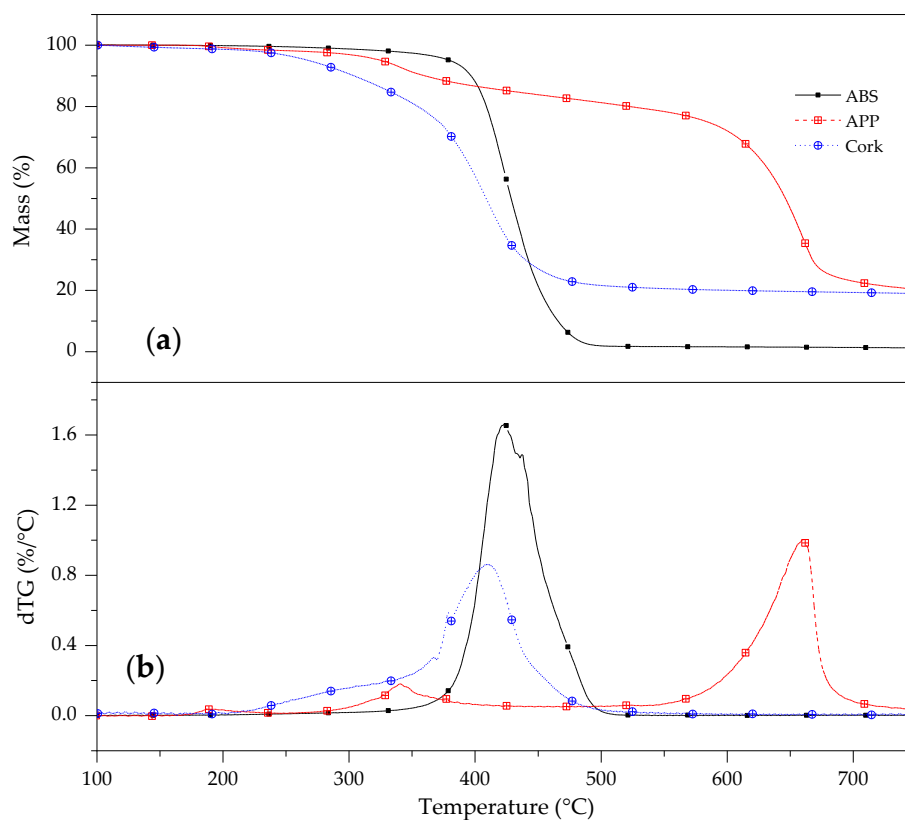
**Figure VI.4.** Storage modulus ( $E'$ ) of ABS / Storage modulus ( $E'$ ) of ABS formulations.

### VI.3.3 Pyrolysis: thermogravimetric analysis

Mass and dTG curves of the individual components, that is, ABS, APP and cork are shown in Figure VI.5 (a) and (b), respectively. Furthermore, the TD steps,  $T_{5\%}$ ,  $T_{peak}$ , ML and residue at 800 °C are summarized in Table VI.3.

ABS decomposed in a single step between 330 °C and 520 °C with a mass loss of 97.8%, with almost no charring ability by itself, and a maximum mass loss rate at 423 °C. It has been previously reported that ABS thermal decomposition starts with the evolution of butadiene monomer and aromatics from the decomposition of the styrenic portion followed by the evolution of the acrylonitrile [158, 159, 235].

APP thermally decomposed in two steps. The first one between 250 °C and 420 °C had a mass loss of 13.1% with the maximum mass loss rate registered at 341 °C attributed to water and ammonia release [13, 236, 237]. The second one between 570 °C and 710 °C related to the degradation of the polyphosphate network, showed a major mass loss of 59.8% and a maximum mass loss rate occurring at 659 °C [238].



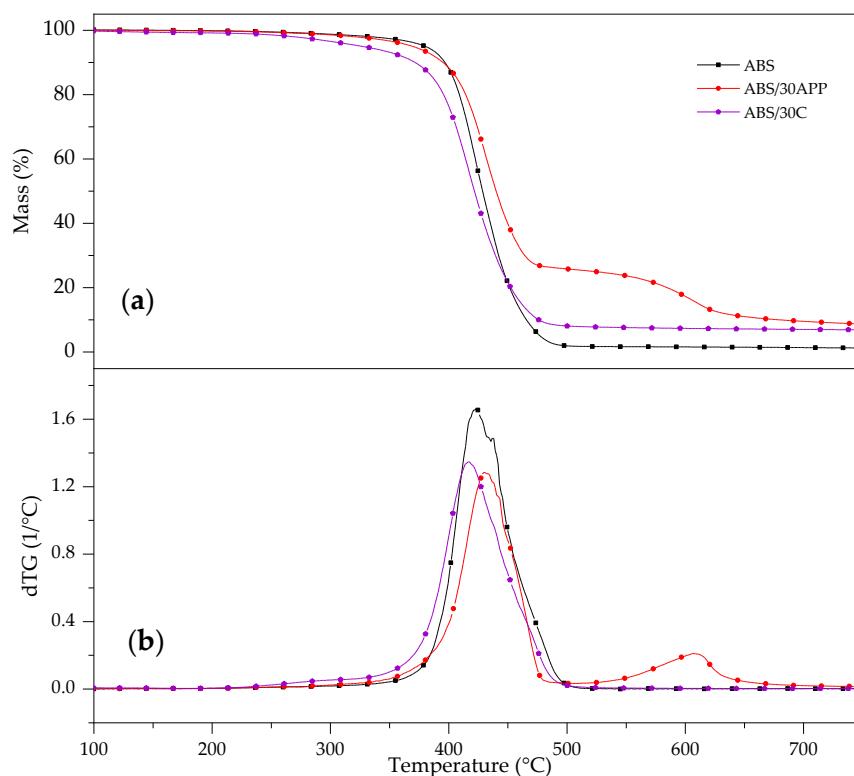
**Figure VI.5.** (a) Mass and (b) dTG curves of ABS, APP and cork powder obtained at 10 °C/min under N<sub>2</sub> atmosphere.

Cork started to decompose at lower temperature compared with APP and ABS, with a T<sub>5%</sub> of 260 °C. It showed one main thermal decomposition step with a mass loss of 78.8% and maximum mass loss rate at 410 °C. The shoulder observed at the beginning of its thermal decomposition, between 200 °C and 350 °C, was related to the polar extractives decomposition followed by polysaccharides and suberin. The higher mass loss rate between 350 °C and 500 °C, was attributed to the decomposition of lignin, suberin and non-polar extractives [95, 170].

**Table VI.3.** Thermal decomposition data obtained from TGA (mass and dTG curves) of ABS, APP and cork (C).

Materials	TD step	T <sub>5%</sub> (°C)	T <sub>peak</sub> (°C)	ML (%)	R <sub>800 °C</sub> (%)
ABS	1	380	423	97.8	1.2
APP	1	321	341	13.1	18.5
	2		659	59.8	
Cork	1	260	410	78.8	18.9

Figure VI.6 shows the comparative of ABS ABS/30C and ABS/30APP Mass and dTG curves. Like the neat ABS, the thermal decomposition of ABS/30C occurred in one main step. Due to the lower thermal stability of cork components, a reduction of 55 °C of T<sub>5%</sub> and a 6 °C of T<sub>peak</sub> were observed for ABS/30C respect to ABS (Table VI.3). Nevertheless, above 475 °C a lower mass loss than that of ABS with a 6.8% residue at 800 °C was registered due to the inner higher cork charring ability. Meanwhile, thermal decomposition of ABS/30APP occurred in two stages similar to APP thermal decomposition. The first and main one, between 260 °C and 510 °C, related to ABS decomposition and partially volatilization of APP, showed a mass loss of 73.3% and a T<sub>peak</sub> of 6 °C higher than that of ABS. The second one, attributed to the main thermal decomposition step of APP, showed a 53 °C reduction in T<sub>peak</sub> compared to neat APP (see Figure VI.5 and Figure VI.6). Also, addition of 30 wt.% APP to ABS exhibited a 7.9% residue yield at 800 °C which was slightly higher than that of ABS/30C (see Table VI.3).



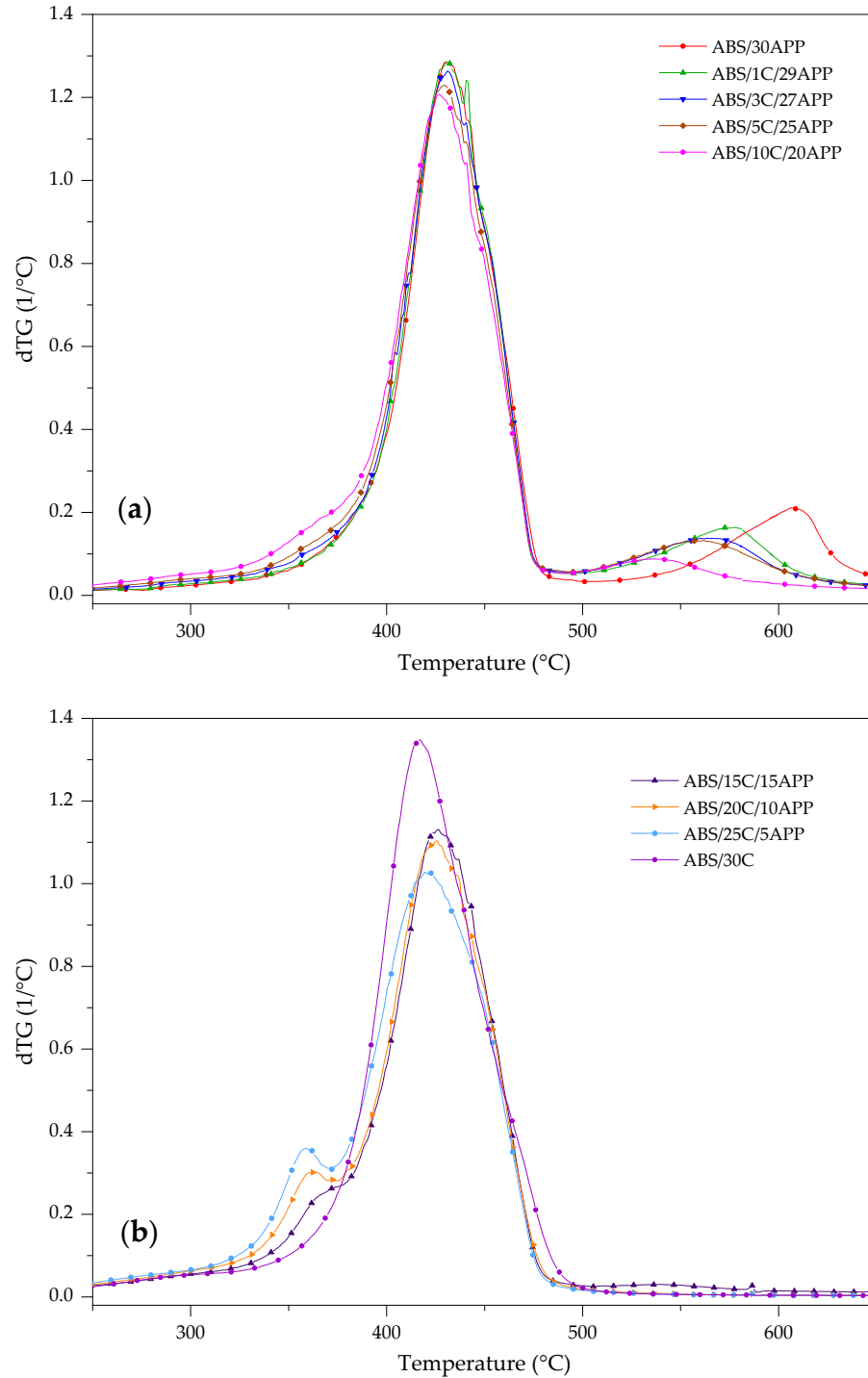
**Figure VI.6.** (a) Mass and (b) dTG of curves of ABS, ABS/30APP and ABS/30C obtained at 10 °C/min under N<sub>2</sub> atmosphere.

Comparative dTG curves of ABS formulations with APP or cork as the main additive are shown in Figure VI.7 (a) and (b) respectively. In general, two different thermal decomposition behaviors were observed and further detailed.

When APP was the major additive (Figure VI.7 (a)), a two-step decomposition similar to ABS/30APP was registered. Nevertheless, the first step between 250 °C and 500 °C showed a slight and gradual increase in mass loss as the cork content increased up to 10 wt.%. While, the second stage between 500 °C and 670 °C displayed a  $T_{\text{peak}}$  shift to a lower temperature as increasing the cork content. In fact, for ABS/10C/20APP a decrease of 70 °C regarding ABS/30APP was noticed, as well as, a higher thermal stable residue formation compared to ABS/30APP (see Table VI.4).

On the other hand, when cork was the major component (Figure VI.7 (b)), a new thermal decomposition step, between 320 °C and 370 °C, was observed. This could be corresponding to a less thermally stable fraction of cork components catalyzed by the presence of APP. Additionally,

between 500 °C and 650 °C, polyphosphate network decomposition of APP was no longer observed.



**Figure VI.7.** dTG curves of ABS formulations with (a) C/APP weight ratio < 1 and (b) C/APP ≥ 1 cork obtained at 10 °C/min under N<sub>2</sub> atmosphere.

**Table VI.4.** Mass and dTG data of ABS and ABS formulations.

<b>Materials</b>	<b>TD step</b>	<b>T<sub>5%</sub>(°C)</b>	<b>T<sub>peak</sub>(°C)</b>	<b>ML(%)</b>	<b>R<sub>800°C</sub>(%)</b>
ABS	1	380	423	97.8	1.2
ABS/30APP	1	368	429	73.3	7.9
	2		606	16.12	
ABS/1C/29APP	1	366	431	73.3	9.1
	2		585	13.5	
ABS/3C/27APP	1	355	431	75.8	9.1
	2		560	12.6	
ABS/5C/25APP	1	350	429	75.2	9.1
	2		556	12.2	
ABS/10C/20APP	1	332	426	78.4	11.3
	2		536	7.4	
ABS/15C/15APP	1	328	426	80.3	14.2
ABS/20C/10APP	1	319	364	14.1	14
	2		425	69.7	
ABS/25C/5APP	1	312	358	16.2	11.9
	2		419	70.3	
ABS/30C	1	325	416	91.2	6.8

To further identify the chemical interactions between APP and cork in ABS matrix, calculated and experimental mass and dTG curves of ABS composites are presented in Figure VI.8. The

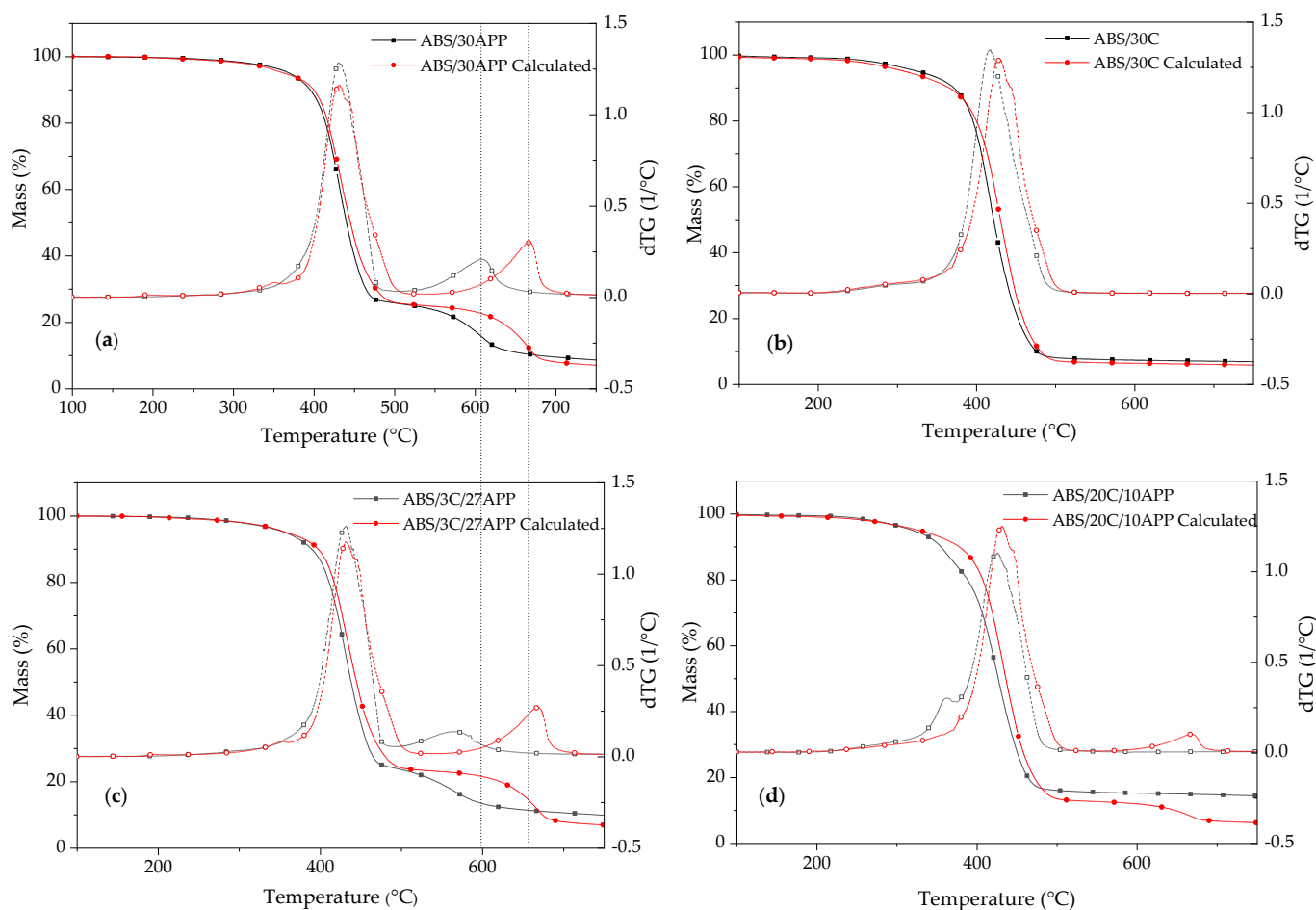


calculated curves were obtained based on the weight percentage of the components in each material and their individual thermogravimetric results, using the rule of mixture.

For ABS/30APP differences were only noticed during the second decomposition step (Figure VI.8 (a)): a 50 °C shift of  $T_{\text{peak}}$  to a lower temperature with respect to the expected value was observed. This fact indicates that the polyphosphate network is less thermally stable and that it decomposes at a lower rate when combined with products of ABS decomposition. On the other hand, no significant differences were noticed for ABS/30C (Figure VI.8 (b)), indicating poor chemical interactions between ABS and cork during composite decomposition.

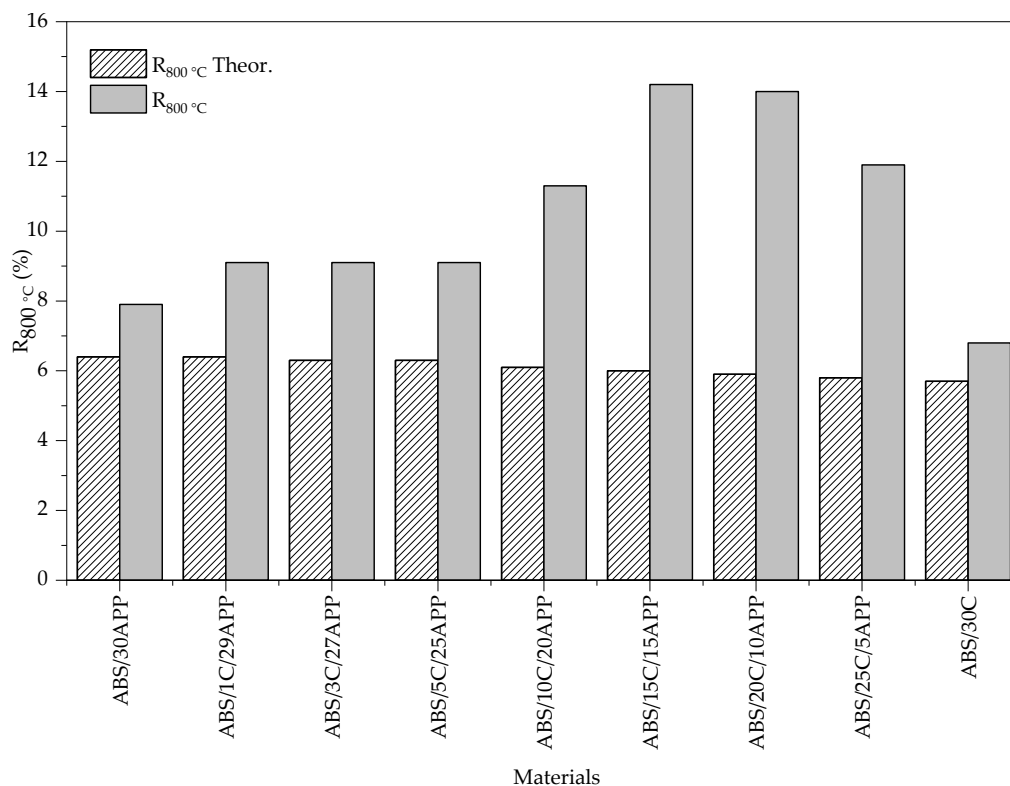
It should be mentioned that, ABS/C/APP formulations with a cork content lower than 15 wt.% ( $C/APP < 1$ ) exhibited similar differences between experimental and calculated curves, as well as, the ones with cork content equal or higher than 15 wt.% ( $C/APP \geq 1$ ). Therefore, ABS/3C/27APP and ABS/20C/10APP are reported as the representative of these two groups of formulations in Figure VI.8 (c) and (d) respectively.

Figure VI.8 (c) shows that the second TD peak of ABS/3C/27APP not only began at lower temperature than the calculated but also that the mentioned decomposition of polyphosphate cross-linked structure started at lower temperature than that of ABS/30APP (see blue lines in Figure VI.8). These observations indicate that cork, as the minor additive, catalyzed APP decomposition during that range of temperature. When cork was the main additive (Figure VI.8 (b)), an unexpected thermal decomposition stage between 320 °C and 370 °C combined with the absence of the second decomposition step of APP also emphasized the presence of chemical interactions between these two additives. The new step observed at the beginning of thermal decomposition could be related with hydrolytic reactions of cork promoted by the presence of phosphoric acid produced during APP first step decomposition. Also, such chemical interactions seem to affect the ending of thermal decomposition with the absence of the second decomposition stage of APP leading to a much higher residue formation than expected for the mentioned composites under pyrolysis conditions (Figure VI.8 (b)).



**Figure VI.8.** Experimental and calculated mass and dTG curves of (a) and (b) composite with individual components (APP and C) in ABS, and representative examples of thermal decomposition behavior of ABS composites with C/APP weight ratio (c) lower than 1 and (d) equal or higher than 1.

Figure VI.9 compares the experimental and calculated residue values of ABS composites at 800 °C. For all composites, the experimental residue value was superior to the calculated one. Under a nitrogen atmosphere, ABS composites with a C:APP weight proposition of 1:1 (ABS/15C/15APP) or 2:1 (ABS/20C/10APP) led to the highest residue formation. It has been reported in the literature that the presence of phosphate enhances the dehydration reactions of lignocellulosic materials, leading to a high amount of residue with condensed structures that were not further degraded [239, 240].



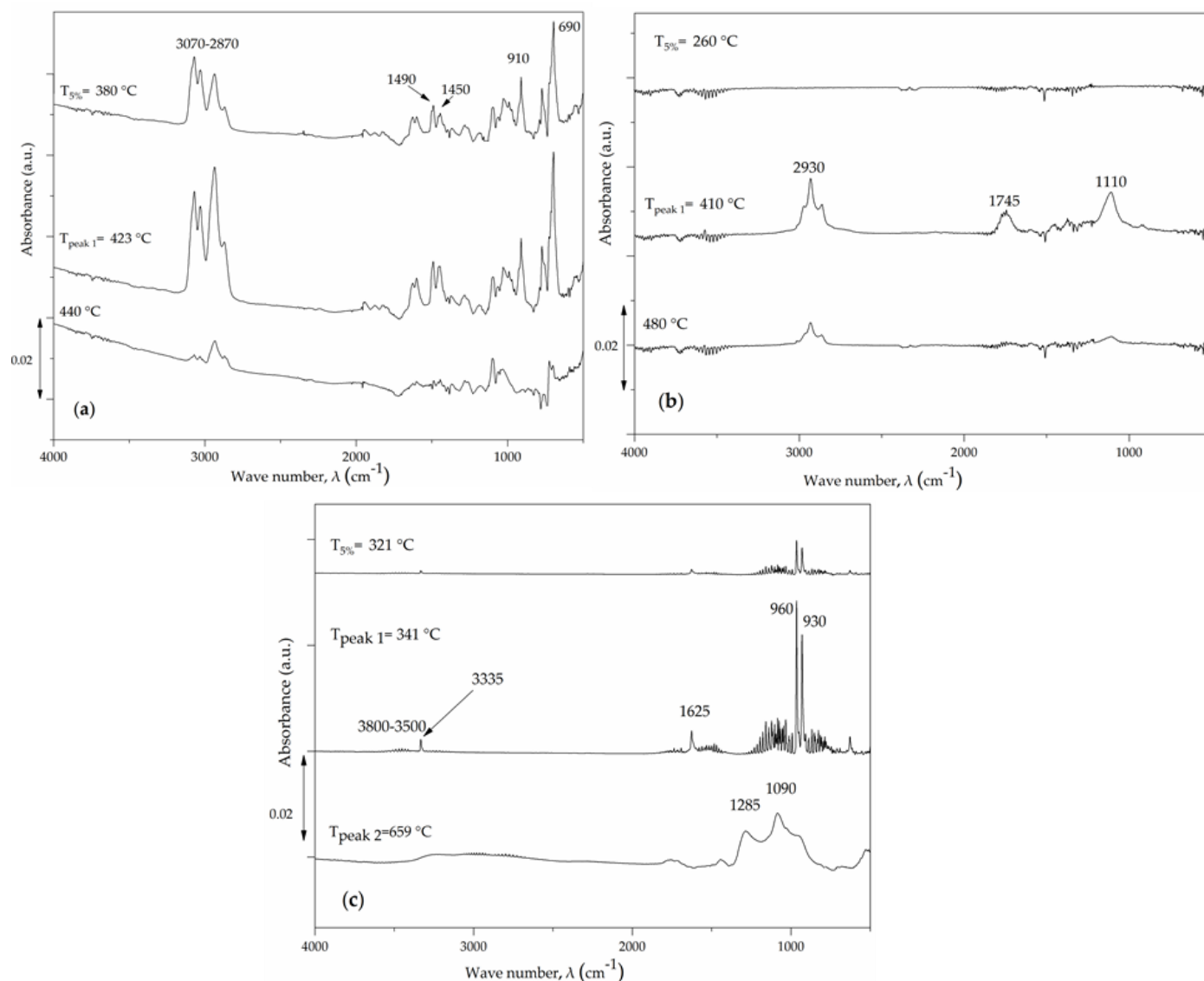
**Figure VI.9.** Experimental and calculated residue value at 800 °C of flame retarded ABS formulations.

### VI.3.4 Evolved pyrolysis gasses: FTIR analysis

The FTIR characteristic spectra of the gaseous pyrolysis products at the beginning of the decomposition ( $T_{5\%}$ ) and at the maximum mass loss rate temperature ( $T_{\text{peak}}$ ) of the main decomposition steps, of ABS, cork powder, APP are presented in Figure VI.10 and spectra of the evolved gaseous products of ABS/30C, ABS/30APP, ABS/3C/27APP and ABS/27C/3APP are shown in Figure VI.11.

FT-IR spectrum of ABS at 380 °C ( $T_{5\%}$ ) showed the aromatic and aliphatic hydrocarbon vibrations at  $3070\text{ cm}^{-1}$ ,  $3030\text{ cm}^{-1}$  and  $2935\text{ cm}^{-1}$ ,  $2870\text{ cm}^{-1}$ , respectively with the highest intensity at 423 °C (see Figure VI.10 (a)). Moreover, absorption bands related to the deformation of  $\text{CH}_2$  of butadiene at  $1490\text{ cm}^{-1}$  and  $1450\text{ cm}^{-1}$ , vibration of  $\text{C}=\text{C}-\text{H}$  and  $\text{C}-\text{H}$  of butadiene at  $910\text{ cm}^{-1}$  were registered [241, 242]. Also, the absorption signal at  $690\text{ cm}^{-1}$  was assigned to the out-of-plane bending of the CH groups in the aromatic ring of styrene units [241]. Acrylonitrile or its decomposition products were not detected, as reported previously in literature [243]. The detected

hydrocarbons were products of the chain scission of the polymer [13, 244], being these mainly from butadiene and styrene monomers and its derivatives.



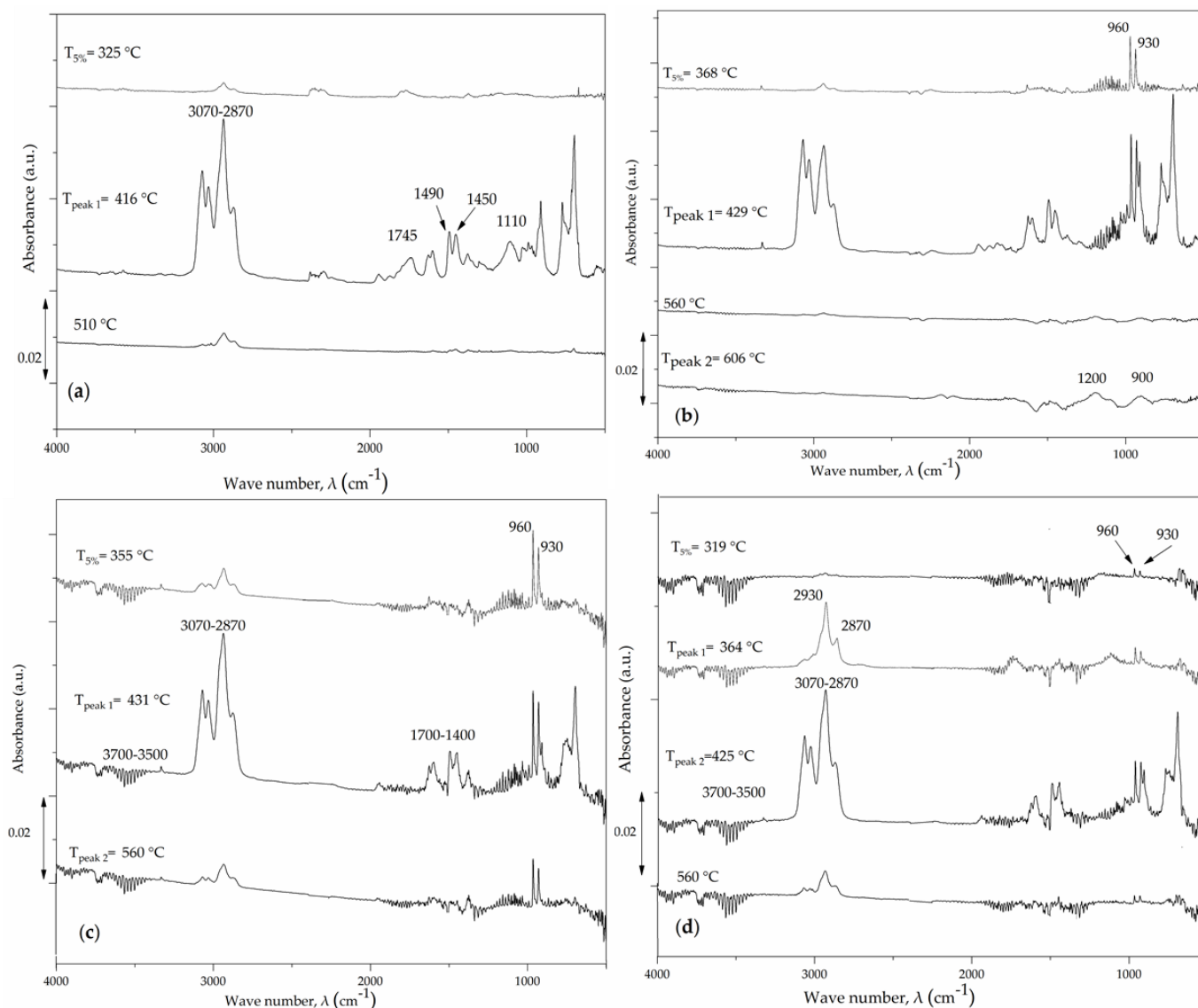
**Figure VI.10.** FT-IR spectra of (a) ABS, (b) cork and (c) APP pyrolysis products between the beginning of decomposition ( $T_{5\%}$ ) and the maximum mass loss rate ( $T_{\text{peak}}$ ).

Figure VI.10 (b) shows the FTIR characteristic spectra of cork gaseous pyrolysis products. At the beginning of decomposition ( $260\text{ }^{\circ}\text{C}$ ), vibrations at  $3800\text{--}3500\text{ cm}^{-1}$  mainly related to water O–H stretching vibration were observed. As pyrolysis proceeded, the absorption band at  $2930\text{ cm}^{-1}$  corresponding to aliphatic C–H bonds resulted from the of  $\text{-OCH}_3\text{-}$  bonds breakage [245, 246],

showed the highest intensity at the maximum mass loss rate temperature (410 °C). The band at 1745  $\text{cm}^{-1}$  was ascribed to the stretching vibration of C-O of carbonyl ( $-\text{C}=\text{O}$ ) and carboxyl functional groups ( $-\text{COOH}$ ), as a result of organic compounds release such as: aldehydes, ketones, acids, and ester [246]. The registered absorbance peak at 1110  $\text{cm}^{-1}$  was attributed to the stretching vibration of C-O from phenols [245]. When the pyrolysis temperature reached above 410 °C, these functional groups of O-H, C-H, and C-O, which were weakly linked to the basic structural unit of cork main components, were gradually cut off by thermal cracking [247]. The liberation of these pyrolysis gasses continued up to 480 °C.

The FTIR spectra of APP pyrolysis decomposition gasses showed two intense peaks at 960  $\text{cm}^{-1}$  and 930  $\text{cm}^{-1}$  characteristics of  $\text{NH}_3$ , with the maximum absorbance at 341 °C. Also, the less intense peak observed at 1630  $\text{cm}^{-1}$  was attributed to the  $\text{NH}_3$  asymmetric bend vibration [13, 244]. The sign at 3335  $\text{cm}^{-1}$  and vibrations between 1250  $\text{cm}^{-1}$  and 750  $\text{cm}^{-1}$ , characteristics of the release of  $\text{NH}_3$ , were also registered. Beside  $\text{NH}_3$  volatilization from APP decomposition, the peaks between 3800-3500  $\text{cm}^{-1}$  and 1700-1400  $\text{cm}^{-1}$  showed evidences of water release [248, 249]. Furthermore, at 659 °C, where the second step of APP thermal decomposition occurred, a broad band between 3400  $\text{cm}^{-1}$  and 2400  $\text{cm}^{-1}$  assigned to P-OH absorption was registered [250]. Also, the signals at 1285  $\text{cm}^{-1}$  and 1090  $\text{cm}^{-1}$  of P=O and P-O, were attributed to the stretching vibration of volatile phosphorus radicals, in accordance with the literature [13].

As it was previously reported in Table VI.4, ABS/30C lost more than 90% of its weight during one step. There was no significant evidence of pyrolysis gasses evolution up to 325 °C, from this temperature on thermal decomposition of both ABS and cork started gradually. In Figure VI.11 (a) the highest intensity of absorption signals at 3070  $\text{cm}^{-1}$ , 3030  $\text{cm}^{-1}$ , 1490  $\text{cm}^{-1}$ , 1450  $\text{cm}^{-1}$ , 912  $\text{cm}^{-1}$  related to the thermal decomposition of ABS and the peaks at 1745  $\text{cm}^{-1}$  and 1110  $\text{cm}^{-1}$  corresponding to cork components thermal decomposition, were registered at 416°C. The bands at 2930  $\text{cm}^{-1}$  and 2870  $\text{cm}^{-1}$  corresponding to C-H, a common aromatic and aliphatic hydrocarbon vibration, were also attributed to both ABS and cork. Since no new peak was observed, it can be concluded that there was no chemical interaction between ABS and cork during pyrolysis thermal decomposition, as previously discussed.



**Figure VI.11.** FT-IR spectra of (a) ABS/30C, (b) ABS/30APP, (c) ABS/3C/27APP and (d) ABS/20C/10APP pyrolysis products between the beginning of decomposition ( $T_{5\%}$ ) and the maximum mass loss rate ( $T_{\text{peak}}$ ).

ABS/30APP formulation lost 73.3 % of its weight during its first thermal decomposition step mainly related to the thermal decomposition of ABS and partial decomposition of APP. From Figure VI.11 (b), it can be noted that APP began to decompose at a slightly lower temperature than ABS, with the liberation of ammonia and water at 368 °C. This evolution of  $\text{NH}_3$  from APP was related to acidic site formation observed in the intumescent reaction [13, 238, 251]. At  $T_{\text{peak}}$  of the second ABS/30APP thermal decomposition step (606 °C), signals related to stretching vibrations

of P=O and P-O volatile phosphorus radicals were registered at  $1200\text{ cm}^{-1}$  and  $900\text{ cm}^{-1}$ , respectively. Furthermore, by comparing the first and second stages of ABS/30APP thermal decomposition in Figure VI.11 (b), it is possible to observe that during the second decomposition stage, the release of pyrolysis gasses was lower regarding the first one [13, 249, 252].

Aromatic and aliphatic hydrocarbon vibrations of ABS at  $3070\text{ cm}^{-1}$ ,  $3030\text{ cm}^{-1}$  and of both ABS and cork at  $2935\text{ cm}^{-1}$  and  $2870\text{ cm}^{-1}$  of ABS/3C/27APP registered at  $T_{5\%}$  ( $335\text{ }^{\circ}\text{C}$ ), are presented in Figure VI.11 (c). The intensity of these peaks at  $335\text{ }^{\circ}\text{C}$  was much higher than the one registered for ABS/30APP at  $368\text{ }^{\circ}\text{C}$ , its corresponding  $T_{5\%}$  (Figure VI.11 (b)), which indicates a lower thermal stability of ABS/3C/27APP regarding with ABS/30APP at the beginning of decomposition, in accordance with TGA analysis results. The absorption signals registered at  $960\text{ cm}^{-1}$  and  $930\text{ cm}^{-1}$  and the peak registered at  $1630\text{ cm}^{-1}$  are characteristic of  $\text{NH}_3$ , as previously discussed, showing their highest intensity at  $431\text{ }^{\circ}\text{C}$  ( $T_{\text{peak}}$  of first step). In addition, the numerous thin peaks between  $750\text{ cm}^{-1}$  and  $1250\text{ cm}^{-1}$  are also characteristic of the release of  $\text{NH}_3$  and the ones between  $1700\text{-}1400\text{ cm}^{-1}$  of the release of water [248]. Compared to ABS/30APP, the  $\text{NH}_3$  release in ABS/3C/27APP started at lower temperature and continued up to a higher temperature  $560\text{ }^{\circ}\text{C}$ . In addition, due to the continuous release of ammonia at higher temperature, the expected P=O and P-O stretching vibrations bands at  $1200\text{ cm}^{-1}$  and  $900\text{ cm}^{-1}$  could not be distinguished from those thin vibrations of  $\text{NH}_3$ . Furthermore, small absorbance signals registered between  $3700\text{-}3500\text{ cm}^{-1}$  related to  $\text{H}_2\text{O}$  vaporization [253], were more intense when both additives were found, and a broader temperature of water release was also observed. The dehydration reaction of cork, promoted by APP, can be the result of the mentioned higher liberation of water.

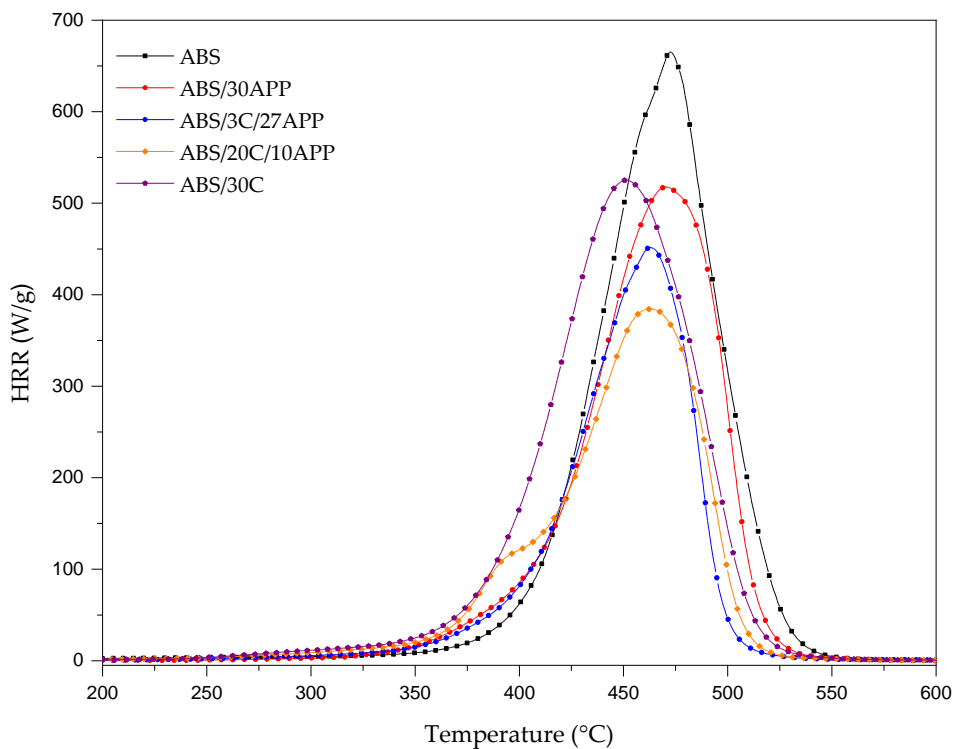
FT-IR spectrum of ABS/20C/10APP exhibited the same absorption signals of ABS/3C/27APP (Figure VI.11 (d)). However, the release of ammonia from hydrolytic decomposition of APP started at lower temperature ( $T_{5\%} = 319\text{ }^{\circ}\text{C}$ ), indicating a direct effect of cork products' decomposition content on the APP thermal stability. Although, the peaks at  $960\text{ cm}^{-1}$  and  $930\text{ cm}^{-1}$  assigned to ammonia release had a lower intensity compared to ABS/3C/27APP as a result of a lower amount of APP in the composite. In addition, at  $T_{\text{peak } 1}$  ( $364\text{ }^{\circ}\text{C}$ ), the intensity of the absorptions bands at  $2930\text{ cm}^{-1}$  and  $2870\text{ cm}^{-1}$  attributed to mainly aliphatic C-H vibration of cork components was higher compared to the other formulations, which can be due to a more intense dehydration reaction of cork in the presence of APP when cork was the major additive. Also, it can be seen that the pyrolysis gasses released during the first thermal decomposition stage of

ABS/20C/10APP were mainly attributed to cork meanwhile APP thermal decomposition mostly occurred in the second step by releasing the highest amount of ammonia gas, in agreement with TGA analysis.

### VI.3.5 Micro-scale combustion calorimetry

HRR curves of ABS, ABS/30C, ABS/30APP, ABS/3C/27APP, and ABS/20C/10APP are shown in Figure VI.12 and the corresponding combustion data are listed in Table VI.5.

The HRR curve of neat ABS shows its high flammability by a sudden increase of heat release reaching its maximum value of 665 W/g. The lowest char formation at the end of consumption was registered for ABS with a 2.6% of residue. This fact indicates that ABS decomposed almost without charring; therefore, more flammable volatiles were released.



**Figure VI.12.** Heat release rate of ABS and ABS formulations obtained by MCC.



The presence of 30 wt.% of APP in ABS decreased the beginning of thermal decomposition temperature in agreement with TGA analysis results. In addition, HRC decreased from 649 J/g-K to 498 J/g-K (22% reduction) and 475 °C to 470 °C, respectively when 30 wt.% of APP was added. Besides pHRR values of ABS/30APP and of ABS/30C were almost similar, the ABS/30C pHRR temperature was 19 °C lower than that of ABS/30APP, which can be due to the lower thermal stability of cork components.

By substituting 3 wt.% of APP with cork (ABS/3C/27APP), a 15.8 % and a 16.6 % reduction of the HRC compared to those of ABS/30APP and ABS/30C was respectively noticed. It should be mentioned that a higher residue formation of 12.8% was also registered for ABS/3C/27APP compared to those of ABS/30APP and ABS/30C in accordance with results obtained by TGA analysis. ABS/20C/10 APP showed the lowest values of HRC and pHRR, with a value of 360 J/g-K and 385 W/g respectively, indicating an improvement in fire performance under pyrolysis when cork was the main additive. This can be related to a combined effect of noncombustible gasses released during a wider range of temperature, as discussed previously in FT-IR analysis of the pyrolysis gasses.

In general, combining cork and APP resulted in a decrease in the flammability potential of FR-ABS composites compared to when they were added individually to ABS, confirming the occurrence of a synergistic interaction between APP and cork during pyrolysis.

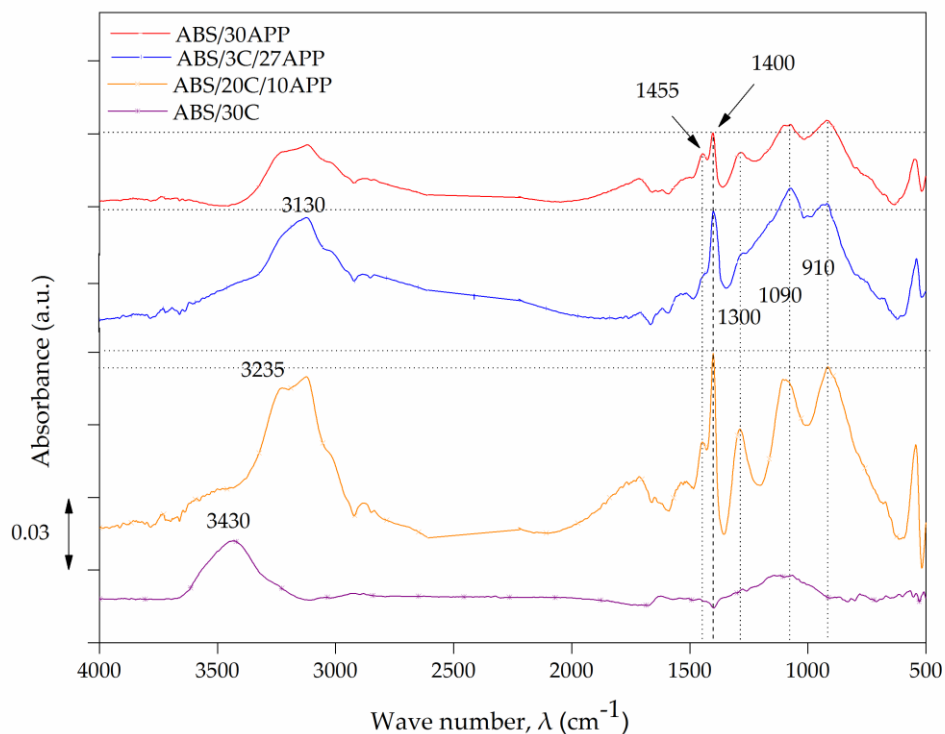
**Table VI.5.** Summary of data obtained by MCC for ABS and ABS composites.

<b>Samples</b>	<b>pHRR (W/g)</b>	<b>HRC (J/g-K)</b>	<b>Temperature to pHRR (°C)</b>	<b>Residue (%)</b>
ABS	665 ± 22	649 ± 18	473 ± 1	2.6 ± 0.1
ABS/30APP	517 ± 13	498 ± 15	470 ± 1	10.7 ± 0.1
ABS/3C/27APP	440 ± 9	419 ± 6	464 ± 1	12.8 ± 0.2
ABS/20C/10 APP	385 ± 2	360 ± 4	463 ± 1	13.3 ± 0.2
ABS/30C	523 ± 16	503 ± 20	451 ± 1	7.1 ± 0.1

### VI.3.6 Chemical analysis of MCC residue

Figure VI.13 shows a comparative of the FTIR spectra of the ABS/30APP, ABS/3C/27APP, ABS/20C/10APP and ABS/30C residue after the MCC test. FTIR spectra of the ABS/30APP exhibited a broad absorption band at 3400-3000  $\text{cm}^{-1}$  related to N-H and OH stretching vibration [166, 254]. The band at 1455  $\text{cm}^{-1}$  and the sharp peak at 1400  $\text{cm}^{-1}$  belonged to asymmetric deformation vibration of  $\text{CH}_3/\text{CH}_2$  and phosphorus oxynitrides, respectively, as a result of dehydration and cross-linking reactions of APP [251, 254]. The peaks at 1300  $\text{cm}^{-1}$  and 1090  $\text{cm}^{-1}$  were attributed to stretching vibration of P=O and P-O-P, respectively, and the peak appeared at 910  $\text{cm}^{-1}$  was assigned to P-O-C structure in P-C complex confirming the existence of P-O-C chemical bonds in char layer, which further indicates a cross-linking reaction between components [166, 255]. For ABS/30C, at 3430  $\text{cm}^{-1}$ , a peak related to O-H stretching and a broad band between 1360  $\text{cm}^{-1}$  and 830  $\text{cm}^{-1}$  assigned to C-O and C-H deformation were observed [256].

ABS/3C/27APP and ABS/20C/10APP showed similar absorbance bands as the ones registered for ABS/30APP, with a small shoulder at 3430  $\text{cm}^{-1}$  related to OH absorbance of cork. By comparing FTIR spectra of ABS/3C/27APP and ABS/30APP, it can be seen that the peak at 1090  $\text{cm}^{-1}$  attributed to P-O-P stretching was more intense by replacing 3 wt% of APP with cork, which is in good agreement with the charring ability of cork and a synergistic effect between cork and APP in the condensed phase. By further substituting APP up to 20%, the intensity of the peak at 1400  $\text{cm}^{-1}$  assigned to phosphorus oxynitrides was increased significantly compared to the other vibrations of phosphorus, also a slight increase in the intensity of the P-O-C band at 910  $\text{cm}^{-1}$  was noticed. The analysis of the MCC residues confirms the ability of cork to retain phosphorus in the condensed phase during pyrolysis.



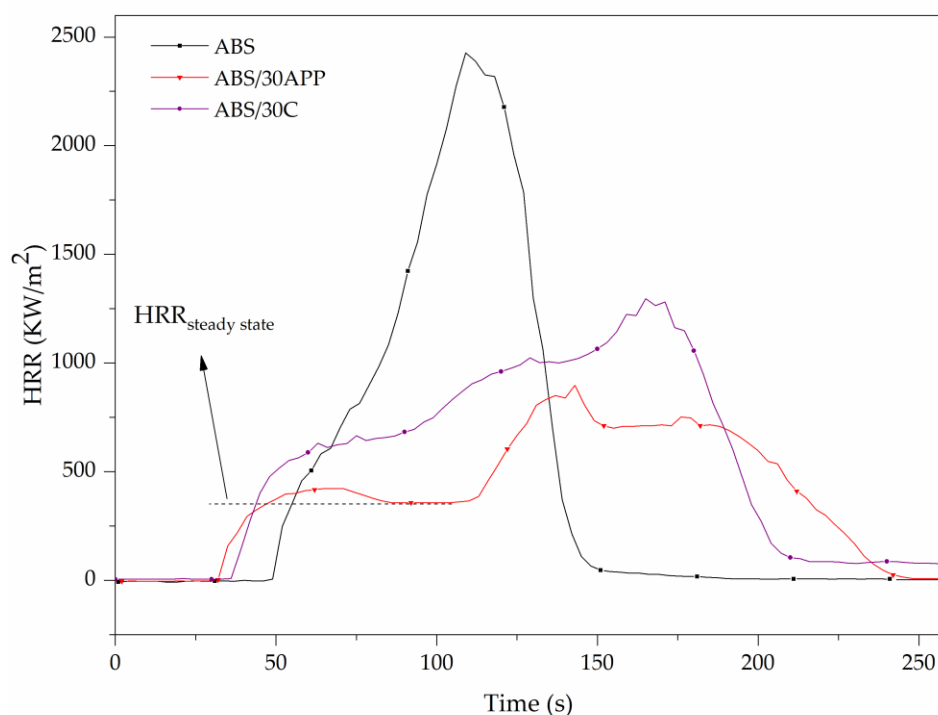
**Figure VI.13.** FTIR spectra of the ABS/30APP, ABS/3C/27APP, ABS/20C/10APP and ABS/30C residue after MCC test.

### VI.3.7 Fire behavior

Cone calorimetry is the most used technique to evaluate the fire behavior of polymeric materials. The combustion environment of the samples in this technique is similar to the real scale fire, so the cone calorimeter results can largely reflect the fire performance of the samples [164].

The HRR curves for ABS, ABS/30APP and ABS/30C, obtained from cone calorimetry test, as a function of time are shown in Figure VI.14. Heat release curve of neat ABS is characteristic of thermally thin samples [164] that elevated quickly after ignition, followed by a less intense increase. The latter increase could be related to a growing pyrolysis zone thickness during the cone test [165]. Finally, this increase reached its maximum value ( $2835 \text{ kW/m}^2$ ), a sharp peak, with a rapid HRR decrease to the end of burning. This peak behavior was strongly associated with increasing thermal feedback from the back of the sample and with the consumption of combustible matrix as the result of the burning. This feature indicates that the ABS combustion flame spreads

rapidly. Also, no remarkable residue formation at the end of ABS consumption was noticed (0.25%).



**Figure VI.14.** Heat release rate vs. time curves of ABS, ABS/30APP and ABS/30C.

Heat release rate of ABS/30APP showed a characteristic of the thermally thick charring materials [164]. It gradually increased after flaming combustion until it reached a quasi-static plateau associated with a char layer formation in the condensed phase and with the liberation of ammonia and water of APP which diluted the combustible gasses in the gas phase. Then, a sudden increase in HRR was observed showing that the char cracked and did not work as an effective thermal insulator and physical barrier to the mass transfer. After reaching the pHRR ( $864 \text{ kW/m}^2$ ), a decrease of HRR with the formation of a new plateau between 150-200s was observed before the end of combustion. This sample showed the highest amount of residue with 25% of char formation. On the other hand, ABS/30C curve exhibited an intermediate thickness non-charring fire behavior and contrary to ABS/30APP, no constant HRR or plateau was registered for ABS/30C [164]. After passing pHRR of  $1374 \text{ kW/m}^2$ , the HRR decreased rapidly implying that the sample was consumed with no char barrier effect. It should also be noted that at the end of the combustion process, this sample continued burning with a constant residual HRR for a long period

of time (250-550s), without flame with significant white smoke release and no remarkable residue remained (see Table VI.6).

**Table VI.6.** Main results obtained from cone calorimeter tests.

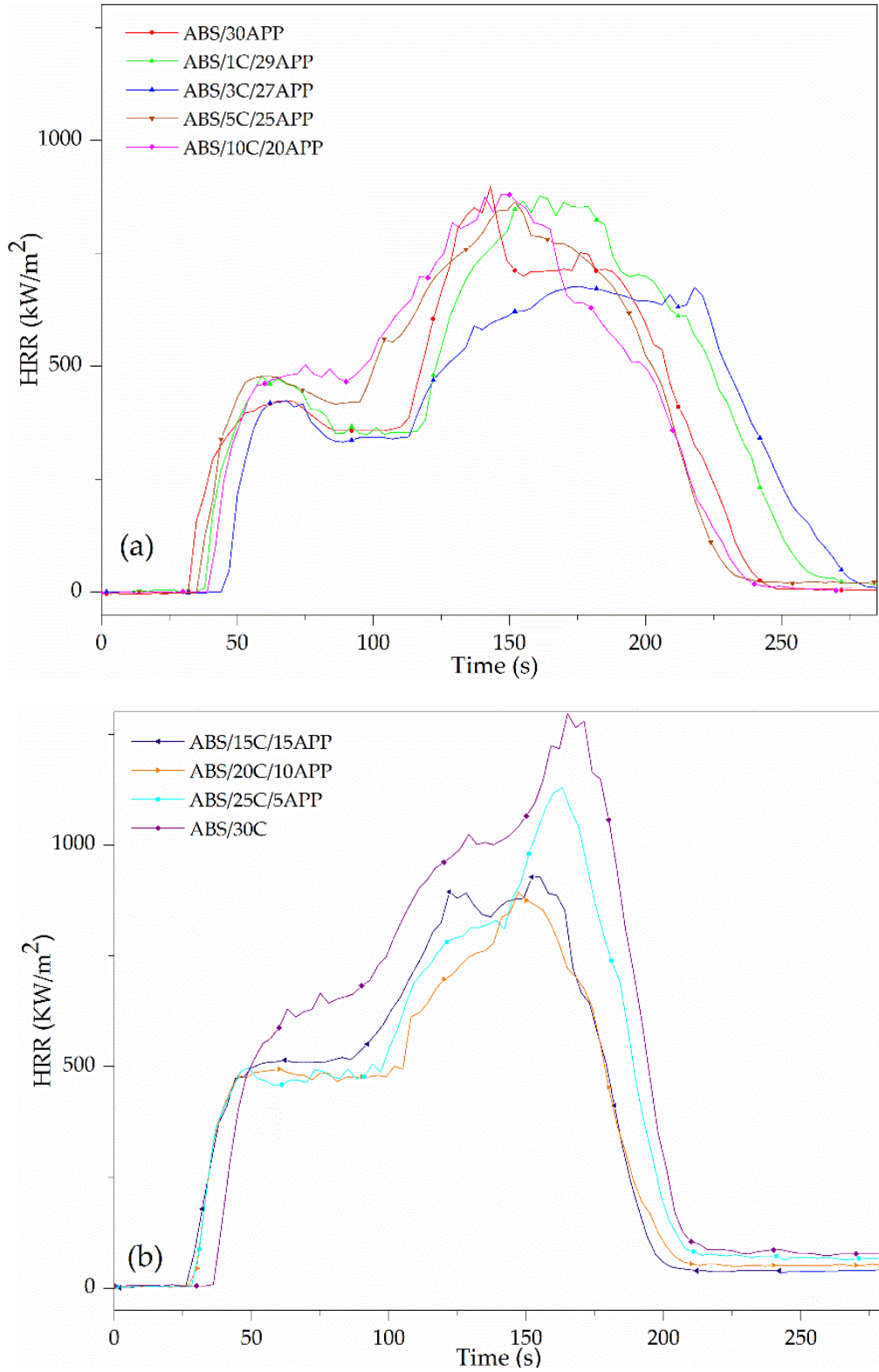
<b>Materials</b>	<b>TTI (s)</b>	<b>pHRR (kW/m<sup>2</sup>)</b>	<b>t<sub>PHRR</sub> (s)</b>	<b>t<sub>combustion</sub> (s)</b>	<b>EHC (MJ/kg)</b>	<b>FRI</b>	<b>Residue (wt%)</b>
ABS	44 ± 8	2835 ± 84	113 ± 1	143 ± 3	35 ± 1	-	0.25 ± 0.01
ABS/30APP	30 ± 2	864 ± 47	144 ± 1	246 ± 3	31 ± 2	3.1	25 ± 0.1
ABS/1C/29APP	32 ± 3	852 ± 32	167 ± 9	251 ± 9	31 ± 1	3.4	25 ± 0.1
ABS/3C/27APP	41 ± 5	680 ± 9	174 ± 2	264 ± 5	29 ± 1	5.3	24 ± 0.1
ABS/5C/25APP	31 ± 1	827 ± 50	147 ± 9	221 ± 5	30 ± 1	2.5	21 ± 0.1
ABS/10C/20APP	33 ± 6	922 ± 60	136 ± 60	220 ± 14	28 ± 1	3.2	18 ± 0.2
ABS/15C/15APP	26 ± 1	941 ± 19	150 ± 19	194 ± 3	28 ± 1	2.4	15 ± 0.1
ABS/20C/10APP	27 ± 1	932 ± 53	150 ± 3	195 ± 7	27 ± 1	2.5	10 ± 0.6
ABS/25C/5APP	29 ± 1	1155 ± 36	162 ± 1	203 ± 3	30 ± 1	2.1	5 ± 0.5
ABS/30C	33 ± 4	1374 ± 99	158 ± 10	143 ± 2	33 ± 1	1.7	0.3 ± 0.01

Regarding the FRI which proposes a classification for flame retarded polymeric materials based on the results obtained from the cone calorimetry test, all ABS/C/APP flame retarded formulations are classified as good with  $10^0 < \text{FRI} < 10^1$  and for ABS/3C/27APP, the highest FRI of 5.3 was achieved (see Table 5).

Figure VI.15 (a) presents the HRR curves of formulations with C/APP < 1. Among these formulations, ABS/3C/27APP showed a significant fire retardancy enhancement compared to ABS/30APP. By substituting 3 wt.% of APP with cork, HRR curve exhibited a later time to ignition and a constantly lower HRR than that of ABS/30APP, with a decrease of the second PHRR of 21% respect to ABS/30APP. As previously discussed in FTIR analysis of the pyrolysis gasses, a higher release amount of water and ammonia before and during the beginning of ABS decomposition, due to the dehydration reactions of cork and volatilization of APP, contributed to an enhancement action on the gas phase by diluting the combustible gasses which led to the

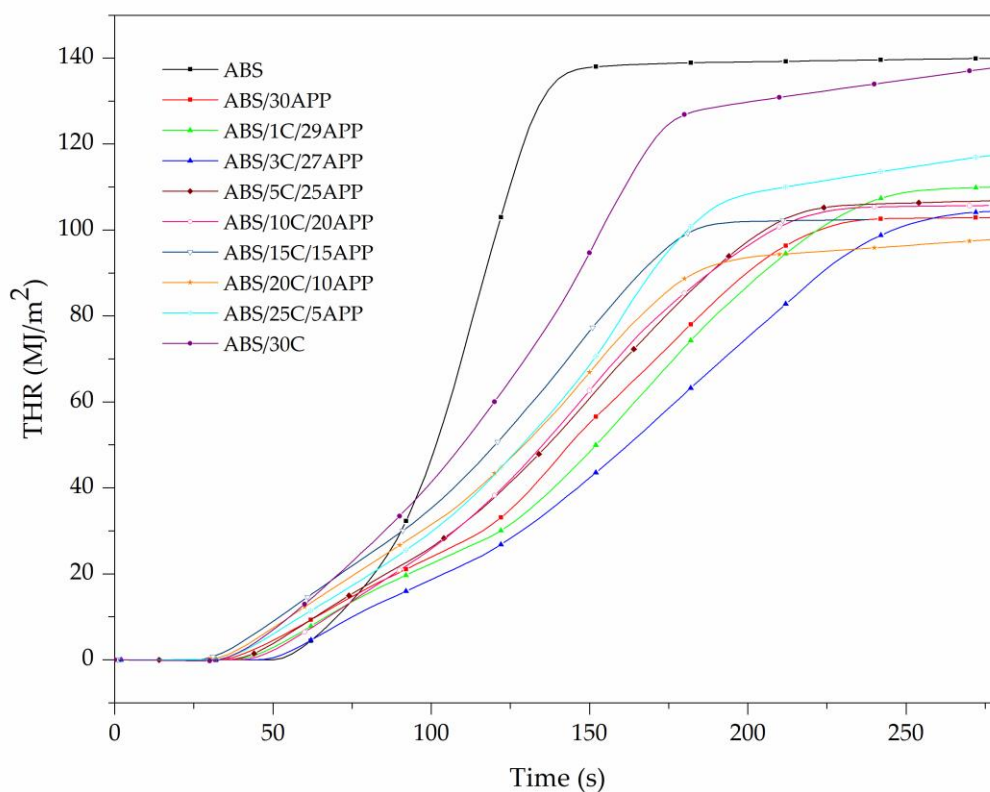
ignition delay and to the lower HRR during combustion of the mentioned composite regarding ABS/30APP. In addition, the time period between the two HRR peaks was relatively longer for the mentioned ABS cork/APP composite, indicating that a more protective carbonaceous layer than that of ABS/30APP was also produced. This fact was a result of the synergistic chemical interaction between cork and APP at the beginning of decomposition observed in TGA that could lead to the formation of a more cohesive and cross-linked char layer acting as a heat and mass transfer barrier. Figure VI.15 (a) shows also that replacement of APP to lower or higher than 3 wt.% of cork has an adverse effect on the fire performance of ABS flame retardant composites.

Figure VI.15 (b) presents the HRR curves of ABS formulations with C/APP ratio  $\geq 1$ . When cork was the major additive, it was observed that 20 wt.% substitution led to the lowest pHRR and a longer period of time that the protective char layer was formed. This was shown as a quasi-static plateau during the 25-110 s in the HRR curve that is typically considered as a barrier effect which controls the polymer degradation rate. However, a slightly higher pHRR was registered for ABS/20C/10APP compared to formulations with C/APP ratio  $< 1$ . This fact was related to thermo-oxidative degradation of char, which decreased its efficiency in protecting the underlying material after 110 s to the end of the combustion. Nevertheless, ABS/20C/10APP showed the lowest EHC (see Table 5), and a low residue formation at the ending of combustion, indicating that a gas phase mechanism of action by continuous water release that led to a dilution of the combustible gasses occurred [257], in agreement with the FTIR analysis of pyrolysis gasses.



**Figure VI.15.** Heat release rate vs. time curves of ABS formulations with (a)  $C/APP < 1$  and ABS/30APP (b)  $C/APP \geq 1$  and ABS/30C.

In Figure VI.16, THR curves of ABS and its composites are presented. It can be seen that THR curve of ABS/3C/27APP exhibited the lowest slope compared to the other formulations, indicating that the highest reduction of the fire spread took place for that formulation. In addition, by increasing the amount of cork, the slope of the curves increased.



**Figure VI.16.** Total heat release rate of ABS and ABS formulations.

In addition, the flammability behavior (reaction to a small flame) of ABS and ABS formulations was assessed by UL-94 horizontal burning tests. The results of UL-94 tests are summarized in Table VI.7. In UL-94 horizontal test, replacing 3 wt.% of APP with cork resulted in the lowest LBR, indicating an enhancement in fire retardancy behavior compared with ABS/30APP, in agreement with the TTI delay, the highest reduction of pHRR and the lowest THR slope for this formulation observed in cone calorimetry. Also, for ABS/20APP/10C, the same LBR as ABS/30APP was noted, implying that by substituting 20 wt.% of APP with cork, similar fire



performance can be achieved, also in agreement with CC analysis. It should be mentioned that for the formulations with C/APP ratio  $\geq 1$ , no dripping during the tests was observed.

**Table VI.7.** UL-94 horizontal results of ABS and ABS composites.

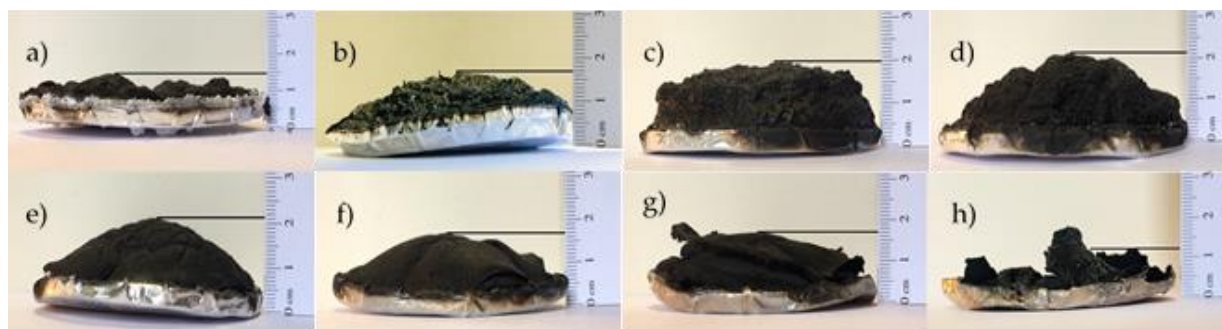
<b>Materials</b>	<b>Linear burning rate (LBR) (mm/min)*</b>	<b>Dripping</b>
ABS	44	Yes
ABS/30APP	24	Yes
ABS/1C/29APP	21	Yes
ABS/3C/27APP	19	Yes
ABS/5C/25APP	28	Yes
ABS/10C/20APP	28	Yes
ABS/15C/15APP	32	No
ABS/20C/10APP	24	No
ABS/25C/5APP	32	No
ABS/30C	41	No

\* Each value is the average of performed experiments with variation coefficients within 1–2.

### *VI.3.8 Morphological and chemical analysis of CC residue*

Digital photographs of residues after cone calorimetry are shown in Figure VI.17. Remarkable differences were noticed between them and related to composition of ABS composites. As is possible to see, ABS/30APP generated a carbonaceous residue with the lowest expansion degree. On the other hand, ABS/30C did not show residue formation ability during combustion, as previously discussed, and for that reason digital photography was not included. In addition, when both cork and APP were added into ABS, different expansion degrees and surface structure were produced. Among all ABS/C/APP formulations, ABS/3C/27APP formed the most stable, uniform and compact char structure with a significant expansion degree, which contributed to fuel and heat transfer reduction in agreement with cone calorimeter results. However, by increasing C/APP ratio,

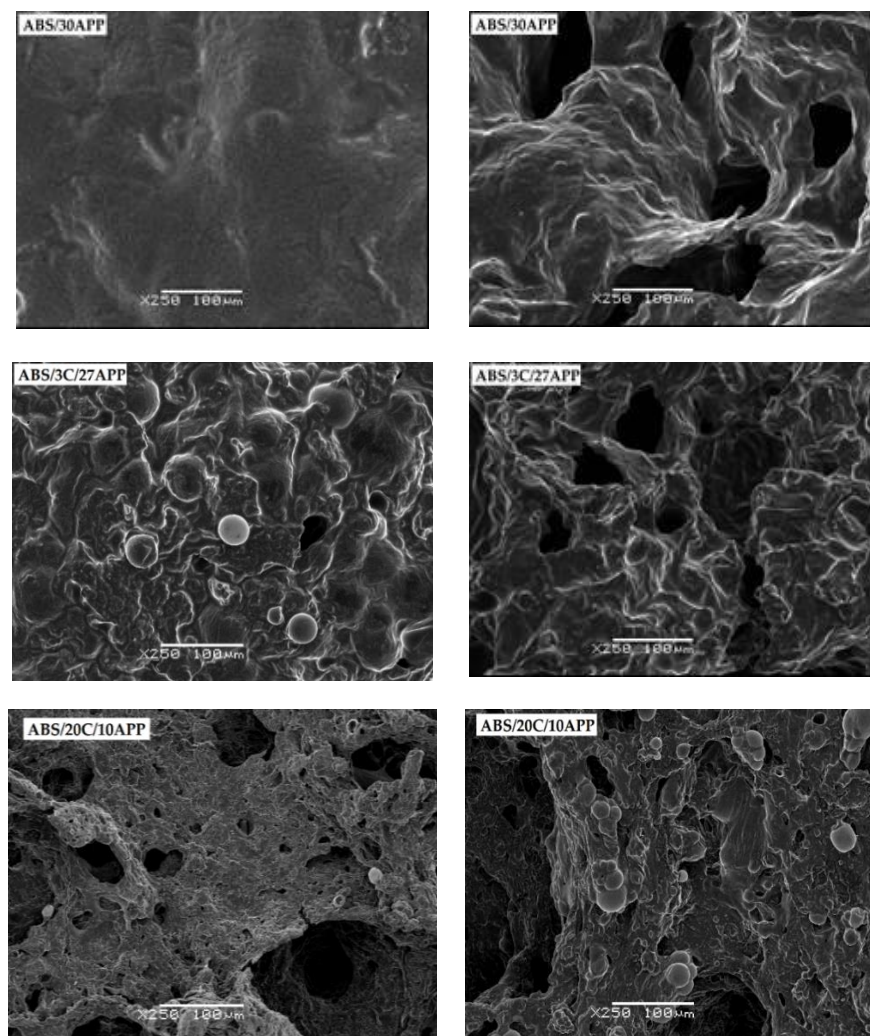
the expansion and uniformity degree of the char layer gradually decreased which reduced barrier effectiveness and shielding efficiency of the residue.



**Figure VI.17.** Digital photographs of (a) ABS/30APP, (b) ABS/1C/29APP, (c) ABS/3C/27APP, (d) ABS/5C/25APP, (e) ABS/10C/20APP, (f) ABS/15C/15APP, (g) ABS/20C/10APP, and (h) ABS/25C/5APP residue after cone calorimetry. The approximate residue thickness is indicated on the scale (in centimeters).

The surface of ABS/30 APP, ABS/3C/27APP and ABS/20C/10APP residue after cone calorimetry was observed by SEM to identify the quality of the protective layer and also to analyze the formed structure under that layer. Heat transfer through the char layer depends on the resistance of the substrate to fire, so the char formation process, intumescent effect and insulation efficiency of the char layer dominate general flame-retardant properties of the system.

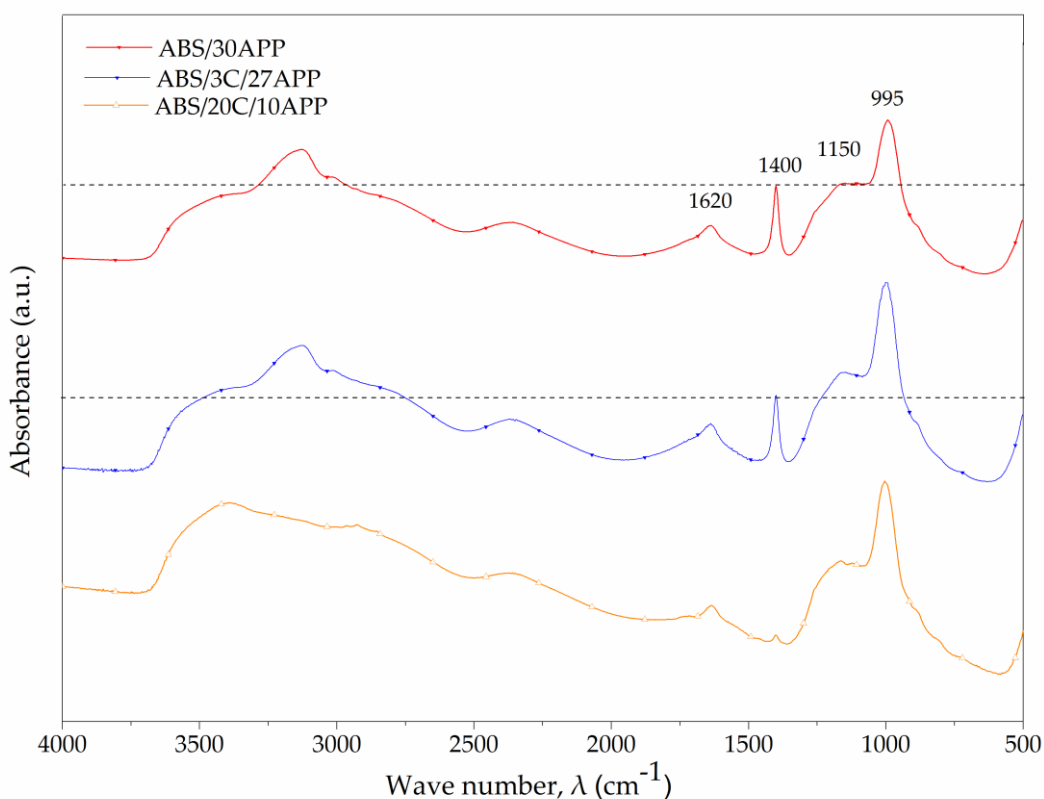
As it is shown in Figure VI.18, ABS/30APP residue has a flat surface and smooth layer surface. By replacing cork with APP, evidence of a higher protective residue was observed, the surface of this residue showed an intumescent layer with a porous inner structure. By having 3 wt.% of cork a more protective and cohesive layer with the formation of a foamed structure, composed by closed microspheres, was noticed. This more effective heat insulating foamed structure combined with the cohesive surface layer resulted in an improved performance on the condensed phase which could also act as a physical barrier against gas transmission which endorses the results previously discussed in cone calorimetry. Furthermore, by increasing the amount of cork up to 20 wt.% a porous morphology with bigger pores was also observed. Due to the increase of the pores size, it can be concluded that the effectiveness of this foamed barrier was diminished that resulted in a higher heat release rate leading to a lower flame retardancy behavior in cone calorimetry compared to ABS/3C/27APP.



**Figure VI.18.** SEM micrographs of the upper (left) and down surface (right) of the ABS formulations after the cone calorimeter tests (at  $250\times$  with a scale bar of  $100\ \mu\text{m}$ ).

Figure VI.19 shows a comparative of the FTIR spectra of the ABS/30APP, ABS/3C/27APP and ABS/20C/10APP residue after cone calorimeter test. FTIR spectra of the ABS/30APP exhibited a broad absorption band at  $3800\text{--}2500\ \text{cm}^{-1}$  related to N-H and OH stretching vibration [166, 254]. The sharp peak which appeared at  $1400\ \text{cm}^{-1}$  belonged to phosphorus oxynitrides as a result of dehydration and cross-linking reactions of APP [251, 254]. In addition, the shoulder at  $1150\ \text{cm}^{-1}$  was attributed to the absorption of C-O-C groups and the peak at  $995\ \text{cm}^{-1}$  was assigned to P-O symmetric stretching in P-O-C chemical bands [166, 255].

ABS/3C/27APP showed similar absorbance bands as the ones registered for ABS/30APP. By comparing FTIR spectra of ABS/3C/27APP and ABS/30APP, it can be seen that the signal at  $995\text{ cm}^{-1}$  attributed to P-O-C absorbance peak was more intense by replacing 3 wt.% of APP with cork, due to the charring ability of cork and a probable synergistic effect between cork and APP in the condensed phase, in accordance with cone calorimetry results. By further substituting APP up to 20 wt.%, the peak at  $1400\text{ cm}^{-1}$  of phosphorus oxynitrides almost disappeared and the intensity of the peaks related to the vibrations of phosphorus were slightly decreased, contrary to the higher intensity vibrations of phosphorus registered for this formulation under non oxidative thermal decomposition in MCC.



**Figure VI.19.** FTIR spectra of the ABS/30APP, ABS/3C/27APP and ABS/20C/10APP residue after cone calorimeter test.

## *VI.4 Conclusions*

In this work, ABS and ABS composites containing APP and/or cork were prepared and characterized. APP and cork particles showed different contributions to the mechanical properties of ABS composites obtained by DMTA. An increase in storage modulus was registered in the case of ABS composite with 30 wt.% of APP, due to the higher stiffness of APP particles. On the other hand, by substituting APP with cork, a continuous reduction of storage modulus was observed. TGA analysis of the composites under pyrolysis showed that when both APP and cork were presented, a higher amount of residue remained at 800 °C compared to when APP and cork were added individually, indicating an enhancement of charring ability and thermal stability of char residue at higher temperature than expected. It was also observed that for the formulations with C/APP ratio lower than 1, the second step began at lower temperature than expected, which implied that cork and APP chemical interaction resulted in an earlier decomposition of the polyphosphate network of APP. On the other hand, when cork was the main additive, an unexpected thermal decomposition stage appeared also confirming the presence of chemical interactions between these two additives that probably resulted in an acceleration and promotion of dehydration reaction of cork combined with APP earlier thermal decomposition.

In addition, FTIR analysis of the pyrolysis gasses showed interactions between cork and APP that promoted the liberation of non-flammable gasses at a wider range of temperatures compared to ABS/30APP that diluted the combustible ones during ABS decomposition. Pyrolysis combustion analysis revealed that substituting APP with cork presented a lower potential flammability of ABS composites by a HRC decrease and an increase of residue compared to ABS/30APP. Furthermore, fire behavior of ABS formulations was studied by cone calorimetry, showing that a small substitution of APP by 3 wt.% of cork imparted optimum improvement in fire retardancy performance with the highest efficiency in reducing the pHRR (21%) and LBR (26%). ABS/20C/10APP also showed a similar pHRR and same burning rate in horizontal UL-94 to the fully synthesized ABS/30APP with the lowest EHC registered among all formulations.

Additionally, from SEM micrographs of ABS/30APP residue was possible to ascertain that a continuous char layer without intumescence was formed. Nevertheless, by only replacing 3 wt.% of APP natural cork powder led to the formation of a protective intumescent char with a foamed and cohesive structure that acted as a more efficient physical barrier against heat and mass transfer.

In the FTIR analysis of residue, by comparing FTIR spectrum of ABS/30APP and ABS/3C/27APP, the same peaks were observed with different intensity for characteristic absorption peaks of P-O-C structure, further indicating a probable cross-linking reaction between cork and APP due to the chemical interaction between them. Based on TGA, FTIR of evolved gasses, fire test results and FTIR of residue of ABS/C/APP formulations, evidences of occurrence of gas phase activity via release of non-flammable gasses and condensed-phase activity through intumescent charring ability were noted.







Effect of cork powder's phosphorylation on  
thermo-mechanical, thermal stability and  
fire behavior of ABS formulations

Chapter  
**VII**



## Chapter VII: Effect of cork powder's phosphorylation on thermo-mechanical, thermal stability and fire behavior of ABS formulations

### *VII.1 Introduction*

Developing new sustainable materials is considered a promising approach that has caught the attention of science and industry due to the many environmental benefits. On the other hand, regarding circular economy, composite containing agricultural and forest waste or by-products have shown an important strategy for bio-waste valorization [23, 76, 169].

Cork, a natural and renewable material has garnered attention in recent years for its potential applications in sustainable and eco-friendly products. One area of particular interest is its use as a flame retardant material, as the inherent properties of cork make it a promising candidate for enhancing fire reaction via its char forming ability. In this context, investigating the effect of phosphorylation and surface modification of cork powder on the improvement of its flame retardancy behavior can be interesting. By incorporating phosphorus based flame retardants and cork phosphorylation, studies aim to improve its charring ability and its effectiveness as a bio-flame retardant.

Several studies have been focused into the using phosphorylated biomaterials, highlighting their potential in advancing sustainable material development. For instance, chitosan derivatives, that are considered as polysaccharides, were phosphorylated with  $P_4O_{10}$  reaction with glycidyl methacrylate in order to prepare a flame retardant material for epoxy. MCC results showed that presence of phosphorylated chitosan led to a 56% reduction of the peak heat release and 50% of total heat release of epoxy composites. FTIR of evolved gasses and the residue revealed that phosphorylation reduced the release of combustible gasses and promoted a more protective residue formation respectively [104].

In another study wheat starch was modified using a phosphate/urea reaction system. It was shown that starch derivatives from phosphate/urea systems could achieve fire protection

efficiencies similar to those of commercial flame retardants currently used in the wood fiber industry. FR efficiency was dependent on the phosphate content, solubility, reaction time, and the additive form such as physical mixture, uncleaned, or cleaned synthesis products. The calorimetric measurements also exhibited a significant reduction in HRR compared to untreated wood fibers indicating an enhancement in fire retardancy behavior of wood fibers [258].

An enhancement of flame retardancy was observed when phosphorylated lignin (P-LIG) with 4.1% of phosphorus content was synthesized and 30 wt.% of P-LIG was added to ABS composites. The thermal stability of P-LIG was significantly enhanced in comparison to that for lignin. Grafting phosphorus onto lignin significantly increased the amount of residue from the polymer blend at high temperature. It was reported that P-LIG promoted char formation by reacting with ABS during thermal decomposition leading to a significant reduction of the peak of heat release rate pHRR and THR of 58% and 20%, respectively. It was shown that P-LIG was acting mainly in the condensed phase by interacting with ABS during the decomposition of the composite. These interactions induced less release of combustibles to the flame while a charring protective barrier was formed on the composite surface. A slight inhibition effect in the flame was observed as well, probably caused by release of phosphorus species into the gas phase [40].

In the previous chapter the effect of combining cork powder and ammonium polyphosphate on thermal stability and fire performance of ABS was reported. In order to achieve further enhancement in fire behavior of ABS composites, cork surface modification was carried out with the aim of the occurrence of a phosphorus chemical bonding on the surface of cork powder by using different phosphorus components. As previously mentioned, the use of phosphorus chemistry in combination with biomaterials is of great interest, as it would give access to renewable resources characterized by intrinsic flame-retardant properties. In the present chapter, firstly, the chemical analysis of phosphorylated cork by using different phosphorus components and under different reaction conditions is reported. Then, the effect of cork phosphorylation on the thermomechanical behavior, thermal stability and fire performance of ABS formulations has been investigated. The cork modification presented in this chapter has been carried out during the stay at Yildiz Technical University in Istanbul, Turkey.

## VII.2 Composition of ABS formulations

The composition of the melt-compounded materials studied in this chapter is listed in Table VII.1.

**Table VII.1.** Materials identification and weight percentage (wt.%) of the components.

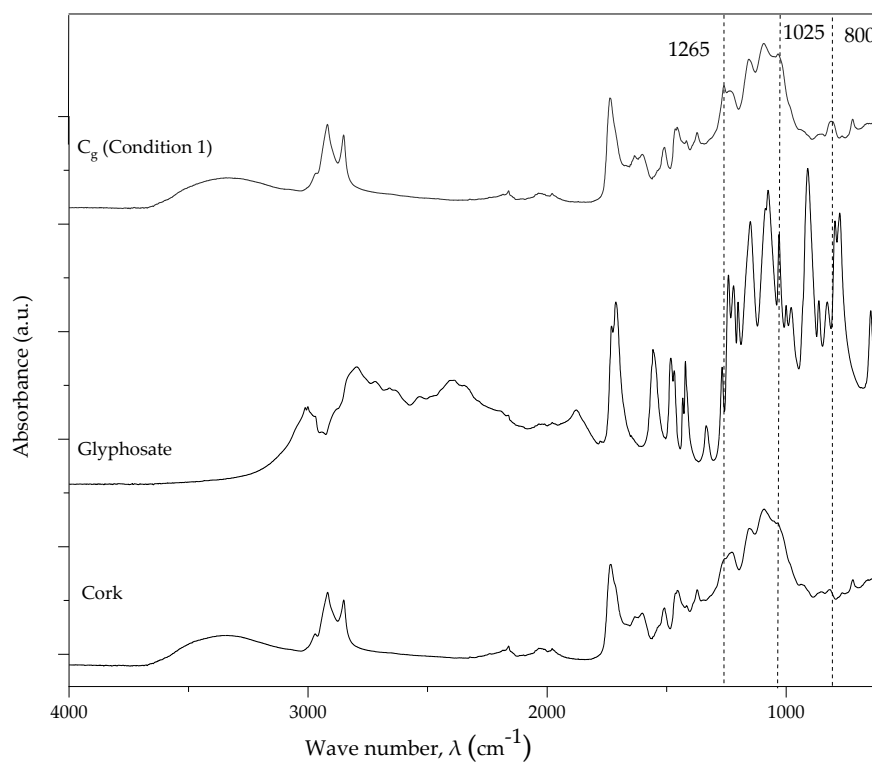
Materials	ABS (wt.%)	APP (wt.%)	C <sub>g</sub> (wt.%)	C <sub>d</sub> (wt.%)
ABS/30C <sub>g</sub>	70	-	30	-
ABS/30C <sub>d</sub>	70	-	-	30
ABS/20C <sub>g</sub> /10APP	70	10	20	-
ABS/20C <sub>d</sub> /10APP	70	10	-	20
ABS/3C <sub>g</sub> /27APP	70	27	3	-
ABS/3C <sub>d</sub> /27APP	70	27	-	3

## VII.3 Results and discussion

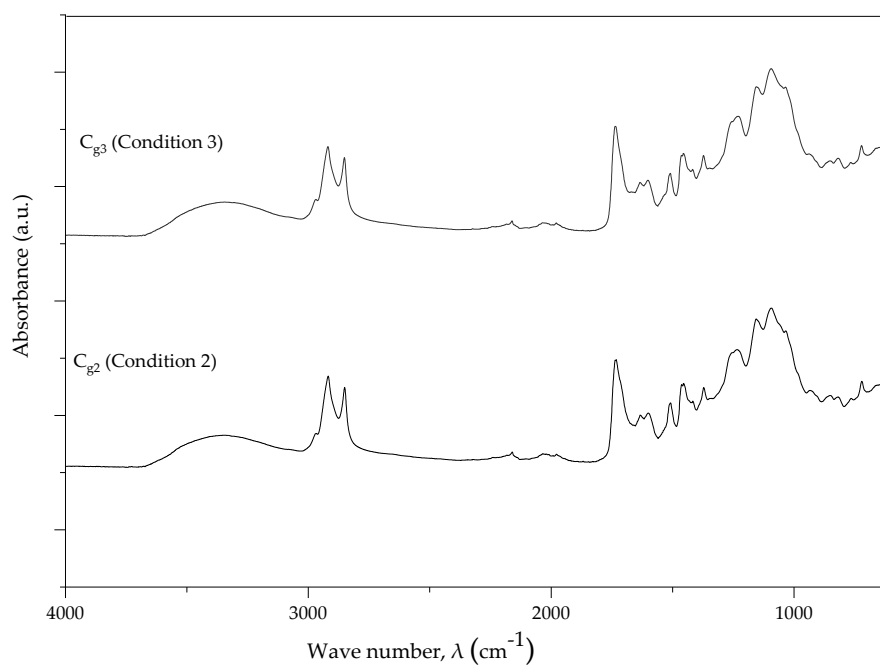
### VII.3.1 Chemical analysis of phosphorylated cork powder

To identify the presence of phosphorus absorbance bands after the phosphorylation and determine the best reaction condition, ATR-FTIR analysis was carried out for the raw materials and the phosphorylated samples. As the cork ATR-FTIR spectra has been discussed in detail in chapter V, in this part the spectrum of glyphosate, TEP, DTSP and the phosphorylated cork under different reaction conditions are presented.

In Figure VII.1 the glyphosate spectrum shows the absorbance peak at 3000 cm<sup>-1</sup> attributed to N-H stretching and the signals at 2800 cm<sup>-1</sup> and 2400 cm<sup>-1</sup> were assigned to C-H stretching. The peaks at 1560 cm<sup>-1</sup> and 1480 cm<sup>-1</sup> were related to NH<sub>2</sub> deformation of glyphosate while P=O stretching vibration of glyphosate PO<sub>3</sub>H group was registered at 1260 cm<sup>-1</sup>. The peaks at 1220 cm<sup>-1</sup>, 1075 cm<sup>-1</sup>, 1029 cm<sup>-1</sup>, 1000 cm<sup>-1</sup> and 800 cm<sup>-1</sup> were also attributed to P-OH, P-O-stretching, CCNC skeletal vibration, P-O symmetric stretching, and POH deformation of glyphosate, respectively [259, 260].



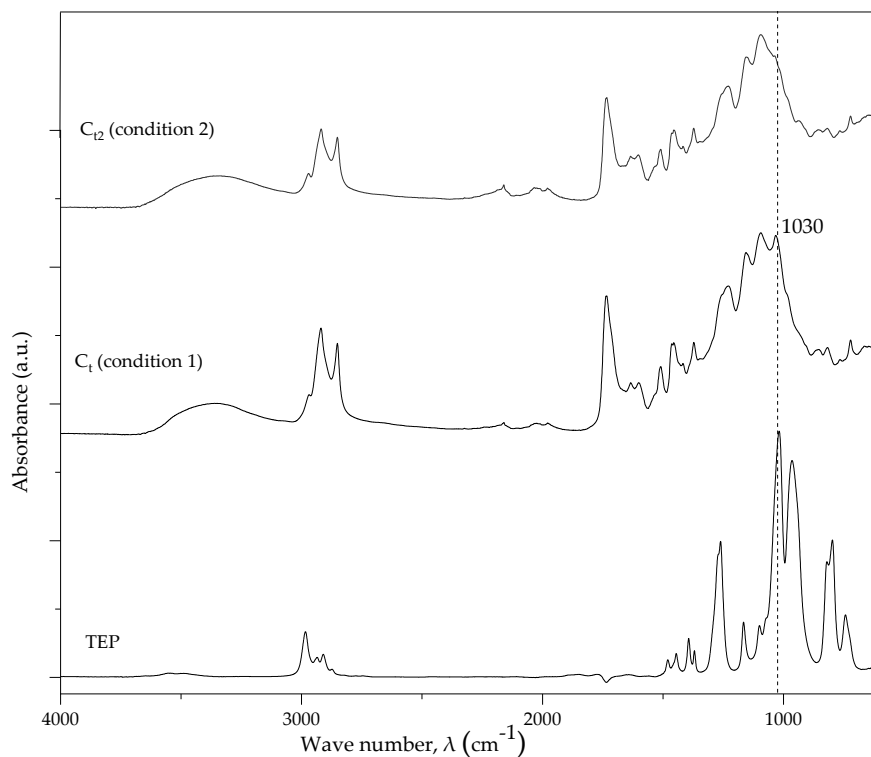
**Figure VII.1.** ATR-FTIR spectra of cork powder, glyphosate and phosphorylated cork with glyphosate under condition 1.



**Figure VII.2.** ATR-FTIR spectra of phosphorylated cork with glyphosate under condition 2 and 3.

As it was explained in chapter III, cork modification with glyphosate was carried out under three different reaction conditions. The  $C_g$  was washed with IPA, firstly; however, in the spectra of  $C_g$ , only main absorbance bands of glyphosate were detected and none of the cork absorbance signals appeared. In order to wash the excessive amount of glyphosate on the surface of the cork powder, a solution of ammonia:water (1:1) was used. After washing, the spectrum of the modified cork, at room temperature for three days (condition 1), showed the more intense absorbance bands at  $1265\text{ cm}^{-1}$ ,  $1025\text{ cm}^{-1}$  and  $800\text{ cm}^{-1}$  related to P=O stretching, CCNC skeletal vibration and POH deformation of glyphosate, respectively. On the other hand, under condition 2 and 3, similar spectra to cork without any changes were registered indicating that neither chemical nor physical bonding between cork and glyphosate occurred (Figure VII.2).

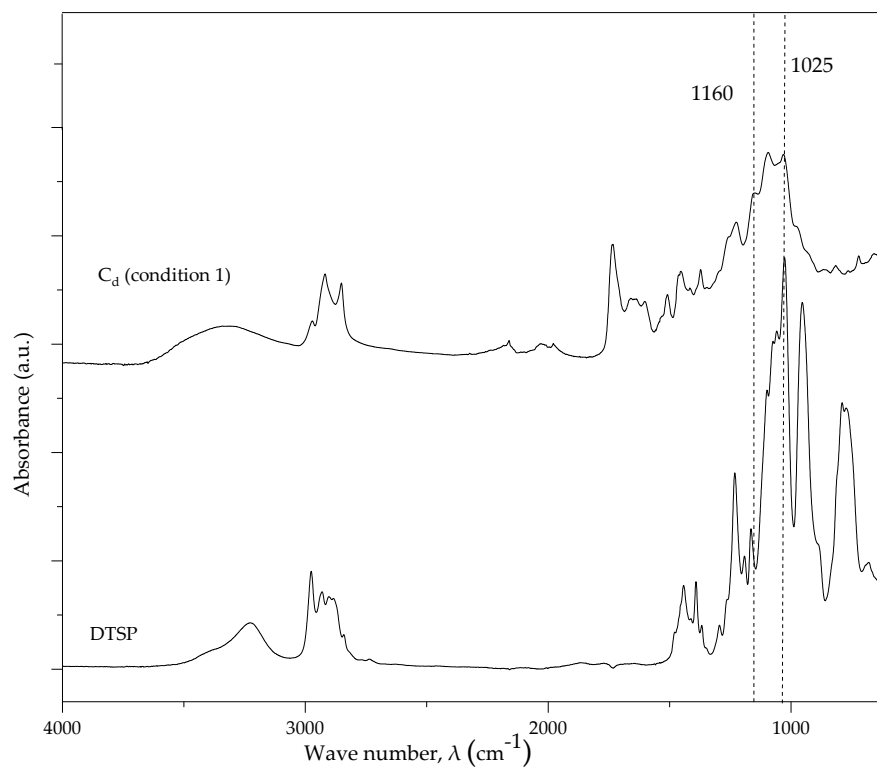
The spectra of TEP and  $C_t$  under two different reaction conditions are shown in Figure VII.3. The peaks at  $2980\text{ cm}^{-1}$ ,  $1445\text{ cm}^{-1}$ ,  $1390\text{ cm}^{-1}$  and  $1370\text{ cm}^{-1}$  were associated to C-H symmetric stretching. The absorbance signals appeared at  $1260\text{ cm}^{-1}$ ,  $1165\text{ cm}^{-1}$  and the sharp peak at  $1030\text{ cm}^{-1}$  were attributed to P=O,  $\text{PO}_3$  and O-P-O stretching vibration of TEP, respectively. Also, the absorbance bands of P-O-C stretching and P-O stretching vibrations were registered at  $965\text{ cm}^{-1}$  and  $795\text{ cm}^{-1}$  [261, 262]. By comparing ATR spectrum of  $C_t$  under two different conditions and cork powder, it can be seen that the modification under the condition 2 was not successful, however; under condition 1 at  $120\text{ }^\circ\text{C}$  for 12 hours, a new peak at  $1030\text{ cm}^{-1}$  attributed to O-P-O stretching vibration of TEP was observed.



**Figure VII.3.** ATR-FTIR spectra of TEP and phosphorylated cork with TEP under condition 1 and 2.

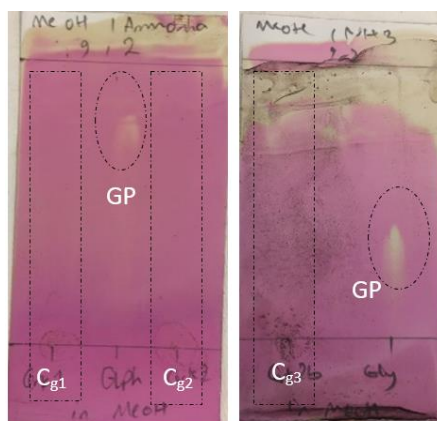
DTSP and  $C_d$  spectra are presented in Figure VII.4. The absorbance band of  $3225\text{ cm}^{-1}$  was attributed to the stretching vibration of the N–H group, and the signals at  $2975\text{ cm}^{-1}$ ,  $2930\text{ cm}^{-1}$  were assigned to the C–H stretching vibrations. Moreover, the phosphoryl (P=O) absorbance peak of DTSP was registered at  $1230\text{ cm}^{-1}$  and the absorption peak corresponding to P–N and Si–O groups appeared at  $1165\text{ cm}^{-1}$  and  $970\text{ cm}^{-1}$ , respectively. The signals of P–O–C at  $1025\text{ cm}^{-1}$  and of O–P–O at  $826\text{ cm}^{-1}$  were registered [141]. After modification of the cork with DTSP and washing several times with DCM and IPA, a more intense peak at  $1025\text{ cm}^{-1}$  corresponding to P–O–C and a small shoulder at  $1160\text{ cm}^{-1}$  related to P–N were observed.





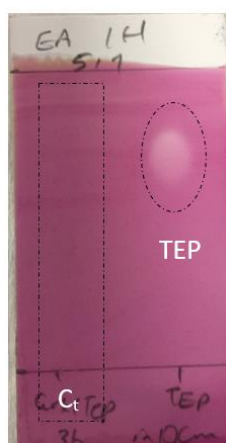
**Figure VII.4.** ATR-FTIR spectra of DTSP and phosphorylated cork with DTSP before and after washing.

TLC method was also carried out to investigate if the reaction and modification of cork powder was completed. Methanol: ammonia mixture was used as a solvent system for glyphosate residue and the best proportion (9:2) of mixture by observing the test results was chosen. Glyphosate is an organic compound, which reacts with a chromogenic reagent, which then forms a yellow colored spot. When the spot appeared for the modified cork indicated that there was some glyphosate remaining on the surface of the cork powder with no chemical or even physical bonding. Therefore, further washing procedure with ammonia and water (1:1) as commented in ATR-FTIR analysis was essential. The washing process continued until no spot was detected for the modified cork in TLC test (Figure VII.5).



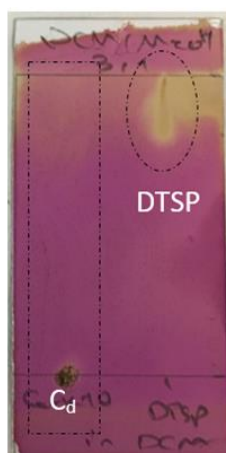
**Figure VII.5.** Digital photographs of TLC plates for glyphosate and phosphorylated cork with glyphosate.

Two solvent systems were prepared by mixing ethyl acetate and hexane 5:1 and 3:1 for detecting TEP residue. The best mixture ratio was chosen as 5 to 1. The presence of a small amount of TEP was observed for  $C_t$ , so it was washed with DCM and again with IPA before repeating the test. As it can be seen in Figure VII.6 no spot regarding the presence of TEP remaining was noticed.



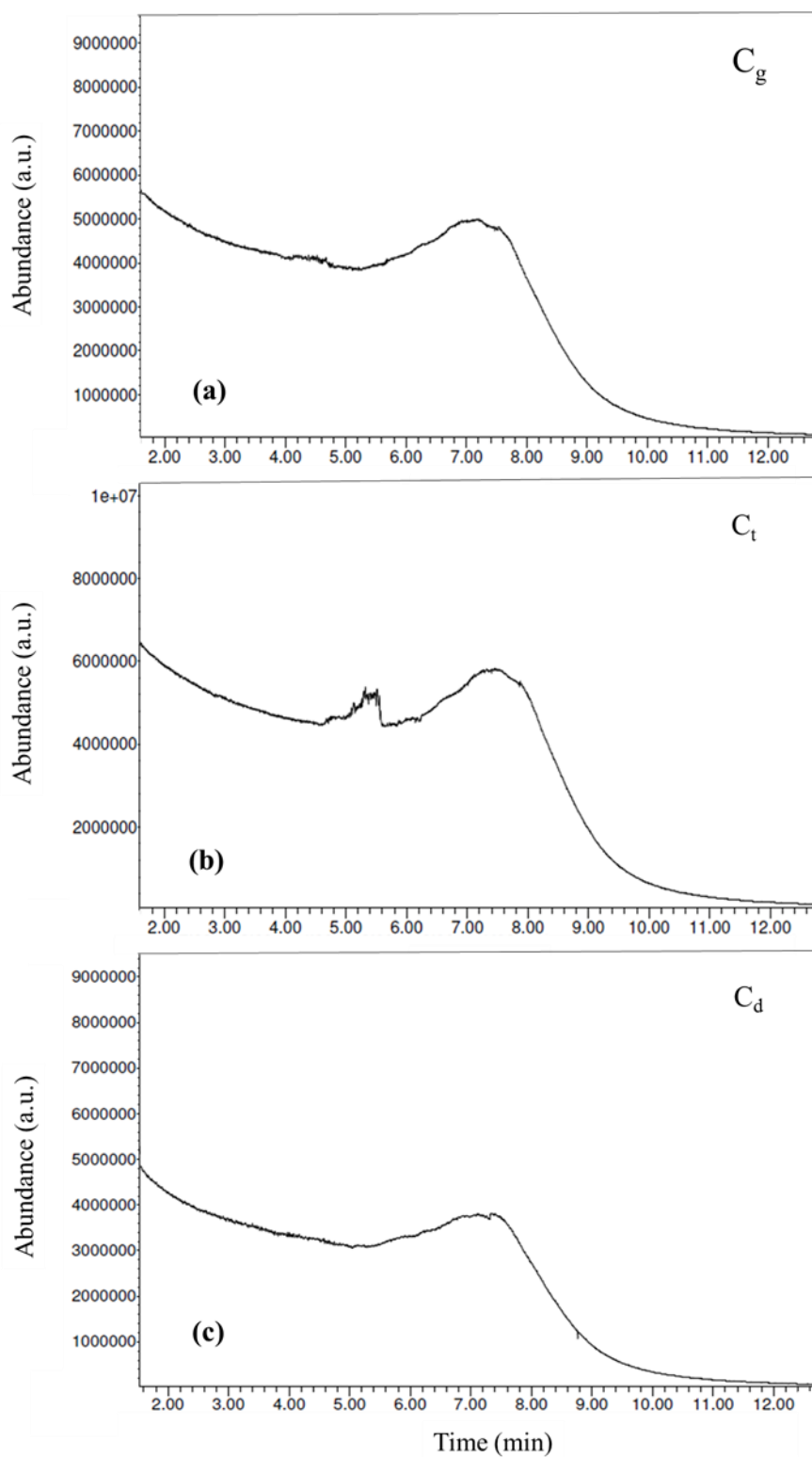
**Figure VII.6.** Digital photograph of TLC plates for TEP and phosphorylated cork with TEP.

In addition, two solvent systems were prepared by mixing DCM: Methanol (2:1 and 3:1) for detecting DTSP residue. The best mixture ratio was chosen as 2 to 1. DTSP was detected in the modified cork sample therefore it was washed with DCM and IPA before repetition of the TLC test. After washing no spot and trace of DTSP remaining was observed in the sample (Figure VII.7).



**Figure VII.7.** Digital photograph of TLC plates for DTSP and phosphorylated cork with DTSP, test was done with the ratio of 2:1 DCM: methanol as the solvent system.

To complete the TLC analysis and confirm that the phosphorylation reactions were successful GC-MS analysis was carried out. For  $C_g$  it can be seen in Figure VII.8, no significant amount of glyphosate residue was observed in the solution and the peak appeared with the retention time of approximately 7 minutes was related to the DCM [263], confirming a successful chemical bonding of glyphosate to the surface of cork.  $C_t$  exhibited the presence of small vibrations of TEP at 5.5 minutes, while, for  $C_d$ , no DTSP residue was observed, confirming the successful phosphorylation of cork powder with DTSP that was also observed in ATR-FTIR.



**Figure VII.8.** GC-MS chromatogram of phosphorylated cork with (a) glyphosate, (b) TEP and (c) DTSP.

In addition, quantitative data from the XPS analysis of the raw cork powder and phosphorylated cork samples are listed in Table VII.2. It shows the presence of C (73.0 wt.%), O (23.4 wt.%), N (2.7 wt.%) and Si (0.9 wt.%) atoms for cork powder. After phosphorylation and surface modification with glyphosate, %C and %Si were decreased to 71.4 wt.% and 0.6 wt.%, respectively, while %O, %N and %P atoms were increased to 23.6 wt.%, 3.6 wt.% and 0.9 wt.%, respectively. In addition, for  $C_t$ , the same trend was observed where the %C and %Si were decreased and %O, %N and %P atoms were increased, however the decrease and increase in the mentioned atoms was lower for  $C_t$  compared to  $C_g$ . Furthermore, by comparing  $C_d$  to other modified samples, the highest decrease in %C to 64.4 wt.% and highest increase in %O, %N, %Si and %P atoms to 25.1 wt.%, 4.4 wt.%, 3.5 wt.% and 2.4 wt.% was registered, respectively. All the obtained results confirmed the achievement of phosphorylation process for each phosphorus compound, where hydroxyl groups on the cork surface was substituted phosphoryl groups and the oxygen content was increased [264].

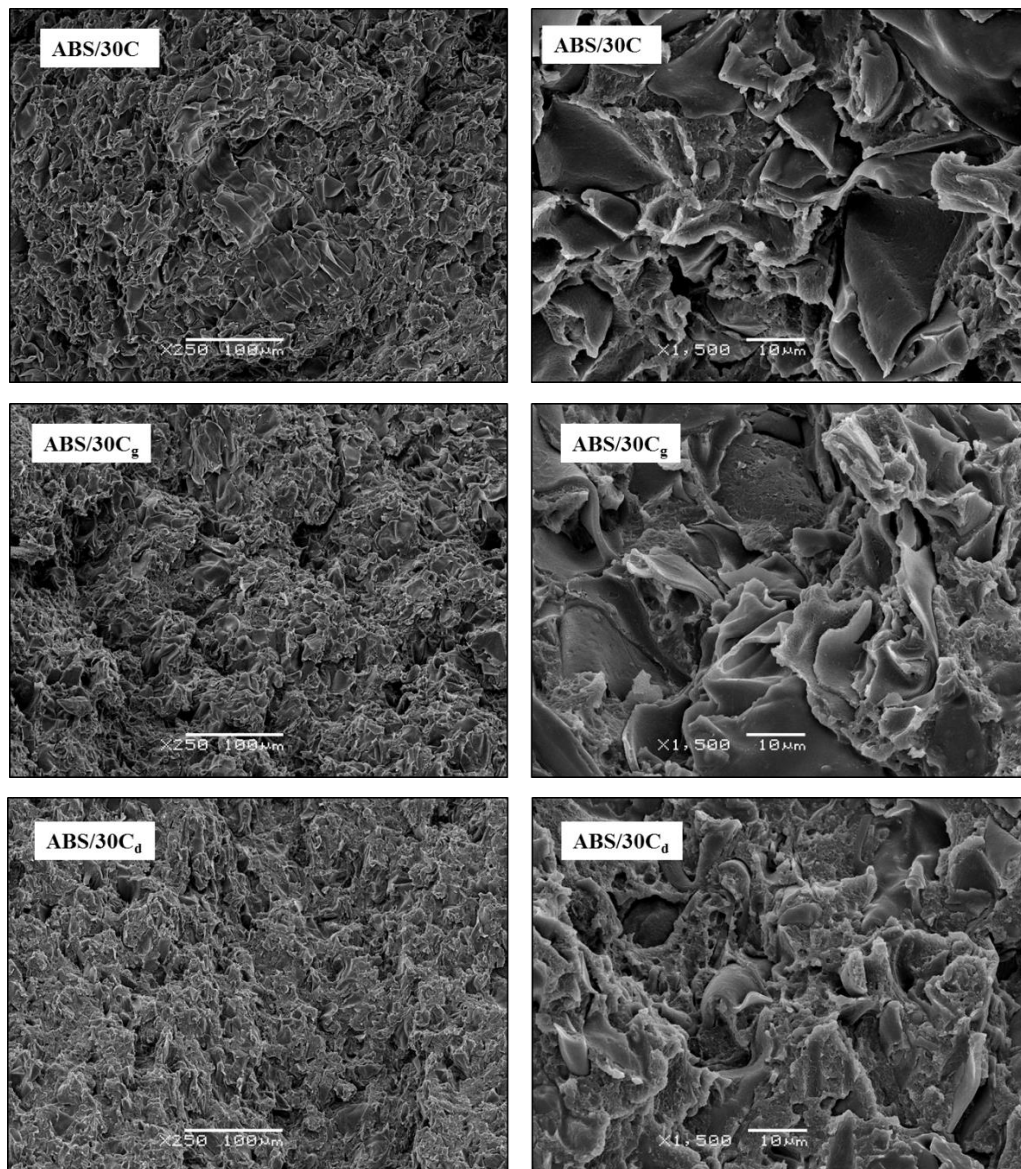
**Table VII.2.** Cork powder, and phosphorylated cork samples XPS component ratios of  $C_{1s}$ ,  $O_{1s}$ ,  $N_{1s}$ ,  $Si_{2p}$  and  $P_{2p}$  elements

Materials	Concentration (wt.%)				
	$C_{1s}$	$O_{1s}$	$N_{1s}$	$Si_{2p}$	$P_{2p}$
Cork powder	73.0	23.4	2.7	0.9	-
$C_g$	71.4	23.6	3.6	0.6	0.9
$C_t$	72.6	23.5	3.0	0.4	0.3
$C_d$	64.6	25.1	4.4	3.5	2.4

After confirming a successful phosphorylation of cork powder, two phosphorylated cork samples with the highest phosphorus content,  $C_g$  and  $C_d$ , were added to ABS composite with or without APP for studying the effect cork's phosphorylation on thermo-mechanical, thermal stability and fire behavior of ABS composites.

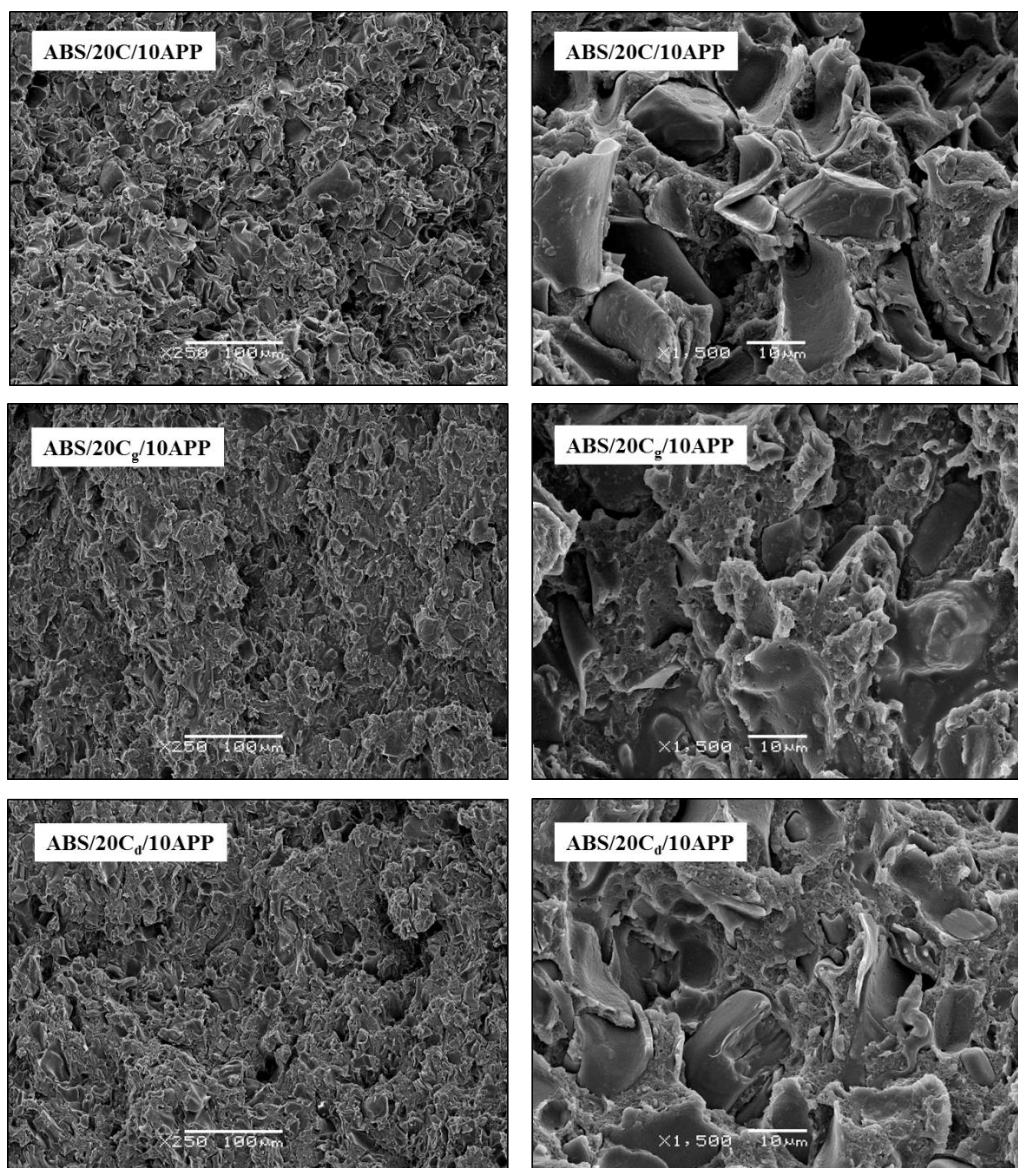
### VII.3.2 Morphology of ABS composites

The morphology of ABS formulations with 30, 20 and 3 wt.% of unmodified cork,  $C_g$  and  $C_d$  was characterized by SEM. By comparing SEM micrographs of ABS/30C with ABS/30C<sub>g</sub> and ABS/30C<sub>d</sub>, it can be noticed that phosphorylation led to a slight improvement in interaction between ABS and cork powder particles, showing them being partially covered by the polymeric matrix (Figure VII.9).

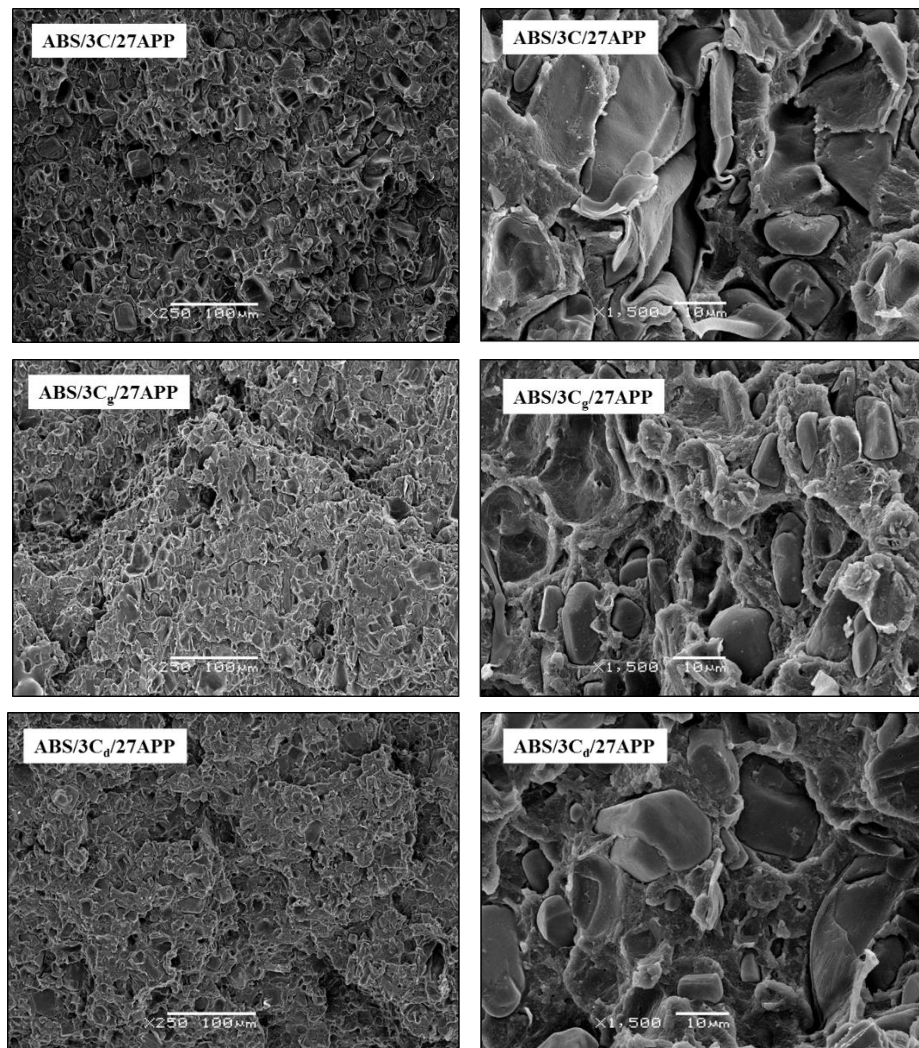


**Figure VII.9.** SEM micrographs of ABS with 30 wt.% of cork and phosphorylated cork, at 250 × and 1500 ×, with a scale bar of 100 and 10 μm, respectively.

Similar observations were also noticed for ABS formulations containing 20 wt.%  $C_g$  and  $C_d$  (Figure VII.10), as well as, a homogeneous microstructure with well dispersed cork and APP particles in the polymeric matrix. In addition, due to the low content of cork, formulations with 3 wt.% of unmodified or modified cork did not show any significant difference between their SEM micrographs (Figure VII.11).



**Figure VII.10.** SEM micrographs of ABS with 20 wt.% of cork and phosphorylated cork, at 250 × and 1500 ×, with a scale bar of 100 and 10 μm, respectively.

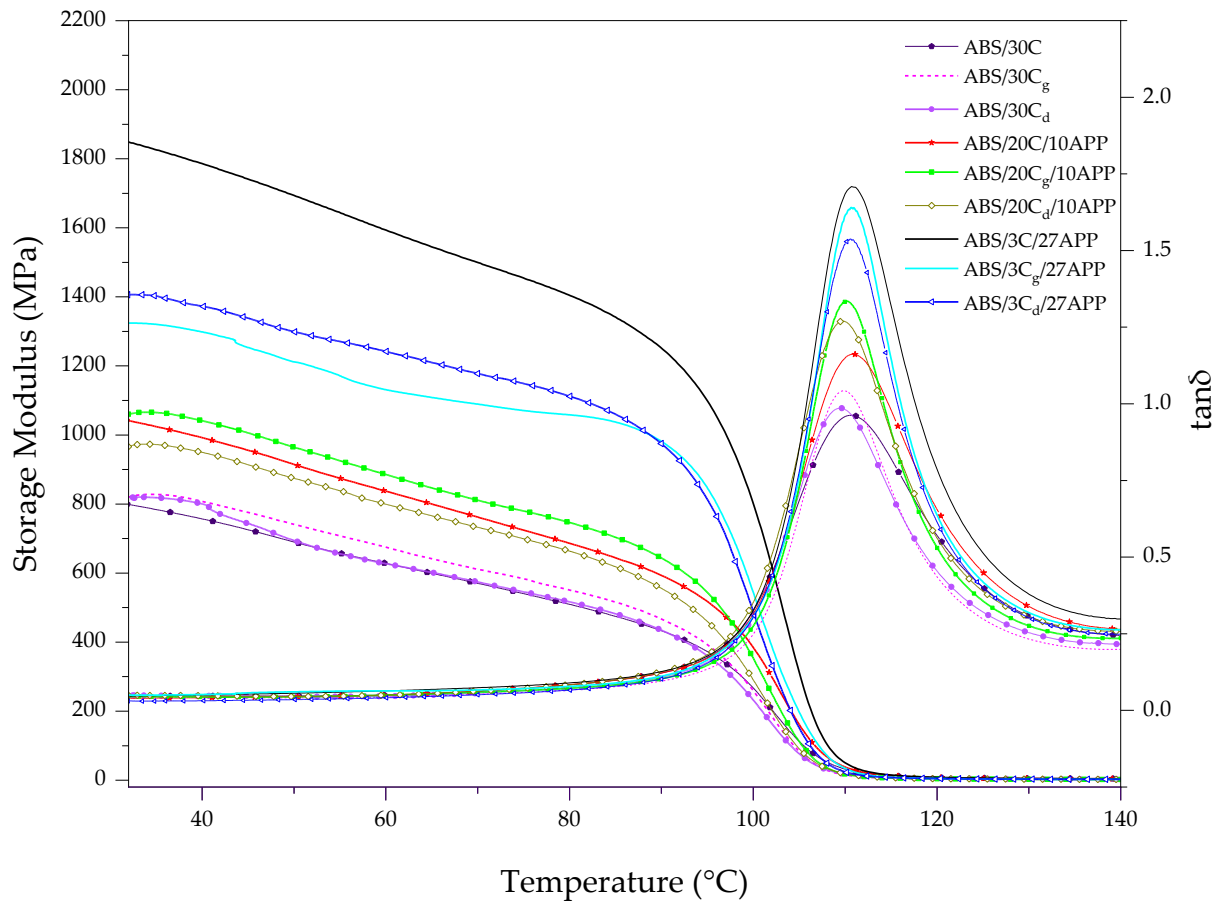


**Figure VII.11.** SEM micrographs of ABS with 3 wt.% of cork and phosphorylated cork, at 250 × and 1500 ×, with a scale bar of 100 and 10 μm, respectively.

### VII.3.3 Dynamic mechanical thermal analysis

Figure VII.12 shows the variation of the storage modulus and  $\tan \delta$  with temperature for ABS formulations with 30, 20 and 3 wt.% of cork and phosphorylated cork. The samples'  $T_g$  was obtained from the temperature corresponding to the maximum of  $\tan \delta$  curves and the  $E'$  was collected at 30 °C from the DMTA curves. There was a difference between the onset and the end of  $\tan \delta$  associated with the glass transition of SAN. The results of DMTA of all samples are presented in Table VII.3.





**Figure VII.12.** Storage modulus ( $E'$ ) and  $\tan \delta$  of ABS formulations, effect of phosphorylation.

In Figure VII.12, it can be seen that as the temperature increased, the storage modulus gradually decreased from room temperature to 90 °C, followed by a sudden decrease until reaching the energy of free movement of the SAN chain segments at approximately 110 °C.

As it was previously shown in chapter VI, the presence of APP or cork particles did not affect the glass transition temperature of the SAN phase of ABS. As it is also reported in Table VII.3, no change was registered for the glass transition temperature of the SAN by the addition of  $C_g$  or  $C_d$  in the ABS composites.

It was exhibited that phosphorylation did not remarkably affect storage modulus of the formulations with 20 and 30 wt.% of cork. Only a slight decrease in it for ABS/20 $C_d$ /10APP. However, at 3 wt.% loading of cork and 27 wt.% of APP, after phosphorylation, a high decrease in storage modulus was observed indicating enhanced softening of the composites.

**Table VII.3.** Storage modulus ( $E'$ ) and glass transition temperature ( $T_g$ ) of ABS formulations, effect of phosphorylation.

Materials	$E'$ at 30 °C (MPa)	$T_g$ (°C)
		Max tan $\delta$
ABS/30C	802	111
ABS/30C <sub>g</sub>	819	110
ABS/30C <sub>d</sub>	815	110
ABS/20C/10APP	1058	111
ABS/20C <sub>g</sub> /10APP	1060	110
ABS/20C <sub>d</sub> /10APP	980	110
ABS/3C/27APP	1854	111
ABS/3C <sub>g</sub> /27APP	1320	111
ABS/3C <sub>d</sub> /27APP	1390	111

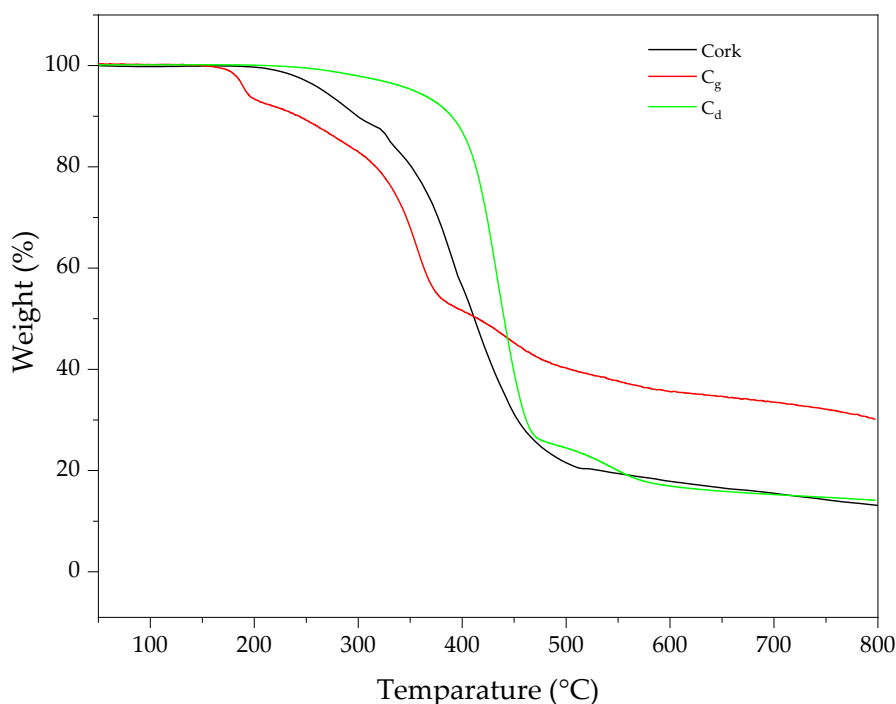
### VII.3.4 Thermal stability

The mass loss curves of cork, C<sub>g</sub> and C<sub>d</sub> are presented in Figure VII.13. Furthermore, TD steps, T<sub>5%</sub>, T<sub>peak</sub>, ML and residue at 800 °C are summarized in Table VII.4. As it was discussed in chapter V, unmodified cork decomposed in two main steps, between 200 °C and 290 °C with a T<sub>5%</sub> of 260 °C and followed by a higher mass loss of 70.1% between 290 °C and 600 °C.

Cork modified by glyphosate, similar to unmodified cork, decomposed in two main step, the first one with a T<sub>5%</sub> of 195 °C, 65 °C lower than that of cork and with a ML of 11.5%, showing that the beginning of cork thermal decomposition was accelerated which can be due to the presence of functional group of glyphosate that started to decompose at lower temperatures [265]. Although C<sub>g</sub> lost its major mass in the second TD step between 220 °C and 450 °C at lower temperatures compared to the unmodified, the mass loss was lower than unmodified cork and a remarkably high amount of residue was registered for this sample at 800 °C, indicating that under pyrolysis, a more stable char residue was formed for C<sub>g</sub>.

C<sub>d</sub> also decomposed in two steps, the main one between 380 °C and 480 °C with temperature of maximum mass loss at 440 °C. Modification of cork with DTSP resulted in an enhancement of thermal stability by delaying the beginning of thermal decomposition to a higher

temperature of 355 °C with can be due to the char-formation ability of silicon, phosphorus containing compounds and polyphosphoric acid formed by DTSP during thermal decomposition [141]. For C<sub>d</sub>, a residue content of 14.2% remained at 800 °C, similar to unmodified cork.



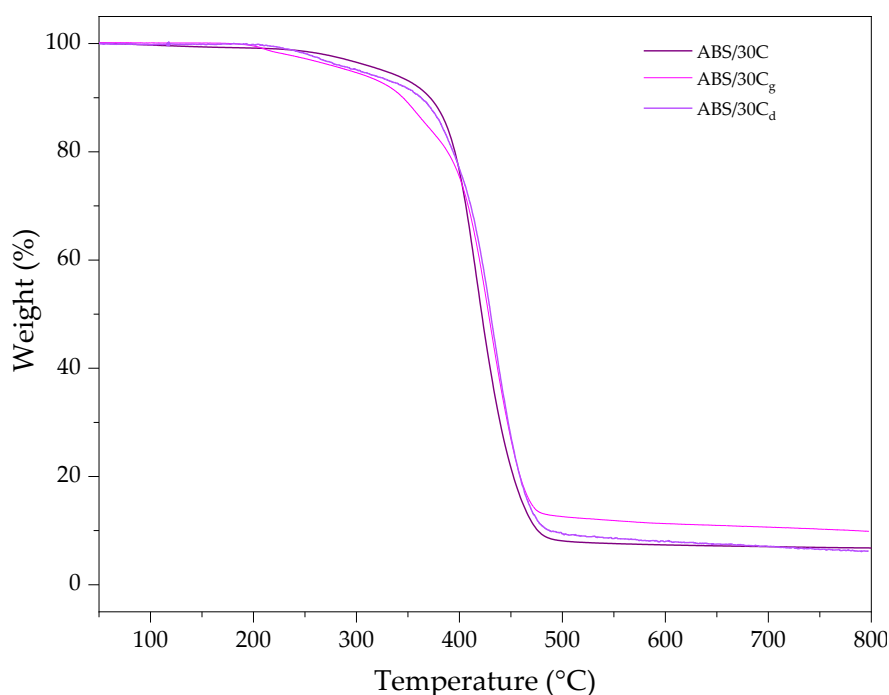
**Figure VII.13.** TG curves of cork and phosphorylated cork samples obtained at 10 °C/min under N<sub>2</sub> atmosphere.

**Table VII.4.** Mass and dTG data of cork and phosphorylated cork samples.

Materials	TD Step	T <sub>5%</sub> (°C)	T <sub>peak</sub> (°C)	ML (%)	R <sub>800 °C</sub> (%)
Cork	1	260	280	10.5	13.0
	2		400	70.1	
C <sub>g</sub>	1	190	195	11.5	30.3
	2		355	48.8	
C <sub>d</sub>	1	355	440	73.2	14.2
	2		545	8.6	

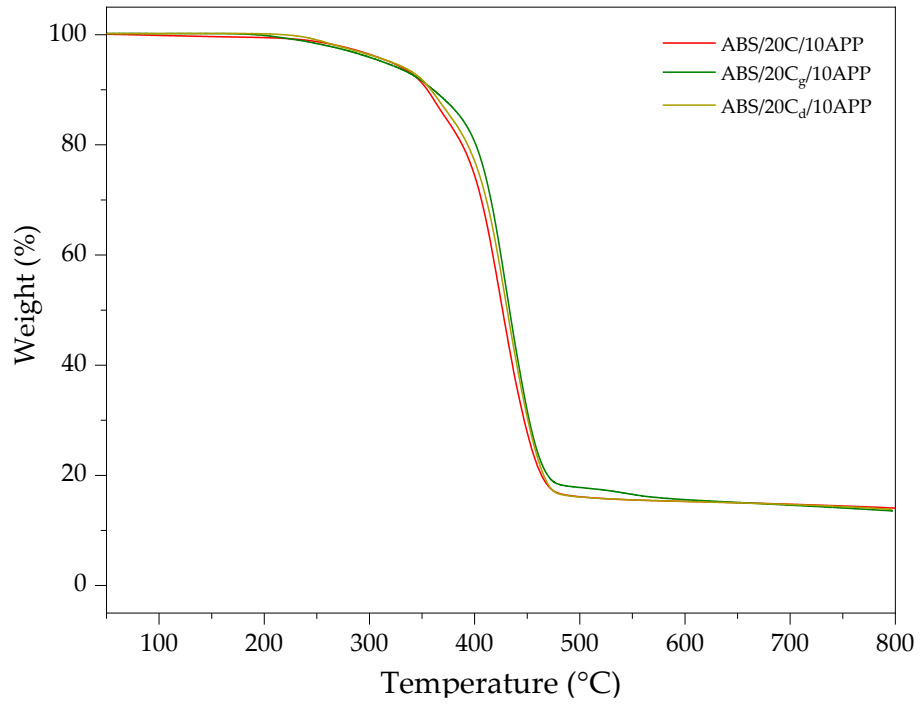
Comparative mass loss curves of ABS formulations with cork and phosphorylated cork with or without APP are shown in Figure VII.14-16. It should be mentioned that the thermal stability

of ABS composite with unmodified cork has been discussed in detail in chapter VI. In Figure VII.14, it can be seen that the addition of 30 wt.% phosphorylated cork resulted in a lower thermal stability at the beginning of decomposition, compared to the formulation with unmodified cork. This fact can be due to the volatilization of phosphorus components that were presented in phosphorylated cork. However, the second and main thermal decomposition step was observed at higher temperatures compared to ABS/30C that can be related to the formation of a more stable char residue as result of probable formation of P-O-C cross-linked structure or Si-O-C in case of ABS/30C<sub>d</sub> (see Table VII.5).

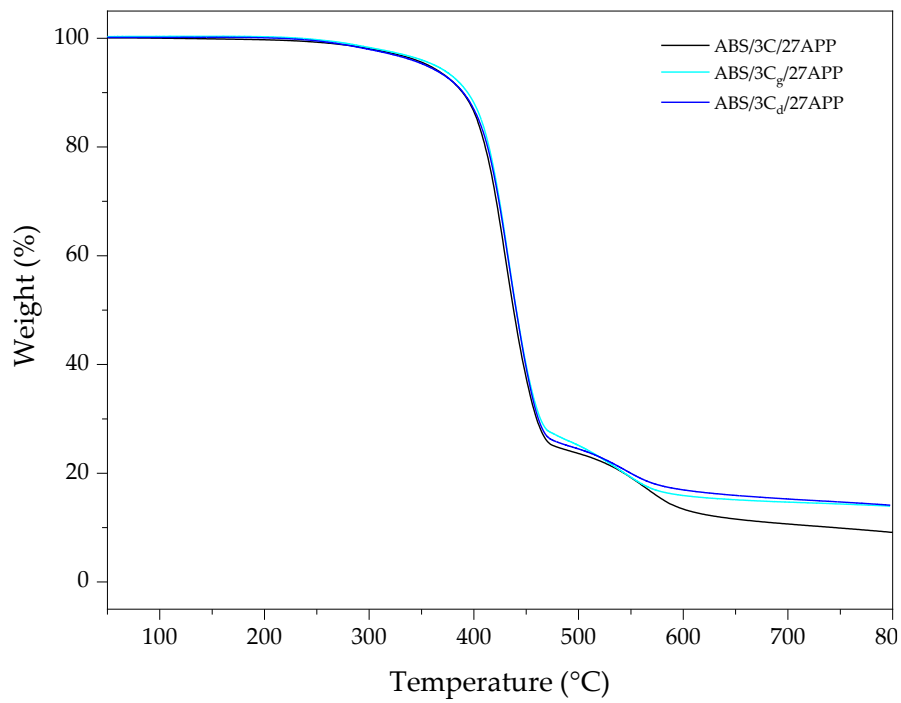


**Figure VII.14.** TG curves of ABS composites containing 30 wt.% of cork or phosphorylated cork, obtained at 10 °C/min under N<sub>2</sub> atmosphere.

As shown in Figure VII.15, for the formulations with 20 wt.% of cork, no significant effect on thermal stability of ABS composites was observed. However, a higher char formation was observed for formulations containing 3 wt.% C<sub>g</sub> or C<sub>d</sub> with 27 wt.% APP which can be due to the presence of phosphorus moieties on the surface of cork that resulted in an enhancement of synergistic effect between phosphorylated cork and APP followed by a higher char formation (see Figure VII.16).



**Figure VII.15.** TG curves of ABS composites containing 20 wt.% of cork or phosphorylated cork with 10 wt.% APP, obtained at 10 °C/min under N<sub>2</sub> atmosphere.



**Figure VII.16.** TG curves of ABS composites containing 3 wt.% of cork or phosphorylated cork with 27 wt.% APP, obtained at 10 °C/min under N<sub>2</sub> atmosphere.

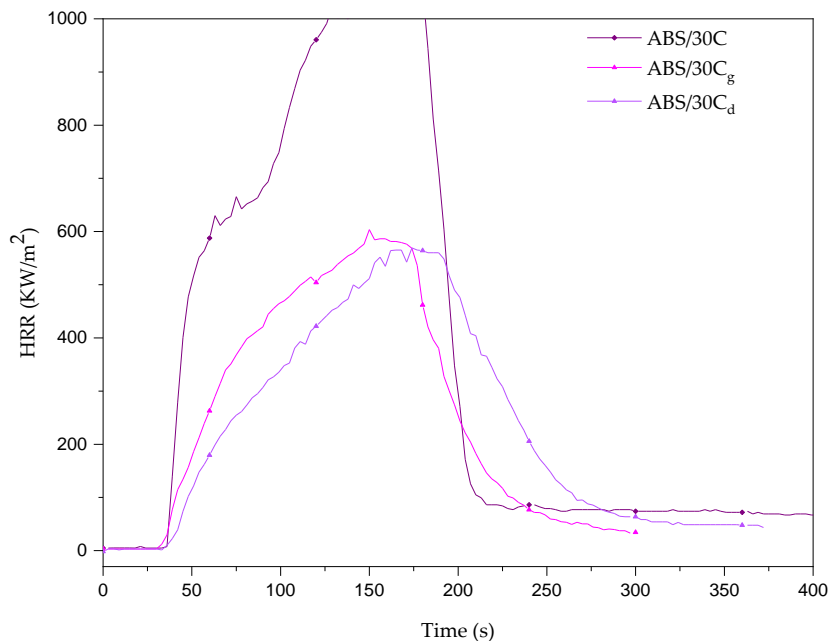
**Table VII.5.** Mass and dTG data of ABS formulations with cork and phosphorylated cork.

Materials	TD Step	T <sub>5%</sub> (°C)	T <sub>peak</sub> (°C)	ML (%)	R <sub>800 °C</sub> (%)
ABS/30C	1	325	416	91.2	6.8
ABS/30C <sub>g</sub>	1	290	210	3.1	9.9
	2		430	83.8	
ABS/30C <sub>d</sub>	1	310	265	5.1	6.9
	2		435	84.2	
ABS/20C/10APP	1	320	365	14.1	14.0
	2		425	69.7	
ABS/20C <sub>g</sub> /10APP	1	315	360	2.1	13.9
	2		430	78.8	
ABS/20C <sub>d</sub> /10APP	1	315	365	2.3	13.8
	2		430	79.1	
ABS/3C/27APP	1	355	431	75.8	9.1
	2		560	12.6	
ABS/3C <sub>g</sub> /27APP	1	355	435	76.7	14.0
	2		550	8.7	
ABS/3C <sub>d</sub> /27APP	1	355	435	74.1	14.1
	2		550	8.8	

### VII.3.5 Fire behavior

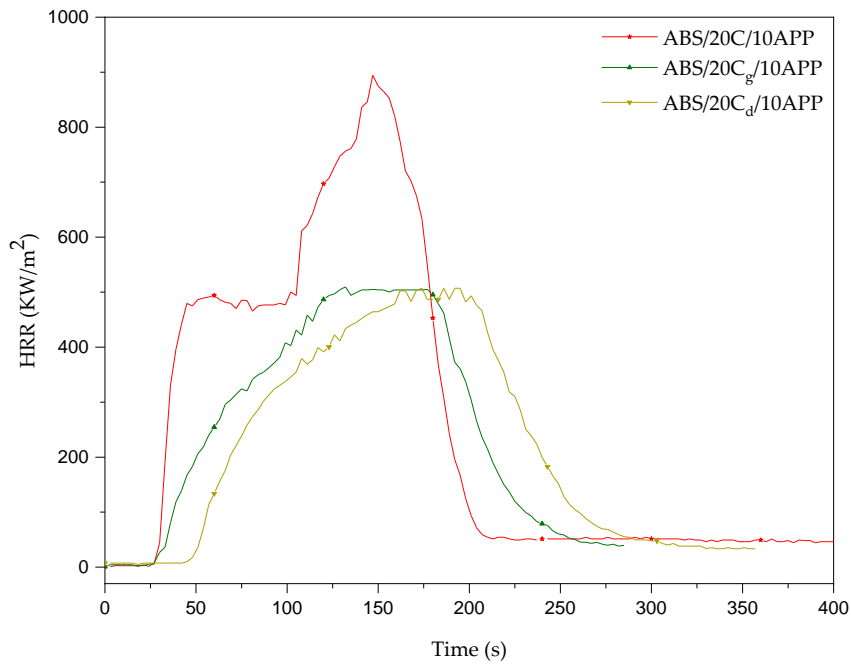
A comparative of HRR curves of ABS formulations with unmodified cork, C<sub>g</sub> and C<sub>d</sub>, obtained from cone calorimetry test, as a function of time is presented in Figure VII.17-19. In chapter VI the flammability of ABS and effect of unmodified cork has been explained. The main cone calorimetry results of ABS composite with 30 wt.%, 20 wt.% and 3 wt.% of cork or phosphorylated cork are listed in Table VII.6. In this part, the effect of cork phosphorylation on the fire retardancy of ABS/C/APP formulations was investigated. The most significant enhancement in flame retardancy, as the results of phosphorylation, can be noticed for the formulations with 30 wt.% of

cork (Figure VII.17). Compared to the unmodified one, the highest pHRR, EHC and MARHE reduction of 57%, 42 % and 51%, was registered for ABS/30C<sub>d</sub>, respectively. The observed enhancement in flame retardancy of the mentioned formulation could be due to the presence of the higher amount of phosphorus, as a result of phosphorylation, leading to an improvement in both gas and condensed phase mechanism by releasing noncombustible gasses and forming a more efficient protective char layer that prevented the heat and mass transfer resulting in the registered lower HRR values to the end of the combustion.

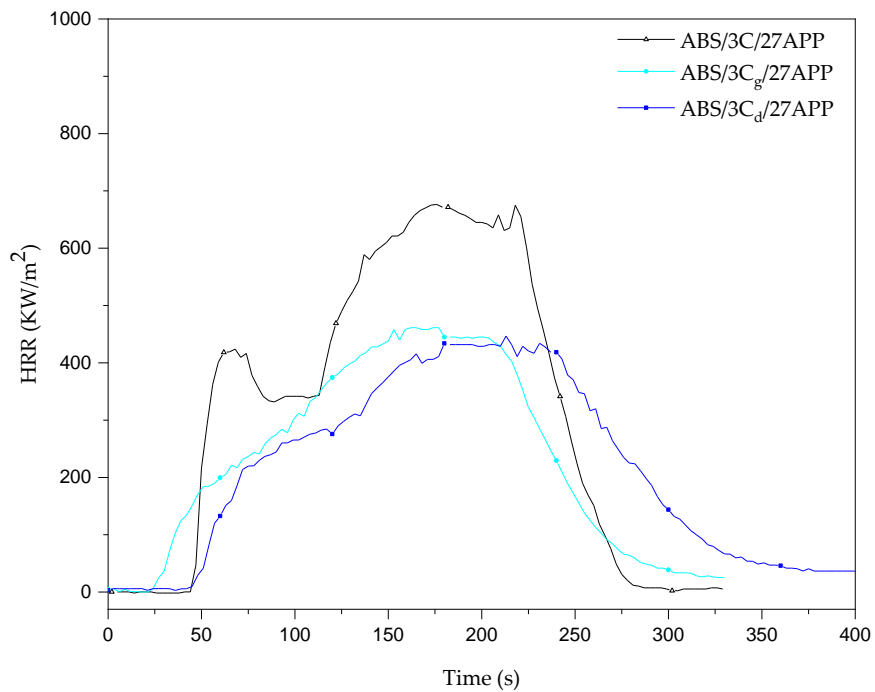


**Figure VII.17.** Heat release rate vs. time curves of ABS formulations with 30 wt.% cork, the effect of phosphorylation.

In Figure VII.18, the same behavior was also observed for the formulations with 20 wt.% of cork; however, in the case of adding 20 wt.% of phosphorylated cork, a lower reduction of pHRR and residue value compared to the ABS/30C<sub>g</sub> and ABS/30C<sub>d</sub> was registered, related to the lower content of phosphorylated cork (Figure VII.18). In Figure VII.19, for formulations with 3 wt.% of C<sub>g</sub> and C<sub>d</sub>, a lower TTI as well as lower HRR values was observed regarding the unmodified one; nevertheless, the phosphorylation did not have a significant effect on the char forming ability of these composites.



**Figure VII.18.** Heat release rate vs. time curves of ABS formulations with 20 wt.% cork and 10 wt.% APP, the effect of phosphorylation.



**Figure VII.19** Heat release rate vs. time curves of ABS formulations with 3 wt.% cork and 27 wt.% APP, the effect of phosphorylation.



**Table VII.6.** Main results obtained from cone calorimeter tests, the effect of cork phosphorylation.

<b>Materials</b>	<b>TTI</b> (s)	<b>pHRR</b> (kW/m <sup>2</sup> )	<b>t<sub>PHRR</sub></b> (s)	<b>t<sub>combustion</sub></b> (s)	<b>EHC</b> (MJ/Kg)	<b>MARHE</b> (kW/m <sup>2</sup> )	<b>Residue</b> (wt%)
ABS/30C	33 ± 4	1374 ± 109	158 ± 10	143 ± 2	33 ± 1	675 ± 22	0.3 ± 0.01
ABS/30C <sub>g</sub>	28 ± 2	599 ± 12	150 ± 1	199 ± 12	19 ± 0.1	334 ± 17	7.8 ± 0.8
ABS/30C <sub>d</sub>	31 ± 1	585 ± 14	168 ± 6	228 ± 3	19 ± 0.1	333 ± 13	7.9 ± 0.1
ABS/20C/10APP	27 ± 1	932 ± 53	150 ± 3	195 ± 7	27 ± 1	492 ± 11	10 ± 0.6
ABS/20C <sub>g</sub> /10APP	25 ± 2	515 ± 5	153 ± 7	203 ± 11	19 ± 0.1	311 ± 9	12.4 ± 0.2
ABS/20C <sub>d</sub> /10APP	34 ± 1	505 ± 11	174 ± 4	210 ± 12	19 ± 0.2	309 ± 4	13.2 ± 0.4
ABS/3C/27APP	41 ± 5	680 ± 9	174 ± 2	264 ± 5	29 ± 1	408 ± 7	24 ± 0.1
ABS/3C <sub>g</sub> /27APP	30 ± 1	460 ± 2	182 ± 5	261 ± 7	20 ± 0.2	278 ± 16	23.9 ± 0.1
ABS/3C <sub>d</sub> /27APP	35 ± 2	440 ± 7	213 ± 1	274 ± 15	20 ± 0.2	274 ± 3	24.0 ± 0.5

In addition, the effect of phosphorylation on the flammability behavior of ABS formulations was assessed by UL-94 horizontal burning tests. The results of UL-94 tests are summarized in Table VII.7. As it was also observed in cone calorimetry, the greatest improvement in flame retardancy was observed for the samples with 30 wt.% of cork, resulting in a 43% reduction of burning rate compared to unmodified ones. It should be noted that the type of phosphorus compound used for phosphorylation did not affect the LBR. Moreover, for formulations with 20 wt.% of cork, a lower burning rate was registered which can be due to a higher charring ability as a result of phosphorylation. On the other hand, no change in LBR of formulations with 3 wt.% of cork was observed due to the low amount of phosphorylated cork.

**Table VII.7.** UL-94 horizontal results of ABS and ABS composites, the effect of cork phosphorylation.

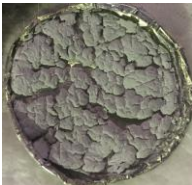
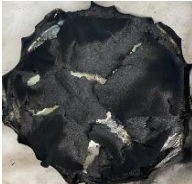



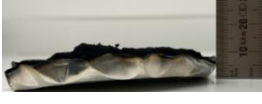



<b>Materials</b>	<b>LBR (mm/min)</b>	<b>Dripping</b>
ABS/30C	41	No
ABS/30C <sub>g</sub>	23	No
ABS/30C <sub>d</sub>	23	No
ABS/20C/10APP	24	No
ABS/20C <sub>g</sub> /10APP	20	No
ABS/20C <sub>d</sub> /10APP	20	No
ABS/3C/27APP	19	Yes
ABS/3C <sub>g</sub> /27APP	19	Yes
ABS/3C <sub>d</sub> /27APP	19	Yes

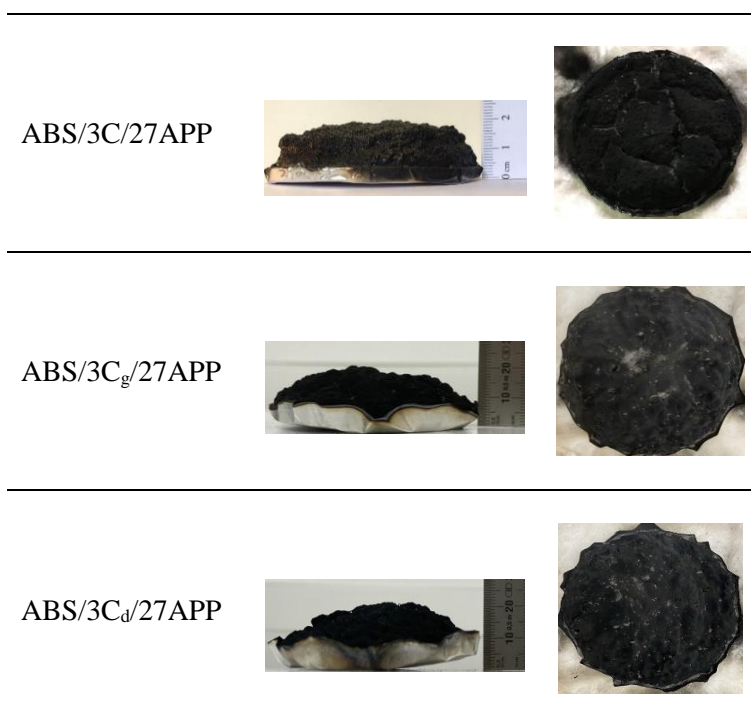
### *VII.3.6 Morphological and chemical analysis of CC residue*

Furthermore, the digital photographs of residues after cone calorimetry are presented in Table VII.8. For the formulations with a higher amount of phosphorylated cork (30 and 20 wt.%), a different structure of residue was formed. After phosphorylation, the FR-ABS produced a more stable, uniform and compact char structure that could reduce the mass and heat transfer during combustion leading to a lower HRR. Furthermore, in case of unmodified cork, it was noticed that for ABS/30C a very small amount of residue (0.3%) was remained which was slightly white in color, while after phosphorylation, the char formation was remarkably increased to 7.8% and 7.9% for ABS/30C<sub>g</sub> and ABS/30C<sub>d</sub>, respectively. Since the samples with 30 wt.% of cork did not show any expansion their lateral side is not presented.

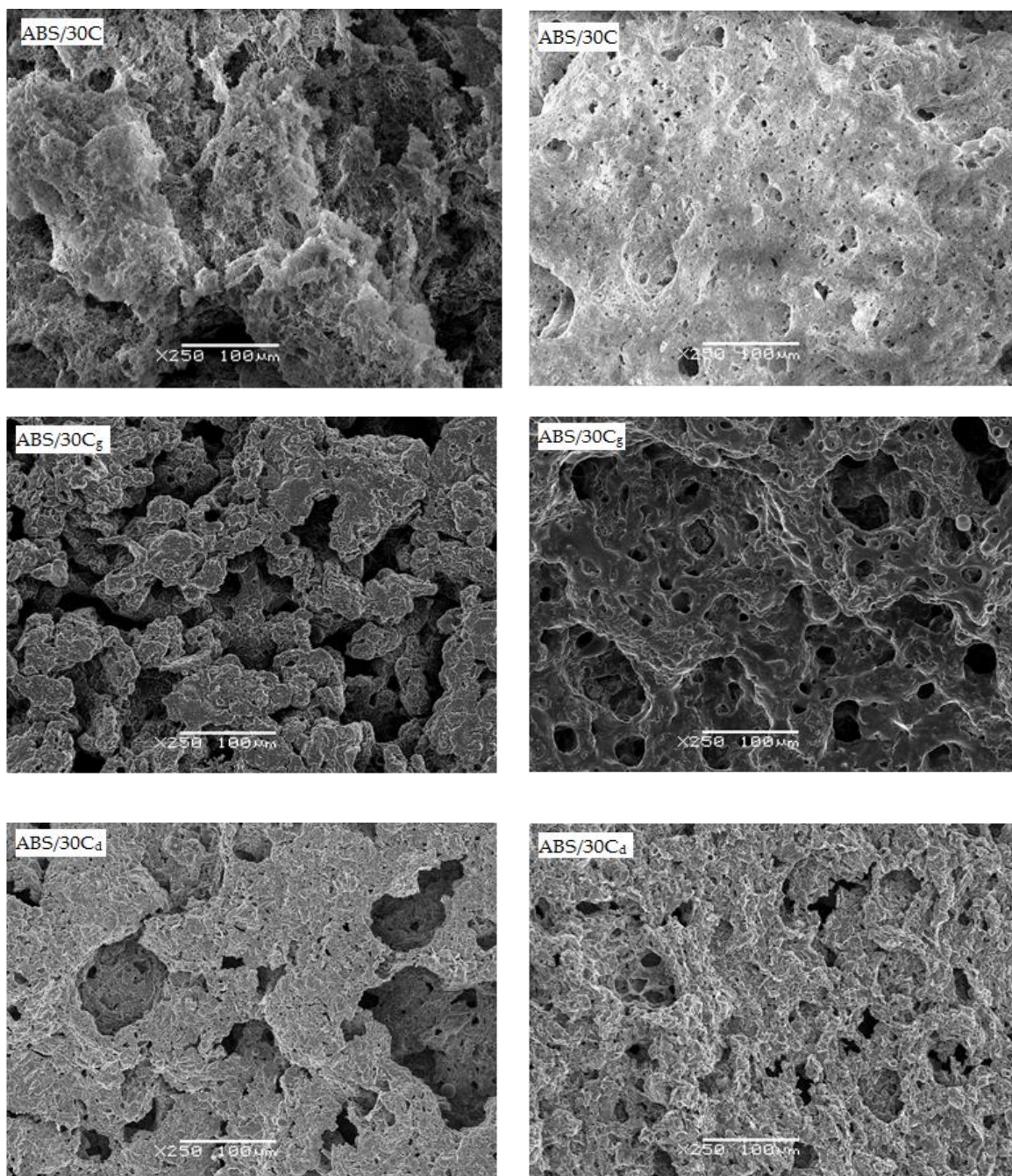
By studying the effect of cork's phosphorylation for 3 wt.% of modified and unmodified cork, a slight reduction in expansion degree of residues can be noted. However, composites with phosphorylated cork residue showed less cracks on the surface compared to the unmodified one that resulted in a more efficient protective layer that resulted in a lower HRR as observed in cone calorimetry.

**Table VII.8.** Digital photographs of ABS formulations residue after cone calorimetry, the effect of phosphorylation.

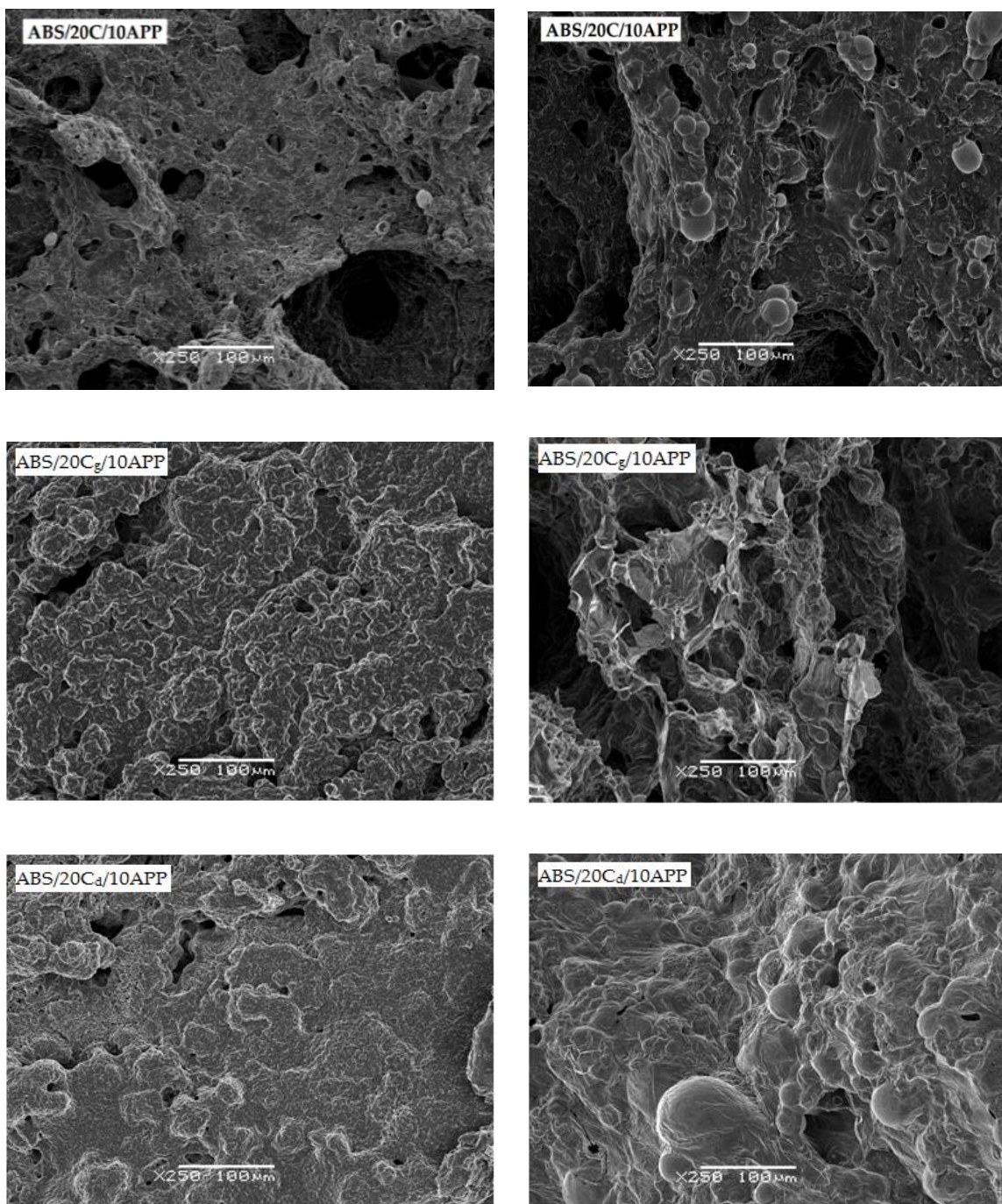
<b>Materials</b>	<b>Lateral side</b>	<b>Upper side</b>
ABS/30C	-	
ABS/30C <sub>g</sub>	-	
ABS/30C <sub>d</sub>	-	
ABS/20C/27APP		
ABS/20C <sub>g</sub> /10APP		
ABS/20C <sub>d</sub> /10APP		



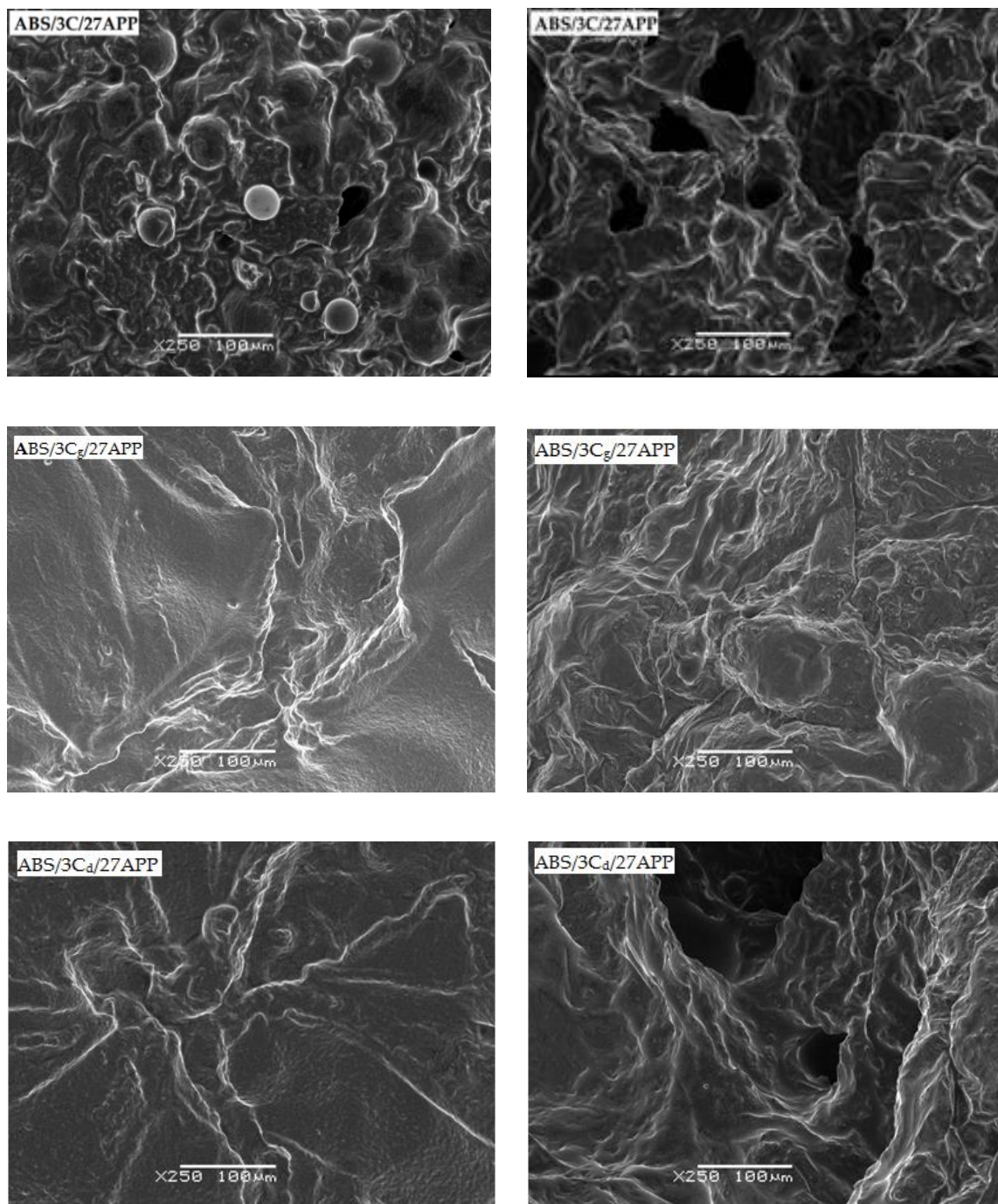
The surface of the ABS composites residue with phosphorylated and unmodified cork after cone calorimetry was observed by SEM to further identify the quality of the protective char layer. As it is shown in Figure VII.20-22 residue of the formulations with phosphorylated cork showed a more compact and cohesive foamed layer compared to the unmodified ones, confirming the enhancement of the protective efficiency of the formed carbonaceous layer. This more effective protective char layer resulted in an improved fire performance on the condensed phase which could also act as a physical barrier against heat and gas transmission in accordance with the results previously discussed in cone calorimetry.



**Figure VII.20.** SEM micrographs of the upper (left) and down surface (right) of the ABS formulations with 30 wt.% of unmodified cork or phosphorylated cork after the cone calorimeter tests (at 250 × with a scale bar of 100 μm).



**Figure VII.21.** SEM micrographs of the upper (left) and down surface (right) of the ABS formulations with 20 wt.% of unmodified cork or phosphorylated cork after the cone calorimeter tests (at 250 × with a scale bar of 100 μm).

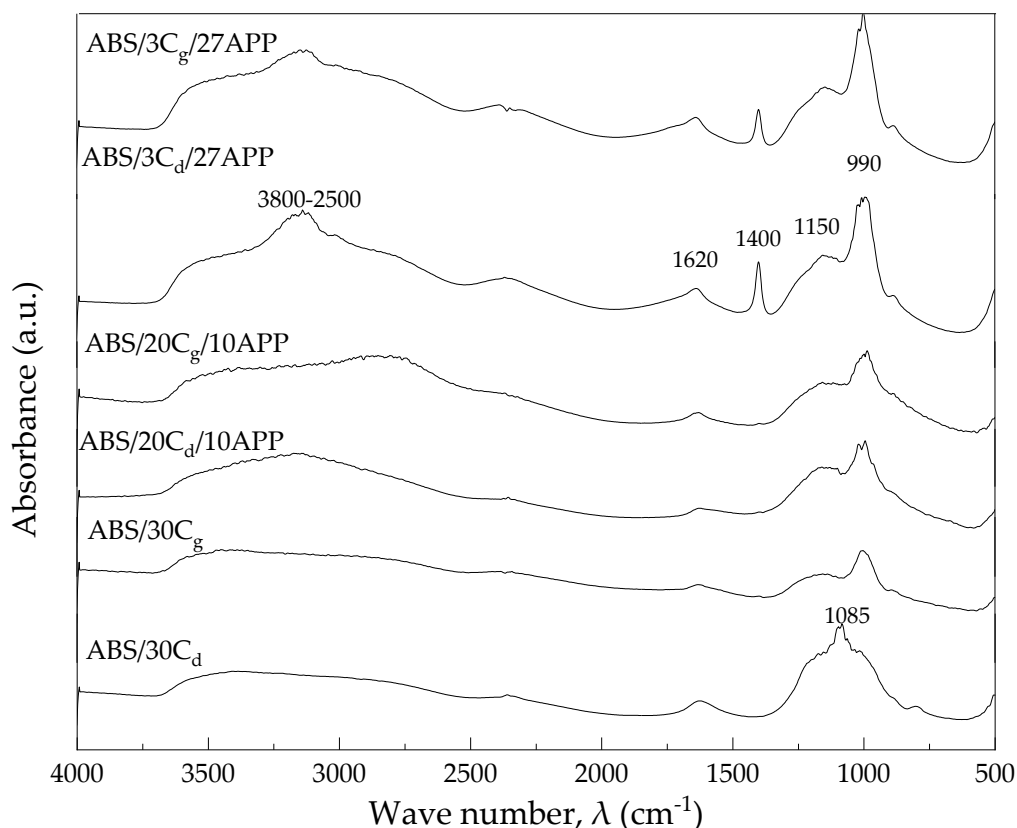


**Figure VII.22.** SEM micrographs of the upper (left) and down surface (right) of the ABS formulations with 3 wt.% of unmodified cork or phosphorylated cork after the cone calorimeter tests (at  $250\times$  with a scale bar of 100  $\mu\text{m}$ ).

Figure VII.23 shows a comparative of the FTIR spectra of the ABS formulations residue after cone calorimeter test. FTIR spectra of ABS/30C<sub>g</sub> and ABS/30C<sub>d</sub> confirmed the presence of P-O-C network structure in char residue observed at  $990\text{ cm}^{-1}$ , in accordance with cone calorimetry

results. By comparing FTIR spectra of these two formulations, it can be seen that the peaks between  $1300\text{-}1000\text{ cm}^{-1}$  were changed into a single broader band due to the presence of the Si-O-C characteristic band at  $1085\text{ cm}^{-1}$  that overlapped them [266].

Both ABS/3C<sub>g</sub>/27APP and ABS/3C<sub>d</sub>/27APP showed similar absorbance bands. The broad absorption band at  $3800\text{-}2500\text{ cm}^{-1}$  registered for these formulations was assigned to N-H and OH stretching vibration [166, 254]. The sharp peak which appeared at  $1400\text{ cm}^{-1}$  belonged to phosphorus oxynitrides as a result of dehydration and cross-linking reactions of APP [251, 254]. The shoulder at  $1150\text{ cm}^{-1}$  was also attributed to the absorption of C-O-C groups and the peak at  $990\text{ cm}^{-1}$  was related to P-O symmetric stretching in P-O-C chemical bands [166, 255]. ABS/20C<sub>g</sub>/10APP and ABS/20C<sub>d</sub>/10APP also presented similar absorbance signals while for these formulations the phosphorus oxynitrides peak of APP at  $1400\text{ cm}^{-1}$  did not appear.



**Figure VII.23.** FTIR spectra of the ABS formulations with 30, 20 and 3 wt.% different phosphorylated cork residue after cone calorimeter test.



## VII.4 Conclusions

In this chapter, cork powder phosphorylation with different phosphorus components, glyphosate and TEP under different reaction conditions as well as phosphorylation with DTSP has been carried out. In the case of glyphosate, the best condition of reaction was set at room temperature and for three days (condition 1), where the phosphorus absorbance bands in ATR-FTIR were detected for C<sub>g</sub>. For C<sub>g</sub>, a phosphorus content of 0.9 wt.% was observed by XPS analysis. For C<sub>t</sub> under condition 1, at 120 °C for 12 hours, the absorbance peaks of phosphorus at 965 cm<sup>-1</sup> and 795 cm<sup>-1</sup> registered by ATR-FTIR, confirmed that the phosphorus moieties were successfully attached on the surface of cork; however, for this sample the lowest phosphorus content was registered in XPS analysis. DTSP was also successfully synthesized and used for cork surface modification. The presence of phosphorus moieties in the C<sub>d</sub> was confirmed by ATR-FTIR and XPS analysis. This sample showed the highest phosphorus content of 2.4 % in XPS analysis. Furthermore, the quality of final phosphorylated cork samples was analyzed by GC-MS and TLC, which showed no sign of phosphorus component weak attachment on the surface of cork powder confirming a successful phosphorylation.

In addition, ABS composites containing APP and phosphorylated cork were prepared and characterized. A homogenous microstructure with an enhanced interaction between particles and polymeric matrix was observed by SEM as an effect of phosphorylation. No significant differences were noticed in thermo-mechanical properties of ABS with high amounts of phosphorylated cork; however, at 3 wt.% its loading, a reduction in storage modulus was registered. TGA analysis of the composites under pyrolysis showed Cork modified by glyphosate showed a lower thermal stability than unmodified cork at the beginning of the thermal decomposition and it lost its major mass in the second TD step at lower temperatures compared to the unmodified; however, the mass loss rate was slower than unmodified cork and a remarkably high amount of residue was registered for this sample at 800 °C. On the other hand, modification of cork with DTSP resulted in an enhancement of thermal stability by delaying the beginning of thermal decomposition to a higher temperature as a result of the catalytic char-formation ability of silicon, phosphorus containing compounds and polyphosphoric acid formed by DTSP during thermal decomposition. It was also shown that under pyrolysis, the formed char by C<sub>d</sub> was less stable than C<sub>g</sub>.

Furthermore, fire behavior of ABS formulations was studied by cone calorimetry and it was observed that the greatest reduction of HRR during combustion regarding ABS composites with unmodified cork as a result of phosphorylation, was registered for the formulations with 30 wt.% of cork. Compared to the unmodified one, the highest pHRR, EHC and MARHE reduction of 57%, 42 % and 51% were observed for ABS/30C<sub>d</sub>, respectively. In the case of adding 20 wt.% of phosphorylated cork, a higher reduction of pHRR and residue value compared to the unmodified one was registered, probably related to the higher phosphorus content that resulted in formation of a cross-linked char structure. An enhancement in flame retardancy of composites with 3 wt.% phosphorylated cork compared to unmodified one was observed. Since the phosphorylation did not have significant effect on the char forming ability of these composites, it can be concluded that the flame retardancy improvement is associated to the higher release of nonflammable gasses at the beginning of the combustion and the formation of a more thermally stable char that efficiently prevent the heat and mass transfer resulting in the registered lower HRR values until the end of the combustion. In general, the observed enhancement in flame retardancy of composites after cork phosphorylation and the presence of the higher amount of phosphorus led to a synergistic improvement in both gas and condensed phase mechanism by releasing noncombustible gasses and forming a more efficient protective char layer that also led to the reduction of burning rate observed in horizontal UL-94.

Additionally, from SEM micrographs of CC residue, it was possible to ascertain that a foamed intumescence char layer was formed and phosphorylation of cork powder resulted in the formation of a more cohesive and protective char with less cavities that acted as a more efficient physical barrier against heat and mass transfer. In the FTIR analysis of residue, for formulation with 30 wt.% of phosphorylated cork, absorption peaks of P-O-C structure were observed, confirming the presence of a cross-linked protective char layer that acted efficiently in the condensed phase observed by CC. In addition, in case of C<sub>d</sub>, the Si-O-C characteristic band was also detected due to the presence of silicone in the DTSP chemical structure.





Confidential

Chapter

VIII



# Patents and scientific dissemination

## Chapter

# IX





---

## Chapter IX: Patents and scientific dissemination

### *IX.1 Patents*

- A European patent application with the number of EP23383250 and the title of "Flame-retardant ABS composition" was filed on **December 4<sup>th</sup>, 2023** to protect the research detailed in the chapter IV of the present thesis.

### *IX.1 Publications*

- Farnaz Ghonjizade-Samani, Laia Haurie, Ramón Malet and Vera Realinho, "The Components' Roles in Thermal Stability and Flammability of Cork Powder", *Materials*, Vol. 16, NO. 10, PP. 3829 (1-17), **18 May 2023**, DOI: 10.3390/ma16103829, Q1 in "Metallurgy Metallurgical Engineering".
- Farnaz Ghonjizade-Samani, Laia Haurie, Ramón Malet, Mark Pérez and Vera Realinho, "Phosphorus based flame retardant ABS with enhanced mechanical properties by combining ultrahigh molecular weight silicone rubber and ethylene methyl acrylate copolymer", *Polymers*, Vol. 16, NO. 7, PP. 923 (1-21), **27 March 2024**, DOI: 10.3390/polym16070923, Q1 in "Polymer Science".
- Farnaz Ghonjizade-Samani, Laia Haurie, Ramón Malet and Vera Realinho, "Study of using cork powder as an adjuvant bio-flame retardant in acrylonitrile-butadiene-styrene flame retardant formulations", *Polymer degradation and stability*, submitted, Q1 in "Polymer Science".
- Farnaz Ghonjizade-Samani, Laia Haurie, Ramón Malet, Tarik Eren and Vera Realinho, "Effect of cork powder's phosphorylation on fire behavior of acrylonitrile-butadiene-styrene flame retardant formulations", to be submitted.

*IX. International conferences*

- GreenCHEM-22, 5<sup>th</sup> International Conference on Green Chemistry and Sustainable Engineering, Rome, Italy, **20-22 July 2022**, ‘‘Cork as synergistic additive in flame retardant systems, oral presentation’’.
- European Meeting on Fire Retardant Polymeric Materials (FRPM23), Zurich, Switzerland, **26-29 June 2023**, ‘‘Effects of combining cork powder and APP in mechanical and flammability of ABS, poster presentation’’.

## References

- [1] Characteristics, Applications and Properties of Polymers, in: H.F. Brinson, L.C. Brinson (Eds.), *Polymer Engineering Science and Viscoelasticity: An Introduction*, Springer US, Boston, MA, 2008, pp. 55-97, [https://doi.org/10.1007/978-0-387-73861-1\\_3](https://doi.org/10.1007/978-0-387-73861-1_3).
- [2] J.A. Brydson, *Plastics Materials*, Butterworths, UK, 1966.
- [3] S.R. Owen, J.F. Harper, Mechanical, microscopical and fire retardant studies of ABS polymers, *Polymer Degradation and Stability* 64(3) (1999) 449-455, [https://doi.org/10.1016/s0141-3910\(98\)00150-5](https://doi.org/10.1016/s0141-3910(98)00150-5).
- [4] N. Wu, X. Li, Flame retardancy and synergistic flame retardant mechanisms of acrylonitrile-butadiene-styrene composites based on aluminum hypophosphite, *Polymer Degradation and Stability* 105 (2014) 265-276, <https://doi.org/10.1016/j.polymdegradstab.2014.04.011>.
- [5] S.V. Levchik, E.D. Wei, New developments in flame retardancy of styrene thermoplastics and foams, *Polymer International* 57(3) (2008) 431-448, <https://doi.org/10.1002/pi.2282>.
- [6] V. Realinho, D. Arencon, M. Antunes, J. Ignacio Velasco, Effects of a Phosphorus Flame Retardant System on the Mechanical and Fire Behavior of Microcellular ABS, *Polymers* 11(1) (2019), <https://doi.org/10.3390/polym11010030>.
- [7] T.F. Webster, M.D. McClean, Exposure to polybrominated diphenyl ethers in the indoor environment, *Fire Technology* 51 (2015) 85-95, <https://doi.org/10.1007/s10694-013-0334-9>.
- [8] P.O. Darnerud, Toxic effects of brominated flame retardants in man and in wildlife, *Environment International* 29(6) (2003) 841-853, [https://doi.org/10.1016/s0160-4120\(03\)00107-7](https://doi.org/10.1016/s0160-4120(03)00107-7).
- [9] K.H. Pawlowski, B. Schartel, Flame retardancy mechanisms of triphenyl phosphate, resorcinol bis(diphenyl phosphate) and bisphenol bis(diphenyl phosphate) in polycarbonate/acrylonitrile-butadiene-styrene blends, *Polymer International* 56(11) (2007) 1404-1414, <https://doi.org/10.1002/pi.2290>.
- [10] M.C. Despinasse, B. Schartel, Aryl phosphate-aryl phosphate synergy in flame-retarded bisphenol A polycarbonate/acrylonitrile-butadiene-styrene, *Thermochimica Acta* 563 (2013) 51-61, <https://doi.org/10.1016/j.tca.2013.04.006>.
- [11] R.-K. Jian, L. Chen, Z. Hu, Y.-Z. Wang, Flame-retardant polycarbonate/acrylonitrile-butadiene-styrene based on red phosphorus encapsulated by polysiloxane: Flame retardance, thermal stability, and water resistance, *Journal of Applied Polymer Science* 123(5) (2012) 2867-2874, <https://doi.org/10.1002/app.34845>.
- [12] Z. Yuan, H. Wen, Y. Liu, Q. Wang, Synergy between piperazine pyrophosphate and aluminum diethylphosphinate in flame retarded acrylonitrile-butadiene-styrene copolymer, *Polymer Degradation and Stability* 190 (2021), <https://doi.org/10.1016/j.polymdegradstab.2021.109639>.
- [13] V. Realinho, L. Haurie, J. Formosa, J. Ignacio Velasco, Flame retardancy effect of combined ammonium polyphosphate and aluminium diethyl phosphinate in acrylonitrile-butadiene-styrene, *Polymer Degradation and Stability* 155 (2018) 208-219, <https://doi.org/10.1016/j.polymdegradstab.2018.07.022>.
- [14] A. Baby, S. Tretsiakova-McNally, M. Arun, P. Joseph, J. Zhang, Reactive and Additive Modifications of Styrenic Polymers with Phosphorus-Containing Compounds and Their Effects on Fire Retardance, *Molecules* 25(17) (2020), <https://doi.org/10.3390/molecules25173779>.
- [15] B. Schartel, Phosphorus-based Flame Retardancy Mechanisms-Old Hat or a Starting Point for Future Development?, *Materials* 3(10) (2010) 4710-4745, <https://doi.org/10.3390/ma3104710>.
- [16] E. Weil, S. Levchik, Flame Retardants, Phosphorus, 2017, <https://doi.org/10.1002/0471238961.1608151923050912.a01.pub3>.
- [17] T.M. Jayaweera, C.F. Melius, W.J. Pitz, C.K. Westbrook, O.P. Korobeinichev, V.M. Shvartsberg, A.G. Shmakov, I.V. Rybitskaya, H.J. Curran, Flame inhibition by phosphorus-containing compounds over a range of equivalence ratios, *Combustion and Flame* 140(1-2) (2005) 103-115, <https://doi.org/10.1016/j.combustflame.2004.11.001>.
- [18] K.S. Lim, S.T. Bee, L.T. Sin, T.T. Tee, C.T. Ratnam, D. Hui, A.R. Rahmat, A review of application of ammonium polyphosphate as intumescent flame retardant in thermoplastic composites, *Composites Part B-Engineering* 84 (2016) 155-174, <https://doi.org/10.1016/j.compositesb.2015.08.066>.

- [19] Kien-Sin Lim, Soo-Tueen Bee, Lee Tin Sin, Tiam-Ting Tee, C.T. Ratnam, David Hui, A.R. Rahmat, A review of application of ammonium polyphosphate as intumescent flame retardant in thermoplastic composites, *Composites Part B: Engineering* 84 (2016) 155-174, <https://doi.org/10.1016/j.compositesb.2015.08.066>.
- [20] Z. Wang, K. Wu, Y. Hu, Study on flame retardance of co-microencapsulated ammonium polyphosphate and dipentaerythritol in polypropylene, *Polymer Engineering & Science* 48(12) (2008) 2426-2431, <https://doi.org/10.1002/pen.21198>.
- [21] Y. Yang, H. Luo, X. Cao, F. Zhou, W. Kong, X. Cai, The synergistic effects of a novel intumescent flame-retardant poly-(4-nitrophenoxy)-phosphazene and ammonium polyphosphate on ABS systems, *Journal of Thermal Analysis and Calorimetry* 137(1) (2019) 65-77, <https://doi.org/10.1007/s10973-018-7934-z>.
- [22] J. Yi, Y. Liu, X. Cai, The synergistic effect of adjuvant on the intumescent flame-retardant ABS with a novel charring agent, *Journal of Thermal Analysis and Calorimetry* 113(2) (2013) 753-761, <https://doi.org/10.1007/s10973-012-2802-8>.
- [23] T. Gurunathan, S. Mohanty, S.K. Nayak, A review of the recent developments in biocomposites based on natural fibres and their application perspectives, *Composites Part a-Applied Science and Manufacturing* 77 (2015) 1-25, <https://doi.org/10.1016/j.compositesa.2015.06.007>.
- [24] C.E. Hobbs, Recent advances in bio-based flame retardant additives for synthetic polymeric materials, *Polymers* 11(2) (2019), <https://doi.org/10.3390/polym11020224>.
- [25] L. Costes, F. Laoutid, S. Brohez, P. Dubois, Bio-based flame retardants: When nature meets fire protection, *Materials Science & Engineering R-Reports* 117 (2017) 1-25, <https://doi.org/10.1016/j.mser.2017.04.001>.
- [26] M.N. Prabhakar, A.U.R. Shah, J.-I. Song, Improved flame-retardant and tensile properties of thermoplastic starch/flax fabric green composites, *Carbohydrate Polymers* 168 (2017) 201-211, <https://doi.org/10.1016/j.carbpol.2017.03.036>.
- [27] P. Song, Z. Cao, S. Fu, Z. Fang, Q. Wu, J. Ye, Thermal degradation and flame retardancy properties of ABS/lignin: Effects of lignin content and reactive compatibilization, *Thermochimica Acta* 518(1-2) (2011) 59-65, <https://doi.org/10.1016/j.tca.2011.02.007>.
- [28] P.A. Costa, M.A. Barreiros, A.I. Mouquinho, P. Oliveira e Silva, F. Paradela, F.A. Costa Oliveira, Slow pyrolysis of cork granules under nitrogen atmosphere: by-products characterization and their potential valorization, *Biofuel Research Journal-Brj* 9(1) (2022) 1562-1572, <https://doi.org/10.18331/brj2022.9.1.3>.
- [29] APCOR's Cork Yearbook, 2020. [https://www.apcor.pt/wp-content/uploads/2021/08/Cork\\_BoletimEstatistico\\_APCOR\\_2020](https://www.apcor.pt/wp-content/uploads/2021/08/Cork_BoletimEstatistico_APCOR_2020). (Accessed 01/11 2023).
- [30] L. Gil, Cork powder waste: An overview, *Biomass & Bioenergy* 13(1-2) (1997) 59-61, [https://doi.org/10.1016/s0961-9534\(97\)00033-0](https://doi.org/10.1016/s0961-9534(97)00033-0).
- [31] A.S. de Leon, F. Nunez-Galvez, D. Moreno-Sanchez, N. Fernandez-Delgado, S.I. Molina, Polymer Composites with Cork Particles Functionalized by Surface Polymerization for Fused Deposition Modeling, *Acs Applied Polymer Materials* 4(2) (2022) 1225-1233, <https://doi.org/10.1021/acsapm.1c01632>.
- [32] L. Gil, Cork composites: A review, *Materials* 2(3) (2009) 776-789, <https://doi.org/10.3390/ma2030776>.
- [33] E.M. Fernandes, V.M. Correlo, J.A.M. Chagas, J.F. Mano, R.L. Reis, Properties of new cork-polymer composites: Advantages and drawbacks as compared with commercially available fibreboard materials, *Composite Structures* 93(12) (2011) 3120-3129, <https://doi.org/10.1016/j.compstruct.2011.06.020>.
- [34] B. Dairi, N. Bellili, N. Hamour, A. Boulassel, H. Djidjelli, A. Boukerrou, R. Bendib, Cork waste valorization as reinforcement in high-density polyethylene matrix, in *Polymer and Mediterranean Fiber International Conference (PMFIC)*. 2021, Bejaia, ALGERIA, <https://doi.org/10.1016/j.matpr.2021.12.420>.
- [35] F. Ben Abdallah, R. Ben Cheikh, M. Baklouti, Z. Denchev, A.M. Cunha, Effect of surface treatment in cork reinforced composites, *Journal of Polymer Research* 17(4) (2010) 519-528, <https://doi.org/10.1007/s10965-009-9339-y>.

- [36] E.M. Fernandes, V.M. Correlo, J.A.M. Chagas, J.F. Mano, R.L. Reis, Cork based composites using polyolefin's as matrix: Morphology and mechanical performance, *Composites Science and Technology* 70(16) (2010) 2310-2318, <https://doi.org/10.1016/j.compscitech.2010.09.010>.
- [37] E.M. Fernandes, V.M. Correlo, J.F. Mano, R.L. Reis, Novel cork-polymer composites reinforced with short natural coconut fibres: Effect of fibre loading and coupling agent addition, *Composites Science and Technology* 78 (2013) 56-62, <https://doi.org/10.1016/j.compscitech.2013.01.021>.
- [38] E.M. Fernandes, J.F. Mano, R.L. Reis, Hybrid cork-polymer composites containing sisal fibre: Morphology, effect of the fibre treatment on the mechanical properties and tensile failure prediction, *Composite Structures* 105 (2013) 153-162, <https://doi.org/10.1016/j.compstruct.2013.05.012>.
- [39] R. Hajj, R. El Hage, R. Sonnier, B. Otazaghine, S. Rouif, M. Nakhl, J.-M. Lopez-Cuesta, Influence of lignocellulosic substrate and phosphorus flame retardant type on grafting yield and flame retardancy, *Reactive & Functional Polymers* 153 (2020), <https://doi.org/10.1016/j.reactfunctpolym.2020.104612>.
- [40] B. Prieur, M. Meub, M. Wittemann, R. Klein, S. Bellayer, G. Fontaine, S. Bourbigot, Phosphorylation of lignin to flame retard acrylonitrile butadiene styrene (ABS), *Polymer Degradation and Stability* 127 (2016) 32-43, <https://doi.org/10.1016/j.polymdegradstab.2016.01.015>.
- [41] P.-B. Dai, F.-D. Meng, X.-L. Wang, Y.-Z. Wang, Effect of an Ultrahigh Rubber ABS Impact Modifier Resin on Mechanical Properties of Intumescent Flame-Retardant ABS Composites, *Journal of Macromolecular Science Part B-Physics* 49(3) (2010) 542-551, <https://doi.org/10.1080/00222341003591484>.
- [42] K. Jaidev, M. Biswal, S. Mohanty, S.K. Nayak, The influence of hybrid flame retardant and impact modifier on recycled blends formulated from keyboard waste plastics: A study on its flame retardant, mechanical, thermal, and chemical properties, *Polymers for Advanced Technologies* 33(2) (2022) 647-657, <https://doi.org/10.1002/pat.5547>.
- [43] G. Ozkoc, G. Bayram, E. Bayramli, Impact essential work of fracture toughness of ABS/polyamide-6 blends compatibilized with olefin based copolymers, *Journal of Materials Science* 43(8) (2008) 2642-2652, <https://doi.org/10.1007/s10853-008-2483-7>.
- [44] C.J. Hilado, *Flammability Handbook for Plastics*, Technomic Publishing Co., Pennsylvania, 1998,
- [45] A.H. Landrock, *Handbook of Plastics Flammability and Combustion Toxicology*, Noyes Publications, Park Ridge, 1983,
- [46] R.E.L.a.M.L. Janssens, *Polymer Flammability*, U.S. Department of Transportation USA, 2005, p. 82.
- [47] F. Laoutid, L. Bonnaud, M. Alexandre, J.M. Lopez-Cuesta, P. Dubois, New prospects in flame retardant polymer materials: From fundamentals to nanocomposites, *Materials Science & Engineering R-Reports* 63(3) (2009) 100-125, <https://doi.org/10.1016/j.mser.2008.09.002>.
- [48] P. Patel, *Investigation of the Fire Behaviour of PEEKbased Polymers and Compounds*, Centre of Fire and Hazard's Science, University of Central Lancashire, England, 2011.
- [49] <https://fire-risk-assessment-network.com/blog/fire-triangle-tetrahedron/>.
- [50] A.F.G.a.C.A. Wilkie, *Fire Retardancy of Polymeric Materials*, Marcel Dekker, New York, 2000,
- [51] A.R.H.a.D. Price, *Fire Retardant Materials*, Woodhead Publishing, England, 2001,
- [52] G. Pal, H. Macskasy, *Plastics: Their behavior in fires*, Elsevier, New York, 1991,
- [53] R.A. Ilyas, S.M. Sapuan, M.R.M. Asyraf, D.A.Z.N. Dayana, J.J.N. Amelia, M.S.A. Rani, M.N.F. Norrahim, N.M. Nurazzi, H.A. Aisyah, S. Sharma, M.R. Ishak, M. Rafidah, M.R. Razman, *Polymer Composites Filled with Metal Derivatives: A Review of Flame Retardants*, *Polymers* 13(11) (2021), <https://doi.org/10.3390/polym13111701>.
- [54] P. Leonards, *EU flammability standards and ENFIRO*, Institute for Environmental Studies VU University Amsterdam, 2012.
- [55] P.E. FIRE, *PU Europe FIRE HANDBOOK*, 2019.
- [56] K.H. Digges, R.G. Gann, S.J. Grayson, M.M. Hirschler, R.E. Lyon, D.A. Purser, J.G. Quintiere, R.R. Stephenson, A. Tewarson, Human survivability in motor vehicle fires, *Fire and Materials* 32(4) (2008) 249-258, <https://doi.org/10.1002/fam.964>.
- [57] B.S. Institution, *Methods of test for assessment of the ignitability of upholstered seating by smoldering and flaming ignition sources*, London, 2006.

- [58] U.L. Inc., UL 94, Test for Flammability of Plastic Materials for Parts in Devices and Appliance, 2001.
- [59] A. Dasari, Z.Z. Yu, G.P. Cai, Y.W. Mai, Recent developments in the fire retardancy of polymeric materials, *Progress in Polymer Science* 38(9) (2013) 1357-1387, <https://doi.org/10.1016/j.progpolymsci.2013.06.006>.
- [60] A.B. Morgan, J.W. Gilman, An overview of flame retardancy of polymeric materials: application, technology, and future directions, *Fire and Materials* 37(4) (2013) 259-279, <https://doi.org/10.1002/fam.2128>.
- [61] F. Laoutid, P. Gaudon, J.M. Taulemesse, J.M.L. Cuesta, J.I. Velasco, A. Piechaczyk, Study of hydromagnesite and magnesium hydroxide based fire retardant systems for ethylene-vinyl acetate containing organo-modified montmorillonite, *Polymer Degradation and Stability* 91(12) (2006) 3074-3082, <https://doi.org/10.1016/j.polymdegradstab.2006.08.011>.
- [62] A.B. Morgan, J.M. Cogent, R.S. Opperman, J.D. Harris, The effectiveness of magnesium carbonate-based flame retardants for polyethylene-co-vinyl acetate and poly (ethylene-co-ethyl acrylate), *Fire and Materials* 31(6) (2007) 387-410, <https://doi.org/10.1002/fam.950>.
- [63] K.H. Pawlowski, B. Scharrel, Flame retardancy mechanisms of aryl phosphates in combination with boehmite in bisphenol A polycarbonate/acrylonitrile-butadiene-styrene blends, *Polymer Degradation and Stability* 93(3) (2008) 657-667, <https://doi.org/10.1016/j.polymdegradstab.2008.01.002>.
- [64] U. Braun, A.I. Balabanovich, B. Scharrel, U. Knoll, J. Artner, M. Ciesielski, M. Doering, R. Perez, J.K.W. Sandler, V. Altstaedt, T. Hoffmann, D. Pospiech, Influence of the oxidation state of phosphorus on the decomposition and fire behaviour of flame-retarded epoxy resin composites, *Polymer* 47(26) (2006) 8495-8508, <https://doi.org/10.1016/j.polymer.2006.10.022>.
- [65] U. Braun, H. Bahr, H. Sturm, B. Scharrel, Flame retardancy mechanisms of metal phosphinates and metal phosphinates in combination with melamine cyanurate in glass-fiber reinforced poly(1,4-butylene terephthalate): the influence of metal cation, *Polymers for Advanced Technologies* 19(6) (2008) 680-692, <https://doi.org/10.1002/pat.1147>.
- [66] B. Scharrel, R. Kunze, D. Neubert, Red phosphorus-control led decomposition for fire retardant PA 66, *Journal of Applied Polymer Science* 83(10) (2002) 2060-2071, <https://doi.org/10.1002/app.10144>.
- [67] S.Y. Lu, I. Hamerton, Recent developments in the chemistry of halogen-free flame retardant polymers, *Progress in Polymer Science* 27(8) (2002) 1661-1712, [https://doi.org/10.1016/s0079-6700\(02\)00018-7](https://doi.org/10.1016/s0079-6700(02)00018-7).
- [68] S.V. Levchik, E.D. Weil, A review of recent progress in phosphorus-based flame retardants, *Journal of Fire Sciences* 24(5) (2006) 345-364, <https://doi.org/10.1177/0734904106068426>.
- [69] S. Fu, P. Song, X. Liu, Thermal and flame retardancy properties of thermoplastics/natural fiber biocomposites, 2017, <https://doi.org/10.1016/b978-0-08-100411-1.00019-4>.
- [70] S. Bourbigot, M. Le Bras, S. Duquesne, M. Rochery, Recent advances for intumescent polymers, *Macromolecular Materials and Engineering* 289(6) (2004) 499-511, <https://doi.org/10.1002/mame.200400007>.
- [71] S. Bourbigot, M. Le Bras, F. Dabrowski, J.W. Gilman, T. Kashiwagi, PA-6 clay nanocomposite hybrid as char forming agent in intumescent formulations, *Fire and Materials* 24(4) (2000) 201-208, [https://doi.org/10.1002/1099-1018\(200007/08\)24:4<201::aid-fam739>3.0.co;2-d](https://doi.org/10.1002/1099-1018(200007/08)24:4<201::aid-fam739>3.0.co;2-d).
- [72] G. Bertelli, G. Camino, E. Marchetti, L. Costa, E. Casorati, R. Locatelli, Parameters Affecting Fire Retardant Effectiveness in Intumescent Systems, *Polymer Degradation and Stability* 25(2-4) (1989) 277-292, [https://doi.org/10.1016/s0141-3910\(89\)81012-2](https://doi.org/10.1016/s0141-3910(89)81012-2).
- [73] G. Camino, L. Costa, G. Martinasso, Intumescent Fire-retardant Systems, *Polymer Degradation and Stability* 23(4) (1989) 359-376, [https://doi.org/10.1016/0141-3910\(89\)90058-x](https://doi.org/10.1016/0141-3910(89)90058-x).
- [74] Y.-W. Yan, L. Chen, R.-K. Jian, S. Kong, Y.-Z. Wang, Intumescence: An effect way to flame retardance and smoke suppression for polystyrene, *Polymer Degradation and Stability* 97(8) (2012) 1423-1431, <https://doi.org/10.1016/j.polymdegradstab.2012.05.013>.
- [75] A.K. Mohanty, M. Misra, L.T. Drzal, *Natural Fibers, Biopolymers, and Biocomposites: An introduction, Natural Fibers, Biopolymers, and Biocomposites*, CRC Press, New York, 2005.

- [76] A.K. Mohanty, M. Misra, L.T. Drzal, S.E. Selke, B.R. Harte, G. Hinrichsen, Natural fibers, biopolymers, and biocomposites: An introduction, *Natural Fibers, Biopolymers, and Biocomposites* (2005) 1-36, <https://doi.org/https://doi.org/10.1201/9780203508206>.
- [77] R. Sonnier, A. Taguet, L. Ferry, J.M. LopezCuesta, *Towards Bio-Based Flame Retardant Polymers, Towards Bio-Based Flame Retardant Polymers* 2018, pp. 1-100, <https://doi.org/10.1007/978-3-319-67083-6>.
- [78] X. Wang, C. Lu, C. Chen, Effect of Chicken-Feather Protein-Based Flame Retardant on Flame Retarding Performance of Cotton Fabric, *Journal of Applied Polymer Science* 131(15) (2014), <https://doi.org/10.1002/app.40584>.
- [79] E. Fahy, A comprehensive classification system for lipids *Journal of Lipid Research* 51(6) (2010) 1618-1618, <https://doi.org/10.1194/jlr.E400004ERR>.
- [80] M. Brebu, C. Vasile, Thermal degradation of lignin—A review, *Cellulose Chemistry and Technology* 44(9) (2010) 353-363.
- [81] G.M. Glenn, W.J. Orts, G.A.R. Nobes, Starch, fiber and CaCO<sub>3</sub> effects on the physical properties of foams made by a baking process, *Industrial Crops and Products* 14(3) (2001) 201-212, [https://doi.org/10.1016/s0926-6690\(01\)00085-1](https://doi.org/10.1016/s0926-6690(01)00085-1).
- [82] G.M. Raghavendra, J. Jung, D. Kim, J. Seo, Step-reduced synthesis of starch-silver nanoparticles, *International Journal of Biological Macromolecules* 86 (2016) 126-128, <https://doi.org/10.1016/j.ijbiomac.2016.01.057>.
- [83] M. Maqsood, G. Seide, Investigation of the Flammability and Thermal Stability of Halogen-Free Intumescent System in Biopolymer Composites Containing Biobased Carbonization Agent and Mechanism of Their Char Formation, *Polymers* 11(1) (2019), <https://doi.org/10.3390/polym11010048>.
- [84] J.Y. Xiaofeng Sui, Mi Zhou, Jun Zhang, Haijun Yang, Weizhong Yuan, Yen Wei, Caiyuan Pan, Synthesis of Cellulose-graft-Poly(N,N-dimethylamino-2-ethyl methacrylate) Copolymers via Homogeneous ATRP and Their Aggregates in Aqueous Media, *Biomacromolecules* 9 (2008) 2615-2620.
- [85] X. Sui, J. Yuan, M. Zhou, J. Zhang, H. Yang, W. Yuan, Y. Wei, C. Pan, Synthesis of Cellulose-graft-Poly(N,N-dimethylamino-2-ethyl methacrylate) Copolymers via Homogeneous ATRP and Their Aggregates in Aqueous Media, *Biomacromolecules* 9(10) (2008) 2615-2620, <https://doi.org/10.1021/bm800538d>.
- [86] D.K. Jena, P.K. Sahoo, Development of biodegradable cellulose-g-poly(butyl acrylate)/kaolin nanocomposite with improved fire retardancy and mechanical properties, *Journal of Applied Polymer Science* 135(11) (2018), <https://doi.org/10.1002/app.45968>.
- [87] M.N.Prabhakar, A.u.R. Shah, J. Song, A Review on the Flammability and Flame Retardant Properties of Natural Fibers and Polymer Matrix Based Composites, *Composites Research* 28(2) (2015) 29-39.
- [88] R. Dunne, D. Desai, R. Sadiku, Material characterization of blended sisal-kenaf composites with an ABS matrix, *Applied Acoustics* 125 (2017) 184-193, <https://doi.org/10.1016/j.apacoust.2017.03.022>.
- [89] M. Durante, C. Leone, M. Ussorio, I.C. Visconti, SOLUTION IMPREGNATION OF NATURAL FIBRES/ABS MATRIX COMPOSITES, in In: *Proceedings of ECCM-11. 2004, Rhodes Greece*.
- [90] A.R. Torrado Perez, D.A. Roberson, R.B. Wicker, Fracture Surface Analysis of 3D-Printed Tensile Specimens of Novel ABS-Based Materials, *Journal of Failure Analysis and Prevention* 14(3) (2014) 343-353, <https://doi.org/10.1007/s11668-014-9803-9>.
- [91] Y. Martensa, A. Ehrmann, *Composites of 3D-Printed Polymers and Textile Fabrics*, *Materials Science and Engineering*, 2017.
- [92] R. Kozłowski, M. Władyska-Przybylak, Flammability and fire resistance of composites reinforced by natural fibers, *Polymers for Advanced Technologies* 19(6) (2008) 446-453, <https://doi.org/10.1002/pat.1135>.
- [93] H. Pereira, *Cork: Biology, production and uses*, Elsevier, Amsterdam, 2007, <https://doi.org/10.1016/B978-0-444-52967-1.X5000-6>.
- [94] S.P. Silva, M.A. Sabino, E.M. Fernandes, V.M. Correlo, L.F. Boesel, R.L. Reis, Cork: Properties, capabilities and applications, *International Materials Reviews* 50(6) (2005) 345-365, <https://doi.org/10.1179/174328005x41168>.

- [95] F. Ghonjizade-Samani, L. Haurie, R. Malet, V. Realinho, The Components' Roles in Thermal Stability and Flammability of Cork Powder, *Materials* 16(10) (2023) 3829, <https://doi.org/10.3390/ma16103829>.
- [96] N. Illy, M. Fache, R. Menard, C. Negrell, S. Caillol, G. David, Phosphorylation of bio-based compounds: the state of the art, *Polymer Chemistry* 6(35) (2015) 6257-6291, <https://doi.org/10.1039/c5py00812c>.
- [97] V.A. Alfonsov, Diastereoselective Synthesis of Enantiopure  $\alpha$ -Aminophosphonic Acid Derivatives: Pudovik Reaction in Stereoselective Synthesis (Dedicated to A. N. Pudovik, 1916-2006), *Phosphorus Sulfur and Silicon and the Related Elements* 183(11) (2008) 2637-2644, <https://doi.org/10.1080/10426500802344022>.
- [98] F.R. Atherton, H.T. Openshaw, A.R. Todd, Studies on phosphorylation. Part II. The reaction of dialkyl phosphites with polyhalogen compounds in presence of bases. A new method for the phosphorylation of amines, *Journal of the Chemical Society (SEP-)* (1945) 660-663, <https://doi.org/10.1039/jr9450000660>.
- [99] L. Montero De Espinosa, J.C. Ronda, M. Galia, V. Cadiz, A Straightforward Strategy for the Efficient Synthesis of Acrylate and Phosphine Oxide-Containing Vegetable Oils and Their Crosslinked Materials, *Journal of Polymer Science Part a-Polymer Chemistry* 47(16) (2009) 4051-4063, <https://doi.org/10.1002/pola.23466>.
- [100] G. Lligadas, J.C. Ronda, M. Galia, V. Cadiz, Synthesis and properties of thermosetting polymers from a phosphorous-containing fatty acid derivative, *Journal of Polymer Science Part a-Polymer Chemistry* 44(19) (2006) 5630-5644, <https://doi.org/10.1002/pola.21691>.
- [101] M. Moreno, G. Lligadas, J.C. Ronda, M. Galia, V. Cadiz, Flame retardant high oleic sunflower oil-based thermosetting resins through aza- and phospho-michael additions, *Journal of Polymer Science Part a-Polymer Chemistry* 51(8) (2013) 1808-1815, <https://doi.org/10.1002/pola.26562>.
- [102] R.A. Sanchez, B.P. Esposito, Preparation of sugarcane bagasse modified with the thiophosphoryl function and its capacity for cadmium adsorption, *Bioresources* 6(3) (2011) 2448-2459.
- [103] Y. Sekiguchi, C. Sawatari, T. Yagi, Durable flame retardant cotton fabric prepared by partial pyrophosphorylation and metal complexation, *Textile Research Journal* 70(1) (2000) 71-76, <https://doi.org/10.1177/004051750007000111>.
- [104] S. Hu, L. Song, H. Pan, Y. Hu, X. Gong, Thermal properties and combustion behaviors of flame retarded epoxy acrylate with a chitosan based flame retardant containing phosphorus and acrylate structure, *Journal of Analytical and Applied Pyrolysis* 97 (2012) 109-115, <https://doi.org/10.1016/j.jaap.2012.06.003>.
- [105] H. He, Y. Wang, Z. Yu, J. Liu, Y. Zhao, Y. Ke, Ecofriendly flame-retardant composite aerogel derived from polysaccharide: Preparation, flammability, thermal kinetics, and mechanism, *Carbohydrate Polymers* 269 (2021), <https://doi.org/10.1016/j.carbpol.2021.118291>.
- [106] H. Ma, L. Tong, Z. Xu, Z. Fang, Y. Jin, F. Lu, A novel intumescent flame retardant: Synthesis and application in ABS copolymer, *Polymer Degradation and Stability* 92 (2006) 720-726.
- [107] Y.Y. Xilei Cao, Hang Luo, Xufu Cai, High efficiency intumescent flame retardancy between Hexakis (4-nitrophenoxy) cyclotriphosphazene and ammonium polyphosphate on ABS, *Polymer Degradation and Stability* 143 (2017) 259-265.
- [108] Y. Zhang, X. Chen, Z. Fang, Synergistic Effects of Expandable Graphite and Ammonium Polyphosphate with a New Carbon Source Derived from Biomass in Flame Retardant ABS, *Applied Polymer Science* (2012) 2424-2432, <https://doi.org/10.1002/APP.38382>.
- [109] D. Ghanbari, Hydrothermal synthesis of CuS nanostructures and their application on preparation of ABS-based nanocomposite, *Journal of Industrial and Engineering Chemistry* 20 (2014) 3709-3713.
- [110] V. Realinho, L. Haurie, J. Formosa, J.I. Velasco, Flame retardancy effect of combined ammonium polyphosphate and aluminium diethyl phosphinate in acrylonitrile-butadiene-styrene, *Polymer Degradation and Stability* 155 (2018) 208-219.
- [111] G.F.L. E. A. MURASHKO, S. V LEVCHIK, D. A. BRIGHT, S. DASHEVSKY, Fire Retardant Action of Resorcinol Bis(Diphenyl Phosphate) in a PC/ABS Blend. I. Combustion Performance and Thermal Decomposition Behavior, *JOURNAL OF FIRE SCIENCES* 16 (1998) 278-295.
- [112] R.-K. Jian, L. Chen, S.-Y. Chen, J.-W. Long, Y.-Z. Wang, A novel flame-retardant acrylonitrile-butadiene-styrene system based on aluminum isobutylphosphinate and red phosphorus: Flame retardance,



- thermal degradation and pyrolysis behavior, *Polymer Degradation and Stability* 109 (2014) 184-193, <https://doi.org/10.1016/j.polymdegradstab.2014.07.018>.
- [113] X. Cao, Y. Yang, H. Luo, X. Cai, High efficiency intumescent flame retardancy between Hexakis (4-nitrophenoxy) cyclotriphosphazene and ammonium polyphosphate on ABS, *Polymer Degradation and Stability* 143 (2017) 259-265, <https://doi.org/10.1016/j.polymdegradstab.2017.07.022>.
- [114] L. Xiong, S. Huang, R. Zhong, W. Tang, C. Liu, Y. Jin, Preparation, Characterization, and Performance of Lignin-based Microencapsulated Red Phosphorus Flame Retardant for ABS, *Journal of Wuhan University of Technology-Materials Science Edition* 37(2) (2022) 292-299, <https://doi.org/10.1007/s11595-022-2530-2>.
- [115] C. Yildiz, Y. Seki, E. Kizilkan, M. Sarikanat, L. Altay, Development of Halogen-Free Flame Retardant Acrylonitrile Butadiene Styrene (ABS) Based Composite Materials, *Chemistryselect* 8(41) (2023), <https://doi.org/10.1002/slct.202300989>.
- [116] R.-K. Jian, L. Chen, B. Zhao, Y.-W. Yan, X.-F. Li, Y.-Z. Wang, Acrylonitrile-Butadiene-Styrene Terpolymer with Metal Hypophosphites: Flame Retardance and Mechanism Research, *Industrial & Engineering Chemistry Research* 53(6) (2014) 2299-2307, <https://doi.org/10.1021/ie403726m>.
- [117] X. Chen, X. Cai, Synthesis of poly(diethylenetriamine terephthalamide) and its application as a flame retardant for ABS, *Journal of Thermal Analysis and Calorimetry* 125(1) (2016) 313-320, <https://doi.org/10.1007/s10973-016-5358-1>.
- [118] T.M. Simionescu, A.A. Minea, P.N. Balbis dos Reis, Fire Properties of Acrylonitrile Butadiene Styrene Enhanced with Organic Montmorillonite and Exolit Fire Retardant, *Applied Sciences-Basel* 9(24) (2019), <https://doi.org/10.3390/app9245433>.
- [119] N. Wu, Z. Xiu, J. Du, Preparation of microencapsulated aluminum hypophosphite and flame retardancy and mechanical properties of flame-retardant ABS composites, *Journal of Applied Polymer Science* 134(33) (2017), <https://doi.org/10.1002/app.45008>.
- [120] X. Yang, H. Wang, X. Liu, J. Liu, Synthesis of a novel aluminium salt of nitrogen-containing alkylphosphinate with high char formation to flame retard acrylonitrile-butadiene-styrene, *Royal Society Open Science* 7(9) (2020), <https://doi.org/10.1098/rsos.200800>.
- [121] Y. Ren, Q. Fu, X. Wang, L. Yang, J. Zhou, B. Zhong, Z. Zhang, Fire retardant synergism of hydroquinone bis(diphenyl phosphate) and novolac phenol in acrylonitrile-butadiene-styrene copolymer, *Fire and Materials* 39(6) (2015) 557-569, <https://doi.org/10.1002/fam.2255>.
- [122] A. Bachinger, A. Sandinge, K.M. Lindqvist, A. Strid, G. Gong, Systematic evaluation of bromine-free flame-retardant systems in acrylonitrile-butadiene-styrene, *Journal of Applied Polymer Science* 139(13) (2022), <https://doi.org/10.1002/app.51861>.
- [123] Y. Liu, J. Yi, X. Cai, Effect of a novel intumescent retardant for ABS with synergist  $\text{Al}(\text{H}_2\text{PO}_4)_3$ , *Polymer Bulletin* 67(2) (2011) 361-374, <https://doi.org/10.1007/s00289-011-0482-3>.
- [124] L.-L. Ge, H.-J. Duan, X.-G. Zhang, C. Chen, J.-H. Tang, Z.-M. Li, Synergistic effect of ammonium polyphosphate and expandable graphite on flame-retardant properties of acrylonitrile-butadiene-styrene, *Journal of Applied Polymer Science* 126(4) (2012) 1337-1343, <https://doi.org/10.1002/app.36997>.
- [125] Z. Zheng, T. Yang, B. Wang, B. Qu, H. Wang, Microencapsulated melamine phosphate via the sol-gel method and its application in halogen-free and intumescent flame-retarding acrylonitrile-butadiene-styrene copolymer, *Polymer International* 64(9) (2015) 1275-1288, <https://doi.org/10.1002/pi.4919>.
- [126] H. Luo, F. Zhou, Y. Yang, X. Cao, X. Cai, Gas-condensed phase flame-retardant mechanisms of tris(3-nitrophenyl) phosphine/triphenyl phosphate/ABS, *Journal of Thermal Analysis and Calorimetry* 132(1) (2018) 263-273, <https://doi.org/10.1007/s10973-017-6906-z>.
- [127] W. Jun, J. Yi, X.-F. Cai, Synergistic Effect of a Novel Charring Agent and Ammonium Polyphosphate on the Flame Retardancy of Acrylonitrile Butadiene Styrene, *Journal of Applied Polymer Science* 120(2) (2011) 968-973, <https://doi.org/10.1002/app.33115>.
- [128] Y. Xia, X.-G. Jian, J.-F. Li, X.-H. Wang, Y.-Y. Xu, Synergistic effect of montmorillonite and intumescent flame retardant on flame retardance enhancement of ABS, *Polymer-Plastics Technology and Engineering* 46(3) (2007) 227-232, <https://doi.org/10.1080/03602550601152895>.

- [129] D. Hoang, W. Kim, H. An, J. Kim, Flame retardancies of novel organo-phosphorus flame retardants based on DOPO derivatives when applied to ABS, *Macromolecular Research* 23(5) (2015) 442-448, <https://doi.org/10.1007/s13233-015-3058-5>.
- [130] Y. Zhang, X. Chen, Z. Fang, Flame retardant ABS with a novel polyphosphate derived from biomass, in International Conference on Advanced Engineering Materials and Technology (AEMT2011). 2011, Sanya, PEOPLES R CHINA, <https://doi.org/10.4028/www.scientific.net/AMR.284-286.187>.
- [131] Q. Wu, F. Ran, L. Dai, C. Li, R. Li, C. Si, A functional lignin-based nanofiller for flame-retardant blend, *International Journal of Biological Macromolecules* 190 (2021) 390-395, <https://doi.org/10.1016/j.ijbiomac.2021.08.233>.
- [132] A. Farzadfar, S.N. Khorasani, S. Khalili, Blends of recycled polycarbonate and acrylonitrile-butadiene-styrene: comparing the effect of reactive compatibilizers on mechanical and morphological properties, *Polymer International* 63(1) (2014) 145-150, <https://doi.org/10.1002/pi.4493>.
- [133] M. Tasdemir, Properties of acrylonitrile-butadiene-styrene/polycarbonate blends with styrene-butadiene-styrene block copolymer, *Journal of Applied Polymer Science* 93(6) (2004) 2521-2527, <https://doi.org/10.1002/app.20708>.
- [134] X.F. Zhang, Y.S. Chen, Y. Zhang, Z.L. Peng, Y.X. Zhang, W. Zhou, Effects of ABS-g-MAH on mechanical properties and compatibility of ABS/PC alloy, *Journal of Applied Polymer Science* 81(4) (2001) 831-836, <https://doi.org/10.1002/app.1502>.
- [135] G. Ozkoc, G. Bayram, E. Bayramli, Effects of olefin-based compatibilizers on the morphology, thermal and mechanical properties of ABS/polyamide-6 blends, *Journal of Applied Polymer Science* 104(2) (2007) 926-935, <https://doi.org/10.1002/app.25848>.
- [136] W.Y. Chiang, G.L. Tzeng, Effect of the compatibilizers on flame-retardant polycarbonate (PC) acrylonitrile-butadiene-styrene (ABS) alloy, *Journal of Applied Polymer Science* 65(4) (1997) 795-805, [https://doi.org/10.1002/\(sici\)1097-4628\(19970725\)65:4<795::aid-app17>3.0.co;2-s](https://doi.org/10.1002/(sici)1097-4628(19970725)65:4<795::aid-app17>3.0.co;2-s).
- [137] J. Lin, J. Li, X. Li, Y. Guan, G. Wang, L. Chen, Flame retardancy and toughening modification of glass fiber-reinforced polycarbonate composites, *Polymer Journal* 51(7) (2019) 657-665, <https://doi.org/10.1038/s41428-019-0181-8>.
- [138] N. Bagotia, B.P. Singh, V. Choudhary, D.K. Sharma, Excellent impact strength of ethylene-methyl acrylate copolymer toughened polycarbonate, *Rsc Advances* 5(106) (2015) 87589-87597, <https://doi.org/10.1039/c5ra18024d>.
- [139] N. Cordeiro, M.N. Belgacem, A.J.D. Silvestre, C.P. Neto, A. Gandini, Cork suberin as a new source of chemicals. 1. Isolation and chemical characterization of its composition, *International Journal of Biological Macromolecules* 22(2) (1998) 71-80, [https://doi.org/10.1016/s0141-8130\(97\)00090-1](https://doi.org/10.1016/s0141-8130(97)00090-1).
- [140] A.V. Marques, J. Rencoret, A. Gutierrez, J.C. del Rio, H. Pereira, Ferulates and lignin structural composition in cork, *Holzforschung* 70(4) (2016) 275-289, <https://doi.org/10.1515/hf-2015-0014>.
- [141] Z. Jiang, D. Xu, X. Ma, J. Liu, P. Zhu, Facile synthesis of novel reactive phosphoramidate siloxane and application to flame retardant cellulose fabrics, *Cellulose* 26(9) (2019) 5783-5796, <https://doi.org/10.1007/s10570-019-02465-2>.
- [142] P. Jove, M. Angels Olivella, L. Cano, Study of the variability in chemical composition of bark layers of cork from different production areas, *Bioresources* 6(2) (2011) 1806-1815, <https://doi.org/10.15376/biores.6.2.1806-1815>.
- [143] A. Sen, I. Miranda, B. Esteves, H. Pereira, Chemical characterization, bioactive and fuel properties of waste cork and phloem fractions from *Quercus cerris* L. bark, *Industrial Crops and Products* 157 (2020), <https://doi.org/10.1016/j.indcrop.2020.112909>.
- [144] H. Pereira, Chemical composition and variability of cork from *Quercus suber* L., *Wood Science and Technology* 22(3) (1988) 211-218, <https://doi.org/10.1007/bf00386015>.
- [145] W. Shangguan, Z. Chen, J. Zhao, X. Song, Thermogravimetric analysis of cork and cork components from *Quercus variabilis*, *Wood Science and Technology* 52(1) (2018) 181-192, <https://doi.org/10.1007/s00226-017-0959-9>.

- [146] L.E. Wise, M. Murphy, A.A. Daddieco, Chlorite holocellulose, its fractionation and bearing on summative wood analysis and studies on the hemicelluloses, *Technical Association Papers* 29(JUN) (1946) 210-218.
- [147] H. Vahabi, E. Movahedifar, B.K. Kandola, M.R. Saeb, Flame Retardancy Index (FRI) for Polymer Materials Ranking, *Polymers* 15(11) (2023), <https://doi.org/10.3390/polym15112422>.
- [148] H. Ma, L. Tong, Z. Xu, Z. Fang, Y. Jin, F. Lu, A novel intumescent flame retardant: Synthesis and application in ABS copolymer, *Polymer Degradation and Stability* 92(4) (2007) 720-726, <https://doi.org/10.1016/j.polymdegradstab.2006.12.009>.
- [149] Y. Zhang, X. Chen, Z. Fang, Synergistic effects of expandable graphite and ammonium polyphosphate with a new carbon source derived from biomass in flame retardant ABS, *Journal of Applied Polymer Science* 128(4) (2013) 2424-2432, <https://doi.org/10.1002/app.38382>.
- [150] N.F. Attia, M.A. Hassan, M.A. Nour, K.E. Geckeler, Flame-retardant materials: Synergistic effect of halloysite nanotubes on the flammability properties of acrylonitrile-butadiene-styrene composites, *Polymer International* 63(7) (2014) 1168-1173, <https://doi.org/10.1002/pi.4653>.
- [151] J. Kim, K. Lee, K. Lee, J. Bae, J. Yang, S. Hong, Studies on the thermal stabilization enhancement of ABS; synergistic effect of triphenyl phosphate nanocomposite, epoxy resin, and silane coupling agent mixtures, *Polymer Degradation and Stability* 79(2) (2003) 201-207, [https://doi.org/10.1016/s0141-3910\(02\)00272-0](https://doi.org/10.1016/s0141-3910(02)00272-0).
- [152] E. Wawrzyn, B. Schartel, M. Ciesielski, B. Kretzschmar, U. Braun, M. Doering, Are novel aryl phosphates competitors for bisphenol A bis(diphenyl phosphate) in halogen-free flame-retarded polycarbonate/acrylonitrile-butadiene-styrene blends?, *European Polymer Journal* 48(9) (2012) 1561-1574, <https://doi.org/10.1016/j.eurpolymj.2012.06.015>.
- [153] S.-T. Bee, K.-S. Lim, L.T. Sin, C.T. Ratnam, S.L. Bee, A.R. Rahmat, Interactive effect of ammonium polyphosphate and montmorillonite on enhancing flame retardancy of polycarbonate/acrylonitrile butadiene styrene composites, *Iranian Polymer Journal* 27(11) (2018) 899-911, <https://doi.org/10.1007/s13726-018-0664-z>.
- [154] A. Mujtaba, M. Keller, S. Ilisch, H.J. Radosch, T. Thurn-Albrecht, K. Saalwaechter, M. Beiner, Mechanical Properties and Cross-Link Density of Styrene-Butadiene Model Composites Containing Fillers with Bimodal Particle Size Distribution, *Macromolecules* 45(16) (2012) 6504-6515, <https://doi.org/10.1021/ma300925p>.
- [155] S. Aid, A. Eddhahak, Z. Ortega, D. Froelich, A. Tcharkhtchi, Experimental study of the miscibility of ABS/PC polymer blends and investigation of the processing effect, *Journal of Applied Polymer Science* 134(25) (2017), <https://doi.org/10.1002/app.44975>.
- [156] Y.I. Malekzadeh, K. Shelesh-Nezhad, The effects of HNO<sub>3</sub>-surface treated carbon fiber and nano-CaCO<sub>3</sub> inclusions on dynamic mechanical and heat properties of PA6/ABS-based composites, *Journal of Thermoplastic Composite Materials* 32(7) (2019) 867-883, <https://doi.org/10.1177/0892705718804604>.
- [157] L. Bazli, A. Khavandi, M.A. Boutorabi, M. Karrabi, Correlation between viscoelastic behavior and morphology of nanocomposites based on SR/EPDM blends compatibilized by maleic anhydride, *Polymer* 113 (2017) 156-166.
- [158] M. Suzuki, C.A. Wilkie, The thermal degradation of acrylonitrile-butadiene-styrene terpolymer as studied by TGA/FTIR, *Polymer Degradation and Stability* 47(2) (1995) 217-221, [https://doi.org/10.1016/0141-3910\(94\)00122-o](https://doi.org/10.1016/0141-3910(94)00122-o).
- [159] M.P.L. Dicortemiglia, G. Camino, L. Costa, M. Guaita, Thermal degradation of ABS, *Thermochemica Acta* 93(SEP) (1985) 187-190, [https://doi.org/10.1016/0040-6031\(85\)85048-6](https://doi.org/10.1016/0040-6031(85)85048-6).
- [160] U. Basuli, T.K. Chaki, S. Chattopadhyay, Thermomechanical and rheological behaviour of polymer nanocomposites based on ethylene-methyl acrylate (EMA) and multiwalled carbon nanotube (MWNT), *Plastics Rubber and Composites* 40(5) (2011) 213-222, <https://doi.org/10.1179/1743289810y.0000000001>.
- [161] J. Zhang, S.Y. Feng, Q.Y. Ma, Kinetics of the thermal degradation and thermal stability of conductive silicone rubber filled with conductive carbon black, *Journal of Applied Polymer Science* 89(6) (2003) 1548-1554, <https://doi.org/10.1002/app.12277>.

- [162] F. Wang, X. Wang, Preparation and thermal stability of micro/nano silicone rubber particles, in International Conference on Chemical, Material and Metallurgical Engineering (ICMME 2011). 2011, Beihai, PEOPLES R CHINA, <https://doi.org/10.4028/www.scientific.net/AMR.399-401.718>.
- [163] A. Atazadeh, E. Ameri, Synthesis of PMHS-PDMS composite membranes embedded with silica nanoparticles and their application to separate of DMSO from aqueous solutions, *Polymer Bulletin* 78(9) (2021) 5003-5028, <https://doi.org/10.1007/s00289-020-03355-5>.
- [164] B. Schartel, T.R. Hull, Development of fire-retarded materials - Interpretation of cone calorimeter data, *Fire and Materials* 31(5) (2007) 327-354, <https://doi.org/10.1002/fam.949>.
- [165] P.-B. Dai, D.-Y. Wang, Y.-Z. Wang, Thermal Degradation and Combustion Behavior of a Modified Intumescent Flame-retardant ABS Composite, *Journal of Thermoplastic Composite Materials* 23(4) (2010) 473-486, <https://doi.org/10.1177/0892705708103404>.
- [166] C.-H. Ke, J. Li, K.-Y. Fang, Q.-L. Zhu, J. Zhu, Q. Yan, Y.-Z. Wang, Synergistic effect between a novel hyperbranched charring agent and ammonium polyphosphate on the flame retardant and anti-dripping properties of polylactide, *Polymer Degradation and Stability* 95(5) (2010) 763-770, <https://doi.org/10.1016/j.polymdegradstab.2010.02.011>.
- [167] A. Aljamal, G. Marosi, B. Szolnoki, Investigation of the modes of action for phosphorous flame retardants in a fully waterborne sugar-based epoxy resin, *Journal of Thermal Analysis and Calorimetry* 148(2) (2023) 281-292, <https://doi.org/10.1007/s10973-022-11736-3>.
- [168] B. Xu, L. Shao, J. Wang, Y. Liu, L. Qian, Enhancement of the intumescent flame retardant efficiency in polypropylene by synergistic charring effect of a hypophosphite/cyclotetrasiloxane bi-group compound, *Polymer Degradation and Stability* 181 (2020), <https://doi.org/10.1016/j.polymdegradstab.2020.109281>.
- [169] E. Gallo, B. Schartel, D. Acierno, P. Russo, Flame retardant biocomposites: Synergism between phosphinate and nanometric metal oxides, *European Polymer Journal* 47(7) (2011) 1390-1401, <https://doi.org/10.1016/j.eurpolymj.2011.04.001>.
- [170] A. Sen, J. Van den Bulcke, N. Defoirdt, J. Van Acker, H. Pereira, Thermal behaviour of cork and cork components, *Thermochimica Acta* 582 (2014) 94-100, <https://doi.org/10.1016/j.tca.2014.03.007>.
- [171] S.P. Magalhaes da Silva, P.S. Lima, J.M. Oliveira, Non-isothermal crystallization kinetics of cork-polymer composites for injection molding, *Journal of Applied Polymer Science* 133(42) (2016), <https://doi.org/10.1002/app.44124>.
- [172] H. De Oliveira, B. Yoon, V. Michaud, J.-D. Nam, J. Suhr, All natural cork composites with suberin-based polyester and lignocellulosic residue, *Industrial Crops and Products* 109 (2017) 843-849, <https://doi.org/10.1016/j.indcrop.2017.09.044>.
- [173] L. Reis, A. Silva, Mechanical behavior of sandwich structures using natural cork agglomerates as core materials, *Journal of Sandwich Structures & Materials* 11(6) (2009) 487-500, <https://doi.org/10.1177/1099636209104523>.
- [174] Z. Xie, E.Z. Luo, J.B. Xu, I.H. Wilson, L.H. Zhao, X.X. Zhang, Construction and characterization of a heating stage for a scanning probe microscope up to 215 degrees C, *Review of Scientific Instruments* 71(5) (2000) 2100-2103, <https://doi.org/10.1063/1.1150587>.
- [175] Y. Lei, T. Jia, X. Song, Chemical composition of cork from *Quercus variabilis*, *Wood and Fiber Science* 44(2) (2012) 214-219.
- [176] H. Pereira, The rationale behind cork properties: A review of structure and chemistry, *Bioresources* 10(3) (2015) 6207-6229, <https://doi.org/10.15376/biores.10.3.Pereira>.
- [177] V. Gopinath, S. Saravanan, A.R. Al-Maleki, M. Ramesh, J. Vadivelu, A review of natural polysaccharides for drug delivery applications: Special focus on cellulose, starch and glycogen, *Biomedicine & Pharmacotherapy* 107 (2018) 96-108, <https://doi.org/10.1016/j.biopha.2018.07.136>.
- [178] M. Poletto, A.J. Zattera, R.M.C. Santana, Structural differences between wood species: Evidence from chemical composition, FTIR spectroscopy, and thermogravimetric analysis, *Journal of Applied Polymer Science* 126 (2012) E336-E343, <https://doi.org/10.1002/app.36991>.
- [179] N. Cordeiro, M.N. Belgacem, A. Gandini, C.P. Neto, Urethanes and polyurethanes from suberin 2: synthesis and characterization, *Industrial Crops and Products* 10(1) (1999) 1-10, [https://doi.org/10.1016/S0926-6690\(98\)00029-6](https://doi.org/10.1016/S0926-6690(98)00029-6).

- [180] A.F. Sousa, A. Gandini, A.J.D. Silvestre, C.P. Neto, Synthesis and characterization of novel biopolyesters from suberin and model comonomers, *Chemsuschem* 1(12) (2008) 1020-1025, <https://doi.org/10.1002/cssc.200800178>.
- [181] A.F. Sousa, A. Gandini, A.J.D. Silvestre, C. Pascoal Neto, J.J.C. Cruz Pinto, C. Eckerman, B. Holmbom, Novel suberin-based biopolyesters: From synthesis to properties, *Journal of Polymer Science Part a-Polymer Chemistry* 49(10) (2011) 2281-2291, <https://doi.org/10.1002/pola.24661>.
- [182] E.M. Fernandes, I.M. Aroso, J.F. Mano, J.A. Covas, R.L. Reis, Functionalized cork-polymer composites (CPC) by reactive extrusion using suberin and lignin from cork as coupling agents, *Composites Part B-Engineering* 67 (2014) 371-380, <https://doi.org/10.1016/j.compositesb.2014.07.028>.
- [183] N. Cordeiro, A. Blayo, N.M. Belgacem, A. Gandini, C.P. Neto, J.F. LeNest, Cork suberin as an additive in offset lithographic printing inks, *Industrial Crops and Products* 11(1) (2000) 63-71, [https://doi.org/10.1016/s0926-6690\(99\)00037-0](https://doi.org/10.1016/s0926-6690(99)00037-0).
- [184] I.M. Aroso, A.R. Araujo, R.A. Pires, R.L. Reis, Cork: Current technological developments and future perspectives for this natural, renewable, and sustainable material, *Acs Sustainable Chemistry & Engineering* 5(12) (2017) 11130-11146, <https://doi.org/10.1021/acssuschemeng.7b00751>.
- [185] J. Heinamaki, M.M. Pirttimaa, S. Alakurtti, H.P. Pitkanen, H. Kanerva, J. Hulkko, U. Paaver, J. Aruvali, J. Yliruusi, K. Kogermann, Suberin fatty acids from outer birch bark: Isolation and physical material characterization, *Journal of Natural Products* 80(4) (2017) 916-924, <https://doi.org/10.1021/acs.jnatprod.6b00771>.
- [186] P. Jedrzejczak, M.N. Collins, T. Jesionowski, L. Klapiszewski, The role of lignin and lignin-based materials in sustainable construction-A comprehensive review, *International Journal of Biological Macromolecules* 187 (2021) 624-650, <https://doi.org/10.1016/j.ijbiomac.2021.07.125>.
- [187] N. Graupner, Application of lignin as natural adhesion promoter in cotton fibre-reinforced poly(lactic acid) (PLA) composites, *Journal of Materials Science* 43(15) (2008) 5222-5229, <https://doi.org/10.1007/s10853-008-2762-3>.
- [188] S.L. Hilburg, A.N. Elder, H. Chung, R.L. Ferebee, M.R. Bockstaller, N.R. Washburn, A universal route towards thermoplastic lignin composites with improved mechanical properties, *Polymer* 55(4) (2014) 995-1003, <https://doi.org/10.1016/j.polymer.2013.12.070>.
- [189] I. Simkovic, Unexplored possibilities of all-polysaccharide composites, *Carbohydrate Polymers* 95(2) (2013) 697-715, <https://doi.org/10.1016/j.carbpol.2013.03.040>.
- [190] J. Lucenius, J.J. Valle-Delgado, K. Parikka, M. Osterberg, Understanding hemicellulose-cellulose interactions in cellulose nanofibril-based composites, *Journal of Colloid and Interface Science* 555 (2019) 104-114, <https://doi.org/10.1016/j.jcis.2019.07.053>.
- [191] A.M. Matos, S. Nunes, J. Sousa-Coutinho, Cork waste in cement based materials, *Materials & Design* 85 (2015) 230-239, <https://doi.org/10.1016/j.matdes.2015.06.082>.
- [192] R. Zhang, X. Xiao, Q. Tai, H. Huang, J. Yang, Y. Hu, Preparation of lignin-silica hybrids and its application in intumescent flame-retardant poly(lactic acid) system, *High Performance Polymers* 24(8) (2012) 738-746, <https://doi.org/10.1177/0954008312451476>.
- [193] T. Shi, S. Zhang, X. Shi, Oxidized regenerated celluloses to fabricate high fire safety for epoxy resin with super expansion char layer, *Cellulose* 28(5) (2021) 2995-3015, <https://doi.org/10.1007/s10570-021-03723-y>.
- [194] A.Q. Barbosa, L.F.M. da Silva, A. Oechsner, J. Abenojar, J.C. del Real, Influence of the size and amount of cork particles on the impact toughness of a structural adhesive, *Journal of Adhesion* 88(4-6) (2012) 452-470, <https://doi.org/10.1080/00218464.2012.660811>.
- [195] M. Flores, M.E. Rosa, C.Y. Barlow, M.A. Fortes, M.F. Ashby, Properties and uses of consolidated cork dust, *Journal of Materials Science* 27(20) (1992) 5629-5634, <https://doi.org/10.1007/bf00541634>.
- [196] L.J. Gibson, K.E. Easterling, M.F. Ashby, The structure and mechanics of cork, *Proceedings of the Royal Society of London Series a-Mathematical Physical and Engineering Sciences* 377(1769) (1981) 99-117, <https://doi.org/10.1098/rspa.1981.0117>.

- [197] A.V. Marques, H. Pereira, D. Meier, O. Faix, Quantitative analysis of cork (*Quercus suber* L.) and milled cork lignin by FTIR spectroscopy, analytical pyrolysis, and total hydrolysis, *Holzforschung* 48 (1994) 43-50, <https://doi.org/10.1515/hfsg.1994.48.s1.43>.
- [198] I. Miranda, J. Gominho, H. Pereira, Cellular structure and chemical composition of cork from the Chinese cork oak (*Quercus variabilis*), *Journal of Wood Science* 59(1) (2013) 1-9, <https://doi.org/10.1007/s10086-012-1300-8>.
- [199] M.H. Lopes, A.S. Barros, C.P. Neto, D. Rutledge, I. Delgadillo, A.M. Gil, Variability of cork from Portuguese *Quercus suber* studied by solid-state C-13-NMR and FTIR spectroscopies, *Biopolymers* 62(5) (2001) 268-277, <https://doi.org/10.1002/bip.1022>.
- [200] S. Gandolfi, G. Ottolina, S. Riva, G.P. Fantoni, I. Patel, Complete chemical analysis of carmagnola hemp hurds and structural features of its components, *Bioresources* 8(2) (2013) 2641-2656, <https://doi.org/10.15376/biores.8.2.2641-2656>.
- [201] C.P. Neto, J. Rocha, A. Gil, N. Cordeiro, A.P. Esculcas, S. Rocha, I. Delgadillo, J.D.P. Dejesus, A.J.F. Correia, <sup>13</sup>C Solid-state nuclear magnetic resonance and Fourier transform infrared studies of the thermal decomposition of cork, *Solid State Nuclear Magnetic Resonance* 4(3) (1995) 143-151, [https://doi.org/10.1016/0926-2040\(94\)00039-f](https://doi.org/10.1016/0926-2040(94)00039-f).
- [202] R. Ferreira, H. Garcia, A.F. Sousa, C.S.R. Freire, A.J.D. Silvestre, L.P.N. Rebelo, C.S. Pereira, Isolation of suberin from birch outer bark and cork using ionic liquids: A new source of macromonomers, *Industrial Crops and Products* 44 (2013) 520-527, <https://doi.org/10.1016/j.indcrop.2012.10.002>.
- [203] A. Sen, A.V. Marques, J. Gominho, H. Pereira, Study of thermochemical treatments of cork in the 150-400 degrees C range using colour analysis and FTIR spectroscopy, *Industrial Crops and Products* 38 (2012) 132-138, <https://doi.org/10.1016/j.indcrop.2012.01.018>.
- [204] B. Esteves, J. Graca, H. Pereira, Extractive composition and summative chemical analysis of thermally treated eucalypt wood, *Holzforschung* 62(3) (2008) 344-351, <https://doi.org/10.1515/hf.2008.057>.
- [205] C.J. Sartori, G.S. Mota, I. Miranda, F.A. Mori, H. Pereira, Tannin extraction and characterization of polar extracts from the barks of two eucalyptus urophylla hybrids, *Bioresources* 13(3) (2018) 4820-4831, <https://doi.org/10.15376/biores.13.3.4820-4831>.
- [206] T.L. Eberhardt, X. Li, T.F. Shupe, C.Y. Hse, Chinese tallow tree (*Sapium sebiferum*) utilization: Characterization of extractives and cell-wall chemistry, *Wood and Fiber Science* 39(2) (2007) 319-324.
- [207] F. Mburu, P. Sirmah, F. Muisu, S. Dumarcay, P. Gerardin, Selected wood properties of prunus africana (Hook) grown in Kenya as possible reasons for its high natural durability, *Drvna Industrija* 64(1) (2013) 19-24, <https://doi.org/10.5552/drind.2013.1238>.
- [208] B.D. Mattos, T.V. Lourencon, D.A. Gatto, L. Serrano, J. Labidi, Chemical characterization of wood and extractives of fast-growing *Schizolobium parahyba* and *Pinus taeda*, *Wood Material Science & Engineering* 11(4) (2016) 209-216, <https://doi.org/10.1080/17480272.2014.970574>.
- [209] A.N. Shebani, A.J. van Reenen, M. Meincken, The effect of wood extractives on the thermal stability of different wood-LLDPE composites, *Thermochimica Acta* 481(1-2) (2009) 52-56, <https://doi.org/10.1016/j.tca.2008.10.008>.
- [210] A.N. Shebani, A.J. van Reenen, M. Meincken, The effect of wood extractives on the thermal stability of different wood species, *Thermochimica Acta* 471(1-2) (2008) 43-50, <https://doi.org/10.1016/j.tca.2008.02.020>.
- [211] P. Jusner, S. Barbini, S. Schiehser, M. Bacher, E. Schwaiger, A. Potthast, T. Rosenau, Impact of residual extractives on the thermal stability of softwood Kraft pulp, *Cellulose* 29(16) (2022) 8797-8810, <https://doi.org/10.1007/s10570-022-04807-z>.
- [212] J.K. Mohammed, A.A. Mahdi, M.I. Ahmed, M. Ma, H. Wang, Preparation, deproteinization, characterization, and antioxidant activity of polysaccharide from *Medemia argun* fruit, *International Journal of Biological Macromolecules* 155 (2020) 919-926, <https://doi.org/10.1016/j.ijbiomac.2019.11.050>.
- [213] C.A.K. Varma, K.J. Kumar, Structural, functional and pH sensitive release characteristics of water-soluble polysaccharide from the seeds of *Albizia lebeck* L, *Carbohydrate Polymers* 175 (2017) 502-508, <https://doi.org/10.1016/j.carbpol.2017.08.017>.

- [214] T.-Q. Yuan, F. Xu, J. He, R.-C. Sun, Structural and physico-chemical characterization of hemicelluloses from ultrasound-assisted extractions of partially delignified fast-growing poplar wood through organic solvent and alkaline solutions, *Biotechnology Advances* 28(5) (2010) 583-593, <https://doi.org/10.1016/j.biotechadv.2010.05.016>.
- [215] M. Teixeira, R. Sonnier, B. Otazaghine, L. Ferry, M. Aubert, T. Tirri, C.-E. Wilen, S. Rouif, Radiation-grafting of flame retardants on flax fabrics - A comparison between different flame retardant structures, *Radiation Physics and Chemistry* 145 (2018) 135-142, <https://doi.org/10.1016/j.radphyschem.2017.10.013>.
- [216] R. Hajj, R. El Hage, R. Sonnier, B. Otazaghine, B. Gallard, S. Rouif, M. Nakhl, J.-M. Lopez-Cuesta, Grafting of phosphorus flame retardants on flax fabrics: Comparison between two routes, *Polymer Degradation and Stability* 147 (2018) 25-34, <https://doi.org/10.1016/j.polymdegradstab.2017.11.006>.
- [217] G. Dorez, L. Ferry, R. Sonnier, A. Taguet, J.M. Lopez-Cuesta, Effect of cellulose, hemicellulose and lignin contents on pyrolysis and combustion of natural fibers, *Journal of Analytical and Applied Pyrolysis* 107 (2014) 323-331, <https://doi.org/10.1016/j.jaap.2014.03.017>.
- [218] L. Ferry, G. Dorez, A. Taguet, B. Otazaghine, J.M. Lopez-Cuesta, Chemical modification of lignin by phosphorus molecules to improve the fire behavior of polybutylene succinate, *Polymer Degradation and Stability* 113 (2015) 135-143, <https://doi.org/10.1016/j.polymdegradstab.2014.12.015>.
- [219] J.S. Renner, R.A. Mensah, L. Jiang, Q. Xu, A critical assessment of the fire properties of different wood species and bark from small- and bench-scale fire experiments, *Journal of Thermal Analysis and Calorimetry* (2022), <https://doi.org/10.1007/s10973-022-11443-z>.
- [220] H. Pereira, The thermochemical degradation of cork, *Wood Science and Technology* 26(4) (1992) 259-269, <https://doi.org/10.1007/bf00200161>.
- [221] G. Huang, W. Chen, T. Wu, H. Guo, C. Fu, Y. Xue, K. Wang, P. Song, Multifunctional graphene-based nano-additives toward high-performance polymer nanocomposites with enhanced mechanical, thermal, flame retardancy and smoke suppressive properties, *Chemical Engineering Journal* 410 (2021), <https://doi.org/10.1016/j.cej.2020.127590>.
- [222] S. Xu, L. Zhang, Y. Lin, R. Li, F. Zhang, Layered double hydroxides used as flame retardant for engineering plastic acrylonitrile-butadiene-styrene (ABS), *Journal of Physics and Chemistry of Solids* 73(12) (2012) 1514-1517, <https://doi.org/10.1016/j.jpcs.2012.04.011>.
- [223] H. Cirmad, S. Tirkes, U. Tayfun, Evaluation of flammability, thermal stability and mechanical behavior of expandable graphite-reinforced acrylonitrile-butadiene-styrene terpolymer, *Journal of Thermal Analysis and Calorimetry* 147(3) (2022) 2229-2237, <https://doi.org/10.1007/s10973-021-10656-y>.
- [224] M. Zhu, P. Jia, G. Yang, L. Song, Y. Hu, B. Wang, Synergistic effects of core-shell structured piperazine pyrophosphate microcapsules on fire safety and mechanical property in styrenic thermoplastic elastomer, *Journal of Colloid and Interface Science* 653 (2024) 1112-1122, <https://doi.org/10.1016/j.jcis.2023.09.147>.
- [225] X. Cheng, J. Wu, C. Yao, G. Yang, Aluminum hypophosphite and aluminum phenylphosphinate: A comprehensive comparison of chemical interaction during pyrolysis in flame-retarded glass-fiber-reinforced polyamide 6, *Journal of Fire Sciences* 37(3) (2019) 193-212, <https://doi.org/10.1177/0734904119836208>.
- [226] U. Braun, B. Scharrel, Flame retardant mechanisms of red phosphorus and magnesium hydroxide in high impact polystyrene, *Macromolecular Chemistry and Physics* 205(16) (2004) 2185-2196, <https://doi.org/10.1002/macp.200400255>.
- [227] H. Vahabi, F. Laoutid, M. Mehrpouya, M.R. Saeb, P. Dubois, Flame retardant polymer materials: An update and the future for 3D printing developments, *Materials Science & Engineering R-Reports* 144 (2021), <https://doi.org/10.1016/j.mser.2020.100604>.
- [228] M. Vale, M.M. Mateus, R.G. dos Santos, C.N. de Castro, A. de Schrijver, J.C. Bordado, A.C. Marques, Replacement of petroleum-derived diols by sustainable biopolyols in one component polyurethane foams, *Journal of Cleaner Production* 212 (2019) 1036-1043, <https://doi.org/10.1016/j.jclepro.2018.12.088>.

- [229] C. Pinto, S. Cravo, S. Mota, L. Rego, J.R.e. Silva, A. Almeida, C.M. Afonso, M.E. Tiritan, H. Cidade, I.F. Almeida, Cork by-products as a sustainable source of potential antioxidants, *Sustainable Chemistry and Pharmacy* 36 (2023), <https://doi.org/10.1016/j.scp.2023.101252>.
- [230] A.M. Mislata, M. Puxeu, R. Ferrer-Gallego, Aromatic Potential and Bioactivity of Cork Stoppers and Cork By-Products, *Foods* 9(2) (2020), <https://doi.org/10.3390/foods9020133>.
- [231] T.E. Motaung, Z. Gqokoma, L.Z. Liganiso, M.J. Hato, The Effect of Acid Content on the Poly(furfuryl) Alcohol/Cellulose Composites, *Polymer Composites* 37(8) (2016) 2434-2441, <https://doi.org/10.1002/pc.23428>.
- [232] A. Lagorce-Tachon, T. Karbowski, D. Champion, R.D. Gougeon, J.P. Bellat, Mechanical Properties of Cork: Effect of Hydration, in 6th Biot Conference on Poromechanics. 2017, Paris, FRANCE.
- [233] A. Lagorce-Tachon, T. Karbowski, D. Champion, R.D. Gougeon, J.-P. Bellat, How does hydration affect the mechanical properties of wine stoppers?, *Journal of Materials Science* 51(9) (2016) 4227-4237, <https://doi.org/10.1007/s10853-015-9669-6>.
- [234] J.F. Mano, The viscoelastic properties of cork, *Journal of Materials Science* 37(2) (2002) 257-263, <https://doi.org/10.1023/a:1013635809035>.
- [235] S.F. Wang, Y. Hu, L. Song, Z.Z. Wang, Z.Y. Chen, W.C. Fan, Preparation and thermal properties of ABS/montmorillonite nanocomposite, *Polymer Degradation and Stability* 77(3) (2002) 423-426, [https://doi.org/10.1016/s0141-3910\(02\)00098-8](https://doi.org/10.1016/s0141-3910(02)00098-8).
- [236] Z.Y. Wang, E.H. Han, W. Ke, Influence of nano-LDHs on char formation and fire-resistant properties of flame-retardant coating, *Progress in Organic Coatings* 53(1) (2005) 29-37, <https://doi.org/10.1016/j.porgcoat.2005.01.004>.
- [237] G. Camino, L. Costa, L. Trossarelli, Study of the mechanism of intumescence in fire retardant polymers: Part V—Mechanism of formation of gaseous products in the thermal degradation of ammonium polyphosphate, *Polymer Degradation and Stability* 12(3) (1985) 203-211, [https://doi.org/10.1016/0141-3910\(85\)90089-8](https://doi.org/10.1016/0141-3910(85)90089-8).
- [238] A. Riva, G. Camino, L. Fomperie, P. Amigouet, Fire retardant mechanism in intumescent ethylene vinyl acetate compositions, *Polymer Degradation and Stability* 82(2) (2003) 341-346, [https://doi.org/10.1016/s0141-3910\(03\)00191-5](https://doi.org/10.1016/s0141-3910(03)00191-5).
- [239] A. Cayla, F. Rault, S. Giraud, F. Salaun, V. Fierro, A. Celzard, PLA with Intumescent System Containing Lignin and Ammonium Polyphosphate for Flame Retardant Textile, *Polymers* 8(9) (2016), <https://doi.org/10.3390/polym8090331>.
- [240] Y. Shu, Q.L. Luo, H.W. Lin, Y.J. Ouyang, X.M. Zhang, L.P. Sheng, S.P. Su, Preparation and Properties of Bio-Based Flame Retardant Polyvinyl Alcohol, *Journal of Renewable Materials* 9(5) (2021) 909-921, <https://doi.org/10.32604/jrm.2021.014216>.
- [241] S.B. Munteanu, C. Vasile, Spectral and thermal characterization of styrene-butadiene copolymers with different architectures, *Journal of Optoelectronics and Advanced Materials* 7(6) (2005) 3135-3148.
- [242] A. Agirre, M. Aguirre, J.R. Leiza, Characterization of grafting properties of ABS latexes: ATR-FTIR vs NMR spectroscopy, *Polymer* 253 (2022), <https://doi.org/10.1016/j.polymer.2022.124997>.
- [243] B. Perret, B. Schartel, The effect of different impact modifiers in halogen-free flame retarded polycarbonate blends - I. Pyrolysis, *Polymer Degradation and Stability* 94(12) (2009) 2194-2203, <https://doi.org/10.1016/j.polymdegradstab.2009.09.005>.
- [244] J. Feng, C. Carpanese, A. Fina, Thermal decomposition investigation of ABS containing Lewis-acid type metal salts, *Polymer Degradation and Stability* 129 (2016) 319-327, <https://doi.org/10.1016/j.polymdegradstab.2016.05.013>.
- [245] X. Yang, Z. Fu, D. Han, Y. Zhao, R. Li, Y. Wu, Unveiling the pyrolysis mechanisms of cellulose: Experimental and theoretical studies, *Renewable Energy* 147 (2020) 1120-1130, <https://doi.org/10.1016/j.renene.2019.09.069>.
- [246] Q. Wang, D. Chu, C. Luo, Z. Lai, S. Shang, S. Rahimi, J. Mu, Transformation mechanism from cork into honeycomb-like biochar with rich hierarchical pore structure during slow pyrolysis, *Industrial Crops and Products* 181 (2022), <https://doi.org/10.1016/j.indcrop.2022.114827>.



- [247] Z. Ma, Y. Yang, Y. Wu, J. Xu, H. Peng, X. Liu, W. Zhang, S. Wang, In-depth comparison of the physicochemical characteristics of bio-char derived from biomass pseudo components: Hemicellulose, cellulose, and lignin, *Journal of Analytical and Applied Pyrolysis* 140 (2019) 195-204, <https://doi.org/10.1016/j.jaap.2019.03.015>.
- [248] S. Bellayer, M. Jimenez, B. Prieur, B. Dewailly, A. Ramgobin, J. Sarazin, B. Revel, G. Tricot, S. Bourbigot, Fire retardant sol-gel coated polyurethane foam: Mechanism of action, *Polymer Degradation and Stability* 147 (2018) 159-167, <https://doi.org/10.1016/j.polymdegradstab.2017.12.005>.
- [249] A. Castrovinci, G. Camino, C. Drevelle, S. Duquesne, C. Magniez, M. Vouters, Ammonium polyphosphate-aluminum trihydroxide antagonism in fire retarded butadiene-styrene block copolymer, *European Polymer Journal* 41(9) (2005) 2023-2033, <https://doi.org/10.1016/j.eurpolymj.2005.03.010>.
- [250] U. Braun, B. Schartel, M.A. Fichera, C. Jaeger, Flame retardancy mechanisms of aluminium phosphinate in combination with melamine polyphosphate and zinc borate in glass-fibre reinforced polyamide 6,6, *Polymer Degradation and Stability* 92(8) (2007) 1528-1545, <https://doi.org/10.1016/j.polymdegradstab.2007.05.007>.
- [251] S.V. Levchik, G. Camino, L. Costa, G.F. Levchik, Mechanism of action of phosphorus-based flame retardants in nylon 6. I. ammonium polyphosphate, *Fire and materials* 19 (1995) 1-10, <https://doi.org/10.1002/fam.810190102>.
- [252] J.-C. Liu, M.-J. Xu, T. Lai, B. Li, Effect of Surface-Modified Ammonium Polyphosphate with KH550 and Silicon Resin on the Flame Retardancy, Water Resistance, Mechanical and Thermal Properties of Intumescent Flame Retardant Polypropylene, *Industrial & Engineering Chemistry Research* 54(40) (2015) 9733-9741, <https://doi.org/10.1021/acs.iecr.5b01670>.
- [253] B. Zhang, E. Leng, P. Wang, X. Gong, J. Zhang, Y. Zhang, M. Xu, Effect of reducing ends on the pyrolysis characteristics and product distribution of cellulose, *Journal of Analytical and Applied Pyrolysis* 114 (2015) 119-126, <https://doi.org/10.1016/j.jaap.2015.05.007>.
- [254] S. Zhou, L. Song, Z. Wang, Y. Hu, W. Xing, Flame retardation and char formation mechanism of intumescent flame retarded polypropylene composites containing melamine phosphate and pentaerythritol phosphate, *Polymer Degradation and Stability* 93(10) (2008) 1799-1806, <https://doi.org/10.1016/j.polymdegradstab.2008.07.012>.
- [255] Z. Zheng, Y. Liu, L. Zhang, B. Dai, X. Yang, H. Wang, Fabrication of halogen-free ammonium phosphate with two components via a simple method and its flame retardancy in polypropylene composites, *Journal of Thermal Analysis and Calorimetry* 127(3) (2017) 2013-2023, <https://doi.org/10.1007/s10973-016-5779-x>.
- [256] F.d.S. Grasel, M.F. Ferrao, C.R. Wolf, Development of methodology for identification the nature of the polyphenolic extracts by FTIR associated with multivariate analysis, *Spectrochimica Acta Part a-Molecular and Biomolecular Spectroscopy* 153 (2016) 94-101, <https://doi.org/10.1016/j.saa.2015.08.020>.
- [257] A. Sut, S. Greiser, C. Jäger, B. Schartel, Aluminium diethylphosphinate versus ammonium polyphosphate: A comprehensive comparison of the chemical interactions during pyrolysis in flame-retarded polyolefine/poly(phenylene oxide), *Thermochimica Acta* 640 (2016) 74-84, <https://doi.org/10.1016/j.tca.2016.08.004>.
- [258] S. Gebke, K. Thuemmler, R. Sonnier, S. Tech, A. Wagenfuehr, S. Fischer, Flame Retardancy of Wood Fiber Materials Using Phosphorus-Modified Wheat Starch, *Molecules* 25(2) (2020), <https://doi.org/10.3390/molecules25020335>.
- [259] R.C. Pereira, P.R. Anizelli, E. Di Mauro, D.F. Valezi, A.C.S. da Costa, C.T.B.V. Zaia, D.A.M. Zaia, The effect of pH and ionic strength on the adsorption of glyphosate onto ferrihydrite, *Geochemical Transactions* 20 (2019), <https://doi.org/10.1186/s12932-019-0063-1>.
- [260] C.V. Waiman, J.M. Arroyave, H. Chen, W. Tan, M.J. Avena, G.P. Zanini, The simultaneous presence of glyphosate and phosphate at the goethite surface as seen by XPS, ATR-FTIR and competitive adsorption isotherms, *Colloids and Surfaces a-Physicochemical and Engineering Aspects* 498 (2016) 121-127, <https://doi.org/10.1016/j.colsurfa.2016.03.049>.
- [261] B. Bardakci, N. Kaya, FT-IR Spectroscopic Study of Triethyl Phosphate Adsorption on FAU Type Zeolite, *Asian Journal of Chemistry* 21(6) (2009) 4914-4918.

- [262] M.C. Basso, A. Pizzi, J.P. Maris, L. Delmotte, B. Colin, Y. Rogaume, MALDI-TOF, <sup>13</sup>C NMR and FTIR analysis of the cross-linking reaction of condensed tannins by triethyl phosphate, *Industrial Crops and Products* 95 (2017) 621-631, <https://doi.org/10.1016/j.indcrop.2016.11.031>.
- [263] E. Deconinck, M. Canfyn, P.Y. Sacre, S. Baudewyns, P. Courselle, J.O. De Beer, A validated GC-MS method for the determination and quantification of residual solvents in counterfeit tablets and capsules, *Journal of Pharmaceutical and Biomedical Analysis* 70 (2012) 64-70, <https://doi.org/10.1016/j.jpba.2012.05.022>.
- [264] M. Bozic, P. Liu, A.P. Mathew, V. Kokol, Enzymatic phosphorylation of cellulose nanofibers to new highly-ions adsorbing, flame-retardant and hydroxyapatite-growth induced natural nanoparticles, *Cellulose* 21(4) (2014) 2713-2726, <https://doi.org/10.1007/s10570-014-0281-8>.
- [265] F.-X. Chen, C.-R. Zhou, G.-P. Li, Study on thermal decomposition and the non-isothermal decomposition kinetics of glyphosate, *Journal of Thermal Analysis and Calorimetry* 109(3) (2012) 1457-1462, <https://doi.org/10.1007/s10973-011-1834-9>.
- [266] E. Wawrzyn, B. Scharrel, H. Seefeldt, A. Karrasch, C. Jäger, What Reacts with What in Bisphenol A Polycarbonate/Silicon Rubber/Bisphenol A Bis(diphenyl phosphate) during Pyrolysis and Fire Behavior?, *Industrial & Engineering Chemistry Research* 51(3) (2012) 1244-1255, <https://doi.org/10.1021/ie201908s>.